UNIVERSITAT DE BARCELONA

Synthesis and performance of heterogeneous catalysts for Fenton-like and photo-Fenton-like reactions at circumneutral pH

Angel Cruz Gonzalo

Programa de doctorat d'Enginyeria i Tecnologies Avançades

SYNTHESIS AND PERFORMANCE OF HETEROGENEOUS CATALYSTS FOR FENTON-LIKE AND PHOTO-FENTON-LIKE REACTIONS AT CIRCUMNEUTRAL pH

Angel Cruz Gonzalo

Director i Tutor:

Dr. Carmen Sans Mazón

Departament d'Enginyeria Química I Química Analítica

Universitat de Barcelona

La Dra. CARMEN SANS MAZÓN, professora titular del Departament d'Enginyeria Química i Química Analítica de la Universitat de Barcelona:

CERTIFICA:

El treball d'investigació titulat "SYNTHESIS AND PERFORMANCE OF HETEROGENEOUS CATALYSTS FOR FENTON-LIKE AND PHOTO-FENTON-LIKE REACTIONS AT CIRCUMNEUTRAL pH" constitueix la memòria que presenta l'Enginyer Químic Angel Cruz Gonzalo per a aspirar al grau de Doctor per la Universitat de Barcelona. Aquesta tesis doctoral ha estat realitzada dins del programa de doctorat "Enginyeria i Tecnologies Avançades", en el Departament d'Enginyeria Química i Química Analítica de la Universitat de Barcelona.

I per a que així consti als efectes oportuns, signa el present certificat a Barcelona, 21 d'abril de 2017.

Dra. Carmen Sans Mazón

Directora y tutora de la tesis doctoral

A mi sobrina Mar, que ha nacido hoy 18 de abril de 2017

Agradecimientos

La primera vez que llegué en 2009 al Departamento de Ingeniería Química de la Universidad de Barcelona era de paso, no conocía lo que era la investigación y venía a hacer un proyecto final de carrera. Desde entonces ha pasado mucho tiempo, he conocido a muchas personas y puedo decir que estoy muy agradecido por haber podido compartir una importante parte de mi vida con ellos, pues ocupan un lugar muy preciado en mi corazón.

Quiero agradecer al Dr. Santiago Esplugas por darme la oportunidad de empezar a trabajar aquí. También merece un gran agradecimiento la Dra. Carmen Sans por dirigir mi tesis, ayudarme, guiarme, enseñarme y sobre todo por aguantarme todos estos años. Gracias a ella he crecido como investigador.

No merecen menos agradecimientos todos mis compañeros, pues no son compañeros sino amigos.

Renato, conseguiste ilusionarme en esos primeros años como investigador, además de ser el alma del grupo y un gran amigo.

Oscar, Roger y Nardi, habéis sido un referente a seguir como investigadores y siempre habéis estado disponibles para debatir cualquier cosa, sea científica o no, contribuyendo a mejorar tanto como investigador como persona.

Ana, Núria, Anto y Mireia, habéis sido mis grandes amigas durante todos estos años y no podría estar más contento. Se que como en todas las amistades ha habido mejores y peores momentos, pero no cambiaría ni uno de ellos, pues la suma de lo bueno y de lo malo hace que seáis una de las mejores razones que se me ocurren para justificar el buen tiempo que he pasado aquí. Habéis estado para ayudarme siempre que lo he necesitado y os lo agradezco de todo corazón.

Meme y Marc, fuisteis una parte muy importante de mi vida de investigador cuando empezaba y aunque ahora nos vemos poco, siempre seréis grandes amigos para mí.

Xavi i Silvia, aunque casi no salís del gimnasio y es difícil de veros, también os considero unos grandes amigos con los que siempre podré contar si lo necesito.

Raül, Follón, Sergi, Carlos, Helios, Angelines, Irene, Albert, Anna... me habéis hecho reír siempre que habéis podido. Sois irremplazables!

No puedo olvidar a todas aquellas personas que pasaron breve pero intensamente por el departamento: Rui, Rodrigo, Bruno S., João, Dani, Chris, Àgueda, Lídia... Nunca os voy a olvidar!

Tampoco aquellos amigos que me ayudaron durante mis estancias en el extranjero: Yuan, Bing, Ana Sofía, Filipa... gracias por vuestra amistad y vuestra ayuda cuando estaba lejos de casa!

También quiero mencionar a las últimas incorporaciones en el Departamento: Alberto, Núria, Víctor, Carme... sois grandes personas y me gustaría haber podido conoceros mejor, pues estoy seguro de que no me arrepentiría. Quiero seguir sabiendo de vosotros aunque ya no esté por aquí.

A mis amigos de siempre: Marc, Álex, Jordi, Ware, Xavi, Christian, Joan, Eric, Fran, Rubén. El tiempo pasa más rápido a vuestro lado. Estoy muy agradecido por vuestra amistad y todos los momentos que pasamos juntos. Consiguen que hasta el peor día pueda ser un gran día!

Por último no quiero olvidar a mi familia. A mis padres, que me han apoyado y ayudado en todo lo que han podido, haciendo que mi vida sea más fácil y sintiéndome más seguro. A mis abuelos, que siempre han estado ahí desde que tengo memoria. Os quiero mucho!

A mi hermana, que además es una magnífica amiga. Muchas gracias por toda tu ayuda y apoyo, y gracias por estar siempre ahí para hablar de todo lo que me preocupa.

De verdad, con este apoyo y estos amigos, siento que sería capaz de lograr cualquier cosa que me proponga. Muchas gracias a todos!

Table of contents

Table of figures

Table of tables

Abstract

As an essential resource for life and most human activities, water resources protection have become one of the major focuses of scientific community, especially the increasing occurrence of emerging pollutants which have its origin in commonly used pharmaceuticals, personal care products, pesticides and some other anthropogenic origin compounds.

Fenton and photo-Fenton are advanced oxidation processes (AOPs) that have been widely proved on the removal of these compounds, but they are conventionally applied at acidic pH, below 3.0, because these processes involve the use of iron (II) salts, which are not soluble above. Also, the acidic effluents must be neutralized and high amounts of iron sludge are formed in the process.

Current research in the field tries to solve this drawback by focusing in two possible solutions: the use of chelating agents to keep iron soluble at circumneutral pH or the use of heterogeneous catalysts containing iron that can be easily removed and reused after its application.

This work is focused on the study, application and improvement of alginate-based heterogeneous catalysts for conducting photo-Fenton reactions at circumneutral pH.

Initially, the preparation process of the conventionally used Fe(III)/alginate catalyst was optimized by evaluating the effect of the parameters involved on its synthesis. Then, the synthetized catalyst was applied to the abatement of antibiotic sulfamethoxazole (SMX), which was used as reference compound. The reaction mechanism of alginate-based catalysts was proposed according to the results obtained. Also, a deep study about catalyst stability revealed a high dependence with water's pH. Fe(III)/alginate catalyst proved to release iron when sample's pH was below alginate's pK_a. Also, due to its organic nature, a significant HO· scavenging effect of alginate itself was observed, which reduced the effective amount of hydroxyl radicals available for the oxidation of the target compound.

Fe(III)/alginate was also tested for disinfection by adjusting the conditions to ensure a minimal iron release. Thus, the contribution of homogeneous reaction was significantly avoided. The catalyst proved being able to be used for disinfection of waters with low organic loads.

In order to improve the Fe(III)/alginate catalyst, some modifications were applied. The first one was the addition of a dehydration stage after its synthesis. The resulting catalyst was tested on the removal of SMX and had a similar effectiveness than the conventionally used Fe(III)/alginate but with a significantly lower iron release, which confirmed its improved stability. This more stable catalyst was also modified by including TiO_2, zero valent iron (ZVI) particles or cerium on its structure with the aim of, not only increase its stability, but its effectiveness. The TiO_2 catalyst proved to increase the effectiveness of the overall removal of SMX while the other two modifications did not.

Red volcanic rocks, iron shavings from metallurgical industry, a commercial Fe/Mn/O catalyst and a self-synthetized Fe/Ce/O catalyst were also tested as heterogeneous catalysts for Fenton and photo-Fenton at acidic and neutral pH. These catalysts were selected as inorganic-based ones and were compared to the Fe(III)/alginate dehydrated catalyst when applied to photo-Fenton at neutral pH. Results proved that only volcanic rocks had a significant activity when applied for photo-Fenton at neutral pH, but the effectiveness on the removal of SMX was low in comparison to the alginate-based catalyst. All other catalysts presented too low activity or major drawbacks that made them not suitable for water purification through Fenton-like and photo-Fenton-like processes.

Thesis director's report

Departament d'Enginyeria Química I Química Analítica
Facultat de Química
Universitat de Barcelona
c/Martí i Franquès, 1
08028 Barcelona, Espanya

Dr. CARMEN SANS MAZÓN, Professor from the Chemical Engineering and Analytical Chemistry Department of the Universitat de Barcelona, PhD thesis director of Angel Cruz Gonzalo, issues the following report related to his participation in the publications and scientific congresses' contributions derived from this PhD thesis:

The experimental work and results discussion included in the publications and Congresses' communications derived from this thesis were mainly developed in the Chemical Engineering and Analytical Chemistry Department of the Universitat de Barcelona by Angel Cruz Gonzalo, under the supervision of his PhD director. Part was also developed at the University of Coimbra under the supervision of Prof. Rosa Quinta-Ferreira. The publications derived from this thesis were not presented in other doctoral thesis or a thesis presented as a summary of publications.

<u>Publications:</u>

Authors (signature): Cruz, A.; Couto, L; Sans, C.; Esplugas, S.
Title: Study of the contribution of homogeneous catalysis on heterogeneous Fe(III)/alginate mediated photo-Fenton process
Journal: Chemical Engineering Journal
Volume: 318 **Pages, initial:** 272 **final:** 280 **Year:** 2016
DOI: 10.1016/j.cej.2016.09.014

Congress communications:

Authors: Cruz, A.; Sans, C.; Esplugas, S.

Title: Inactivation of Escherichia Coli by Fe/alginate heterogeneous photo-Fenton at neutral pH

Type of participation: Presentation of communication

Conference: 2nd International Conference of Recycling and Reuse

Publication: Book of Abstracts: ISBN: 978-975-518-364-0, pg 63-64

National / International: International

City: Istanbul   **Country:** TURKEY   **Year:** 2014

Authors: Cruz, A.; Li, M.; Sans, C.; Esplugas, S.; Qiang, Z.

Title: Assessment of Fe Fouling on LP UV lamp sleeves

Type of participation: Poster

Conference: 13th.Mediterranean Congress of Chemical Engineering.

Publication: Electronic Proceedings, 22_012_P

National / International: International

City: Barcelona   **Country:** SPAIN   **Year:** 2014

Authors: Cruz, A.; Sans, C.; Esplugas, S.

Title: Synthesis and evaluation of a new Fe/alginate heterogeneous catalyst for photo-Fenton at neutral pH

Type of participation: Speech

Conference: 7th European Meeting on Chemical Industry and Environment (EMChIE 2015)

Publication: Conference Proceedings, Volume 2. ISBN: 978-84-8424-367-0

National / International: International

City: Tarragona   **Country:** SPAIN   **Year:** 2015

xx

Authors: Sans, C.; Cruz, A.; Esplugas, S.

Title: Synthesis and evaluation of a new Fe/alginate heterogeneous catalyst for photo-Fenton and simulated solar photo-Fenton at neutral pH

Type of participation: Presentation of communication

Conference: 4th European Conference on Environmental Applications of Advanced Oxidation Processes EAAOP4

Publication: Proceedings

National / International: International

City: Athens   **Country:** GREECE   **Year:** 2015

Authors: Cruz, A.; Sans, C.; Esplugas, S.

Title: Study of pH stability of Fe/alginate catalyst for heterogeneous photo-Fenton

Type of participation: Poster

Conference: 3rd WATER RESEARCH Conference

Publication: Electronic Proceedings.

National / International: International

City: Shenzhen   **Country:** CHINA   **Year:** 2015

Dr. Carmen Sans Mazón

Barcelona, 21st of April 2017

Nomenclature

English

AOP	Advanced Oxidation Process
ATP	Adenosin Tri-Phosphate
BET	Brunauer-Emmett-Teller
BJH	Barret-Joyner-Halenda
BLB	Black-Light-Blue
CAFO	Concentrated Animal Feeding Operations
CFU	Colony Forming Units
DBP	Disinfection By-Products
EFOM	Effluent Organic Matter
FTIR	Fourier Transform Infrared
HO·	Hydroxyl Radical
ICP-AES	Inductive Coupled Plasma Atomic Emission Spectrometry
ICP-OES	Inductive Coupled Plasma Optical Emission Spectrometry
MFSD	Modified Fluorescence Silica Detector
MSB	Modified Scholten's Brooth
NGO	Non-Governmental Organizations
NOM	Natural Organic Matter
NSAiD	Non-Steroidal Anti-inflamatory Drugs
PCP	Personal Care Products
PFC	Perfluorinated Compounds
PFU	Plaque Forming Unit
SEM	Scanning Electron Microscopy
SMX	Sulfamethoxazole
TOC	Total Organic Carbon
TP	Transformation Products
WWTP	Wastewater Treatment Plants
ZVI	Zero Valent Iron

Spanish

CE	Contaminante Emergente
COT	Carbono Orgánico Total
POA	Proceso de Oxidación Avanzada

1. Introduction

1.1. WATER RESOURCES

Since ancient times water has been the most precious natural resource and villages and cities have prospered near rivers and lakes. As centuries passed, humankind increased in number and water supply became a challenge that engineering was able to solve, allowing the transportation and storage of the existent water resources. Nowadays, human population have grown until being almost 7.5 billion people, what supposes a new challenge for society.

Unlike other planets, water is the most abundant compound in Earth's surface (71 %), but 97.4 % of this water is saltwater and only a 2.5 % is freshwater. From this 2.5 %, almost 69 % can be found as ice in poles and glaciers and the rest is groundwater (30.1 %). Only a 1.2 % of the total freshwater is on the surface in the form of ground ice, permafrost, lakes, swamps, marshes, rivers and also as atmospheric water of part of living beings (Figure 1.1)
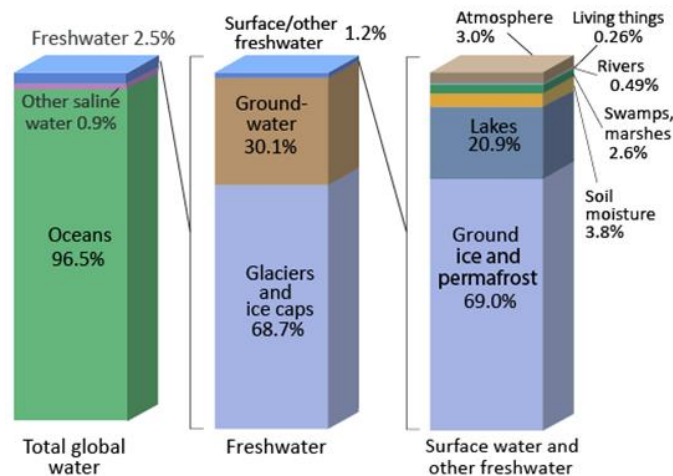
Figure 1.1. Water distribution on Earth. Image source: Igor Shiklomanov's chapter "World fresh water resources" in Peter H. Gleick (Editor), 1993, Water in Crisis: A Guide to the World's Fresh Water Resources.

This small amount of total water that can be used by humans is still considered enough to sustain basic needs as drinking water, cooking or personal hygiene of all Earth's population. Even so, freshwater is also essential for agriculture and industry. This processes are the ones consuming the highest amount of freshwater resources [1]. Also, "water use has been growing much faster than population for at least a century" [2].

Furthermore, water resources are not equally distributed, so there exist zones of the planet with more water than need but also zones in which water scarcity, due to physical or economic reasons, is a proved fact (Figure 1.2).
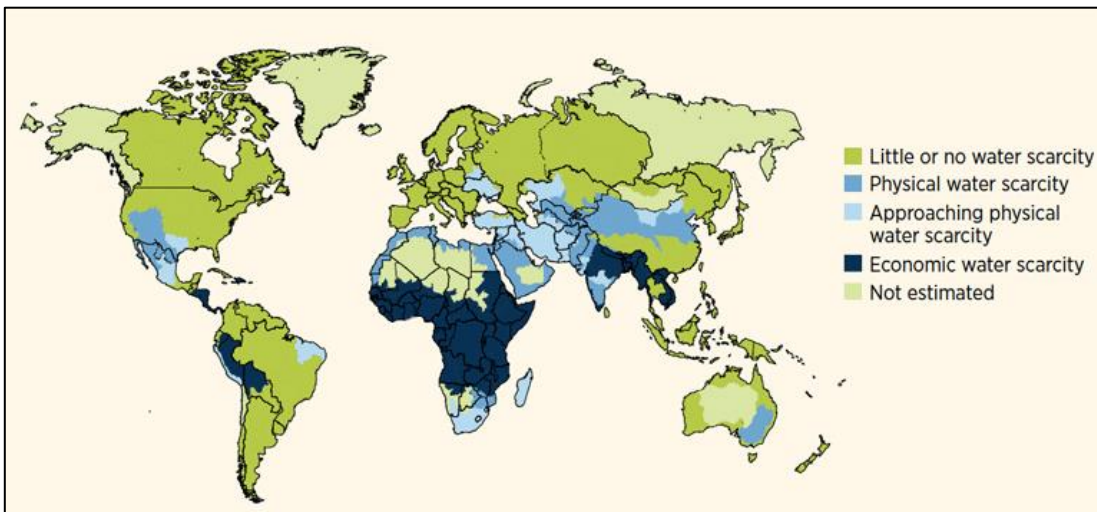
Figure 1.2. Water stress versus water scarcity. Source: World Water Development Report 4. World Water Assessment Programme (WWAP), March 2012.

A country is considered to suffer from a shortage of water when its annual available freshwater reserve is less than 1,000 m³ per capita [3].

According United Nations, "around 1.2 billion people, or almost one-fifth of the world's population, live in areas of physical scarcity, and 500 million people are approaching this situation. Another 1.6 billion people, or almost one quarter of the world's population, face economic water shortage (where countries lack the necessary infrastructure to take water from rivers and aquifers)" [4].

United Nations also estimated on its *Human Development Report* (2006) that by year 2025 more than 3 billion people could be living in water-stressed countries [2].

Considering all this facts and forecasts, the management and conservation of the existent water resources must be a critical point for society.

1.2. CONTAMINATED WATER AND WASTEWATER TREATMENT PLANTS

As previously mentioned, water is used in almost all human activities. All these uses inevitably produce an impact over water quality and contaminate it by incorporating organic matter and chemical compounds into it.

Environmental engineering tries to minimize or solve these anthropogenic impacts by applying several treatments. Otherwise, the discharge of untreated water into environment would produce the progressive reduction of water resources quality and the consequent reduction of available "clean" resources and an increase of global water scarcity.

For this purpose, wastewater treatment plants (WWTPs) have been designed and are in a constant improving process by incorporating new technologies and processes to reduce the amount of pollutants what have been incorporated into these resources.

Conventional WWTPs consist of diverse stages of treatment the sum of what achieve a sufficient water quality to allow the natural self-purification system processes of water resources to begin. This plants use to incorporate a combination of physical, chemical and biological processes and operations to remove solids, organic matter and nutrients from wastewater. These processes can be classified as preliminary, primary, secondary and tertiary treatments [5]. An example of a conventional WWTP configuration scheme proposed by Melgarejo et al. can be found in Figure 1.3 [6].
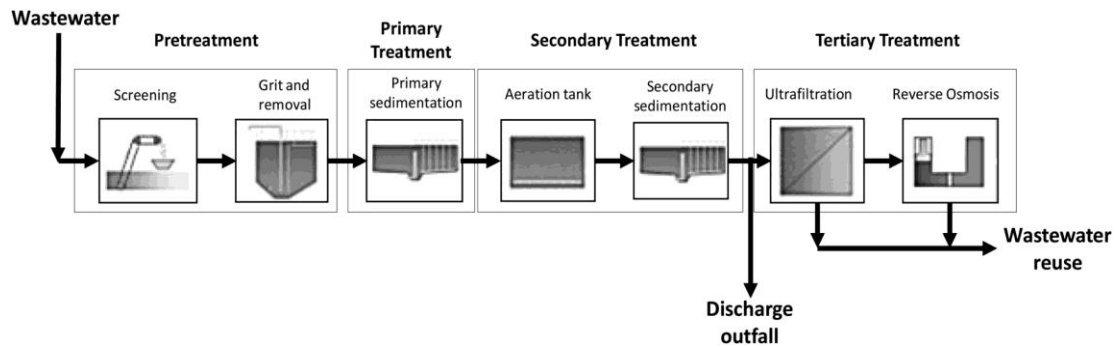
Figure 1.3. Example of a conventional WWTP process configuration.

The preliminary treatment is in charge of the removal of solids and other large materials which can be found in raw wastewater by using coarse screening and grit removal.

The primary treatment removes settleable organic and inorganic solids by sedimentation, and also removes materials that will float (scum) by skimming.

Secondary treatment follows primary treatment and involves the removal of biodegradable dissolved and colloidal organic matter using aerobic biological treatment processes. In the presence of oxygen, aerobic microorganisms metabolize the organic matter in the wastewater producing more microorganisms and inorganic end-products which are usually settled on a secondary settling tank.

In some cases, secondary treatment is not enough to remove non-biodegradable and other compounds which cannot be discharged and are still detected after the treatment [7–9], so a tertiary or advanced treatment process must follow it. These treatments are focused to the removal of specific wastewater constituents as nitrogen, phosphorus, additional suspended solids, refractory organics, heavy metals and dissolved solids.

4

1.3. GENERAL LEGAL FRAMEWORK OF WATER

1.3.1. Directive 2000/60/CE

Due to the importance of protecting water resources and water environments, the 23rd of October of 2000 the Directive 2000/60/EC of the European Parliament and of the Council was created, establishing a framework for the Community action in the field of water policy.

This directive, demanded and discussed not only by the European Council but also by local and regional authorities, water users and non-governmental organisations (NGOs) stablished a framework with the following key aims [10]:

- Expanding the scope of water protection to all waters, surface waters and groundwater.
- Achieving "good status" for all waters by a set deadline.
- Water management based on river basins.
- "Combined approach" of emission limit values and quality standards.
- Getting the prices right.
- Getting the citizen involved more closely.
- Streamlining legislation.

Other Directives at European level were issued since 2000, which modified and amplified the scope of Directive 2000/60/EC:

- Directive 2008/105/EC of the European Parliament and of the Council of 16 December 2008 on environmental quality standards in the field of water policy, amending and subsequently repealing Council Directives 82/176/EEC, 83/513/EEC, 84/156/EEC, 84/491/EEC, 86/280/EEC and amending Directive 2000/60/EC of the European Parliament and of the Council (European Commission, 2008).
- Commission Directive 2009/90/EC, of 31 of July 2009, laying down, pursuant to Directive 2000/60/EC of the European Parliament and of the Council, technical

specifications for chemical analysis and monitoring of water status (European Commission, 2009a).

The Directive 2000/60/EC of the European Parliament and of the Council included a list of priority pollutants that have been actualized since then through revisions and thanks to the scientific community that confirmed the danger posed by these compounds. The actual list of compounds [11] can be found in Table 1.1.

Table 1.1. List of the 33 priority compounds in water policy stablished by European Legislation.
(Last update 08/06/2016)

Number	CAS number	Compound
1	15972-60-8	Alachlor
2	120-12-7	Anthracene
3	1912-24-9	Atrazine
4	71-43-2	Benzene
5	Not applicable	Brominated diphenyleteriv
6	7440-43-9	Cadmium and its compounds
7	85535-84-8	Chloroalkanes, C-10-13 iv
8	470-90-6	Chlorfenvinphos
9	2921-88-2	Chlorpyrifos (Chlorpyrifos-ethyl)
10	107-06-2	1,2-Dichlorethane
11	75-09-2	Dichloromethane
12	117-81-7	Di(2-ethylhexyl)phthalate (DEHP)
13	330-54-1	Diuron
14	115-29-7	Endosulfan
15	206-44-0	Fluoranthene
16	118-74-1	Hexachlorobenzene
17	87-68-3	Hexachlorobutadiene
18	608-73-1	Hexachlorocylohexane
19	34123-59-6	Isoproturon
20	7439-92-1	Lead and its compounds
21	7439-97-6	Mercury and its compounds
22	91-20-3	Naphthalene
23	7440-02-0	Nickel and its compounds
24	25154-52-3	Nonyphenols
25	1806-26-4	Octylphenols
26	608-93-5	Pentachlorobenzene

<div align="center">**Table 1.1. (Continuation)**</div>

Number	CAS number	Compound
27	87-86-5	Pentachlorophenol
28	Not applicable	Polyaromatic hydrocarbons
29	122-34-9	Simazine
30	Not applicable	Tributyltin compounds
31	12002-48-1	Trichlorobenzenes
32	67-66-3	Trichloromethane
33	1582-09-8	Trifluralin

1.4. EMERGING POLLUTANTS

Until early 90s non-polar hazardous compounds such as persistent organic pollutants (POPs) and heavy metals were the major concern as priority pollutants and were subdued to intensive monitoring programs. Today, these compounds have been controlled through the adoption of appropriate measures to reduce dramatically their emissions [12].

However, the emission of so-called "emerging" or "new" unregulated contaminants has become an environmental problem and the major focus for scientific community.

According to Farré et al., emerging pollutants are defined as compounds that are not currently covered by existing water-quality regulations, have not been studied before, and are thought to be potential threats to environmental ecosystems and human health and safety [13].

Under this definition, a wide amount of compounds can be englobed. Among them, pharmaceuticals, drugs of abuse, personal-care products (PCPs), steroids and hormones, surfactants, perfluorinated compounds (PFCs), flame retardants, industrial additives and agents, and gasoline additives, as well as their transformation products (TPs) are the main ones. Lately, new ones are also being identified as emerging pollutants, such as nanomaterials, 1,4-dioxane or swimming pool disinfection by-products (DBPs) [14].

Table 1.2 summarizes the sources of major emerging pollutants categories found in aquatic environment [15].

Table 1.2. Sources of micropollutants in the aquatic environment.

Category	Important subclasses	Major sources	
		Distinct	Non-exclusive
Pharmaceuticals	NSAIDs*, lipid regulator, anticonvulsants, antibiotics, β-blockers and stimulants	Domestic wastewater (from excretion) Hospital effluents Run-off from CAFOs** and aquaculture	Sources that are not exclusive to individual categories include: Industrial wastewater (from product manufacturing discharges) Landfill leachate (from improper disposal of used, defective or expired items)
Personal care products	Fragrances, disinfectants, UV filters and insect repellents	Domestic wastewater (from bathing, shaving, spraying, swimming and etc.)	
Steroid hormones	Estrogens	Domestic wastewater (from excretion) Run-off from CAFOs and aquaculture	
Surfactants	Non-ionic surfactants	Domestic wastewater (from bathing, laundry, dishwashing and etc.) Industrial wastewater (from industrial cleaning discharges)	
Industrial chemicals	Plasticizers and flame retardants	Domestic wastewater (by leaching out of the material)	
Pesticides	Insecticides, herbicides and fungicides	Domestic wastewater (from improper cleaning, run-off from gardens, lawns and roadways and etc.) Agricultural runoff	

*NSAIDs: Non-steroidal Anti-Inflammatory Drugs, **CAFOs: Concentrated Animal Feeding Operations

Despite the efforts of authorities, as emerging pollutant's definition says, there is still not legislation regarding them. Also, most of these pollutants are not removed through the standard treatments at WWTP because of their recalcitrant properties and because WWTP are not specifically designed for their removal so they end being released into the environment [16–19]. These pollutants can be found in microgram per litre or nanogram per litre concentrations so they are also called micropollutants. Although these low amounts don't pose an immediate risk for human health or environment, the World Health Organization pointed out that there is still not enough knowledge about the risks of long-term exposure to these low concentrations or the mixture of different compounds.

Scientific community believes that, among all emerging contaminants, antibiotics are of greatest concern, since their emission in the environment can increase the occurrence of resistant bacteria in the environment [20]. Muñoz et al. reviewed the occurrence of emerging pollutant detected in WWTP effluents from around the world [21]. Table 1.3 shows an extract of it referencing some antibiotics.

Table 1.3. Occurrence of antibiotics in wastewater effluents (ng L^{-1}).

Compound	Effluent concentration, medium-maximum	Country
Trimethoprim	550-1900	USA
	320-660	Germany
	58-188	South Korea
Ciplofloxacin	239-514	Italy
	170-860	USA
	120-400	Canada
Ofloxacin	652-1081	Italy
Erythromycin	89-353	Italy
	130-294	South Korea
	17-30	Croatia
Sulfamethoxazole	390-820	Croatia
	400-2000	Germany
	136-407	South Korea

1.4.1. Sulfamethoxazole

Sulfamethoxazole (SMX) is a sulfonamide antibiotic which is effective against both, gram negative and positive bacteria. It has been widely prescribed to treat bacterial infections in human and veterinary medicine [22]. Its biostatic ability works by inhibiting bacterial enzyme dihydropteroate synthetase [23] and consequently the production of folic acid in bacteria, which is a requirement for the production of nucleic acids [24]. SMX is also specially efficacious as antibacterial agent in aquaculture with a combination of sulfamethoxazole-trimethoprim at the ratio of 5:1 [25–27]. SMX is slight soluble (0.5 g L^{-1}) and hydrophilic (octanol water partition coefficient: log K_{ow} = 0.27). Considering this an its poor metabolism, a large portion of SMX is excreted unchanged into the sewage system[28,29], which supposes a great concern.

1.5. ADVANCED OXIDATION PROCESSES

The increasing concern about water pollution has generated a response as an increase of the research activities focused on environmental protection. New and improved detection techniques allowed observing the inability of conventional wastewater treatment plants to eliminate recalcitrant compounds from effluents before discharge into rivers, lakes or into the sea. In this context, the necessity to incorporate tertiary treatments to solve these problems was considered imperative.

These tertiary technologies mainly consist on separation techniques (adsorption or stripping techniques) or methods for the destruction of the pollutant (chemical oxidation or reduction). Oxidation processes transform the pollutants into smaller and usually more biodegradable and less harmful compounds. They can also achieve the total mineralization by transforming pollutants into carbon dioxide, water and inorganic salts. Obviously, the processes based on the pollutant destruction, when properly designed, provide a full solution to the problem. On the contrary, separation techniques isolate the problem, but it still exists [30].

Advanced Oxidation Processes (AOPs) are defined as the processes that generate hydroxyl (HO·) and other radicals (e.g. sulfate radicals) in sufficient quantities to be able to oxidize majority of the complex recalcitrant, toxic and non-biodegradable compounds to various by-products and eventually to inert end-products [31,32]. Also, it is well known that AOPs can be applied as powerful disinfection processes due to its ability to oxidize cell membrane of bacteria and other microorganism [33–38].

1.5.1.   Hydroxyl radical oxidation reactions

Hydroxyl radicals (HO·) are the main specie responsible for oxidation when applying an AOP. HO· is considered the most oxidant specie known after fluorine, with an oxidation potential of 2.80 V [39] (see Table 1.4). HO· is an oxidative specie with a very low selectivity, a very short life and able to react with almost all kind of organic compound, degrading it to less complex ones [40,41].

Table 1.4. Oxidation potential of various oxidants.

Oxidant	Oxidation potential (V)
Fluorine	3.03
Hydroxyl radical	2.80
Sulfate radical	2.60
Atomic oxygen	2.42
Ozone	2.07
Hydrogen peroxide	1.78
Perhydroxyl radical	1.70
Permanganate	1.68
Hypobromous acid	1.59
Chlorine dioxide	1.57
Hypochlorous acid	1.57

Hydroxyl radicals, once they are generated through an AOP reaction, are able to oxidize organic and inorganic molecules by using different reaction mechanisms according to the

nature and structure of the molecule. The oxidative mechanisms that can occur are the electrophilic addition, the hydrogen abstraction or the electron transfer.

A brief explanation of each one of these reactions initiated by hydroxyl radicals can be found below (The R included in reaction equations makes reference to a generic organic molecule. M^n makes reference to a generic element with a valence charge of n).

- Electrophilic addition: A double bond C=C is eliminated through electrophilic addition and the HO· is incorporated into the chain forming an organic radical. This reaction constitutes the most common mechanism produced by HO·.

  HO· + R_2C=CR2 → ·CR_2-C(OH)R_2 (Equation 1.1)

- Hydrogen abstraction: A hydrogen is abstracted from an organic compound. The formed organic radical can react with molecular oxygen (O_2) to produce peroxide radicals, which initiate chain reactions of oxidative degradation that led to mineralization of the compound.

  HO· + R-H → R· + H_2O (Equation 1.2)
  R· + O_2 → RO_2· (Equation 1.3)

- Electron transfer: HO· takes an electron from the compound, which can be an inorganic compound that gets oxidized.

  HO· + M^n → M^{n+1} + HO^- (Equation 1.4)

1.5.2. AOPs classification

Diverse classifications of the AOPs can be done depending on different aspects of the process, the inclusion of light, the use of precursors for HO· production, etc. Table 1.5 shows

a classification of the most common AOPs evaluated for water and wastewater according to its photochemical nature [42].

Table 1.5. Most common AOPs evaluated for water and wastewater treatment (Gültekin and Ince, 2007)

Advanced Oxidation Processes	
Photochemical processes	Non-photochemical processes
UV oxidation processes	Ozonation (O_3)
$\quad$ UV/H_2O_2	Fenton
$\quad$ UV/O_3	Ultrasound (US)
$\quad$ UV/H_2O_2/O_3	$\quad$ US/H_2O_2, US/O_3, US/Fenton
$\quad$ UV/Ultrasound	Electrochemical oxidation
Photo-Fenton	Supercritical water oxidation
Photocatalysis	Ionizing radiation
Vacuum UV (VUV)	Electron-beam irradiation
Microwave	Wet-air oxidation
Sonophotocatalysis	Pulsed plasma

1.5.1. AOPs implementation

All advanced oxidation processes, when applied for the degradation of organic compounds, share the same reactions pattern (Figure 1.4). There are producing simultaneously the AOP reaction that generates the oxidative specie and the oxidation reactions that degrade the organic compounds.

The first stage of the oxidative process involves the parameters affecting the AOP reaction rate and consequently the rate of production of the oxidative specie, which use to be the hydroxyl radical (HO·).

In the second stage, which is produced simultaneously to the first one, the oxidative species generated react with the recalcitrant organic compounds and oxidize them into biodegradable compounds or mineralize them into water, carbon dioxide and inorganic salts. The extent of these reactions is mainly controlled by parameters such as the amount and nature of the organic load in water, amount of oxidant produced, the presence of

scavenging compounds or the amount of other organic compounds competitive for the oxidant species. According to these parameters, the original recalcitrant organic compounds can be partially oxidized into biodegradable compounds or totally mineralized.
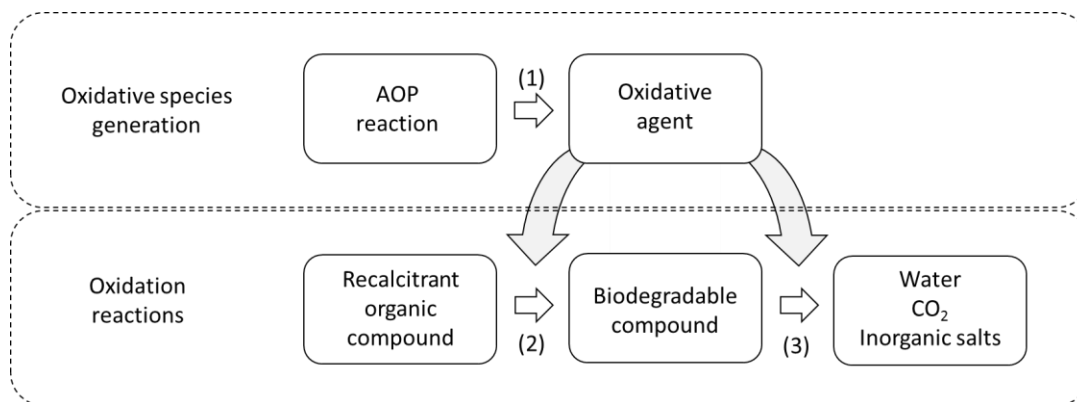
Figure 1.4. Stages involved in the degradation of a recalcitrant organic compound by using an AOP.

To achieve the desired extent of pollutants removal, sometimes it is convenient to couple some processes to optimize the AOP performance. Some possibilities, according to Comninellis et al. can be found below [43]:

- Simultaneous application of different AOPs to promote higher organic oxidation rates (i.e. UV/H_2O_2, $UV/H_2O_2/TiO_2$, UV/Fenton, UV/ozone, $Ozone/H_2O_2$, $Ultrasound/UV/TiO_2$, etc.). These combinations may lead to treatment efficiencies that are greater than the sum of efficiencies that could be achieved by the individual processes applied alone.

- Sequential application of various AOPs to containing several classes of organic compounds that exhibit different levels of oxidation towards different reactive moieties. In this way, a selectivity enhancement can be achieved.

- Application of a separation treatment prior to AOP. Thus, organic non-target compounds, such as organic matter in wastewater, can be separated and a lower amount of effluent with a higher concentration of pollutant can be treated by the AOP, so their removal is easier.

- Application of AOPs as a pre-treatment stage to enhance biodegradability and reduce toxicity, followed by biological post-treatment. Biological treatments are cheaper than AOPs but cannot remove recalcitrant compounds, so the application of an AOP to achieve not mineralization but to transform non-biodegradable pollutants into biodegradable compounds can solve the problem.
- Complex treatments comprising various physical, advanced oxidation and biological processes.

Due to the use of expensive reactants such as H_2O_2 or the high power consumption of most AOPs, it is not economically viable to apply them for replacing the more economical biological treatment [44]. Thus, they must be installed in the global water treatment process to optimize its effect and to satisfy the necessity of removing refractory organic compounds that the common biological treatments cannot eliminate. So, the configuration of AOPs in the global process of a water treatment plant depends mainly on the influent.

Figure 1.5, extracted from Petrovic et al. (2002), shows a schematic diagram of where to apply AOPs on a wastewater treatment plant and on a drinking water treatment plant.

Regarding wastewater treatment plants, the influent water usually contains high organic matter load, which produces a high competition for the oxidative species. Thus, the application of an AOP for the elimination of trace recalcitrant compounds would be not economically viable to be applied to raw water. In this case, the AOPs are usually applied as tertiary treatments, once the secondary biological treatment have already removed the higher amount of organic matter and allows a more efficient removal of trace refractory compounds. Even so, if the organic load in the influent is low, AOPs could eventually be applied after primary treatment, which also would enhance wastewater biodegradability.
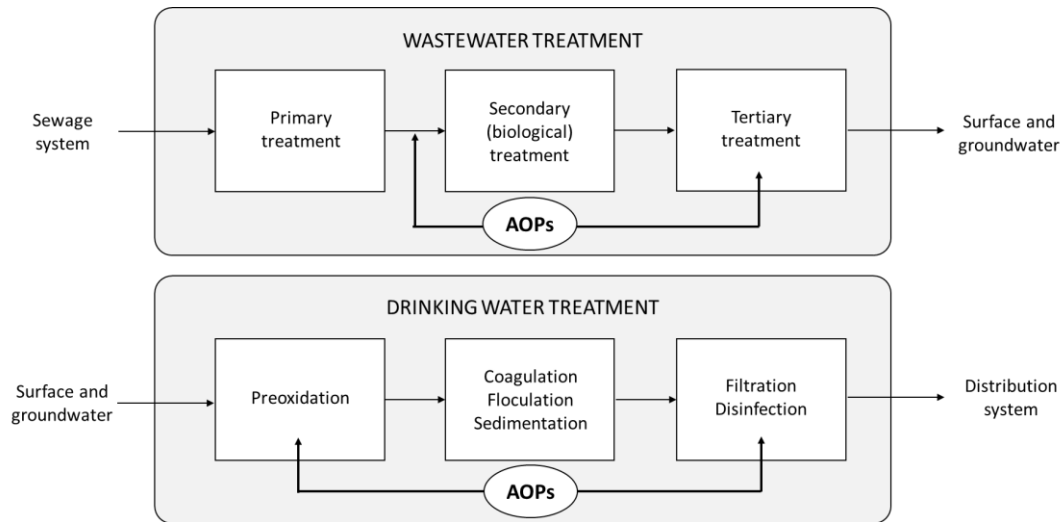
Figure 1.5. Possible applications of AOPs in wastewater and drinking water treatment [45]**.**

In the case of drinking water treatments, the influent coming from surface and groundwater use to contain a very low load of organic matter. The low competition for the oxidant species allow to apply AOPs as a preoxidation as the initial treatment to remove these refractory trace organic compounds or also as a posttreatment after the process, which could remove the trace organic compounds and act as disinfection process at the same time.

1.5.2. Water parameters affecting AOPs efficiency

As previously mentioned, the influent water composition can affect significantly the performance of AOPs. Due to the non-selectivity of hydroxyl radical, the presence of organic and inorganic compounds other than the target pollutants in water acts as competition. Thus, the more scavenging compounds in water, the less will be the efficiency on the removal of recalcitrant target compounds.

A list of the most relevant water parameters influencing the effectiveness of AOPs can be found below:

-*Alkalinity:* Carbonate and bicarbonate act as strong scavengers of HO· forming carbonate radicals according to the following reactions [46]:

$$HO· + HCO_3^- \rightarrow CO_3^- · + H_2O \qquad K_{·OH,M} = 8.5 \times 10^6 \text{ L mol}^{-1} \text{ s}^{-1} \qquad \text{(Equation 1.5)}$$

$$HO· + CO_3^{2-} \rightarrow HO^- + CO_3^- · \qquad K_{·OH,M} = 3.9 \times 10^8 \text{ L mol}^{-1} \text{ s}^{-1} \qquad \text{(Equation 1.6)}$$
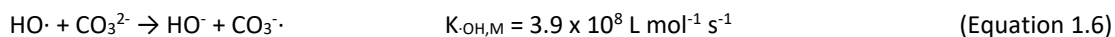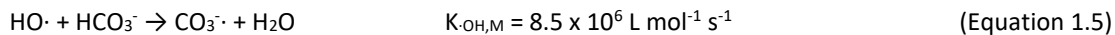
These carbonate radicals can also oxidize organic and inorganic compounds, but at a much lower rate. Despite their reaction rate constants are slower compared to several recalcitrant compounds [40], carbonates reactions with hydroxyl radical are of second order and their reaction rate depends of the carbonates concentration, which use to be much higher than the concentration of the target micropollutants. Thus, HO· radicals end being consumed by carbonates instead of micropollutants.

-*Organic matter load:* As it happened with carbonates, organic matter can establish a competition for the oxidative species produced by AOPs, which consequently reduces their availability for the oxidation of the target recalcitrant compounds and the global efficiency of the process [47]. Organic matter, usually quantified as TOC or DOC, and also called NOM if its origin is natural or EFOM if it is the WWTP effluents, can be also present in concentrations several orders of magnitude higher than the recalcitrant target compounds, so independently of the reaction rate constants, due to the low selectivity of HO·, the efficiency on the degradation of micropollutants will be consequently reduced by these competitive reactions.

-*Nitrates and nitrites:* These compounds have a UV light absorption peaks in 230-240 nm and 300-310 nm ranges. Due to this, all AOPs involving the use of UV light in these ranges will be affected by the competition for light absorbance. Thus, high concentration of nitrates and nitrites will produce a reduction in the HO· formation reaction and consequently a lower efficiency on target compounds removal.

-*Turbidity:* This water property also affects the HO· production reaction in photochemical-based AOPs. A high turbidity lowers water transmittance, what consequently reduces the

penetration of light into the source water. Thus, the production of HO· will be drastically reduced and so the global efficiency on target compounds removal.

-*Other:* There are also some other compounds that have high reaction kinetics with HO· and can act as strong scavengers. Even so, these compounds don't have a common natural occurrence as the previously mentioned. This is the case of substances as tert-butyl alcohol (TBA, $k_{HO·,TBA}$ = 6.50 x 10^8 L mol^{-1} s^{-1}), which can be used as HO· scavengers for scientific purposes.

1.6. FENTON AND FENTON-LIKE REACTIONS

1.6.1. Conventional Fenton

Henry H. Fenton discovered that the use of Fe(II) salts as catalyst for hydrogen peroxide decomposition highly enhanced the production of HO·.

The cheapness and non-toxicity of hydrogen peroxide and iron salts combined to the potentially non-harmful residues produced by this reaction made the Fenton process very convenient as an environmental application for water purification.

Iron species naturally can be found in Fe(II) and Fe(III) valences. When in solution and not complexed by organic agents, both can be found as several hydrolyzed and/or inorganic complexed species depending on the pH value of the solution. While Fe(II) can be mainly found as Fe^{2+}(aq) in a pH range of 2-7, Fe(III) presents a more diverse speciation. An speciation diagram of Fe(III) species according to solution pH can be found in Figure 1.6 [48].

Considering this speciation, Fe(III) can be found as $Fe(OH)_3$ at circumneutral pH, which is a non-soluble specie and will precipitate [49]. Hence, reducing pH value of solution to an acidic one is required to conduct the conventional Fenton reaction [50]

18
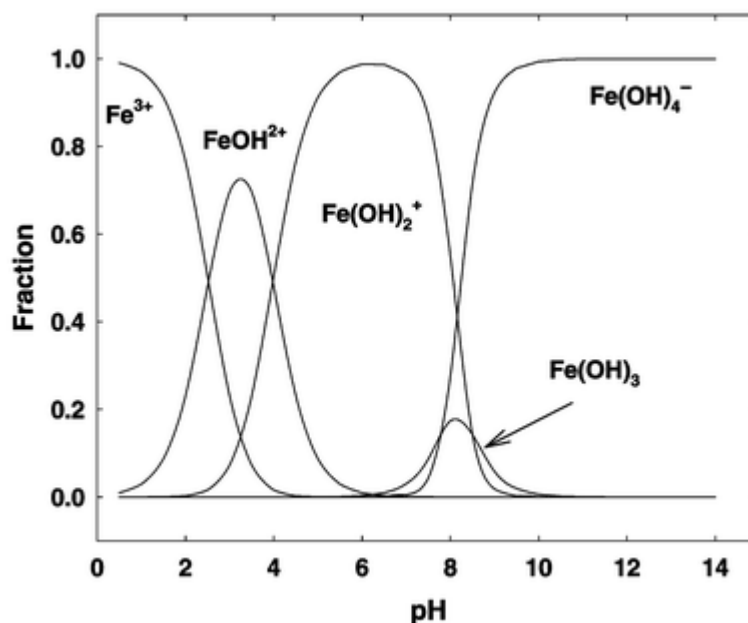
Figure 1.6. Speciation diagram of Fe(III) according to pH (Millero et al., 2001).

The Fenton process mechanism is a complex chain of radical reactions which start with the decomposition of hydrogen peroxide in the presence of Fe(II). Then, iron cyclically passes from the oxidation state 2 to 3 and vice versa. The main reactions occurring after putting in contact hydrogen peroxide with Fe(II) can be found in Table 1.6.

Table 1.6. Main reactions occurring in Fenton process.

Reaction	k (L mol^{-1} s^{-1})	Reference	Eq.
Initiation			
$Fe^{2+} + H_2O_2 \rightarrow Fe^{3+} + HO^- + HO\cdot$	76	[51]	1.7
$Fe^{3+} + H_2O_2 \rightarrow FeOOH^{2+} + H^+ \leftrightarrow Fe^{2+} + HO_2\cdot + H^+$	0.001-0.01	[52]	1.8
$H_2O_2 \rightarrow H_2O + \frac{1}{2} O_2$			1.9
Propagation			
$HO\cdot + H_2O_2 \rightarrow HO_2\cdot + H_2O$	2.7×10^7	[40]	1.10
$HO_2\cdot + H_2O_2 \rightarrow HO\cdot + H_2O + O_2$	1.1-3.7		1.11
Termination			
$Fe^{2+} + HO\cdot \rightarrow Fe^{3+} + HO^-$	3.2×10^8	[40]	1.12
$Fe^{3+} + HO_2\cdot \rightarrow Fe^{2+} + H^+ + O_2$	1.2×10^6	[53]	1.13
$Fe^{2+} + HO_2\cdot + H^+ \rightarrow Fe^{3+} + H_2O_2$	1.3×10^6	[53]	1.14
$HO\cdot + HO_2\cdot \rightarrow H_2O + O_2$	6.6×10^9	[40]	1.15
$HO\cdot + HO\cdot \rightarrow H_2O_2$	5.2×10^9	[40]	1.16
$HO_2\cdot + HO_2\cdot \rightarrow H_2O_2 + O_2$	1.3×10^6	[40]	1.17

By observing the reaction mechanism and considering the kinetic constants, it can be seen tan equation 1.7 is main responsible for the production of the oxidative specie HO·, with the higher reaction rate constant and turning Fe^{2+} into Fe^{3+}. Equation 1.8 can recover Fe^{2+} but their kinetic constants are far lower, so once Fe^{2+} initially added is consumed, this reaction becomes the limiting reaction in Fenton mechanism [54], so a drastically reduction in HO· production rate is produced and consequently also in the target compounds' degradation rates. Thus, the addition of large relatively amounts of Fe2+ at the beginning of the reaction may be required to ensure a proper degradation rate of the target compounds. In equation 1.10 it is observable that H_2O_2 can also act as HO· scavenger, by consuming the oxidative specie, so an excess of this reactant is not desired.

It has been proved that by conducting this reaction at acidic pH down a value of 3.0 the presence of Fe^{2+} is favoured respect Fe^{3+} so it is usually considered the optimum pH for this reaction [55].

Fenton process is able to oxidize organic refractory compounds due to the formation of HO·, but it has been proven that the application of this process can't achieve their total mineralization, which use to be in a range from 40 % to 60 % depending on the amount and ratio of the initial reagents.

A resume of the main strengths and weaknesses of the application of Fenton reaction for water purification purposes can be founds below:

Strengths:

- No potential formation of bromates, which are an especially toxic compound produced when applying some other AOPs.
- No off-gas treatment is required.
- The simplicity and the low energy requirements made the process very cheap and easy to conduct.

20

<u>*Weaknesses:*</u>

- The addition of iron into water requires a removal after the process to ensure compliance with legislation.

- The acidic pH required (pH < 3.0) demands the use of acidic effluents or a previous acidification.

- To comply with legislation, the effluent must be adjusted to a pH near the neutrality before its discharge. This generates a cost of reagent and also a high amount of ferrous sludge is formed due to the precipitation of Fe(III) compounds, which at the same time increases operational costs and require a proper disposal.

1.6.2. Photo-Fenton

Photo-Fenton is a modification of the conventional Fenton (Fe(II)/H_2O_2) by including the irradiation with UV-Vis light to enhance the HO· production. This improvement is achieved by promoting the reduction of Fe(III) to Fe(II), which is the most reactive iron specie.

According to the speciation diagram of Fe(III), when pH is around 3.0, the most favored specie is $FeOH^{2+}$, which have its maximum abundance at a pH of 2.8 (Figure 1.6). By observing the Fe(III) species absorption spectrum (Figure 1.7), this Fe(III) specie absorbs light up to 400 nm. Due to this, by using UV-A or solar light, the following reaction (Equation 1.18) [56] is included into the overall reaction mechanism already mentioned for conventional Fenton (also called dark Fenton).

$$FeOH^{2+} + h\nu \rightarrow Fe^{2+} + HO·$$ (Equation 1.18)

As it can be observed, this reaction promoted by UV-A light not only recovers Fe(II) as reactive specie but also acts as a new source of hydroxyl radicals, achieving a significantly higher efficiency. Moreover, due to this new reaction, the consumption of H_2O_2 gets reduced to achieve the same HO· production in comparison to conventional Fenton. Also, as the rate of this reaction is high and only depends of the amount of radiation, it is not

necessary to add high amounts of iron to achieve good results because a sufficient irradiation ensures the availability of Fe(II) for the main Fenton HO· production reaction. Thus, in comparison to conventional Fenton, the production of iron sludge is lower.
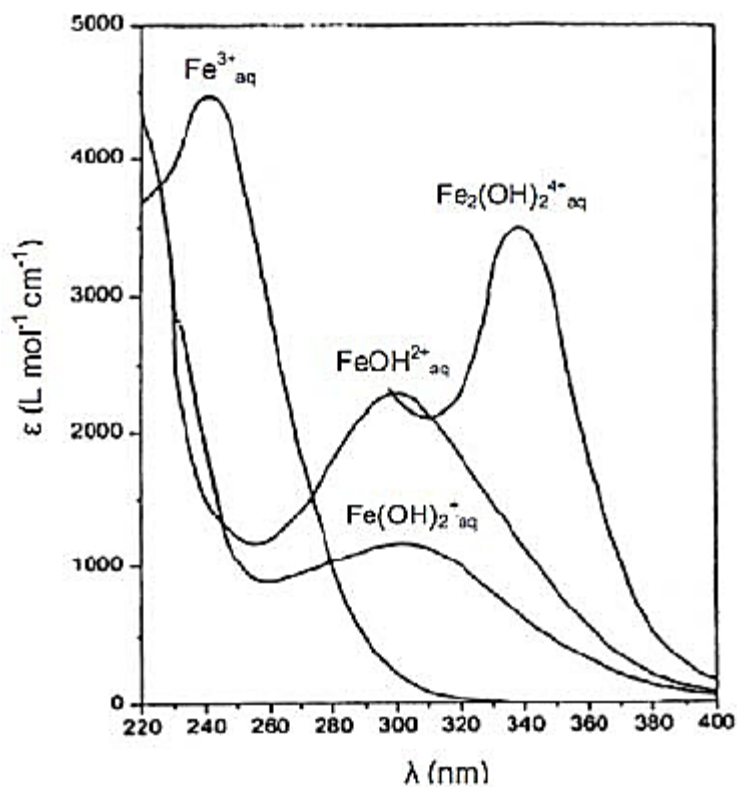
Figure 1.7. Fe(III) species absorption spectrum from 220 to 400 nm. Extracted from Loures et al., 2013 [57]**.**

Even so, as happened with dark Fenton, the necessity of conducting the reaction at acidic pH is not possible to overcome because of Fe(III) precipitation, that removes iron from solution and because the species favored at circumneutral pH have a very low catalytic activity.

Also, the incorporation of light into the reaction achieves significant improvements for the global efficiency, but it has to be considered that the cost of the process becomes higher due to the power consumption involved if using solar light does not perform it. In this last

case, the absorbed light is then conditioned by weather, day and night cycles and geographical location.

Rahim Pouran et al. (2015) reviewed the effectiveness of photo-Fenton for the degradation of recalcitrant compounds (Table 1.7).

Table 1.7. Efficiency of photo-Fenton treatment of some organic compounds in recalcitrant effluents.

Compound	Initial value	Operational conditions					Optimal performance	Ref.
		$[H_2O_2]$	Iron	pH	[Ox]	T		
	(mg L^{-1})	(mg L^{-1})	(mg L^{-1})	-	(mg L^{-1})	(°C)		
Pharmaceuticals								
Pharmaceutical wastewater	TOC_0 = 125	5250	55	3	325	32	84% TOC removal within 115 min at $H_2C_2O_4$:Fe^{3+} ratio of 3	[58]
Penicilin G	200	680	55	3.5	-	-	83.3% Pen-G degradation within 30 min	[32]
Amoxicilin	104	H_2O_2/COD = 1.5	5.2	3	-	-	Complete degradation within 2 min; COD and DOC removal of 80.8% and 58.4% at 50 min	[59]
Ampicillin	105		5.25					
Cloxacillin	103		5.15					
Amoxicillin	138	H_2O_2/COD = 2.5	6.9	3	-	-	Complete degradation within 1 min; 89% COD removal and complete nitrification with combined photo-Fenton-SBR	[60]
Cloxacillin	84		4.2					
Lincomycin (LCM)	25	170	11.17	-	-	-	DOC removal of 65% for LCM and 80% for DZP within 60 min irradiation	[61]
Diazepam (DZP)	25							
Hospital wastewater	COD:H_2O_2:Fe^{2+} 1:4:0.1			3	-	-	Increasing BOD5/COD ratio from 0.3 to 0.52 and oxidation degree from −1.14 to +1.58	[60]

Table 1.7 (Continuation)

Compound	Initial value	Operational conditions					Optimal performance	Ref.
		[H_2O_2]	Iron	pH	[Ox]	T		
	(mg L^{-1})	(mg L^{-1})	(mg L^{-1})	-	(mg L^{-1})	(°C)		
Amoxicillin	50	120	2.8	2.5 - 2.8	-	-	73–81% TOC removal after 240 min, AMX removal after 5–15 min using Fe-Ox and $FeSO_4$ respectively	[62]
Nalidixic acid	45	300	20	2.6 - 2.8	-	-	15% DOC and 100% NXA removal after 210 min	[63]
Dichlorodiphenylamine (DCDPA), Diclofenac sodium (NaDCF), meclofenamic acid sodium salt (NaMCF)	5 each	10	10	3.5	-	-	99% DCF and MCF and 96% DCDPA degradation within 120 min; rate constant order of $k_{DCDPA} < k_{DCF} < k_{MCF}$	[64]
Sulfamethoxazole (SMX)	200	>300	10	2.8	-	25	98% SMX removal, BOD_5/COD improvement from 0.0 to 0.3, 2.4–79.9% TOC removal with H_2O_2 doses from 50 to 1000 mg L^{-1}	[65]
Paracetamol	157.5	200	20	-	-	-	83.33% reduction in reagent cost, 79.11% reduction in costs of reaction time (from 3.4502 $/m^3 to 0.7392 $/m^3)	[66]
Sulfadiazine (SDZ)	25	170	-	2.5	17.6	-	Complete degradation after 8 min irradiation, 92% and 90% mineralization of SDZ and STZ after 42 min of irradiation	[67]
Sulfathiazole (STZ)	25							
Mitoxantrone (MTX)	31.11	640	30	3	47.5	-	60%, 77% and 82% mineralization using Fe^{2+}, Fe^{3+} and Fe-Ox respectively within 140 min	[68]

Table 1.7 (Continuation)

Compound	Initial value	Operational conditions					Optimal performance	Ref.
		[H$_2$O$_2$]	Iron	pH	[Ox]	T		
	(mg L^{-1})	(mg L^{-1})	(mg L^{-1})	-	(mg L^{-1})	(°C)		
Agrochemicals								
Malathion	10	1000	25	3	-	-	Malathion removal to desired level (0.1 mg L^{-1}) after 135 min	[69]
Diuron and Linuron	TOC$_0$ = 50	202	15.9	2.8	-	25	Herbicides degradation within 60 min irradiation with UV-A, 30% TOC removal by ph-F alone and 87% by ph-F-SBR	[70]
Lindane (γ-HCH)	1.01	1000	125	3	-	-	95% and 99.91% TOC removal after 2 and 4 h of irradiation	[71]
Laition, Metasystox, Sevnol and Ultracid	50 each	100	20	2.8	-	30	Up to 80% mineralization of the mixture after 45 min, 31% DOC removal with only ph-F within 140 min and 90% with ph-F-SBR after 7 h	[72]
Alachlor, atrazine, chlorfenvinphos, diuron, isoproturon, pentachlorophenol	50 each	100	20	2.8	-	-	Degradation of the all pesticides into intermediates, 90% TOC removal after <15 min	[73]
Methomyl	20	34	28	3	-	-	100% methomyl removal within 30 min	[74]
Linuron	10	13.6	2.2	4	-	25	Complete linuron degradation after 20 min, 90% TOC removal after 25hwith formation of chloride, nitrate and ammonium ions	[75]

Table 1.7 (Continuation)

Compound	Initial value	Operational conditions					Optimal performance	Ref.
		[H_2O_2]	Iron	pH	[Ox]	T		
	(mg L^{-1})	(mg L^{-1})	(mg L^{-1})	-	(mg L^{-1})	(°C)		
Abamectin	9	204	28	2.5	-	-	70% Abamectin degradation within 60 min, 60% mineralization after 180min	[76]
Metalaxyl	150	80	2	2.8	-	-	96.3% metalaxyl degradation after 180 min	[77]
Petroleum refinery								
Oxalates	182	1020	[Fe^{3+}] = 280	3.9	-	-	Faster degradation of formates than oxalates, [a]EEC$_{TOC=15}$(UV-C) = 1.30 €m^{-3}, EECTOC=15(UV-A) = 2.37 €m^{-3}	[78]
Formats	92		[Fe^{3+}] = 447					
Sourwater from refinery plant	-	4000	400	-	-	-	87% DOC removal with ph-F within 60 min	[79]
Diesel oil	-	1700	5.6	3	-	-	99% TOC removal within 30 min	[80]
Petroleum extraction wastewater	1.6	16,500	0.93	3	-	-	92% and 96% polycyclic aromatic hydrocarbons and aromatic removal within 7 h sunlight exposure	[81]
Phenol	200	1080	5	3	10	-	98% COD removal within 120 min, 90% phenol degradation at 10 min	[82]
Phenol	100	>18.2%	AMKC[b] 2.23 g	5.4	-	-	99.15% phenol degradation within 5 min	[83]
Xylene	15	5100	14.5	2.5 - 3.0	-	-	94.5% xylene removal after 60 min, 100% TOC removal within 90 min	[84]

Table 1.7 (Continuation)

Compound	Initial value	Operational conditions					Optimal performance	Ref.
		[H$_2$O$_2$]	Iron	pH	[Ox]	T		
	(mg L^{-1})	(mg L^{-1})	(mg L^{-1})	-	(mg L^{-1})	(°C)		
Phenol	DOC0 = 500	6400	22	3	-	-	95.1% DOC removal after 180 min under solar irradiation,	[85]
p-Nitroaniline (PNA)	25	340.15	2.8	3	-	20	>98% degradation efficiencies of PNA within 30 min solar irradiation	[86]
Protocatechuic acid (PCA), p-coumaric acid (p-CA), gallic acid (GA)	20	400	20	4	60	25-39	100% PCA removal within 4 min, 100% p-CA degradation within 2 min, 100% GA degradation (within 3 min, 94% TOC removal after 194 min	[73]

[a] EEC$_{TOC=15}$:electrical energy costs required to achieve reference value of 15 mg C L^{-1}.
[b] AMKC: acid modified kaolin clay supported ferric-oxalate catalyst.

The achievement of high removal rates when applying conventional photo-Fenton at acidic pHs (higher than 90% in most cases) can be observed from the data extracted from this review. Also, a wide dispersion in the amounts of H$_2$O$_2$ (10-6400 mg L^{-1}) and iron (0.93-400 mg L^{-1}) have been applied, which indicates that the optimal amounts of these compounds depend mostly of the effluent composition.

1.6.3. Fenton and photo-Fenton at neutral pH

Fenton and photo-Fenton reactions have been widely proved to be able to remove recalcitrant compounds in water. Even so, the necessity of conducting these reactions at acidic pH and the subsequent formation of high amounts of iron sludge after effluent neutralization is a major drawback that makes difficult and expensive to apply these technologies at plant scale.

Current research in the field tries to solve this drawback by focusing in two possible solutions. The first one is to keep iron as soluble specie at neutral or circumneutral pH (near the neutrality, pH = 6.5-7.5) by using chelating agents. By doing this, no iron precipitates will be formed after the process but iron will still be released within the effluent. Thus, iron concentration in the effluent must comply with legislation limits and also the chelating agent must be not harmful.

Chelating agents can bind iron, then the initiation of Fenton-like reactions (Fenton reactions that occur on a similar way but with some modifications respect conventional Fenton) takes place as described by the following reactions [87]:

$Fe^{3+} + L \rightarrow Fe(III)L$ (Equation 1.19)

$Fe(III)L + H_2O_2 \rightarrow Fe(II)L + H^+ + HO_2\cdot$ (Equation 1.20)

$Fe(III)L + HO_2\cdot \rightarrow Fe(II)L + H+ + O_2$ (Equation 1.21)

$Fe(III)L + O_2^-\cdot \rightarrow Fe(II)L + O_2$ (Equation 1.22)

$Fe(II)L + H_2O_2 \rightarrow Fe(III)L + HO\cdot + OH^-$ (Equation 1.23)

Also, when conducting photo-Fenton-like (photo-Fenton reactions that occur on a similar way but with some modifications respect conventional photo-Fenton), the reactions below should be added to the global mechanism [88]:

$Fe(III)L + h\nu \rightarrow Fe^{2+} + L\cdot$ (Equation 1.24)

$Fe(III)L\text{-}OH + h\nu \rightarrow Fe(II)L + HO\cdot$ (Equation 1.25)

$Fe(II)L\text{-}O_2H + h\nu \rightarrow Fe(II)L + HO_2\cdot$ (Equation 1.26)

The second possible solution to conventional acidic Fenton and photo-Fenton is the use of heterogeneous catalysts containing iron. Iron can be supported in a wide variety of materials such as neutral organic polymers, ion exchange membranes or resins and

inorganic materials (clay, zeolites, etc.) and also residual materials containing iron [89–94]. The use of stable heterogeneous catalysts could totally solve the problem of iron sludge, so they are easy and cheap to remove from the effluent by using physical filtration operations, but there must not be iron leaching.

The global reaction mechanism for heterogeneous Fenton-like and photo-Fenton-like catalysts varies depending on the species of iron included in the support, but a general mechanism very similar to the one by using chelating agents can be accepted. The following reactions simplify the process by considering Fe(II)* and Fe(III)* as generic iron species in the state of oxidation 2 or 3 and S as a generic support.

$Fe(III)*/S + H_2O_2 \rightarrow Fe(II)*/S + H^+ + HO_2\cdot$ (Equation 1.27)

$Fe(III)*/S + HO_2\cdot \rightarrow Fe(II)*/S + H+ + O_2$ (Equation 1.28)

$Fe(III)*/S + O_2^-\cdot \rightarrow Fe(II)*/S + O_2$ (Equation 1.29)

$Fe(II)*/S + H_2O_2 \rightarrow Fe(III)*/S + HO\cdot + OH^-$ (Equation 1.30)
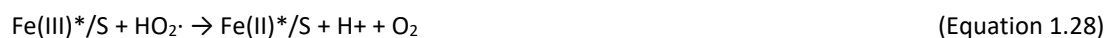
Also, when conducting photo-Fenton-like, the reaction below should be added to the global mechanism:

$Fe(III)*/S\text{-}OH + h\nu \rightarrow Fe(II)*/S + HO\cdot$ (Equation 1.31)

1.6.4. Alginate-based heterogeneous Fenton and photo-Fenton catalysts

Alginate is a natural polysaccharide that comprises from 30 to 60% (on dry weight basis) of brown algae (*Phaeophyceae*). Its main industrial applications as a natural polymeric material are linked to its stabilizing, viscosifying and gelling properties. As it is a non-hazardous and edible substance, alginate have been used in pharmaceutical industry as a binding agent [95,96] and also in the food industry as thickener or for gelification processes [97–99].

Alginate structure is formed as chains of two different configurations, the β-D-mannuronic acid (M) and the α-L-guluronic acid (G). As such, alginates do not possess a regular repeating unit. Thus, they can be described as linear binary copolymers of 1-4 linked M and G units arranged in a blockwise pattern with homopolymeric regions of G-blocks and M-blocks and regions in which the two units coexist as MG-blocks (Figure 1.8) [100].
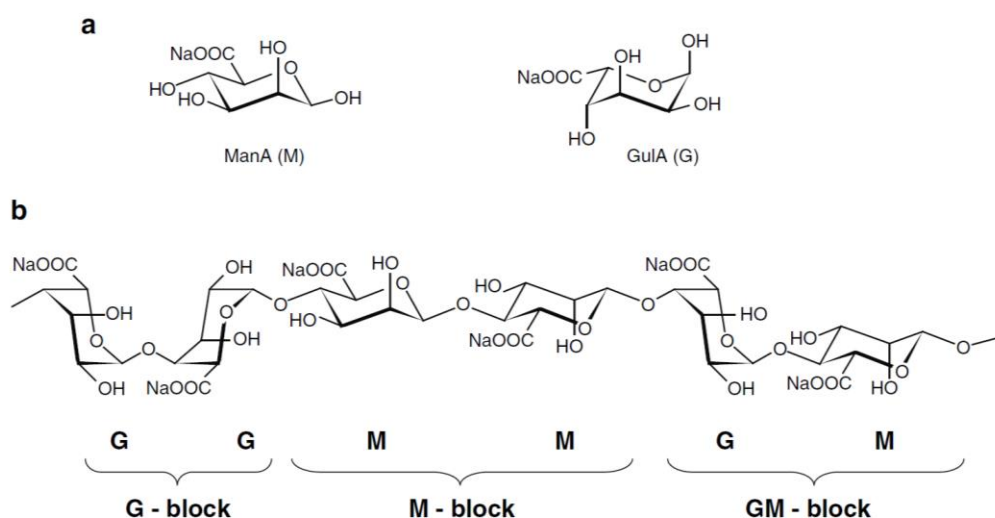
Figure 1.8. Alginate chemical structure. a) The $^4C_1$ conformation of β-D-mannuronic acid (M) sodium salt and the $^1C_4$ conformation of α-L-guluronic acid (G) sodium salt. b) The block composition of alginate with G-blocks, M-blocks, and MG-blocks. [101]

As it can be seen in Figure 1.8, each unit of G or M alginate have a carboxylic group which is bonded to sodium when it is in the form of salt. When in aqueous solution, this sodium dissociates and leave an available (+) linking spot. When an alginate aqueous solution is put in contact with divalent or trivalent cations at a pH over its pK_a, which was found between 4.2 and 5.0 [102–104], an hydrogel is formed by using these cations as crosslink between alginate chains.

By taking advantage of this property of alginates, Fe(II) and Fe(III) cations have been used to produce heterogeneous catalysts for Fenton-like reactions. The main advantage of the use of alginate as support for iron is that it is not harmful, so even using this catalyst, effluents for water supply and human consumption could be safely treated.

Even so, only a few works can be found in scientific literature in which these alginate-based catalysts are applied to Fenton, photo-Fenton or electro-Fenton. Table 1.8 shows a list of these works including the catalyst preparation conditions used and the most significant data about the experimental conditions when applied.

Table 1.8. List of published works in which alginate based catalysts were applied to Fenton and Fenton-like reactions and the major data about catalyst preparation and experimental conditions when applied.

Compound	Alginate solution	Iron source	Other elements	Reaction process	[H_2O_2]	pH	Ref.
Fenton							
Ofloxacin 20 mg L^{-1}	2.5 % (w/v)	Fe^{2+} 0.1 M	Ca^{2+} 2.5% (w/v)	Fenton	40 mM	3	[105]
Indole 20 mg L^{-1}	3% (w/v)	Fe^{2+} 0.1 M	Ca^{2+} 0.5 M	Fenton	9.8 mM	2-6	[106]
		-	Cu^{2+} 0.1 M				
		-	Ca^{2+} 0.5 M				
3-methyl-indole 20 mg L^{-1}	2% (w/v)	Fe_3O_4	Ca^{2+}	Fenton	9.8 mM	4.65	[107]
Norfloxacin 50 mg L^{-1}	2.5 g L^{-1}	Fe^{2+}/Fe^{3+} Ratio (0/5-5-0) 0.2 mM	-	Fenton	0-44 mM	3.5-9.5	[108]
Photo-Fenton							
Reactive Blue 19 50 mg L^{-1}	3 % (w/w)	Fe^{2+} 0.1 M	Cl^{2+} 0.1 M	Fenton Photo-Fenton	25-100 mg L^{-1}	3-5	[109]
Orange II	3% (w/v)	Fe^{3+} 0.05 M	Pluronic L 68 0.25 mg L^{-1}	Fenton Photo-Fenton	4.85 mM	5.6-7.8	[110]
E. Coli 107 CFU mL^{-1}	20 g L^{-1}	Iron enriched Montmorillonite 40 g L-1	Ca^{2+} 0.1 M	Photo-Fenton	10 mg L^{-1}	7.0	[111]
Reactive blue 222 Acid Black 234 5 g L^{-1}	3 mM	Fe^{3+} 0.25- 12 mM	-	Photo-Fenton	3 mM	3-8	[112]
Sulfamethoxazole 10 mg L^{-1}	2.5 % (w/w)	Fe^{3+} 0.05M	-	Photo-Fenton	20 mg L^{-1}	3-11	[113]
Reactive Blue 222 50 mg L^{-1}	-	Fe^{3+} 0.1 M	-	Photo-Fenton	3 mM	3	[114]

Table 1.8 (Continuation)

Compound	Alginate solution	Iron source	Other elements	Reaction process	[H$_2$O$_2$]	pH	Ref.
4-nitrophenol 10 mg L^{-1}	2 % (w/v)	Iron enriched Montmorillonite 20 g L^{-1}	Ca^{2+} 0.1 M	Solar photo-Fenton	0-500 mg L^{-1}	7.0	[115]
Electro-Fenton							
Indole 20 mg L^{-1}	3 % (w/w)	Fe^{2+} 0.1 M	Ca^{2+} 0.1 M	Electro-Fenton	-	3	[116]
Imidacloprid 100 mg L^{-1}	2 % (w/v)	Fe^{3+} 0.05 M	-	Electro-Fenton	-	2	[117]
Lissamine Green B 8.5 mg L^{-1} Azure B 4.83 mgL^{-1}	2 % (w/v)	Fe^{3+} 0.5 M	Ba^{2+} 0.15 M	Electro-Fenton	-	2-8	[118]
Reactive Black 5 100 mg L^{-1} Imidacloprid 100 mg L^{-1} 4-Nitrophenol 50 mg L^{-1} Di-2-ethylhexyl phthalate 0.250 mg L^{-1}	2.0 % (w/v)	-	Mn^{2+} 0.2 M	Electro-Fenton	-	2	[119]

From the review of data in Table 1.8 some conclusions can be extracted about the state of art of alginate-based catalysts intended for Fenton-like reactions.

There is not a consensus about the optimal conditions of preparation of these catalysts, which make it difficult comparing results from one author to another. Also, in most cases authors don't use exclusively iron cations as hardening solution for the preparation of the catalysts. Ca^{2+}, which is the usual cation used for alginate gelification when applied in pharmaceutical or food industry, is in most cases used simultaneously to iron cations to produce alginate gelification.

Moreover, only a few authors use target compounds different than dyes, and only one work was found applying the catalyst for disinfection.

By doing a deep research about all these works, only a few authors evaluated the presence of soluble iron during reaction and no one deeply studied the possible contribution of the homogeneous reaction to the overall removals obtained, which can be considered a significant gap that must be explored.

2. Objectives and thesis structure

2.1. MOTIVATION AND OBJECTIVES

AOPs are known for being one of the few solutions able to remove recalcitrant compounds in water. Among them, Fenton and photo-Fenton reactions are considered powerful tools for this purpose but the current need of performing these processes at acidic pH and the production of high amounts of ferrous sludge after the necessary neutralization are very important drawbacks for their implantation.

This thesis has the main aim of exploring the use of heterogeneous iron catalysts as a possible solution to perform photo-Fenton reactions at circumneutral pH. Special attention has been given to alginate-based catalysts for being not harmful to human health and to environment. Sulfamethoxazole and *Escherichia Coli* have been used as reference compounds for the study of micropollutant removal and disinfection performance, respectively.

To achieve this goal, some interim targets are also objectives of this work:

- To perform and optimize the synthesis of alginate-based catalysts and stablish a standard method for the synthesis of the catalyst for the application to photo-Fenton heterogeneous reaction.
- To study the performance of alginate-based catalysts when applied to Fenton and photo-Fenton reactions on the degradation of antibiotic sulfamethoxazole. The contribution of the homogeneous photo-Fenton reaction on the overall performance will be deeply investigated, as well as heterogeneous catalyst reaction mechanism and stability.
- To survey the application of Fe/alginate based catalyst performance for disinfection purposes.

- To improve the efficiency of the hydrogel catalyst to achieve better removal rates and a higher stability by including different modifications into the catalyst synthesis process and composition.
- To evaluate the performance of the improved alginate-based catalyst in comparison to other heterogeneous catalysts which are currently being researched as heterogeneous alternatives for conventional homogeneous Fenton and photo-Fenton reactions.

2.2. THESIS STRUCTURE

This thesis follows a classical structure of introduction (chapter 1), objectives (chapter 2), materials and methods (chapter 3), results and discussion (chapters 4-8) and conclusions and recommendations (chapter 9). Also, an extra chapter including a brief resume of some other works performed during this PhD thesis that don't have direct relation to the thesis topic have been included (chapter 10). Chapters presenting results and discussion also have a brief introduction, some specific information about materials and methods to simplify the understanding of the experiments included on each chapter and the conclusions extracted from them.

A brief explanation of the content included in chapters 4 to 8 can be found below:

Chapter 4: Fe/alginate catalyst development

This chapter focuses on the study of the different parameters affecting the synthesis of Fe/alginate-based gel beads in order to propose and optimize a standard method for the synthesis of the catalysts.

Chapter 5: Fe(III)/alginate catalyst mechanism and stability

In this chapter, an Fe(III)/alginate catalyst, synthetized according to the previous standard method stablished, is tested for the removal of sulfamethoxazole as target compound. The results obtained from experimentation helped to propose a reaction mechanism accordingly

to the observed phenomena and to evaluate the contribution of homogeneous reaction in the overall performance of the catalytic process. Finally, the stability of the Fe(III)/alginate catalyst after several applications is also evaluated.

The publication below was derived from the work performed in this chapter:

A. Cruz, L. Couto, S. Esplugas, C. Sans, **Study of the contribution of homogeneous catalysis on heterogeneous Fe(III)/alginate mediated photo-Fenton process**, Chem. Eng. J. 318 (2016) 272–280. doi:10.1016/j.cej.2016.09.014.

Chapter 6: Fe(III)/alginate catalyst applied for disinfection

In this chapter, according to the previous results obtained, the Fe(III)/alginate is tested for disinfection. *Escherichia Coli* culture is used as reference disinfection indicator.

The work included on this chapter is included on a publication in collaboration with the Department of Microbiology of University of Barcelona which is under preparation.

Chapter 7: Fe/alginate catalyst modifications

In this chapter, some modifications regarding the commonly used Fe(III)/alginate catalyst are proposed and tested for the degradation of sulfamethoxazole as target compound in order to evaluate the scope of the improvement achieved. Modified catalysts include preparation and/or composition variations, which are described in detail.

A publication derived from the work included in this chapter and entitled "Fe(III)/alginate mediated photo-Fenton reaction: Enhancement of heterogeneous catalyst stability and photocatalytic activity at circumneutral pH" will be sent soon.

Chapter 8: Heterogeneous catalysts intended for Fenton and photo-Fenton at neutral pH

This chapter compares the alginate-based catalyst that obtained better results on previous studies with some other catalysts with potential activity for heterogeneous Fenton-like reactions.

Part of the experiments included in this chapter was performed during a three months stage in the Chemical Engineering Department of the University of Coimbra (Portugal).

3. Materials and methods
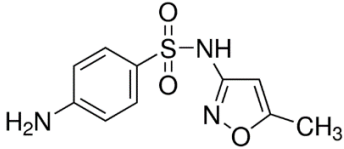
3.1. CHEMICALS AND REAGENTS

3.1.1. Model compound: Sulfamethoxazole

Sulfamethoxazole (SMX) is a sulfonamide antibiotic which is effective against both, gram negative and positive bacteria. It was used as reference compound to evaluate the performance of the oxidative treatments applied in this thesis.

SMX was purchased from Sigma-Aldrich (Spain). Most important data about SMX can be found at Table 3.1.

Table 3.1. Main chemical data of sulfamethoxazole (SMX).

Chemical formula	$C_{10}H_{11}N_3O_3S$
Chemical name	4-Amino-N-(5-methyl-3-isoxazolyl) benzenesulfonamide, N^1-(5-Methylisoxazol-3-yl) sulfanilamide
Chemical structure	
Molar mass	253.28 g mol^{-1}
CAS number	723-46-6

3.1.2. Other

Hydrogen peroxide solution (30% w/v) stabilized, sodium alginate, iron (III) chloride anhydrous (97%), sodium hydrogen sulphite solution (40% w/v) and L(+)-ascorbic acid and auxiliary chemicals used for initial pH adjustment (hydrochloric acid (HCl) and sodium

hydroxide (NaOH)) and acetonitrile HPLC grade used for chromatographic analyses was supplied by Panreac Química (Spain).

1,10-phenantroline (99%), tert-Butanol (99.7%), catalase from bovine liver (lyophilized powder, 2,000-5,000 units mg^{-1} protein), Ce(III) chloride hepta-hydrate (99.9%), Ce(III) nitrate hexa-hydrate (99.5 %), Fe(II) nitrate 9-hydrate (98 %) and iron powder (356 mesh, 97%) were supplied by Sigma-Aldrich.

Ammonium (meta) vanadate (99.0%) was supplied by Fluka.

Aeroxide® TiO$_2$ P25 was supplied by Degussa.

Filters used were Chmlab Group 0.45 μm (pore size) PVDF membrane filters.

3.2. CATALYSTS SYNTHESIS AND PREPARATION

3.2.1. Fe(III)/alginate hydrated catalyst

Fe(III)/alginate hydrated catalyst was prepared for all experiments according to the standard method developed after the study of the influence of diverse variables over catalyst properties, which can be found on chapter 4, "Fe/alginate catalyst development".

The detailed procedure for the production of an approximated amount of 3 g of Fe(III)/alginate hydrated catalyst in dry basis can be found below.

A 2.5% (w/w) sodium alginate aqueous solution was prepared by mixing sodium alginate powder in distilled water with an ultraturrax (IKA®-Werke) to achieve homogeneity (2 minutes at 24000 min^{-1}).

Sodium alginate solution was warmed to 40°C for 24 hours to allow air bubbles formed during mixing to escape. Then it was introduced on syringes with a 10 μL micropipette tip on the top of a vacuum chamber containing 1 L of 0.05 M FeCl$_3$ hardening solution. The full system was placed on top of an orbital stirrer at 55 rpm. By activating the vacuum, the

alginate solution was added drop-wise into iron hardening solution to produce Fe(III)/alginate catalyst. Each drop became a solid gel sphere when put in contact with $FeCl_3$ solution.

A 6 hours curing time of alginate drops inside hardening solution allowed $FeCl_3$ to diffuse and achieve total gelification. Each drop became a solid and mechanically resistant sphere of catalyst. After hardening stage was finished, catalyst spheres were removed from hardening solution and submitted to a cleaning process as explained below:

1. Filtering the catalyst spheres through a strainer to separate the hardening solution from the catalyst.
2. Introduce the catalyst inside 2 L of distilled water for 5 minutes and let iron cations to diffuse outside.
3. Filter again the catalyst through a strainer.
4. Repeat steps 2 and 3 four times.
5. Store catalyst spheres into a vessel with 2 L of distilled water placed on top of an orbital stirrer (120 rpm) for 24 h.
6. Filter the catalyst through a strainer.

After this cleaning process, catalyst was stored in distilled water until its use to avoid dehydration.

The obtained catalyst had an average diameter of 1.9 mm and an iron content of 11.15% (w/w) in dry base.

3.2.2. Fe(III)/alginate dehydrated catalyst

In order to prepare the dehydrated Fe(III)/alginate catalyst, the hydrated form of the catalyst was used as base. The hydrated catalyst was submitted to a thermal dehydration process by introducing it in an oven at 40°C. The oven ventilation was settled fully open to allow the air to flow outside avoiding water air saturation.

After 24 h the catalyst was totally dried and was removed from the oven. Some of the catalyst spheres got attached one into another during this process, so the catalyst was sieved to obtain single spheres.

3.2.3. Fe(III)/Ce/alginate catalyst

To prepare the Fe/Ce/alginate catalyst, a modification of the already established method for the dehydrated Fe/alginate catalyst was done. In this case, cerium (III) was included on the catalyst structure by taking advantage of the affinity of alginate for divalent and trivalent cations, as it was done with Fe. During catalyst preparation, cerium chloride ($CeCl_3$) was mixed with iron chloride ($FeCl_3$) at molar ratio 1:1 on the hardening solution to a final concentration of 0.05M each. On these conditions, the alginate chains were bonded with both, Fe^{3+} and Ce^{3+} cations, forming a Fe/Ce/alginate hydrated catalyst. The same dehydration process explained before was then applied, obtaining the Fe/Ce/alginate catalyst.

3.2.4. Fe(III)/TiO₂/alginate catalyst

The Fe(III)/TiO_2/alginate catalyst was prepared by mixing 0.4 g L^{-1} of TiO_2 particles were mixed into sodium alginate aqueous solution forming a suspension. Then, the production process was the same as it was on the Fe(III)/alginate dehydrated catalyst but replacing the sodium alginate solution for the new one prepared for the TiO_2 catalyst modification. The process entrapped the solid particles into the full volume of the catalysts using alginate as cohesive agent and forming the Fe/TiO_2/alginate modified catalyst.

3.2.5. Fe(III)/ZVI/alginate catalyst

For the preparation of the Fe(III)/ZVI/alginate catalyst 0.4 g L^{-1} of zero valent iron (ZVI) particles were mixed into sodium alginate aqueous solution forming a suspension. Then, the production process was the same as it was on the dehydrated Fe(III)/alginate catalyst but replacing the sodium alginate solution for the new one prepared containing ZVI particles.

The process entrapped the solid particles into the full volume of the catalysts using alginate as cohesive agent and forming the Fe/ZVI/alginate modified catalyst.

3.2.6. Fe/Ce/O catalyst

Fe/Ce/O catalyst was prepared by means of a co-precipitation method.

A 100 mL solution of Fe(II) and Ce(III) in distilled water was prepared on a molar ratio 70:30 by using cerium and iron nitrates. Then, 200 mL of a 3 M NaOH solution was added dropwise over the solution containing cerium and iron, which produced their instant precipitation as hydroxides. The solution containing the precipitate was filtered through filtering paper (1 µm pore size) by using a Buchner and a void pump. The precipitate obtained over the filtering paper was then cleaned with abundant distilled water to remove the residual NaOH solution. The filtering paper with the precipitate was dried overnight (12 h) at 105°C. Dried solids were removed from the filter and calcined at 300°C for 3 h, obtaining the Fe/Ce/O catalyst. Then, the catalyst was crushed and sieved until obtaining a catalyst particle size lower than 250 µm.

Main catalyst properties can be found on Table 3.2. A more detailed characterization of the catalyst can be found elsewhere [92,93,120].

Table 3.2. Main properties of the heterogeneous inorganic catalysts used for experimentation.

Catalyst	Average pore diameter (Å)	B.E.T. surface area ($m^2\,g^{-1}$)	Fe content (w/w)
Fe/Ce/O	66	188	51-56%*
Fe/Mn/O	16.7	133	42%
Volcanic rocks	0.00158	3.49	6 %
Iron shavings	0.00443	1.14	> 99%

*Calculated in based of the Fe/Ce ratio used on synthesis (70:30).

3.2.7. Other heterogeneous catalysts

Fe/Mn/O catalyst is the commercial catalyst Norit N-150, provided by Süd-Chemie AG, Munich (Germany). Raw catalyst was in the shape of cylindrical pellets that were crushed and sieved to a particle size lower than 250 µm before its use. According to the supplier, its composition is 60 % Fe_2O_3 and 30 % MnO_x (w/w). Its main properties can be found in Table 3.2. Further information about this catalyst can be found elsewhere [120,121].

Volcanic rocks catalysts are red volcanic rocks collected from the soil in Azores islands. Rocks were crushed and sieved to a particle size lower than 250 µm before its use. Main properties of the resulting catalyst can be found in Table 3.2. More information about this catalyst can be found elsewhere [93].

Iron shavings catalysts were wastes from iron industry and were collected from a local iron processing plant (Coimbra). Previous analysis performed indicated that their main composition was ferritic stainless steel. Due to its nature as a residue, iron shavings were used as collected, with diameters between 0.841 and 1.140 mm. The main properties of this catalyst can be found in Table 3.2. A more detailed characterization can be found elsewhere [93].

3.3. MAIN TECHNIQUES AND ANALYTICAL EQUIPMENT

3.3.1. High Performance Liquid Chromatography

High Performance Liquid Chromatography (HPLC) was used for the determination of the antibiotic sulfamethoxazole concentration in aqueous samples during the experiments.

For this purpose a HPLC-UB supplied by Agilent was used. The HPLC column was a Teknokroma C-18 Tracer Extrasil ODS2 (250 mm x 4.6 mm) and the mobile phase consisted of a 60:40 solution of acetonitrile and MilliQ water adjusted to pH 3 by using ortho-phosphoric acid (H_3PO_4), respectively. By using a flowrate of 1 mL min-1 and the UV

detector set at a wavelength of 270 nm, an isolated peak viable for its quantification was observed after 5 minutes of the injection.

3.3.2. Dissolved iron measurement

Soluble iron (Fe(II) and Fe(III)) quantification during catalytic reactions was done by means of a modification of the standard 1,10-phenantroline spectrophotometric method at 510 nm (Standard Method 310A modified) [122] with a detection limit of 0.09 mg·L^{-1}. 4 mL of sample containing Fe were mixed with 1 mL of ammonium acetate/acetic acid buffer (pH = 4) and 1 mL of 1 g L^{-1} 1,10-phenantroline. A small amount of ascorbic acid (30 mg) was added to reduce all Fe(III) into Fe(II), which is the reactive species. 1,10-phenantroline reacted with Fe(II) cations forming a colored complex which was measured by using a Hach Lange DR 3900 spectrophotometer at a wavelength of 510 nm.

Due to the possibility of iron precipitation at non acidic pH, neutral pH samples containing iron were measured after 20 minutes of reaction with 1,10-phenantroline, which was found enough time to ensure solid suspended iron particles dissolution. Samples were filtered through a 0.45 µm pore size filter to remove suspended iron particles when needed.

3.3.3. Determination of hydrogen peroxide

H_2O_2 concentration was determined through a metavanadate spectrophotometric procedure at 450 nm with a detection limit of 0.33 mg·L^{-1} throughout all experiments [123]. 3 mL of sample containing H_2O_2 were mixed with 3 mL of 5.14 g L^{-1} of ammonium metavanadate (acidic medium, 19.2 mL H_2SO_4 L^{-1}). Ammonium metavanadate reacted with H_2O_2 according to equation 3.1 and forming an orange-red colored compound (VO_2^{3+}) which was measured at a wavelength of 450 nm by using a Hach Lange DR 3900 spectrophotometer.

$$VO_3^- + 4\ H^+ + H_2O_2 \rightarrow VO_2^{3+} + 3\ H_2O \qquad \text{(Equation 3.1)}$$
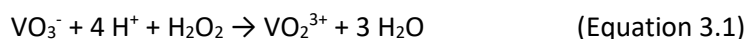
3.3.4.   Determination of Total Organic Carbon (TOC)

TOC determination was performed by using a Shimadzu 5055 TOC-VCSN analyzer equipped with an ASI-V Autosampler. The device conducted aqueous samples catalytic combustion at 680°C according to Standard Method 5220D procedures [122].

3.3.5.   Viscosimetry

Viscosimetry assays of alginate aqueous solutions were performed by using a rheometer HAAKEMARS (Modular Advanced Rheometer System) at a controlled temperature of 25°C or 40°C. Serrated plate-plate geometry with a diameter of 35 mm was used. After loading, samples were kept for 5 min prior test in order to allow stress and temperature equilibration.

3.3.6.   *Escherichia Coli* culture and determination

Escherichia Coli inoculum preparation

Escherichia Coli WG5 strain was provided as a stock solution by the Microbiology Department of the Faculty of Biology of the University of Barcelona and was stored at -20°C until its use.

To prepare the inoculum for disinfection experiments, a volume of the *Escherichia Coli* stock solution was defrosted and added into a 50 mL Falcon vial containing sterilized Modified Scholten's Broth (MSB) (Table 3.3) in a proportion 1:100 (v/v). Then it was incubated at 37°C with gentle agitation for 155 minutes. After this time, bacteria grew to the end of the exponential growth stage, in which an approximated concentration of 10^9 CFU mL^{-1} was obtained. This sample was stored at 4°C for no more than 3 hours until its use as inoculum.

Table 3.3. Modified Scholten's Broth (MSB) composition

Component	Amount
Peptone	10 g
Yeast extract	3 g
Meat extract	12 g
NaCl	3 g
Na_2CO_3 (150 g L^{-1})	5 mL
$MgCl_2 \cdot 6H_2O$ (2,000 g L^{-1})	0.3 mL
MilliQ water	1 L

<u>*Escherichia Coli quantification*</u>

Samples from experimental reactors were collected by using sterilized syringes to avoid microbiological contamination. Samples were submitted to decimal dilution (1:10, 1:100, 1:1,000, 1:10,000) by using Phosphate Buffer Saline (PBS) (Table 3.4) as eluent to avoid osmotic stress of bacteria cells.

Table 3.4. Phosphate Buffer Saline (PBS) composition

Compound	Amount
NaCl	8.0 g
KCl	0.2 g
KH_2PO_4	0.2 g
$NaHPO_4 \cdot 12H_2O$	1.52 g
MilliQ water	1 L

Raw and diluted samples containing the reference bacteria were cultured on 100 mm diameter petri plates by using the mass culture technique. 1 mL of each sample's dilution was added in the center of each plate. Then, a Chromocult® TBX Agar solution, kept at 40°C after its preparation to avoid gelification, was added on top until filling the full plate surface. This agar was specifically design to be a selective agar for *Escherichia Coli*. The plates' contents were gently mixed by submitting each plate to circular movements to ensure a more homogeneous distribution of bacteria over plate's volume. The already mixed plates were covered and left at room temperature until agar jellified and then were introduced in an incubator at 44°C for 18-24 hours. *Escherichia Coli* colonies grew on the full volume of plates as purple circular cumulus of bacteria, which were counted and calculated according to the original dilution.

3.3.7. Actinometrical measures

Photon flow emitted by UV-A black light blue (BLB) lamps included on the experimental reactors was measured by means of an actinometrical method based on o-Nitrobenzaldehyde (o-NB) reaction [124,125] and adapting the method proposed by Willet and Hites [126]. o-NB was considered a suitable actinometer due to its property of absorbing light in a range from 290 to 400 nm, which enclosed the emission wavelength of UV-A BLB lamps.

3.4. SAMPLES PREPARATION AND CHARACTERIZATION

Samples were prepared by spiking sulfamethoxazole on distilled water, bottled drinking water or wastewater to a final concentration of 10 mg L^{-1}.

Bottled drinking water was selected as a slightly buffered natural water matrix. Its main composition before SMX addition can be found on table 1. Wastewater was collected from the secondary effluent of the WWTP of Calafell (Spain). Before its use, it was filtered through a 1 μm pore size filter to remove big particles as a simulation of a filtering operation through a sand filter. The specifications for water after filtration can be found on Table 3.5.

48

Table 3.5 Bottled drinking water and secondary effluent from Calafell (Spain) WWTP characterization.

	Drinking water	Wastewater
TOC	< 0.2 mg L^{-1}	10.6 mg L^{-1}
pH	7.9	7.6
Sulfate	15.8 mg L^{-1}	-
Chloride	13 mg L^{-1}	-
Calcium	35.5 mg L^{-1}	71.5 mg L^{-1}
Magnesium	8.6 mg L^{-1}	59.7 mg L^{-1}
Sodium	11.9 mg L^{-1}	392.2 mg L^{-1}
Conductivity	280 μS cm^{-1}	1820 μS cm^{-1}
Alkalinity (HCO$_3^-$)	144 mg L^{-1}	518.4 mg L^{-1}
Turbidity	< 0.2 NTU	1.9 NTU
Total Suspended Solids	< 0.1 mg L^{-1}	3.3 mg L^{-1}
Total Volatile Solids	< 0.1 mg L^{-1}	2.7 mg L^{-1}
COD	< 5 mg L^{-1}	49.8 mg L^{-1}

3.5. CATALYST CHARACTERIZATION TECHNIQUES

3.5.1. SEM

The morphologies of the catalysts were observed by means of scanning electron microscopy (SEM) using a field emission scanning electron microscope JEOL J-7100 at 20.0 kV. Samples were covered by a gold coating before its analysis.

3.5.2. BET-porosimetry

The surface area of Fe(III)/alginate dehydrated catalyst was measured using the Brunauer-Joyner-Teller (BET) nitrogen adsorption method, and mesopore size distribution was quantified by the Barett-Joyner-Halenda (BJH) method using an adsorption isotherm (TriStar 3000 V 6.04 A surface area and pore analyzer). The samples were degassed under vacuum at 40°C.

3.5.3. ICP-OES

Fe, Ce and Ti contents in catalysts were measured by means of an ICP-OES Optima 3200 RL from Perkin Elmer with a previous digestion in $HNO_3/HClO_4$ for Fe, HNO_3/H_2SO_4 for Ce and $HNO_3/H_2O_2/HF$ for Ti.

3.5.4. FTIR

FTIR analysis was performed by means of a React IRTM 4000 (Applied Systems) and using a silicon probe.

3.6. EXPERIMENTAL DEVICES

3.6.1. UV-A Photo-reactor 1

UV-A Photo-Fenton-like experiments performed by using the Fe(III)/alginate hydrated catalyst for SMX depletion were performed by using this reactor.

The reactor was a 2 L Pyrex jacketed stirred batch reactor with an inner diameter of 11 cm and a height of 23 cm. It was equipped with three immersed UV-A black light blue (BLB) lamps Philips TL 8W, 08 FAM wrapped in three Duran glass sleeves to avoid direct contact with water. Lamps were axially positioned and symmetrically. Each lamp emitted UV-A radiation in a range of 350 to 400 nm of wavelength, with a maximum at 365 nm. Lamps' photon flow emitted was measured with an o-nitrobenzaldehyde actinometrical method, as

explained before, and it was found to be 4.74 x 10^{-6} Einstein s^{-1}. The reactor was covered with an aluminum foil shield to avoid not absorbed radiation to escape the reactor and protect the user of possible exposure. Temperature was controlled at 25.0 ± 0.8 °C by connecting a thermostatic water bath (Haake C-40) to the reactor jacket and circulating water through it. Sample mixing was provided by a magnetic stirrer set at 700 rpm. Samples were taken through a sampling aperture on top of the reactor.

A schematic design of the reactor can be seen on Figure 3.1.
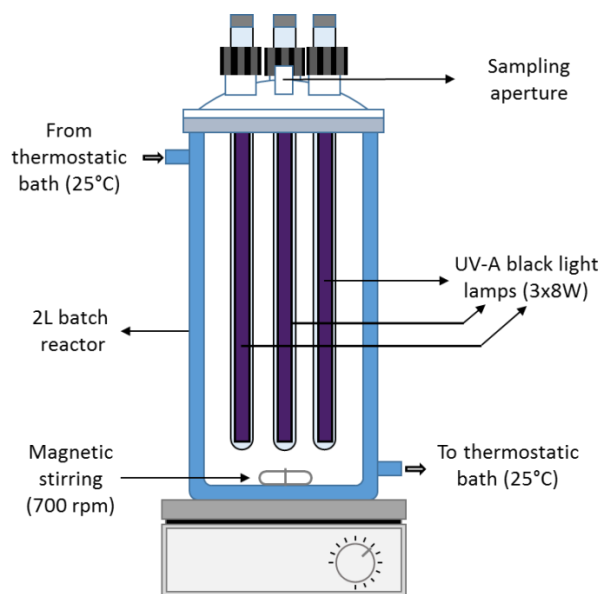
Figure 3.1. UV-A photo-reactor used for SMX depletion experiments performed by using Fe(III)/alginate hydrated catalyst.

3.6.2. UV-A Photo-reactor 2

UV-A Photo-Fenton-like experiments performed by using the Fe(III)/alginate hydrated catalyst for disinfection were performed by using this reactor.

The reactor was a modification of the UV-A photo-reactor 1 used for SMX depletion but changing the three UV-A BLB lamps for a single UV-A BLB lamp. This lamp was also a Philips

TL 8W, 08 FAM. Its photon flow emitted was measured with an o-nitrobenzaldehyde actinometrical method and it was found to be 1.58 x 10^{-6} Einstein s^{-1}. Other design parameters of the reactor were the same as the previous one.

Due to the microbiological nature of experiments, reactor was disinfected between experiments by using a 5 % H_2SO_4 solution (v/v) and then rinsed with abundant MilliQ water.

A schematic design of the reactor can be seen on Figure 3.2.
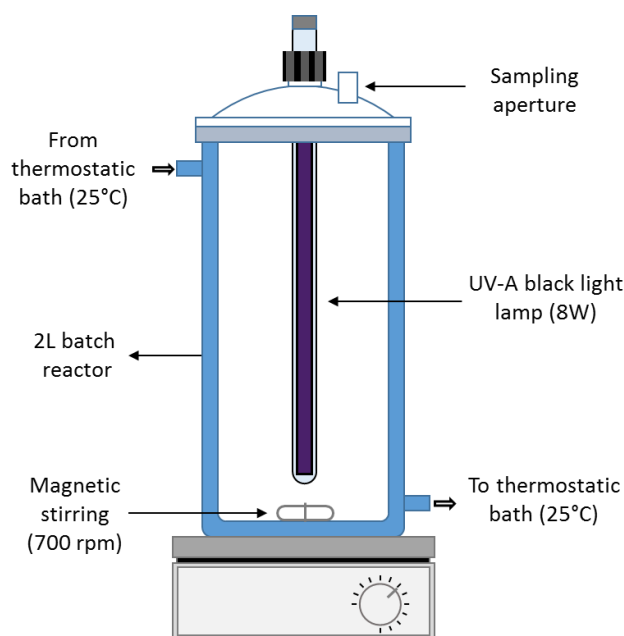
Figure 3.2 UV-A photo-reactor used for disinfection experiments performed by using Fe(III)/alginate hydrated catalyst.

3.6.3. UV-A Photo-reactor 3

UV-A Photo-Fenton-like experiments performed by using the Fe(III)/alginate dehydrated catalyst and its modifications were performed by using this reactor. Also, experiments performed by using the hydrated catalyst were repeated by using this reactor in order to compare. A schematic design of the reactor can be seen on Figure 3.3.
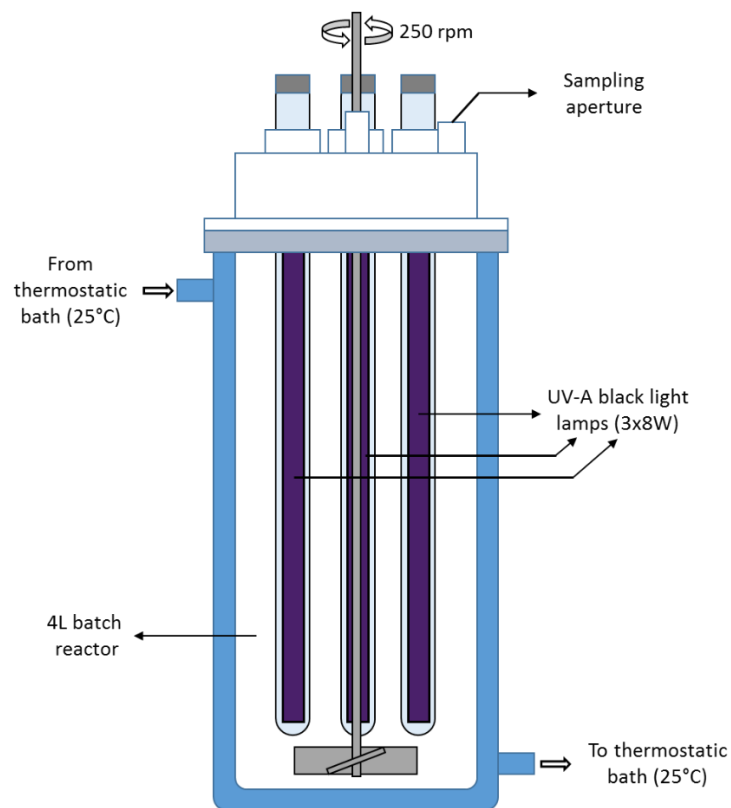
Figure 3.3. UV-A photo-reactor used for SMX depletion experiments performed by using Fe(III)/alginate dehydrated catalyst and its modifications.

The reactor was a 4 L Pyrex jacketed stirred batch reactor with an inner diameter of 12.5 cm and a height of 40 cm. It was equipped with three immersed UV-A black light blue (BLB) lamps Philips TL 8W, 08 FAM wrapped in three quartz glass sleeves to avoid direct contact with water. Lamps were axially positioned and symmetrically. Each lamp emitted UV-A radiation in a range of 350 to 400 nm of wavelength, with a maximum at 365 nm. Lamps' photon flow emitted was measured with an o-nitrobenzaldehyde actinometrical method, as explained before, and it was found to be 5.13 x 10^{-6} Einstein s^{-1}. The reactor was covered with an aluminum foil shield to avoid not absorbed radiation to escape the reactor and protect the user of possible exposure. Temperature was controlled at 25.0 ± 0.8 °C by connecting a thermostatic water bath (Haake C-40) to the reactor jacket and circulating water through it. Due to the higher density of Fe(III)/alginate dehydrated catalyst, sample mixing was provided by mechanical stirring set at 250 rpm. The stirring device consisted on

53

4 blades set on the bottom of the reactor designed to create an ascending flow in order to keep the catalyst homogeneously distributed during reaction. Samples were taken through a sampling aperture on top of the reactor.

4. Fe(III)/alginate catalyst development

4.1. INTRODUCTION

The use of alginate on the preparation of solid gel spheres has been widely reported on literature for different purposes, although few works detail their synthesis as heterogeneous catalyst for Fenton like reactions.

When it is intended for alimentary or pharmaceutical industry, calcium (II) is usually used as linking agent, which allows encapsulating different substances or active principles in the alginate structure, ensuring its edibility. If it is not intended for human consumption, a lot of other different divalent or trivalent cations can be used as binding agents due to the alginate chains ability of being linked by.

When applied to catalytic Fenton like reactions, the most used compound is Fe, which is known as the best specie intended for this purpose. Despite this, some other elements have been also tested by themselves or in combination with Fe.

Although it is not difficult to find literature about this topic, authors do not come to an agreement and they use different conditions on alginate-based catalysts preparation. Due to this, it is important to evaluate how the resulting catalyst is affected by all the variables that can be controlled on its preparation.

On this chapter, the principles of how is the Fe/alginate catalyst synthetized and also an overview of the different parameters involved in the preparation of a Fe/alginate catalysts have been studied in order to determine their best combination and stablish a standard methodology for its synthesis, which has already been detailed on the Materials and Methods section.

4.2. CATALYST SYNTHESIS

The synthesis of Fe/alginate catalysts is based on the ability of alginate of forming solid gel structures when is put in contact with a solution containing divalent or trivalent cations.

Sodium alginate salt has carboxylic groups on its polymeric chains which are bond with Na^+ (Figure 4.1.a). Divalent or trivalent cations which are put in contact with alginate salt can replace this ionic bond with Na^+, but their higher charge allows them to bond more than one carboxylic group at the same time (Figure 4.1.b). When this happens, several alginate chains get bonded one to each other, which results in the solid gel structure that forms the Fe/alginate catalysts.
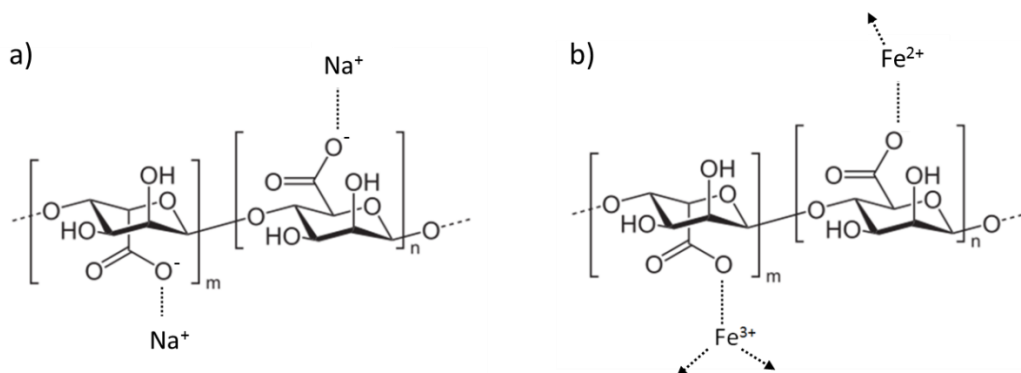
Figure 4.1. a) Sodium alginate salt structure. b) Alginate chain bonded with Fe^{2+} and Fe^{3+} cations.

At macroscopic level, when a drop of alginate aqueous solution is added over a solution containing iron cations, the previously explained process of substitution and bonding of iron cations with alginate instantly occur on the contact surface of alginate and the hardening solution forming a solid gel crust that separates both (Figure 4.2.a). As both, alginate and hardening solutions are aqueous based and as the solid gel structure which separates them is permeable, the difference in iron concentration between the inside and the outside acts as driving force for iron cations diffusion through this crust to the inside phase resulting in the growth of this solid gel crust from the outside to the inside (Figure 4.2.b). Despite Fe/alginate is permeable, it opposes a resistance to iron cations diffusion, which increasingly

slows the crust growth as it becomes thicker. After enough time, iron cations reach the sphere center completing the growth of this crust and obtaining a full volume of solid gel (Figure 4.2.c). As long as there is bonding spots in alginate chains, iron cations that diffuse through alginate can form new bonds, increasing the degree of linking until total saturation of alginate chains and the disappearance of this driving force. Even so, as higher is this saturation degree, higher is the resistance that alginate oppose to diffusion, which gradually turns the process slower. The moment the catalyst is taken out of hardening solution and introduced in distilled water, the absence of iron cations in the outside phase reverts this driving force and starts a lixiviation phase in which iron cations that are not bond to alginate start being released from the catalyst (Figure 4.2.d). The bonds that iron and alginate stablished during the growth phase are strong enough to be unaltered in absence of hardening solution, so the catalyst sphere maintains its integrity [102].
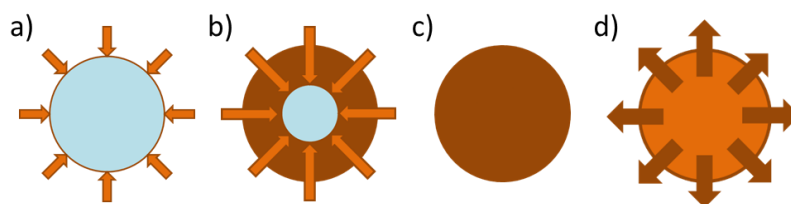
Figure 4.2. Fe/alginate synthesis process.

4.3. PARAMETERS RELATED TO FE/ALGINATE CATALYSTS PREPARATION

4.3.1. Iron source

As alginate can form solid gel structures when it is put in contact with divalent and trivalent cations, iron cations can act as binding agent for alginate chains on its Fe(II) and Fe(III) forms. Thus, it is important to evaluate how the use of different valence species from the same element affects to the resulting catalyst.

For this purpose, two catalysts were prepared, one by using $FeSO_4$ as Fe(II) precursor and the other one by using $FeCl_3$ as a source of Fe(III) cations.

57

Both catalysts were prepared by means of the same procedure and keeping constant all variables except for the iron specie. Alginate solution was prepared in a mass ratio of 2.5%. Both hardening solutions containing Fe(II) or Fe(III) were prepared in a concentration of 0.05 M each. The contact time of alginate drops with hardening solution was 6 h. The resultant catalysts' spheres were submitted to a standard 24 h cleaning process in distilled water to remove the remaining iron solution from preparation.

After their synthesis, a significant difference on both catalysts' mechanical properties was easily observed at first glance. The catalyst prepared by using Fe(III) as binding agent presented a higher mechanical resistance than the one prepared by using Fe(II). This second one was softer and with a little pressure with the bare fingers the spheres got easily crushed. On the contrary, the ones prepared by using Fe(III) were more elastic and resistant, turning them into a more suitable catalyst for its manipulation and its use inside a stirred reactor.

The explanation to this difference resides on the amount of bindings stablished between alginate and iron at molecular level. Fe(III) cations have three binding spots which can link three different alginate chains, but Fe(II) have only two linking spots to bind with the carboxylic groups of alginate, so the resulting structure is weaker.

Due to this, the use Fe(III) as linking agent resulted more convenient for the preparation of an Fe/alginate catalyst intended for water treatments inside a stirred reactor. Most authors used Fe(III) salts as source of iron for the preparation of Fe/alginate catalysts [110,112–114,117,118].

4.3.2. Alginate concentration and viscosity

Alginate concentration on the aqueous solution used for the catalyst preparation is an important parameter to determine in order to settle a standard procedure to synthetize a Fe/alginate catalyst.

Various alginate concentration values up to 3 % (w/w) can be found on literature for the preparation of alginate solutions c.

For the determination of the effect of this parameter over the resulting catalyst, four different concentrations of alginate aqueous solution (1%, 2%, 2.5% and 3%) were tested. A concentration higher than 3% was not possible to prepare because it was impossible to solubilize homogeneously with the available equipment. Also, the 3% solution was very difficult to homogenize, so the 2.5% one was considered the maximum concentration reasonable to prepare. All catalysts were prepared by using a hardening solution containing Fe(III) as binding specie in a concentration of 0.05 M and 6 h of hardening time. Lately, the resulting catalysts' spheres were submitted to a standard cleaning process for 24 h in distilled water.

A significant difference in the time needed for the addition of alginate aqueous solution dropwise over the Fe(III) hardening solution was noticed during the preparation of the four different catalysts. A small increase on alginate solution concentration resulted on a very significant viscosity variation, which was determinant on catalyst preparation. The higher was the concentration, the higher was the viscosity and the longer was the time needed for a drop to pass through the syringe tip and fall into the hardening solution.

Shear stress (τ) respect shear rate ($\dot{\gamma}$) of the four different alginate solutions measured at room temperature and at 40°C can be found on Figure 4.3. The profiles observed clearly show a non-Newtonian pseudoplastic behavior which implies that viscosity varies with temperature and shear stress [127].
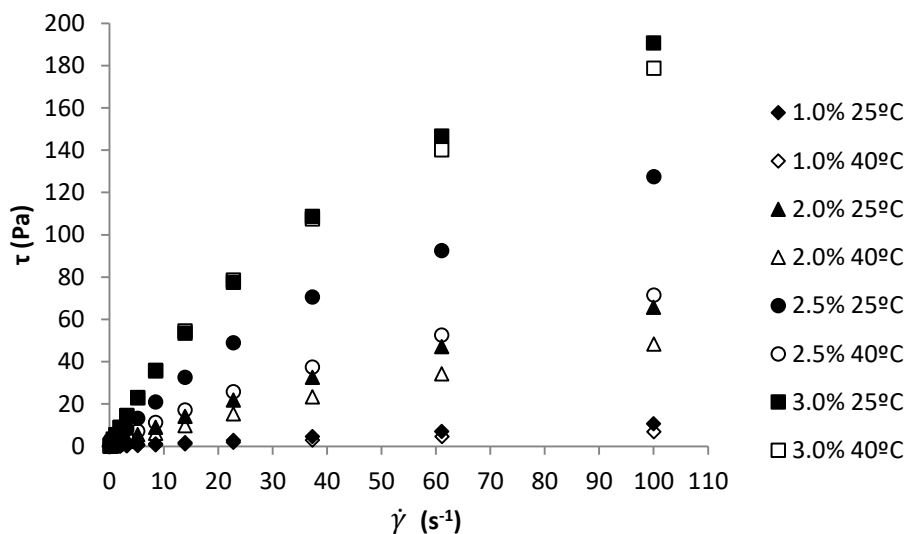
Figure 4.3. Shear stress (τ) respect shear rate (γ̇) of four different concentrations of sodium alginate aqueous solutions at 25°C and 40°C.

In order to evaluate the effect of alginate concentration over catalyst iron load, the four catalysts were introduced in a strong acidic medium (1% H_2SO_4) in which iron from the catalyst was totally released and then quantified.

Fe content in catalysts increased while increasing alginate concentration (Figure 4.4). The explanation for this is related to the amount of binding spots on the alginate structure. The higher alginate concentration on the initial solution, the higher amount of alginate chains are available to absorb Fe(III) cations during the hardening stage of preparation.
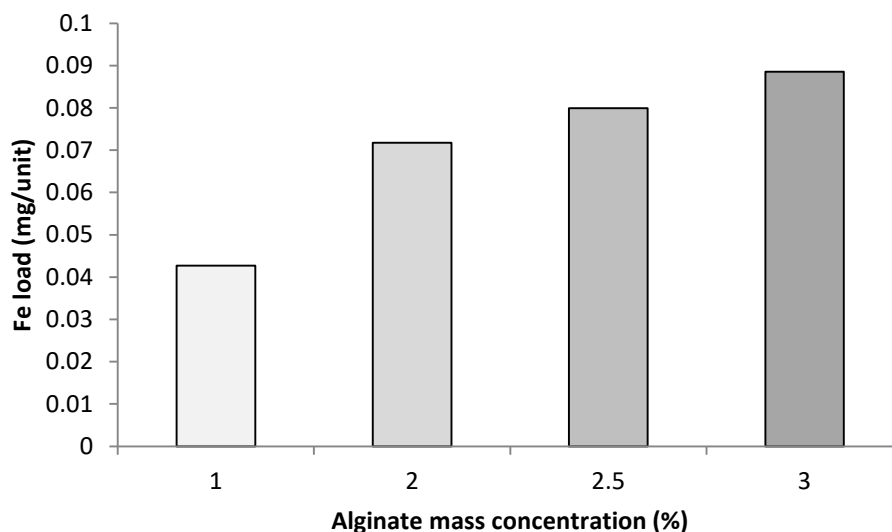
Figure 4.4. Iron load of catalysts prepared by using 1%, 2%, 2.5% and 3% alginate aqueous solution. Hardening solution consisted of FeCl$_3$ 0.05 M and hardening time was of 6 h.

Relating to the obtained catalysts, the one prepared with 1 % alginate aqueous solution was discarded because its consistency was very low, which means that there weren't enough links between chains.

4.3.3.   Iron concentration

Fe(III) hardening solution concentration used during catalyst preparation is also an important parameter which can be found in disparity on literature [107,110,112,116,118,128–132].

In order to evaluate its effect over the catalyst synthesis and performance, four different concentrations of Fe(III) hardening solution were tested (0.01 M, 0.05 M, 0.1 M and 0.5 M). All other parameters were kept constant for the four different catalysts prepared (2.5% of alginate, 6 h of hardening time and a standard cleaning process of 24 h after preparation).

Fe load in the four catalysts was evaluated for the different catalysts prepared (Figure 4.5), revealing that a higher concentration of iron in the hardening solution resulted in a

catalyst with a higher content of Fe. The higher is the iron concentration in hardening solution, the higher is the driving force for iron cations diffusion through the catalyst. This produces an increase of the amount and the rate of formation of Fe-alginate bonds in catalyst. This relation between the hardening solution concentration and the iron load in catalyst looks to be linear while keeping other parameters constant.
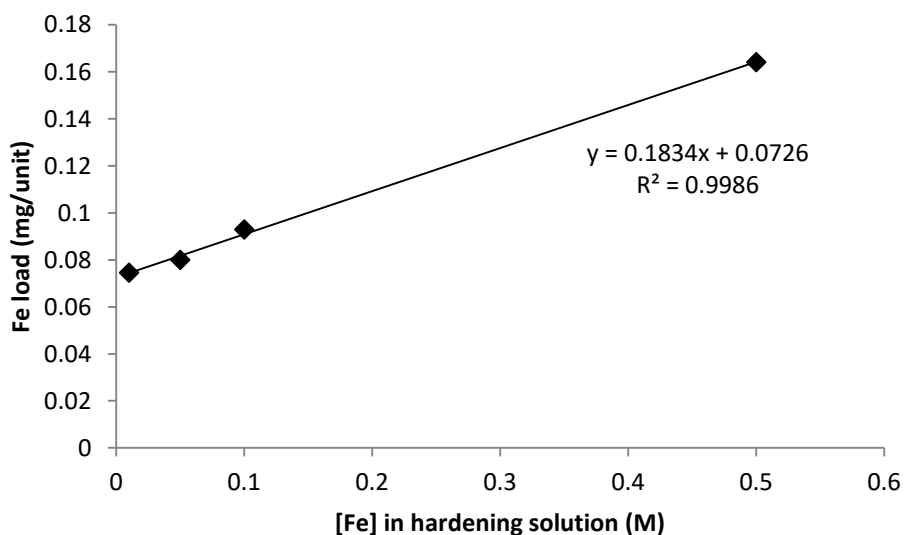
Figure 4.5. Iron load of catalysts prepared by using FeCl₃ 0.01 M, 0.05 M, 0.1 M and 0.5 M as hardening solution. Alginate aqueous solution was 2.5% (w/w) and hardening time was of 6 h.

In reference to the catalysts obtained, the one prepared with 0.01 M FeCl$_3$ solution presented a low consistency and its core was still liquid after the 6 h of hardening time. Also, the low concentration of hardening solution resulted in a low gelification rate. This produced the formation of catalyst aggregates because the alginate drops did not instantly solidify in contact with hardening solution and merge one to each other. Due to this, 0.01 M solution was discarded for catalyst preparation. Catalyst spheres prepared by using 0.5 M FeCl$_3$ solution presented a very good mechanical resistance but a high number of non-spherical units and also irregular cumulus of grouped units were observed after its preparation. The higher density of the hardening solution resulted in alginate drops to float

over it so alginate drops fell over the already formed spheres of catalyst and fused with them. For this reason 0.5 M $FeCl_3$ hardening solution was also discarded.

4.3.4. Hardening time

The amount of time the alginate drops are immersed inside the hardening solution is also a parameter that determines the resulting structure of the Fe(III)/alginate catalyst. The higher is the contact time of alginate and the hardening solution containing Fe(III) cations, the higher is the diffusion of Fe(III) cations through alginate drops and the higher is the amount of Fe-alginate bonds formed.

Preliminary experiments revealed that the minimum time iron cations needed to diffuse from the surface to the core and form a totally solid gel structure was of about 5 h. Lower hardening times by using this preparation conditions produced catalyst spheres consisting on a solid gel crust with a sodium alginate liquid core, which was undesired.

To evaluate the effect of the hardening time on the iron load of the catalyst, three different catalysts were prepared: the first one with a contact time of alginate and hardening solution of 6 h, the second one with a contact time of 12 h and the last one of 24 h. Other parameters were kept the same for all (2.5% of alginate, 0.05 M of Fe(III) in hardening solution and a standard cleaning process of 24 h after preparation).

Iron load of the catalysts prepared was higher as hardening time increased while keeping a linear increase rate of 0.0011 mg per unit every hour (Figure 4.6). As long as there are available binding spots in alginate chains, iron cation will continue diffusing and Fe-alginate links will be forming. Linearity respect both, iron concentration in hardening solution and hardening time, revealed that diffusion through the already formed Fe(III)/alginate is the controlling stage on the formation of this kind of catalyst.

y = 1.10E-03x + 7.31E-02
R^2 = 9.99E-01
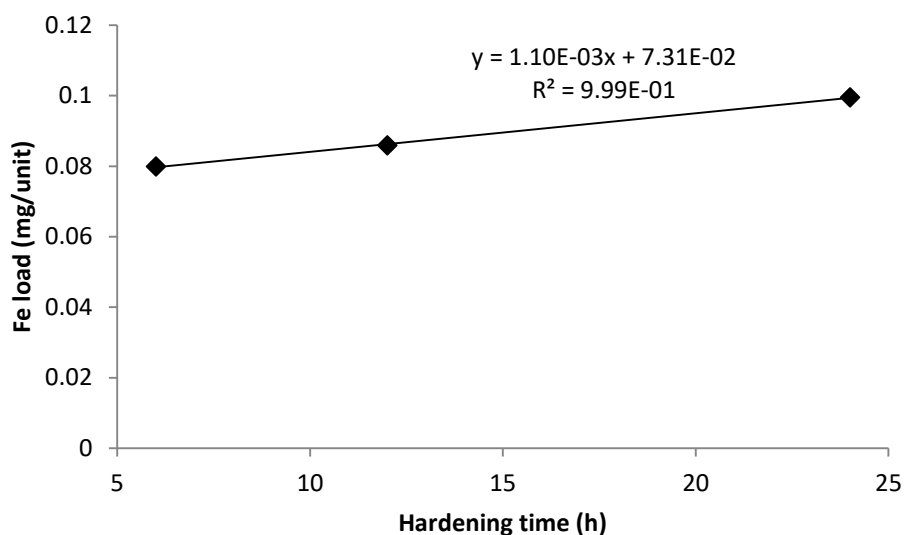
Figure 4.6. Iron load of catalysts prepared by using 2.5% (w/w) alginate aqueous solution, FeCl$_3$ 0.05 M as hardening solution and hardening times of 6 h, 12 h and 24 h.

4.3.5. Catalyst size

Catalyst size is an important variable to consider when referring to heterogeneous reactions. As the reaction is supposed to occur on catalyst surface, the lower is the size of the catalyst, the higher is the ratio surface/catalyst mass and so the active surface. For this reason, it was necessary to prepare the catalyst with the smallest possible size.

In this kind of alginate gelification procedures, the final size depends on the size of the drops added into hardening solution, so reducing the alginate aqueous solution drops one results into smaller catalyst spheres.

The major responsible for drops size was the dimension of syringes tips. Common syringes have a standard 1 mm inner diameter tip. By adapting the tip of a 10 µL micropipette on the common syringes one, a considerable reduction of the drops size was achieved, from 4 mm to 2.5 mm when working at room temperature.

Also, viscosity of a fluid is a determinant physical parameter involved on the size of the drops formed by it. The lower the viscosity of the fluid is, the smaller the drops formed will be. Alginate aqueous solution viscosity is affected by its alginate concentration but this parameter has already been fixed by the synthesis conditions. As alginate is a high viscosity pseudoplastic, a small increase of temperature can produce a significant reduction of its viscosity (Figure 4.3). For this purpose, 2.5% alginate aqueous solution was warmed to 40°C before its addition over the hardening solution, resulting in a higher reduction of drops size, from 2.5 mm to 1.9 mm.

4.4. PREPARATION PROCESS OPTIMIZATION

4.4.1. Catalyst preparation conditions

According to the previously studied parameters and its influence over the resulting catalysts prepared, the synthesis conditions for the preparation of the catalyst used for all experimentation was settled.

Despite Fe(III) is not the active specie for the production of HO· radicals through Fenton reaction, it was selected as the most suitable iron source because of the better mechanical properties of the resulting catalyst. When applied into photo-Fenton reaction, the iron on catalyst surface would turn into Fe(II) by means of the UV-A radiation, which made it an active specie while keeping the full volume of the catalyst with good mechanical resistance and able to be introduced inside a stirred reactor without being crushed by the stirrer blades.

Sodium alginate aqueous solution concentration was decided to be the higher possible, allowing the maximum availability of binding spots for Fe(III) cations to link. The concentration was settled as 2.5 % (w/w). This concentration was the higher one that could be prepared without homogeneity problems.

While alginate concentration determined the amount of available binding spots, iron concentration on hardening solution was the responsible for the amount of this spots to be linked by Fe(III) cations. The more concentrated it was, the higher was the driving force for diffusion and so the percentage of carboxylic groups in alginate chains that got bond by Fe(III) cations. Even so, it was decided that it was not necessary to prepare a heavily loaded catalyst because it could produce a higher iron release during experimentation and also the lixiviation stage became longer. For this reason, a 0.05 M $FeCl_3$ aqueous solution was selected as hardening solution.

In reference to hardening time, it was necessary to ensure that there was no liquid alginate core, so a hardening time higher than 5 h was needed. The higher the time of contact, the higher was the iron load of the catalyst, but as for iron concentration in hardening solution, it was considered not to load the catalyst in excess with Fe. For this reasons, 6h were selected as enough hardening time.

4.4.2.   Alginate aqueous solution addition system

The need to prepare large batches of catalyst discarded the manual addition of alginate aqueous solution by using a syringe, as some authors do [110,132].

An automatic system that allows preparing a large amount of catalyst in low time was required. Some authors use peristaltic pumps with low inner diameter pipes to add alginate dropwise over the hardening solution [118]. But this system limits the amount of catalyst produced because only allows operating from 1 to 6 pipes simultaneously. Also, the addition of high concentrated alginate solutions produced difficulties on pumping and pipes cleaning after the addition.

For this reason, it was decided to use void pressure instead of positive pressure for the addition of alginate aqueous solution. For this purpose, a void chamber was equipped with a cover in which multiple syringes were adapted according to the needs, allowing operating up to 24 simultaneously. The chamber was equipped with a void pressure regulator that enabled to control the inner pressure according to the requirements, which changed depending on the amount of syringes connected and the viscosity of the alginate solution to add (Figure 4.7).
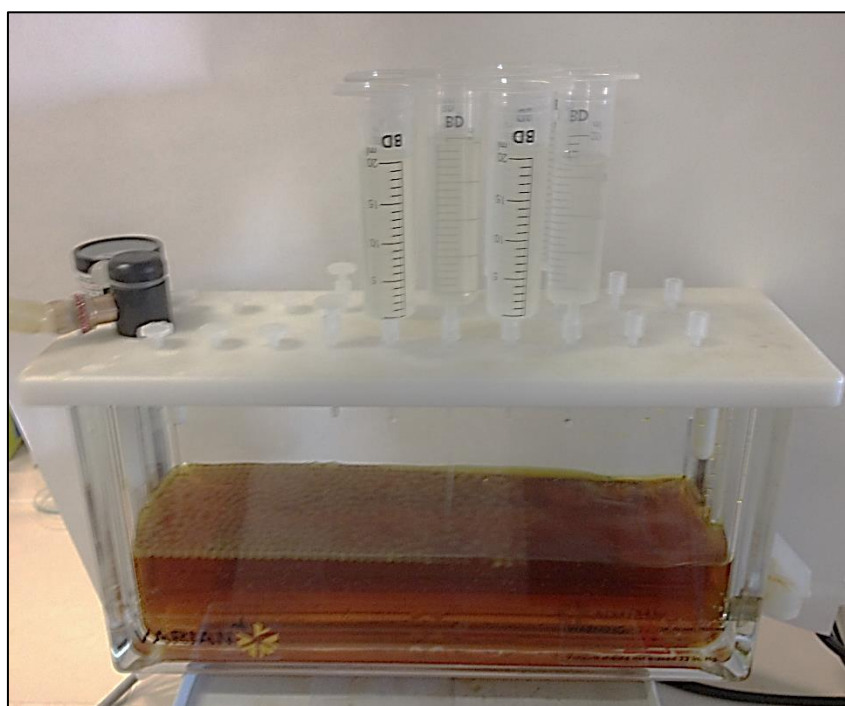
Figure 4.7. Void chamber for the preparation of Fe/alginate catalysts.

This device allowed adding up to 300 mL of 2.5 % alginate aqueous solution dropwise over the hardening solution, which was placed inside the void chamber, in less than 20 min. Thus, the difference of the hardening time of the first drop and the last drop added into hardening solution represented less than a 5% of the total 6 h hardening time, which didn't represent a significant variation of catalyst properties.

4.4.3. Catalyst cleaning

Preparation methodologies for Fe/alginate catalysts found in literature usually incorporate a cleaning stage after the preparation of the catalyst [112,118,129,130,132,133]. A rinsing with abundant water is the most suggested method for removing the hardening solution from the catalyst.

To stablish a standard method for the preparation of the catalyst it was considered that some tests should be performed to ensure the total removal of the solution containing iron cations, which had to diffuse back outside of the catalyst.

As there is not a detailed explanation about the rinsing process, it was decided to follow the steps below:

7. Filtering the catalyst spheres through a strainer to separate the hardening solution from the catalyst.
8. Introduce the catalyst inside 2 L of distilled water for 5 minutes and let iron cations to diffuse outside.
9. Filter again the catalyst through a strainer.
10. Repeat steps 2 and 3 four times.

After each repetition, rejected water was less colored, indicating fewer iron concentration.

The resulted catalyst, clean from hardening solution, was stored in distilled water to avoid its dehydration until its use. After 5 hours of storing, water started to dye in pale orange, indicating the presence of Fe. This exposed that the initial rinsing with abundant water was not enough to avoid the total lixiviation of Fe. Hardening solution that had diffused through alginate for 5 hours until reaching the catalyst core was not able to diffuse outside with this methodology. For this reason, it was decided to submit the catalyst to a long time lixiviation stage after the initial cleaning with abundant water. The catalyst was introduced for 24 h in 2 L of distilled water and putted on top of an orbital stirrer at 120 rpm

to ensure the catalyst to be in suspension. After this lixiviation stage, the catalyst was submitted again to the same initial rinsing process and then stored in distilled water.

A control of iron concentration of the water in which the catalyst was stored after 24 h, 48 h and 7 days didn't detect soluble Fe, so the cleaning process was settled as previously detailed.

The catalyst cleaning was considered an essential stage because the lixiviation of iron cations during its use on reaction could initiate homogeneous photo-Fenton.

4.5. CONCLUSIONS

Fe (III) resulted to be the more convenient oxidation state to use for the catalyst synthesis due to the better mechanical properties of the catalyst after preparation.

Alginate solution concentration proved to determine the amount of iron that the catalyst can absorb as cross-linking agent.

Iron concentration in hardening solution determined the diffusion rate of iron cations through alginate during hardening stage. Thus, the higher the concentration, the higher the amount of iron that got bond with alginate in a same period of time.

Regarding catalyst size, alginate solution temperature was found to be determinant because it varied significantly the solution viscosity, which allowed producing smaller drops of the alginate solution when added over hardening solution.

Finally, the cleaning stage was considered essential to remove the non-cross-linked iron from catalyst and consequently avoid the contribution of homogeneous reactions due to the residual iron from hardening solution.

As a result of the study performed in this chapter, the standardized method for the preparation of Fe/alginate catalyst (detailed in chapter 3, "Materials and methods") was

developed. The selected conditions for its preparation (Figure 4.8) were 2.5 % (w/w) alginate solution, a FeCl$_3$ 0.05 M hardening solution and 6 hours of hardening time

Figure 4.8. Fe(III)/alginate catalyst after its preparation.

5. Fe(III)/alginate catalyst mechanism and stability

5.1. INTRODUCTION

Some works on Fe/alginate as a photo-Fenton and electro-Fenton catalyst focused on its preparation and the degradation ratios obtained during the catalyst application can be found in literature [105,110,116,118,129,131,132,134], but little is done to deeply study catalyst mechanism, catalyst stability and the possible contribution of homogeneous photo-Fenton reaction the overall removal.

Some authors already pointed out the effect of pH on the stability of Fe/alginate catalysts [112,128]. The release of cross-linked iron from Fe/alginate catalysts when introduced into acidic samples is even accepted as a method for the determination of iron content in catalysts [112].

It is known that photo-Fenton reactions generate intermediate compounds (carboxylic acids) that tend to acidify the samples, but the effect of this pH decrease during the reaction process and its relation to catalyst stability have not been deeply studied.

The aim of this chapter is to evaluate the performance and stability of the Fe(III)/alginate heterogeneous catalyst in circumneutral conditions. The influence of pH on the catalyst stability has been deeply studied and a mechanism of homogeneous-heterogeneous pathway contribution in correlation to pH has also been proposed.

To perform this study, antibiotic sulfamethoxazole has been selected as reference compound to follow the efficiency of photo-Fenton reaction.

5.2. MATERIALS AND METHODS

5.2.1. Reactor set-up

In order to perform the experiments which results can be found in this chapter, a 2 L batch reactor was used. The reactor included magnetic stirring and temperature control (25°C). Also, three 8 W UV-A lamps (λ_{max} = 365 nm) with a total emission of 4.74 x 10^{-6} Einstein s^{-1} were immersed inside the reaction volume. (A detailed description of the experimental device can be found in chapter 3, "Materials and Methods".

5.2.2. Samples preparation and characterization

2 L samples were prepared by spiking SMX into a distilled or bottled water matrix to an initial concentration of 10 mg L^{-1}. Solutions were mixed overnight with a magnetic stirrer to ensure the total dissolution of the antibiotic.

Bottled drinking water was selected as a natural buffered water matrix to perform the experiments. A detailed explanation about it and its characterization can be found in chapter 3, "Materials and Methods".

5.2.3. Catalyst synthesis

Fe(III)/alginate catalyst used in this chapter was prepared according to the standard method previously developed. A detailed description about it can be found in chapter 3, "Materials and Methods".

5.3. RESULTS AND DISCUSSION

5.3.1. Blank experiments

Before studying catalyst effectiveness, blank experiments were performed to evaluate the effect of direct oxidation of H_2O_2, UV-A irradiation and absorption in Fe(III)/alginate

catalyst on SMX removal per separate. A fourth blank experiment by combining Fe(III)/alginate catalyst and H_2O_2 in absence of UV-A light was also performed to evaluate the possible contribution of Fenton reaction to the process.

Sulfamethoxazole was spiked into a 2 L sample of distilled water to achieve an initial concentration of 10 mg L^{-1} on each of the four experiments. The first blank experiment was carried out by adding only H_2O_2 to an initial concentration of 20 mg L^{-1} (without UV-A light nor catalyst). The second one was performed by activating the UV-A lamps of the experimental reactor (without the addition of H_2O_2 nor catalyst). The third one was carried out by adding 0.5 g L^{-1} of the catalyst in dry basis (without UV-A radiation nor H_2O_2). The last one was done by adding 0.5 g L^{-1} of the catalyst in dry basis and an initial concentration of 20 mg L^{-1} of H_2O_2.

Results showed that there was no significant sulfamethoxazole removal through UV-A photolysis, adsorption in catalyst or H_2O_2 direct oxidation during 120 minutes of experiment when H_2O_2, UV-A radiation or the catalyst were used separately (Figure 5.1).
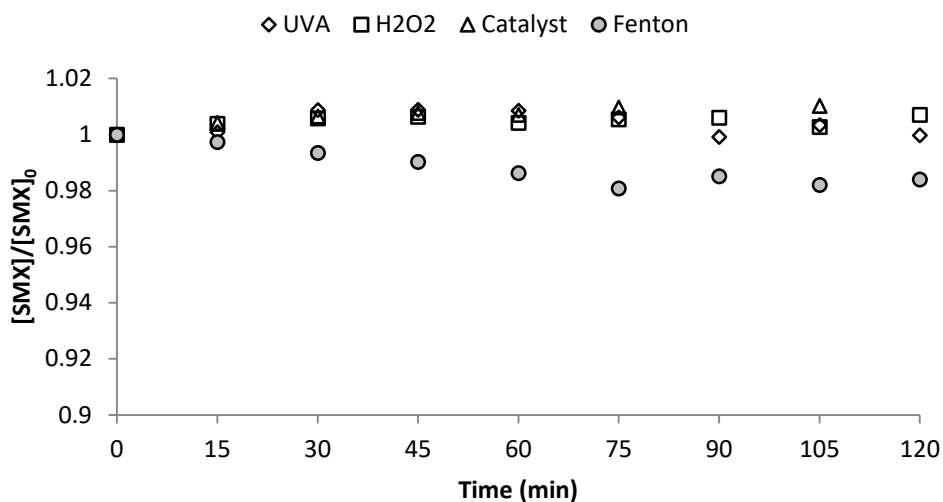
Figure 5.1. Effect of UV-A irradiation, H_2O_2 direct oxidation ([H_2O_2] = 20 mg L^{-1}), absorption over Fe(III)/alginate catalyst (0.5 g L^{-1} of catalyst in dry basis) and heterogeneous Fenton reaction ([H_2O_2] = 20 mg L^{-1}, 0.5 g L^{-1} of catalyst in dry basis) on a sample of distilled water containing 10 mg L^{-1} of SMX.

A very low degradation rate of sulfamethoxazole (1.02×10^{-3} mg L^{-1} min^{-1}) was measured when evaluating the effects of Fenton reaction. The initial iron species present in catalyst structure is Fe(III), which has very low catalytic activity, and as long as it is not reduced to +2 valence due to the effect of UV-A radiation, Fenton reaction cannot occur. This reduction from Fe(III) to Fe(II) is naturally produced in order to achieve the species equilibrium, but it is very slow if it is not boosted by applying UV-A light. According to that, less than 0.2 mg L^{-1} of SMX was depleted in two hours of experiment, with hydrogen peroxide consumption lower than 2 %.

5.3.2. Non-buffered water matrix experiments

In order to evaluate Fe(III)/alginate catalyst effectiveness depending on the initial sample pH a set of heterogeneous photo-Fenton reactions in distilled water adjusted to different pHs (2.0, 3.0, 5.5, 7.0, 9.0 and 11.0) was performed. This initial pH was adjusted by using HCl or NaOH depending on the needs, but samples were not buffered. 0.5 g L^{-1} of Fe(III)/alginate catalyst in dry basis and 20 mg L^{-1} of H_2O_2 were used and the reactor was irradiated for

120 minutes. Sulfamethoxazole removal, soluble iron concentration, H_2O_2 concentration, TOC and pH were monitored along the treatment.

Figure 5.2 shows the results of SMX removal along experiments performed at different initial pH. Results proved a very significant difference in the initial SMX degradation rate of those experiments performed at acidic pH (pH ≤ 3) compared to the ones performed at a higher pH. Thus, after 30 minutes of treatment, SMX was completely removed at $pH_0 = 2$ and $pH_0 = 3$, while only 20 % of initial SMX was depleted when working at pH higher than 5.5. After that time, degradation rates of samples with an initial pH higher than 3 increased on all working pH tested, except for $pH_0 = 11$, in which almost no degradation was detected.
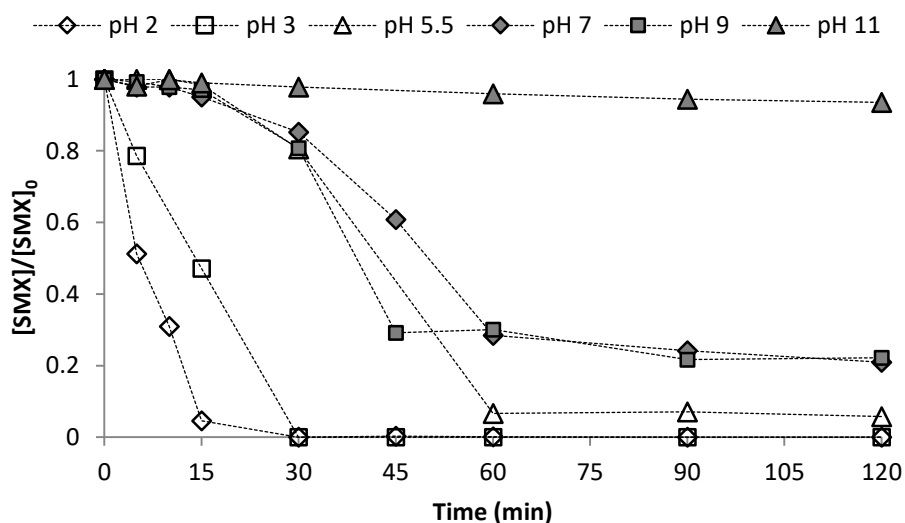
Figure 5.2. Sulfamethoxazole removal by heterogeneous photo-Fenton at different initial pH using 0.5 g L^{-1} (dry basis) of Fe(III)/alginate catalyst, $[H_2O_2]_0$ = 20 mg L^{-1}, $[SMX]_0$ = 10 mg L^{-1} and distilled water as matrix.

After 60 minutes (except experiment at $pH_0 = 9$), degradation of SMX barely stopped due to the reduction of H_2O_2 concentration (see Figure 5.2).

As it can be seen in Figure 5.3, H_2O_2 is consumed from the beginning of all experiments. Only the one conducted at $pH_0 = 11$ decreases with a lower rate. Since almost no SMX depletion was observed at $pH_0 = 11$, the H_2O_2 reduction observed can be attributed to the

disproportionation reaction of H_2O_2, which was produced almost at its maximum rate because pH was near its pK_a (11.6) [135].
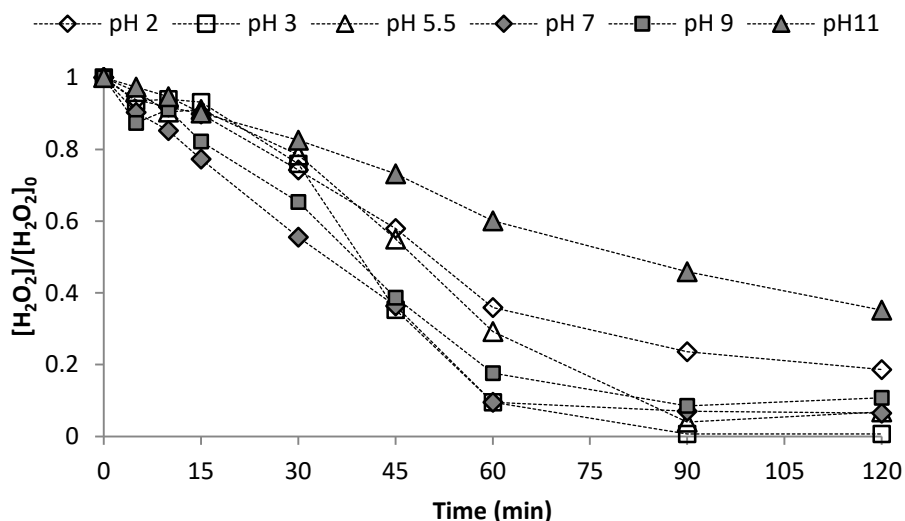
Figure 5.3. H_2O_2 consumption during heterogeneous photo-Fenton treatment at different initial pH using 0.5 g L^{-1} (dry basis) of Fe(III)/alginate catalyst, $[H_2O_2]_0$ = 20 mg L^{-1}, $[SMX]_0$ = 10 mg L^{-1} and distilled water as sample matrix.

   pH evolution measured along the experiments (Figure 5.4) shows the already known tendency of Fenton related reactions in the presence of organic compounds to acidify the samples due to the formation of carboxylic acids and other species that contribute to reduce the pH [136,137]. In this case, carboxylic acids can be formed mainly by the degradation of alginate chains, which contain carboxylic groups and can be released as soluble acidic by-products. It can be seen that the tendency of experiments at an initial pH over the pK_a of alginate is to reduce pH to an equilibrium value of approximately 4.2. Alginate pK_a has been reported to be in the range of 3.4-5.0 [102–104], depending on factors such as ionic strength, dissociation degree or mannuronic and guluronic acid proportion [101]. On the contrary, at the experiments that started at a pH lower than alginate pK_a it remained constant over time. This happens because the acidification effect of the by-products produced is negligible when the medium pH is below the pK_a of alginate.
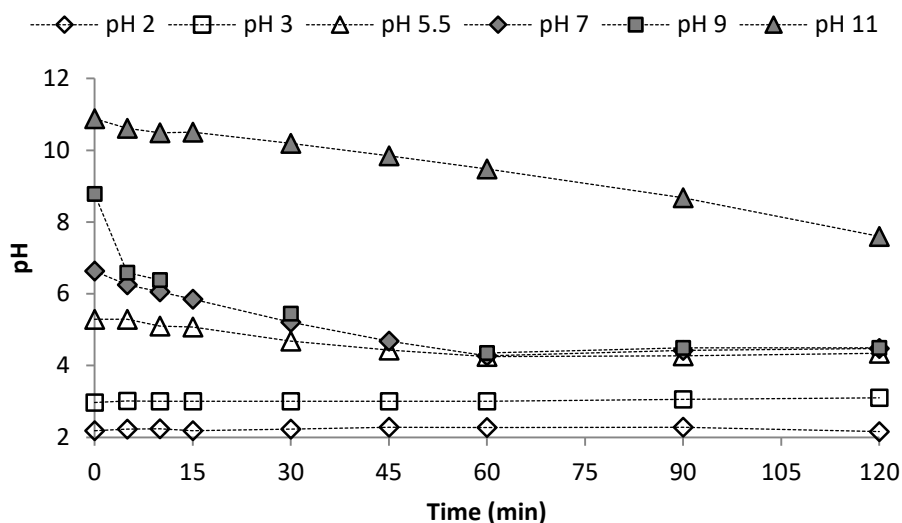
Figure 5.4. pH evolution during heterogeneous photo-Fenton treatment at different initial pH using 0.5 g L^{-1} (dry basis) of Fe(III)/alginate catalyst, [H$_2$O$_2$]$_0$ = 20 mg L^{-1}, [SMX]$_0$ = 10 mg L^{-1} and distilled water as sample matrix.

The monitoring of soluble iron and TOC can be found in Figure 5.5. Results show that iron started being released at some point during the experiments for all samples. In comparison with pH variation of the same experiments in Figure 5.4, it can be appreciated that iron release rate increases as the matrix pH drops near or below alginic acid pK$_a$ (3.4-5.0), after 45-60 minutes of reaction. It can also be seen that the experiments conducted at pH$_0$ = 2, pH$_0$ = 3 and pH$_0$ = 11 started releasing iron from the beginning of the experiments. Furthermore, the ones adjusted to pH$_0$ = 2 and pH$_0$ = 11 have a different performance, with a very high iron release rate (see explanation later on this section).This release of iron at pHs 2.0, 3.0, 5.5, 7.0, 9.0 and 11.0 supposed the lixiviation of approximately the 33%, 18%, 14%, 17%, 16% and 19% of the total iron content in catalyst, respectively.

Initial SMX spike provides an initial TOC of about 5 mg L^{-1}. Consequently, any increase of soluble organic carbon must come from the degradation and solubilization of alginate chains from the catalyst because it is the only possible TOC source. When looking at TOC results, a similar profile to iron release can be observed, except for the experiment

conducted at pH_0 = 2. In this case, the TOC release is not substantially higher than the one of the experiments conducted at different pH.
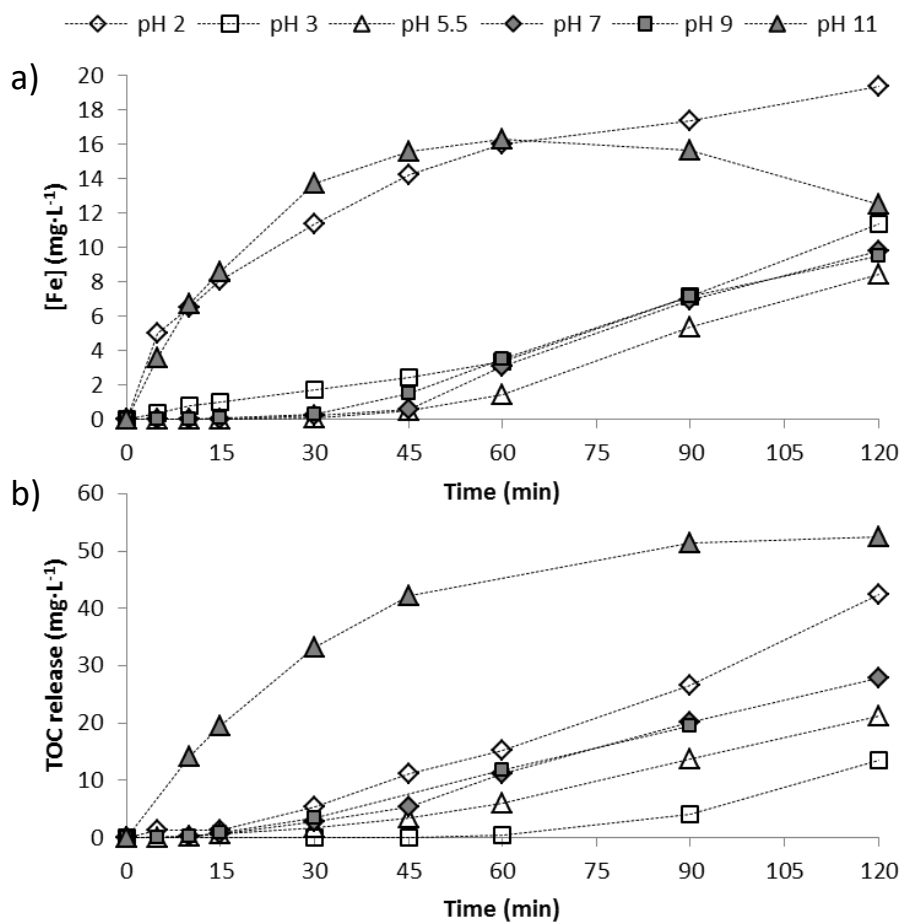
Figure 5.5. (a) [Fe] and (b) TOC release during heterogeneous photo-Fenton treatment at different initial pH using 0.5 g L^{-1} (dry basis) of Fe(III)/alginate catalyst, $[H_2O_2]_0$ = 20 mg L^{-1}, $[SMX]_0$ = 10 mg L^{-1} and distilled water as sample matrix.

From all these results in which the only different variable was the initial pH, it was observed that pH is the most important parameter affecting both performance and catalyst stability. There is a limit pH value beyond which the catalyst destabilizes and iron is released at a very high rate. According to the results, this lower limit is determined by alginate pK_a (pH = 3.4-5.0). Thus, experiments conducted at pH_0 = 2 and pH_0 = 3 owe the

antibiotic removal mainly to the contribution of homogeneous photo-Fenton reaction. Iron release to the reaction media occurs from the beginning of the process, thus SMX depletion occurs mainly on the bulk solution. On the other hand, reactions performed at an initial pH higher than pK_a of alginic acid (5.5, 7.0 and 9.0) started on the surface of the catalyst by the heterogeneous pathway but turned into homogeneous as reaction goes forward. The high H_2O_2 consumption during the first 30 minutes of reaction without a correlation in SMX removal suggests that the heterogeneous reaction produces a significant amount of HO· on the catalyst surface, but they are instantly consumed by the alginate itself, which would act as a strong hydroxyl radical scavenger. As it is a big chained organic molecule, HO· can be consumed in a partial organic complex oxidation without observing a significant increase of iron or TOC content in solution. This effect reduces the available HO· to oxidize SMX and other compounds in the bulk water solution. During this process, pH slowly decreases. When pH reaches pK_a of alginic acid, both effects contribute on the increase of iron release to the reaction media, turning the heterogeneous reaction into homogeneous progressively. The lower the pH is, the higher is the homogeneous contribution because a higher amount of iron can be found in solution. As pH is a logarithmic function of protons concentration, a reduction of 1 unit of pH implies a significant increase of proton, which have a direct relation to the iron release, as it will be explained deeply later in the "Fe(III)/alginate photo-Fenton mechanism" section. This justifies the significant variation from experiments at $pH_0 = 2$ and $pH_0 = 3$. Thus, after iron release starts due to pH reduction, higher SMX removal rates and an increase in iron and TOC release to the reaction media can be observed.

Finally, the different TOC release profiles observed at $pH_0 = 2$ and $pH_0 = 11$ experiments but not in the iron release ones suggest that the iron release mechanism of both experiments is not the same. In the experiment performed at $pH_0 = 11$, the simultaneous increase of TOC and iron from the beginning of the experiment suggests a mechanism in which the integrity of the catalyst is compromised. A side experiment introducing the catalyst in a high pH solution (pH = 13) for 6 hours was done. After this time, the catalyst totally solubilized becoming a source of soluble iron and TOC. This confirmed that Fe(III)/alginate catalysts are not stable at high pH. On the contrary, as TOC does not

79

suddenly increase when working at pH_0 = 2, the iron release follows the mechanism previously explained at acidic pH. As a result of this, the TOC profile at pH_0 = 2 is due to the release of Fe, which produces a high contribution of homogeneous photo-Fenton and degrades the alginate solubilizing it and increasing TOC value. On the contrary, at pH_0 = 11, alginate is directly solubilized due to high pH.

These results suggest a direct relation between iron and TOC release with pH, which becomes the most important parameter to evaluate and control when applying this kind of catalyst (Table 5.1). Barona and co-workers [138] obtained similar conclusions when studying the degradation of resorcinol using the solar photo-Fenton process. The mechanism initiated at neutral pH was mainly heterogeneous, with low degradation rates but the process turned more homogeneous as pH decreased, accelerating resorcinol degradation and hydrogen peroxide consumption.

Table 5.1. Main events observed when using Fe(III)/alginate heterogeneous catalyst applied for photo-Fenton at different pHs.

pH > pK_a		pH < pK_a	
No soluble Fe		Fe release because of acidic pH	
Heterogeneous reaction (low rate)		Homogeneous reaction (high rate)	
TOC release by catalyst oxidation (low rate)	Fe release by catalyst oxidation (low rate)	TOC release by catalyst oxidation (high rate)	Fe release by catalyst oxidation (high rate)

In order to compare the effectiveness of the heterogeneous catalyst with the conventional homogeneous photo-Fenton, experiments with distilled water at initial pHs of 3.0 and 5.5 were performed. The initial amount of iron used was equal to the final amount of soluble iron detected at the end of the ones performed by using the Fe(III)/alginate heterogeneous catalyst (11.3 mg L^{-1} and 8.4 mg L^{-1} respectively).

Figure 5.6 shows a higher SMX degradation rate on the homogeneous experiments respect the heterogeneous ones. Despite the final amount of soluble iron is the same at the end of the experiments, at the homogeneous ones, iron is available from the beginning of

the experiment, increasing significantly its effectiveness. Also, at homogeneous experiments the initial iron specie added into samples is Fe(II), which is the most active specie at photo-Fenton reaction, but on the heterogeneous ones, as it will be seen later on "Fe(III)/alginate photo-Fenton mechanism" section, the soluble iron species released are less active at photo-Fenton reaction.
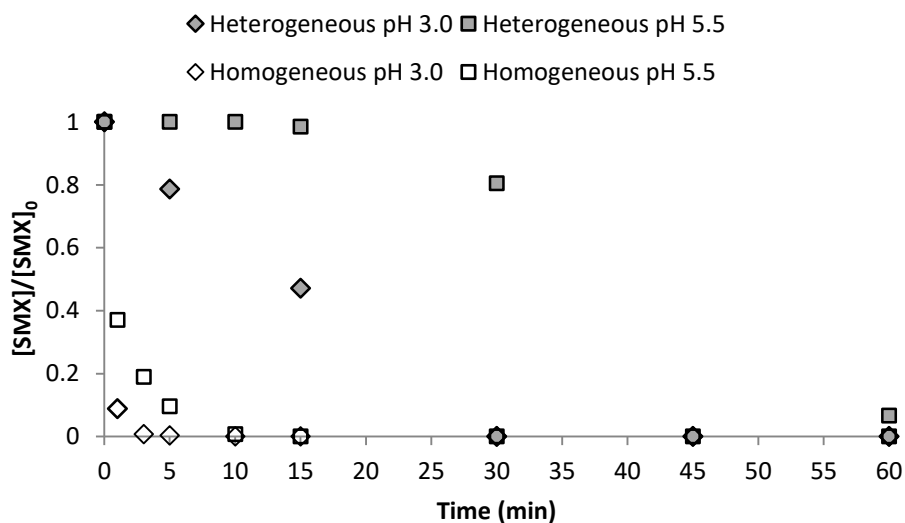
Figure 5.6. Sulfamethoxazole removal by heterogeneous and homogeneous photo-Fenton at pHs 3.0 and 5.5 using $[H_2O_2]_0 = 20$ mg L^{-1}, $[SMX]_0 = 10$ mg L^{-1}, distilled water matrix and 0.5 g L^{-1} (dry basis) of Fe(III)/alginate catalyst at the heterogeneous experiments and 11.3 mg L^{-1} and 8.4 mg L^{-1} of Fe(II) for the homogeneous experiments at pHs 3.0 and 5.5, respectively.

It can be conclude that the effectiveness of the heterogeneous catalyst reaction is less than the homogeneous one but the iron release produced by using the Fe/alginate catalyst allows a total removal of the reference compound at higher reaction times.

5.3.3. Slightly buffered water matrix experiments

Photo-Fenton experiments conducted at different initial pHs were repeated by changing the sample matrix into mineral bottled water. The natural buffering compounds in bottled water helped to keep the pH more constant along the experiments. This allowed a more accurate evaluation of the pH effect over soluble iron release during reaction.

Figure 5.7 shows the variation of concentration of SMX, TOC and H_2O_2 using bottled drinking water as sample matrix. It can be observed that the profiles are totally different than when using distilled water as sample matrix.
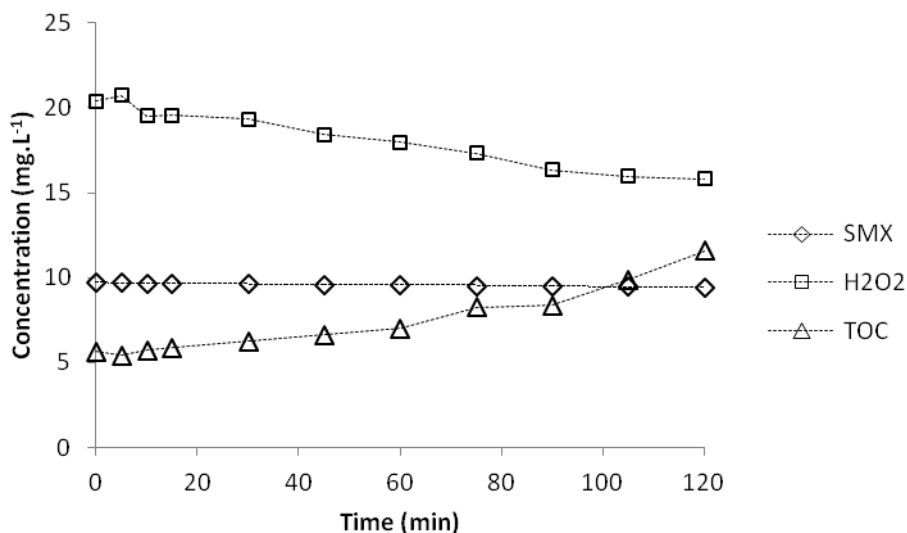
Figure 5.7. Sulfamethoxazole removal, H_2O_2 consumption and TOC release by heterogeneous photo-Fenton in bottled water matrix by using 0.5 g L^{-1} (dry basis) of Fe(III)/alginate catalyst, $[H_2O_2]_0$ = 20 mg L^{-1} , $[SMX]_0$ = 10 mg L^{-1}, pH_0 = 7.0.

The buffering effect of bottled drinking water matrix was able to keep pH barely constant, much above alginate pK_a (from 7.0 to 6.2), throughout the 120 minutes of the experiment, and almost no iron release was observed along the reaction (0.25 mg L^{-1} after 120 minutes of experiment). This ensured that iron was not released due to a pH decrease, as seen on previous experiments. Also, at this pH soluble iron does not present a significant photo activity.

With these results, it can be assured that the low SMX degradation rate of the experiment performed with bottled water (2.02×10^{-3} mg L^{-1} min^{-1}) was only due to the contribution of the heterogeneous photo-Fenton reaction. Thus, less than 0.4 mg L^{-1} was depleted after 2 hours of treatment, with a total H_2O_2 consumption of 4.8 mg L^{-1}. The

consumed H_2O_2 was turned into HO· through photo-Fenton process on the surface of the catalyst, but these HO· were rapidly consumed by the oxidation of the catalyst itself and the presence of carbonates in drinking water matrix, which are well known HO· scavengers [139,140]. Although there was a very small iron release from the degradation of catalyst surface, as long as the pH was not reduced because of the buffering properties of water, there was no significant amount of soluble iron and the homogeneous reaction was considered negligible.

Regarding TOC, a constant increase was produced because of the heterogeneous degradation of the catalyst itself on the surface, which solubilized. As the homogeneous reaction was minimized due to the low amount and low photoactivity of soluble iron at this pH, TOC in water was not mineralized.

5.3.4. Fe(III)/alginate photo-Fenton mechanism

From the results observed and taking into account literature on alginate complexes [112], an overall mechanism is proposed to explain the different pathways when Fe(III)/alginate catalyst is used to promote photo-Fenton reaction at circumneutral pH.

Fe(III)/alginate catalyst structure can be seen in Figure 5.8. Fe(III) cations can link up to three carboxyl groups of different alginate chains with ionic bonds, forming a solid gel structure.
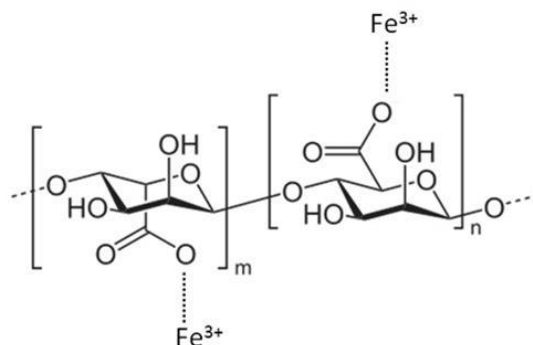
Figure 5.8. Fe(III)/alginate structure. Fe^{3+} cations can be seen bond to carboxylic groups in alginate chains.

When Fe(III) is coordinated with carboxylic groups on alginate, the proposed main reactions occurring on the surface of heterogeneous catalyst during the photo-Fenton process are expressed by equations (5.1) – (5.3):

Fe(III)/Alginate + H_2O_2 + hv → Fe(II)/Alginate + $HO_2\cdot$ + H^+ (Equation 5.1)

Fe(II)/Alginate + H_2O_2 → Fe(III)/Alginate + OH^- + $HO\cdot$ (Equation 5.2)

Fe(III)/Alginate + $HO_2\cdot$ → Fe(II)/Alginate + O_2 + H^+ (Equation 5.3)
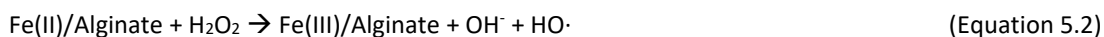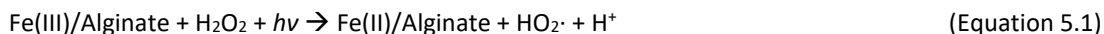
Equation 5.1 is supposed to occur on the irradiated surface of the catalyst. H_2O_2 gives an electron to Fe(III) linked to the alginate structure and turns into Fe(II). The charge variation on the cation produces the loss of a bond with a carboxylic group, and remains as an available binding site with a (-) charge. As a result of that reaction, an H+ and a $HO_2\cdot$ are formed (Figure 5.9).
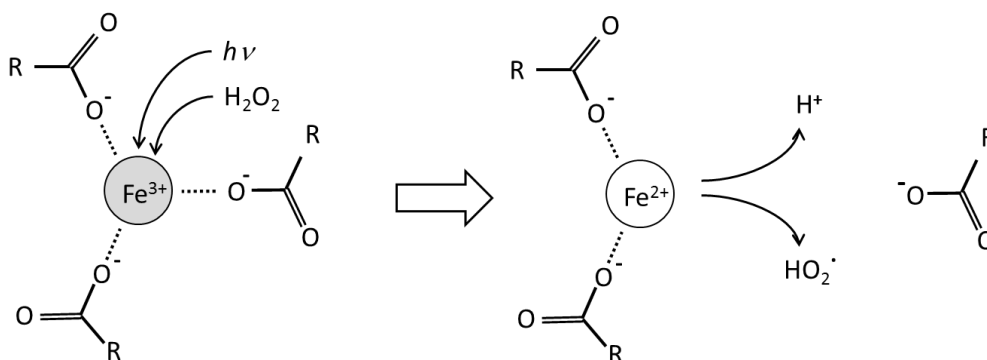
Figure 5.9. Equation 5.1 of Fe(III)/alginate applied as photo-Fenton heterogeneous catalyst.

Similarly, he reaction described in equation 5.2 can only be produced on the surface of the catalyst where there is contact from the aqueous phase containing H_2O_2 and the catalyst. Fe(II) cations linked on the alginate structure act as electron donors and oxidize to Fe(III) again by reacting with H_2O_2. As a result of that reaction, an OH^- and an $HO\cdot$ are formed (Figure 5.10). The resulting $HO\cdot$ from this reaction is the main oxidant specie

responsible of the degradation of both, alginate itself and organic substances in the bulk solution.
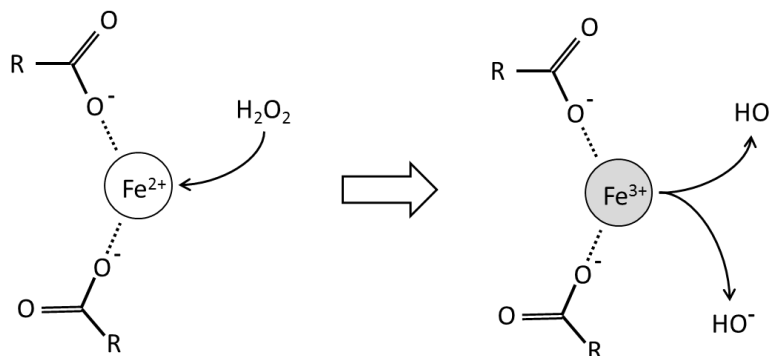
Figure 5.10. Equation 5.2 of Fe(III)/alginate applied as photo-Fenton heterogeneous catalyst.

In equation 5.3, $HO_2\cdot$ radical from equation 5.1 can react with Fe(III)/alginate acting as electron donor and reducing Fe(III) to Fe(II) again. As in equation 5.1, a bond with a carboxylic group is broken, and remains as an available binding site with a (-) charge. Fe(III), that have a (+) charge, could create a new bond with alginate structure linking an available binding site of (-) charge if this sites are available on carboxylic groups.
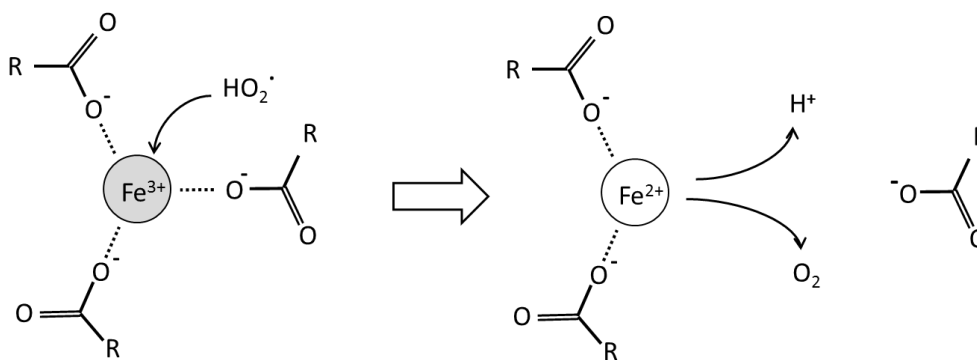
Figure 5.11. Reaction (5.3) of Fe(III)/alginate applied as photo-Fenton heterogeneous catalyst.

5.3.5. Iron release mechanism

Considering the proposed mechanism for Fe(III)/alginate when applied as photo-Fenton heterogeneous catalyst, the observed iron release during its application at acidic pHs can be explained.

According to literature alginate pK_a lies on a range between 3.4-5.0 [102–104]. Thus, below a pH of about 5.0, the alginate structure will tend to be on its protonated form.

When the reaction described in equation 5.1 occurs, if pH of the solution is under alginate pK_a, the resulting H^+ will tend to protonate that binding site of alginate, disabling it for future links while the pH remains below that pK_a (Figure 5.12).
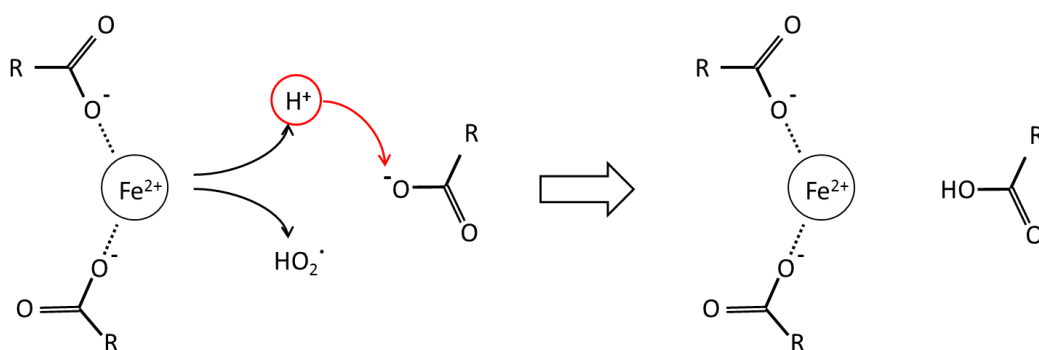
Figure 5.12. Result of equation 5.1 when sample pH is under alginate pK_a.

In the same way, when equation 5.3 occurs at a pH below 5.0, the carboxylic group that unlinks from iron can also be protonated cancelling itself for future links with available Fe.
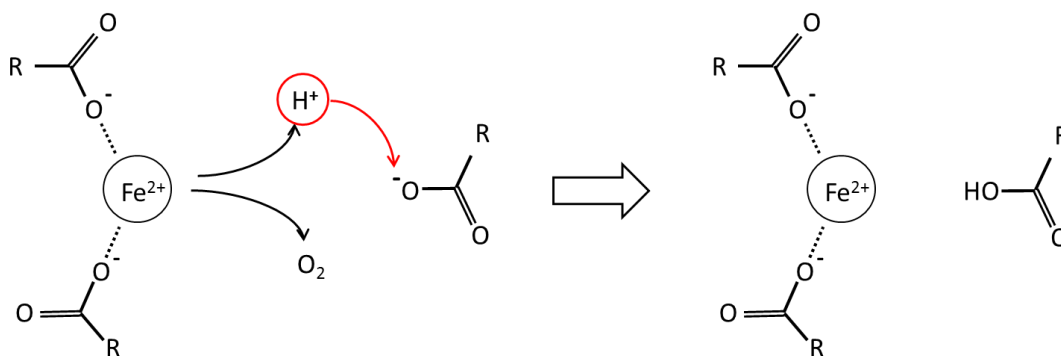
Figure 5.13. Result of equation 5.3 when sample pH is under alginate pK$_a$.

While pH is below 5.0, almost all binding sites will be protonated, so the iron tends to remain with a (+) charge and unbounded with alginate. The Fe(III) cations that are not able to establish a new connection with alginate because of the alginate protonation, can absorb the OH$^-$ anion resulting from equation 5.2, forming a FeOH^{2+} linked to the alginate structure (Figure 5.14).
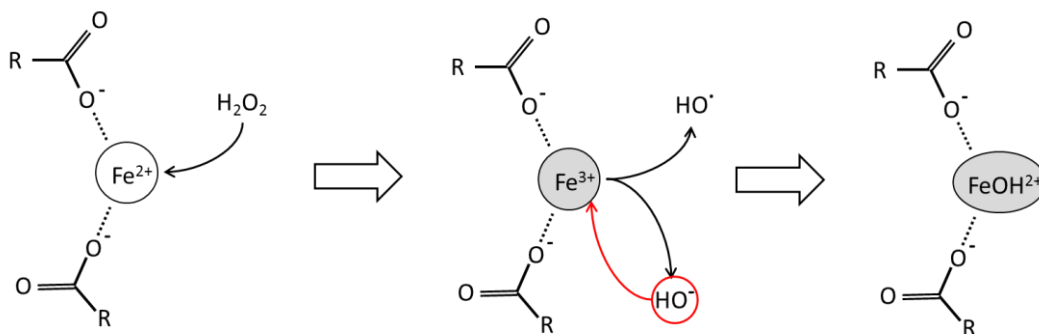
Figure 5.14. Result of equation 5.2 when sample pH is under alginate pK$_a$.

When reactions described in equations 5.1 and 5.3 are produced sequentially at a pH under pK$_a$, binding points in alginate chains continue being cancelled and the previously formed Fe(OH)$^{2+}$ turns into Fe(OH)$^+$, which is bond to alginate only by one single link.

87
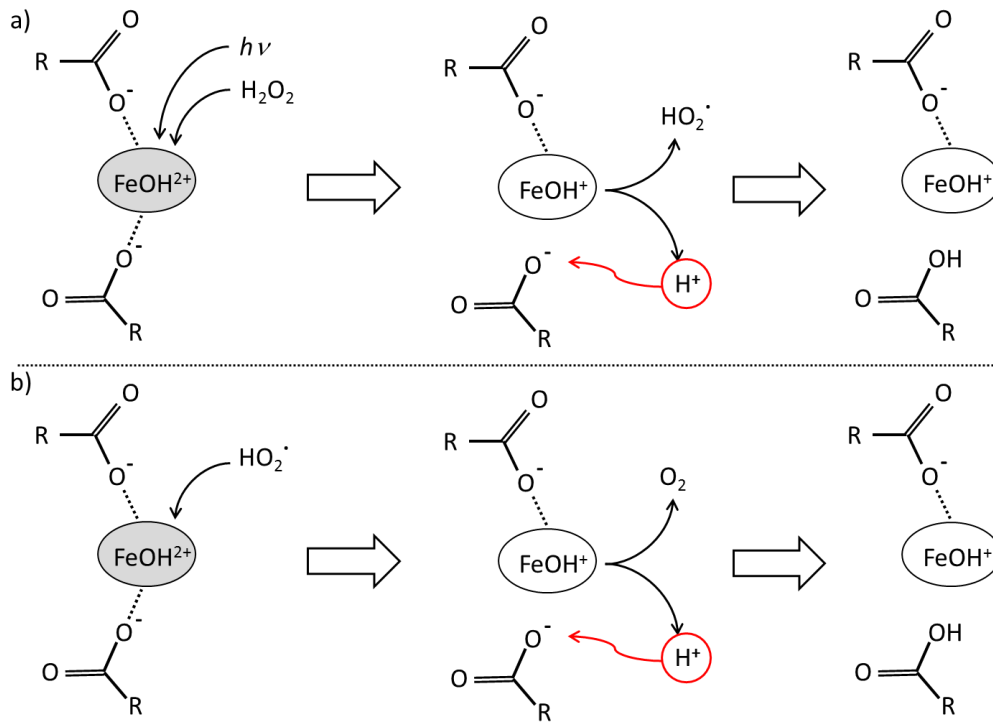
Figure 5.15. a) Equation 5.1 and b) equation 5.3 occurring to an Fe^{3+} which already had accepted an OH$^-$ due to equation 5.2 at pH below alginate pK$_a$.

If equation 5.2 occurs to an Fe(II) that has already accepted a OH-, Fe(OH)$_2^+$ is formed and only one link keeps iron bond to alginate (Figure 5.16).
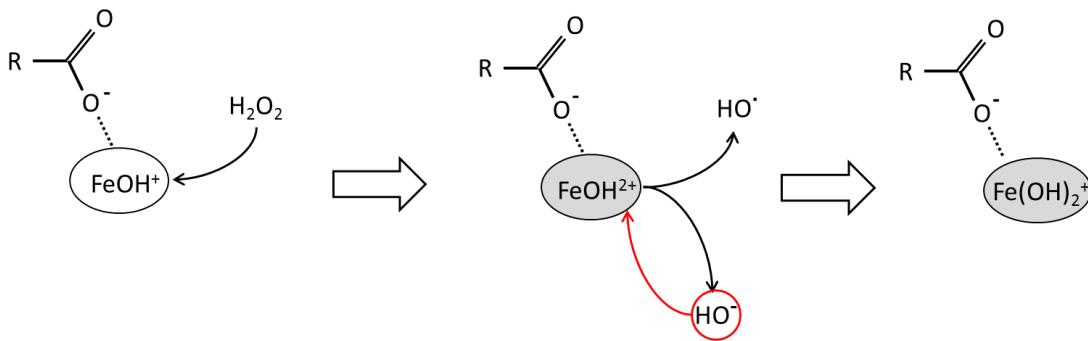
Figure 5.16. Result of equation 5.2 occurring to an Fe^{2+} which already had accepted an OH$^-$ when sample pH is under alginate pK$_a$.

At this point, when equations 5.1 or 5.2 are produced again, the last bond of iron and alginate is broken and an $Fe(OH)_2^+$ cation is released to the medium, generating a soluble iron source
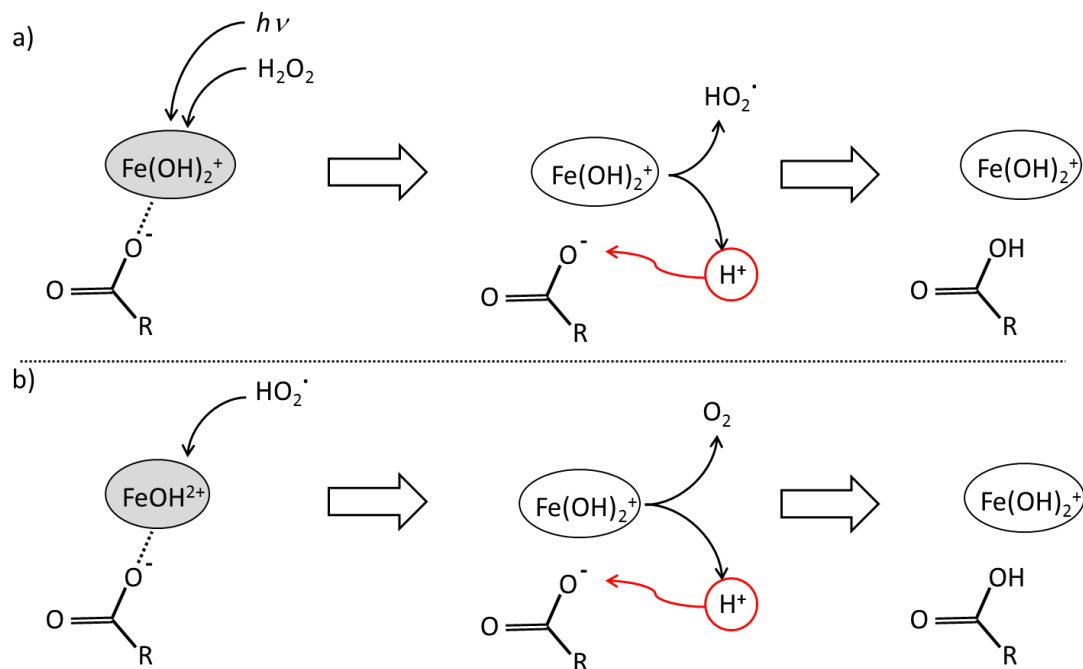
Figure 5.17. a) Equation 5.1 and b) equation 5.3 occurring to an Fe^{3+} which already had accepted two OH^- due to equation 5.2 at pH below alginate pK_a.

As a result of this iron release, apart from the surface reactions, homogeneous photo-Fenton reactions involving soluble iron occur (Equations 5.4-5.6) [30]. These reactions increase the HO· generation rate, accelerating catalyst destabilization.

$Fe^{2+}(aq)+H_2O_2 \rightarrow Fe^{3+}+OH^-+HO·$ (Equation 5.4)

$Fe^{3+}(aq)+H_2O_2 \rightarrow Fe^{2+}+HO_2·+H^+$ (Equation 5.5)

$Fe^{3+}(aq)+H_2O + hv \rightarrow Fe^{2+}+HO·+H^+$ (Equation 5.6)

Reactions described in equations 5.2, 5.4 and 5.6 involve the generation of hydroxyl radicals, which are able to oxidize almost every organic compound, but also the alginate organic chains which form the catalyst. Alginate solubilization due to oxidation produces an even higher release of iron and TOC, accelerating the radical generation exponentially due to the homogeneous photo-Fenton reaction. The increasing amount of soluble iron ends turning the homogeneous pathway as the main cause of HO· production.

According to this mechanism and the experimental results, it can be observed that there is always iron and TOC release due to the attack of HO· to the catalyst structure itself, but the contribution of this effect is negligible in comparison to the one produced by the homogeneous reaction triggered by soluble iron released when medium pH is under alginate pK_a.

5.3.6. Sequential reutilization

The recyclability of the catalyst is very important for practical application. Sequential reutilizations of the catalyst were performed along four experiments using the same initial conditions as previous experiments ($[H_2O_2]_0$ = 20 mg L^{-1}, $[SMX]_0$ = 10 mg L^{-1}, pH_0 = 5.5, 0.5 g L^{-1} of Fe(III)/alginate catalyst in dry basis). The catalyst was recovered by filtration between experiments and rinsed with abundant distilled water. Afterwards, it was reused in the successive SMX degradation experiments.

Performance of Fe(III)/alginate catalyst reutilization for SMX removal and iron and TOC release can be observed in Figure 5.18.

As can be observed on SMX removal profiles, the initial degradation rate on the freshly prepared catalyst experiment is very low. After some minutes of treatment, reaction rate increases considerably. On the second, third and fourth run, this initial lag on SMX removal cannot be observed. After this first use, sequential experiments have similar degradation rate profiles, which slightly reduce after every reutilization.
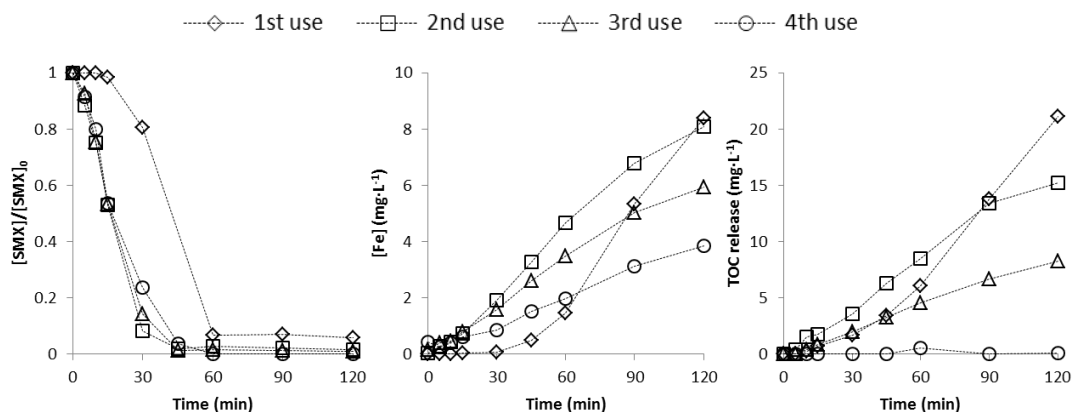
Figure 5.18. SMX removal, iron concentration and TOC release on 4 consecutive photo-Fenton experiments reutilizing the catalyst using 0.5 g L^{-1} (dry basis) of Fe(III)/alginate catalyst, [H$_2$O$_2$]$_0$ = 20 mg L^{-1}, [SMX]$_0$ = 10 mg L^{-1}, pH$_0$ = 5.5.

The first catalyst use also presents an initial delay on iron release, unlike the following ones, which start releasing iron from the beginning. Moreover, each consecutive cycle releases a lower amount of iron to the medium. The TOC release with catalyst recycling also decreased but at a higher extend, thus in the last run almost no TOC release was observed.

This behavior is explained taking into the account the mechanism of iron and TOC released introduced previously. When the first experiment starts, iron in the catalyst is all on the Fe(III) form. Thus, UV-A light needs to turn Fe(III) into Fe(II) before starting the production of the oxidative species. On the following experiments, catalyst recovered from a previous experiment has both, Fe(III) and Fe(II) on its coordinated structure with alginate, so the photo-Fenton process takes place from the beginning of the experiment, promoting the mechanisms of iron and TOC removal explained previously.

The TOC release produces a gradual reduction of catalyst size (from an initial average diameter of 2.5 mm to 1.6 mm after the fourth use), which means a reduction of the reaction surface on the catalyst. This surface reduction along experiments leads to a reduction of iron and TOC release rates, which are directly related to it.

This effect can also be observed in SMX removal but is less influenced than the other two parameters.

5.4. CONCLUSIONS

Fe/alginate based catalysts can be found in literature as heterogeneous catalysts for Fenton reactions. This work demonstrates that the contribution of homogeneous catalysis on the performance of heterogeneous Fe(III)/alginate photo-Fenton process strongly depends on pH. Solution pH has proven to be the most important parameter on the stability of Fe(III)/alginate catalysts, together with the self-degradation of the catalyst structure promoted by the hydroxyl radicals. A destabilization mechanism in which iron is released to the medium has been proposed according to sample pH and alginate carboxylic groups' pK_a.

The heterogeneous photo-Fenton catalytic activity of Fe(III)/alginate spheres has been proved but its efficiency on SMX removal was low because alginate itself acts as an strong scavenger of the HO· produced. The overall antibiotic removal efficiency increased significantly at lower pHs because the reaction mechanisms shift from heterogeneous to homogeneous due to the release of significant amounts of Fe. It becomes clear that when working at pH 5.0 or below, the main HO· production pathway is the homogeneous, leaving the heterogeneous one as a minor contribution. Regarding catalyst reutilization, it was also demonstrated that Fe(III)/alginate catalyst can be sequentially reused with a small reduction on the global efficiency after each reutilization (except the first use, that has a delay), produced by the catalyst size reduction.

6. Fe(III)/alginate catalyst applied for disinfection

6.1. INTRODUCTION

According to previous results, the heterogeneous activity as photo-Fenton catalyst of Fe(III)/alginate was confirmed. Even so, the exponential increase of homogeneous photo-Fenton due to the release of iron from catalyst makes the catalyst shortly recommended if soluble iron is not desired in solution.

Despite the inevitable release of iron after some time of reaction due to both, acidic pH release and direct oxidation of the catalyst, on the initial stage of reaction the amount of soluble iron is low and can be considered negligible, so the heterogeneous oxidation pathway is the most significant. For this reason, an application which required low amounts of HO· produced for its success was considered in order to apply Fe(III)/alginate catalyst on mild conditions avoiding a major iron release.

Disinfection of waters with low organic loads require the use of lower amounts of reactive oxidant species to achieve the total water disinfection due to the less competence of organic matter [141]. These kinds of samples are mainly those aimed to human consumption, as tap water supply or bottled drinking water supply. For this reason, the treatments applied for disinfection must satisfy the requirement of not producing any by-product and not affecting the effluent in any way that could harm human health.

Alginate is a non-hazardous and edible substance, commonly used in the pharmaceutical industry as a binding agent in tablets [95,96] and also in the food industry as a thickener or for gelification processed [97–99]. As iron is also not harmful for human health in the working concentrations, the resulting Fe(III)/alginate catalyst is a very suitable candidate to conduct heterogeneous photo-Fenton reaction intended for disinfection of drinking water and other human consumption effluents.

On this chapter, a study of Fe(III)/alginate used as heterogeneous catalyst for photo-Fenton reaction at circumneutral pH has been done. For this purpose, the reactions were conducted in mild conditions to minimize iron release while ensuring enough HO· production to disinfect the samples.

Coliform bacteria *Escherichia Coli* was used as reference of disinfection because it is the most usual microorganism referenced in legislation for the microbiological control of waters intended for human consumption (Council Directive 98/83/EC).

An experiment by using the bacteriophage virus M4 as target microorganism was also performed in order to evaluate the effectiveness of the disinfection process for a more resistant microorganism than *Escherichia Coli*. This microorganism was isolated by the *Microbiology of water related to the health* group (*MARS*) from the Microbiology Department of the University of Barcelona. This bacteriophage virus was found and cultured from the survivors of experiments performed with real wastewater submitted to solar photo-Fenton treatments [33], so it was considered a strain very resistant to AOPs and a possible disinfection indicator.

6.2. MATERIALS AND METHODS

6.2.1. Reactor set-up

In order to reduce the intensity of photo-Fenton reaction, a 2 L batch reactor incorporating a single 8W UV-A lamp (λ_{max} = 365 nm) with a total emission of 1.58×10^{-6} Einstein s^{-1} was used. The reactor was magnetically stirred and temperature was controlled at 25°C by means of a jacket connected to a thermostatic bath. A more detailed explanation about the experimental reactor can be found in chapter 3, "Materials and Methods".

6.2.2. Samples preparation

Escherichia Coli and M4 bacteriophage virus were cultured in a low TOC culture media just before the experiment and then spiked into a 2 L distilled water or bottled water matrix to the desired initial concentration. A more detailed explanation about *Escherichia Coli* and M4 bacteriophage virus culturing process can be found in chapter 3, "Materials and Methods".

6.2.3. Catalyst synthesis

Fe(III)/alginate catalyst used in this chapter was prepared according to the standard method previously developed. A detailed description about it can be found in chapter 3, "Materials and Methods".

6.3. RESULTS AND DISCUSSION

6.3.1. Blank experiments

Before studying catalyst effectiveness for the inactivation of *Escherichia Coli*, blank experiments were performed to evaluate the effect of direct oxidation of H_2O_2, UV-A irradiation and absorption in Fe(III)/alginate catalyst per separate. A fourth blank experiment by combining Fe(III)/alginate catalyst and H_2O_2 in absence of UV-A light was also performed to evaluate the possible contribution of Fenton reaction to the process.

Escherichia Coli was cultured in a low TOC culture media and then spiked into a 2 L sample of distilled water to an approximate initial concentration of 5 Log (10^5 CFU mL^{-1}) on each of the four experiments. The first blank experiment was carried out by adding only H_2O_2 to an initial concentration of 20 mg L^{-1} (without UV-A light nor catalyst). The second one was performed by activating the UV-A lamp of the experimental reactor (without the addition of H_2O_2 nor catalyst). The third one was carried out by adding 0.5 g L^{-1} of the catalyst in dry basis (without UV-A radiation nor H_2O_2). The last one was done by adding 0.5 g L^{-1} of the catalyst in dry basis and an initial concentration of 20 mg L^{-1} of H_2O_2.

95

Results on Figure 6.1 confirmed that UV-A irradiation, H_2O_2 direct oxidation nor absorption at the conditions selected for experimentation did not produced a significant effect over Escherichia Coli population. Also, heterogeneous Fenton reaction by using Fe(III)/alginate catalyst was proven to be negligible.

◇ UVA   ☐ H2O2   △ Catalyst   ⊙ Fenton
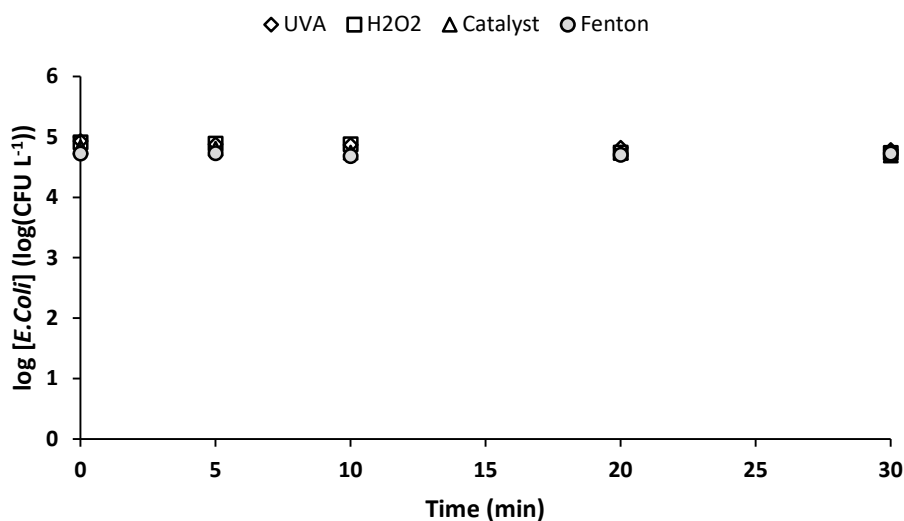
Figure 6.1. Effect of UV-A irradiation, H_2O_2 direct oxidation ([H_2O_2] = 20 mg L^{-1}), absorption over Fe(III)/alginate catalyst (0.5 g L^{-1} of catalyst in dry basis) and heterogeneous Fenton reaction ([H_2O_2] = 20 mg L^{-1}, 0.5 g L^{-1} of catalyst in dry basis) on a sample of distilled water containing 10^5 CFU L^{-1} of *Escherichia Coli*.

6.3.2. *Escherichia Coli* inactivation experiments

In order to evaluate Fe(III)/alginate catalyst effectiveness on *Escherichia Coli* inactivation two heterogeneous photo-Fenton reactions by using 0.5 g L^{-1} of Fe(III)/alginate catalyst in dry basis, 20 mg L^{-1} of H_2O_2 and 10^4 CFU L^{-1} of *Escherichia Coli* were performed using distilled water and bottled drinking water as sample matrixes. Samples were irradiated for 60 minutes. *Escherichia Coli* inactivation, soluble iron concentration, H_2O_2 concentration, TOC and pH were monitored along the treatment.

Results (Figure 6.2) show that using both, distilled and bottled drinking water matrixes produces the inactivation of *Escherichia Coli*. When using distilled water matrix an initial population of 1.1 x 10^4 CFU mL^{-1} of *Escherichia Coli* was totally inactivated before 30 min

with an approximated logarithmic inactivation rate of 0.16 log [*E.Coli*] min^{-1}. The experiment performed by using bottled water as matrix, with an initial population of 1.4 x 10^4 CFU mL^{-1} of *Escherichia Coli*, showed a lower inactivation rate (0.07 log [CFU mL^{-1}] min^{-1}) and also was not able to achieve the total disinfection after 60 min of experiment. At the end of this experiment, 14 CFU mL^{-1} of *Escherichia Coli* were still detected.
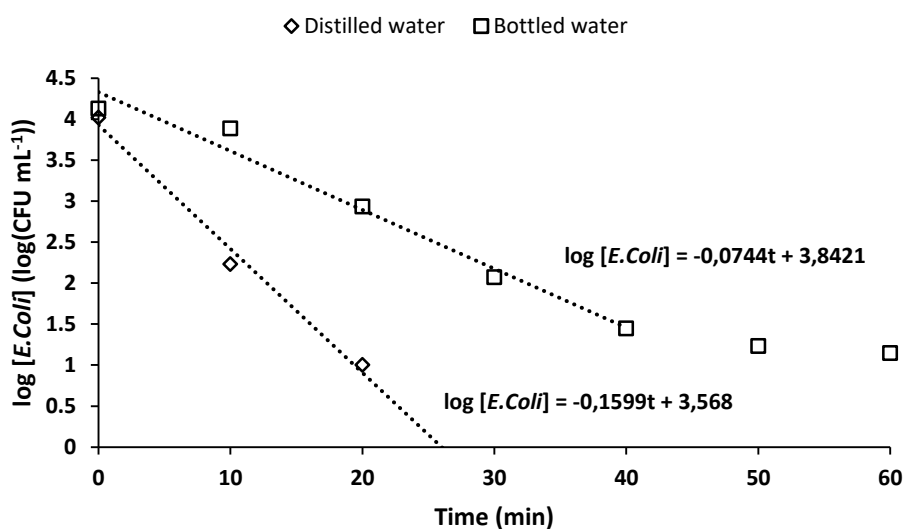
Figure 6.2. *Escherichia Coli* **inactivation by heterogeneous photo-Fenton in distilled water and drinking bottled water matrixes. Experimental conditions: 0.5 g L^{-1} of Fe(III)/alginate catalyst (dry basis) and 20 mg L^{-1} of H$_2$O$_2$.**

Figure 6.3.a shows the values of iron concentration measured along both experiments. It can be seen that the use of distilled water produced an iron release of 0.25 mg L^{-1} after 60 min. Even so, total disinfection was achieved before iron was firstly detected at 40 min ([Fe] = 0.04 mg L^{-1}) so it complied with the 0.2 mg L^{-1} soluble iron limit in legislation when water is intended for human consumption (Council Directive 98/83/EC). The start of iron leaching was produced when sample pH reduced from pH 5.14 at 30 min to pH 4.89 at 40 min. This agrees to the already proposed mechanism for iron release explained in chapter 5, which supposes that iron starts being released when pH goes below alginate pK$_a$ (4.2-5.0). Experiment performed by using drinking bottled water matrix did not produce any

measurable amount of soluble iron for 60 min of experiment. In this case, pH kept barely constant near 7.2, which was the initial pH of the sample.
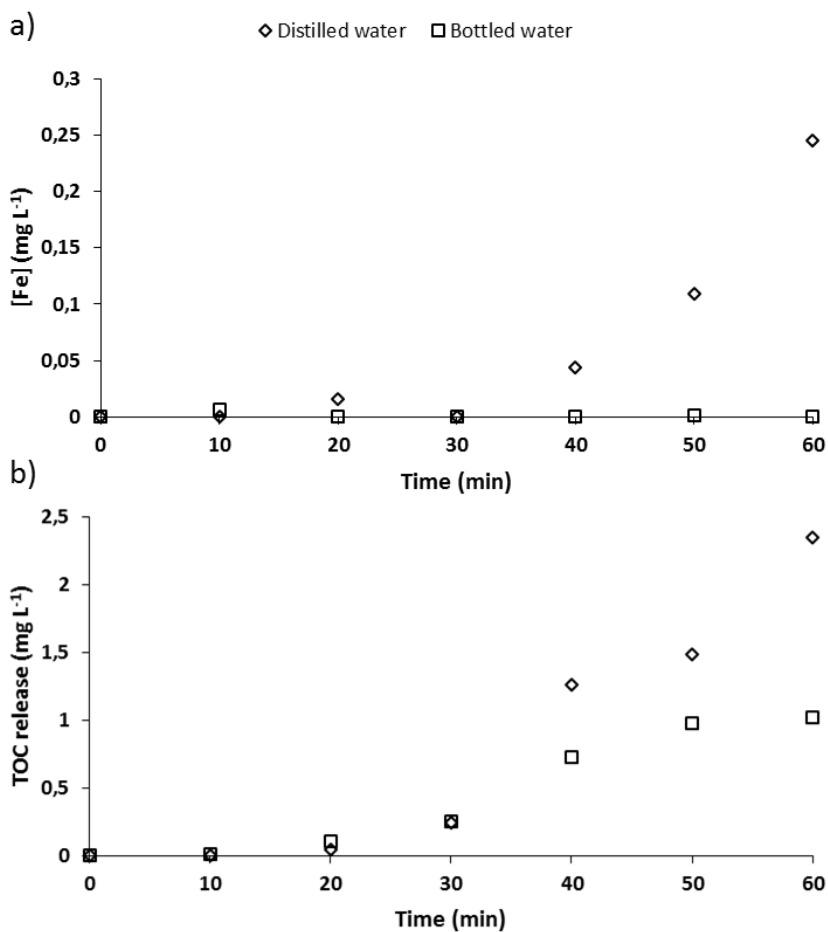
Figure 6.3. a) [Fe] and b) TOC release measured along two heterogeneous photo-Fenton disinfection experiments by using distilled water and drinking bottled water as matrixes. Experimental conditions: 10^4 CFU mL^{-1} of Escherichia Coli, 0.5 g L^{-1} of Fe(III)/alginate catalyst (dry basis) and 20 mg L^{-1} of H_2O_2.

Figure 6.3.b. shows the TOC release produced during reaction for the experiment performed by using distilled water as sample matrix (TOC_0 = 1.7 mg L^{-1}) and the one by using bottled drinking water (TOC_0 = 1.9 mg L^{-1}). Both initial TOC values include the TOC added by the culture medium in which the microorganisms where cultured and spiked into the matrix. A TOC increase can be observed in both experiments' profiles. TOC coming from *Escherichia*

Coli was considered as its maximum before the experiment. Thus, this increase is mainly attributed to the oxidation of alginate in catalyst surface due to the heterogeneous photo-Fenton reaction. A similar increasing profile can be observed for both matrixes till 30 min of reaction. After this time, TOC of experiment performed with distilled water matrix increased its TOC release rate to 0.066 mg L^{-1} min^{-1}, while the one performed with bottled water increased to 0.036 mg L^{-1} min^{-1}. This agrees with the Fe(III)/alginate iron release mechanism. At this time, iron started being released due to pH decay when using distilled water matrix. This increase of soluble iron triggered homogeneous photo-Fenton reaction, which attacked more intensely the catalyst surface, producing a higher TOC release than when using bottled drinking water as sample matrix.
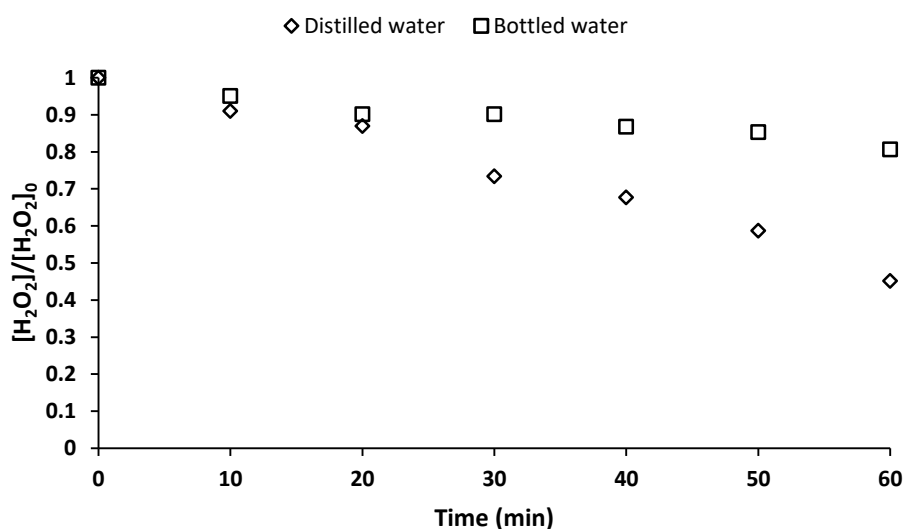
Figure 6.4. [H$_2$O$_2$] measured along two heterogeneous photo-Fenton disinfection experiments by using distilled water and drinking bottled water as matrixes. Experimental conditions: 10^4 CFU mL^{-1} of Escherichia Coli, 0.5 g L^{-1} of Fe(III)/alginate catalyst (dry basis) and 20 mg L^{-1} of H$_2$O$_2$.

Results of H_2O_2 consumption on Figure 6.4 show a similar initial consumption rate ($\approx$ 0.1 mg L^{-1} min^{-1}) for both experiments, using distilled water and drinking bottled water as sample matrixes. Even so, after 30 min of experiment, the one performed by using distilled water as matrix presented a subtle increase, which can also be related to the incipient iron

release and the start of homogeneous photo-Fenton reaction, as it happened with iron and TOC.

6.3.3. M4 bacteriophage virus inactivation experiment

In order to check the efficiency of Fe(III)/alginate as heterogeneous photo-Fenton catalyst when applied to disinfection of microorganisms more resistant than Escherichia Coli, M4 bacteriophage virus was selected as target microorganism.

The experiment was conducted on the same conditions as the previous *Escherichia Coli* ones, but spiking 5.3×10^4 PFU mL^{-1} of M4 virus at the beginning of the experiment ($[H_2O_2]_0 = 20$ mg L^{-1}, 0.5 g L^{-1} of Fe(III)/alginate catalyst, $pH_0 = 7.0$, bottled drinking water matrix).

Results of M4 bacteriophage virus inactivation in comparison to the previously *Escherichia Coli* ones can be observed on Figure 6.5.

A reduction of about 2 logarithmic units, from 5.3×10^4 PFU mL^{-1} to 7.5×10^2 PFU mL^{-1}, in 40 min was observed. Compared to the Escherichia Coli inactivation profile, the disinfection process achieves a lower reduction when applied to M4, which is consistent with the higher resistance of M4 virus to AOPs. Thus, Fe(III)/alginate catalyst can be considered effective for the inactivation of M4, but its efficiency is not enough to achieve total disinfection. Even so, the process is able to eliminate the 98.5% of the initial M4 virus in samples. The softening of the inactivation profile as time advances suggests that an increase of the treatment time will not be followed linearly by an increase in M4 virus inactivation. This effect could be the result of the competence of alginate for HO·, which reduces the available amount of the oxidant specie by the direct degradation of the catalyst and the increasing TOC that results from it.
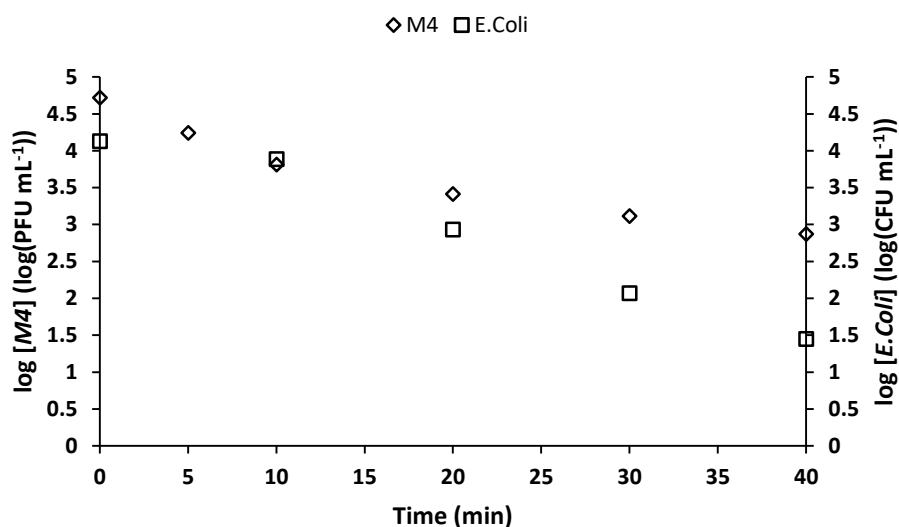
Figure 6.5 M4 bacteriophage virus and Escherichia Coli inactivation by heterogeneous photo-Fenton in bottled drinking water matrix. Experimental conditions: $[M4]_0 = 5.3 \times 10^4$ PFU mL^{-1}, $[E.Coli]_0 = 1.4 \times 10^4$ CFU mL^{-1}, 0.5 g L^{-1} of Fe(III)/alginate catalyst and 20 mg L^{-1} of H_2O_2.

Considering that this virus is specifically resistant to this kind of processes, the results can be considered as a reference to compare with other experimental conditions and AOPs if applied to disinfection, which could solve the difficulties of comparison when using *Escherichia Coli* as reference due to its high sensitivity to oxidative processes.

6.4. CONCLUSIONS

As seen on this chapter, Fe(III)/alginate catalyst is able to inactivate Escherichia Coli when applied as photo-Fenton heterogeneous catalyst.

Despite the iron release drawback, when working in mild reaction conditions by reducing UVA irradiation, iron release rate was highly reduced in distilled water and totally avoided in bottled drinking water. Thus, after 30 min of experiment in distilled water, total inactivation of Escherichia Coli was achieved and iron concentration in samples was still under the legislation limit value for waters intended for human consumption (0.2 mg L^{-1}), which made it suitable for this purpose.

Even so, when tested in bottled drinking water, inactivation rate was reduced in comparison to the experiment using distilled water as matrix. In this case, total disinfection was not achieved in 60 min of experiment.

The inactivation experiment performed by using M4 bacteriophage virus revealed that the applied conditions are still not enough intense to ensure the total disinfection of resistant microorganisms.

Considering the global results, Fe(III)/alginate catalyst can be applied for disinfection and iron leaching can be controlled to ensure compliance with legislation, but experimental conditions must be adjusted on each case according to the effluent to be treated and the microorganisms it contains. Compared to other disinfection technologies, the non-harmful nature of alginate catalysts supposes an advantage when applied to waters intended for human consumption if iron leaching and TOC release are minimized. Even so, its application to waters with higher organic loads, as wastewater, requires the increase of HO· production rate, what as seen on chapter 5 triggers the homogeneous reaction and produces a high TOC and iron release.

7. Fe(III)/alginate catalyst modifications

7.1. INTRODUCTION

As the objective of heterogeneous catalysts is to avoid the homogeneous reaction by performing it on the surface of the catalyst, it was considered important to find a way to stabilize the iron release previously observed when applying Fe(III)/alginate as photo-Fenton heterogeneous catalyst.

The use of cerium (Ce) on iron-based catalysts have been proved as effective on Fenton-like reactions [92,120,142], which made it a suitable candidate for the improvement of the catalytic efficiency of the basic Fe(III)/alginate catalyst. Cerium is a specie with a Fenton-like performance very similar to Fe(II)/Fe(III) [143], so the Fe/alginate mechanism could be adapted for cerium.

$$Ce\ (IV)/Alginate + H_2O_2 + h\nu \rightarrow Ce\ (III)/Alginate + HO_2\cdot + H^+ \qquad \text{(Equation 7.1)}$$

$$Ce\ (III)/Alginate + H_2O_2 \rightarrow Ce\ (IV)/Alginate + OH^- + HO\cdot \qquad \text{(Equation 7.2)}$$

$$Ce\ (IV)/Alginate + HO_2\cdot \rightarrow Ce\ (III)/Alginate + O_2 + H^+ \qquad \text{(Equation 7.3)}$$
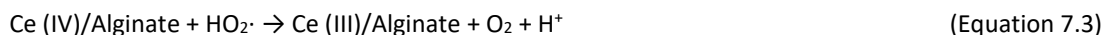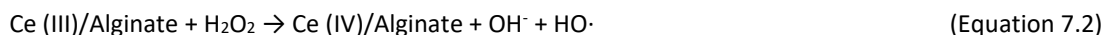
Ionically cross-linked alginate hydrogels have efficiently encapsulated cells, proteins, and drugs with different biomedical applications, among others. Entrapping zero valent iron (ZVI) and TiO$_2$ was also considered as a promising modification for the improvement of the catalytic activity of Fe(III)/alginate catalyst at circumneutral pH. As it can be found in literature [144,145], Fe^0 gets oxidized in the presence of an oxidative specie like O$_2$ (Equation 7.5) or at acidic pH (Equation 7.4), but also by stronger oxidant as H$_2$O$_2$ (Equation 7.6).

$$Fe^0 + 2\,H^+ \rightarrow Fe^{2+} + H_2\uparrow \qquad\text{(Equation 7.4)}$$

$$2Fe^0 + O_2 + H_2O \rightarrow 2\,Fe^{2+} + 4\,OH^- \qquad\text{(Equation 7.5)}$$

$$Fe^0 + H_2O_2 + 2\,H^+ \rightarrow Fe^{2+} + 2H_2O \qquad\text{(Equation 7.6)}$$

According to these reactions, alternative pathways to obtain the photoactive Fe^{2+} specie can be triggered by ZVI. This specie is slowly released as soluble iron that contributes to homogeneous photo-Fenton, which in the case of Fe/ZVI/alginate catalyst should increase the global efficiency as well.

Likewise, TiO_2 particles have been applied successfully for the treatment of water due to its own oxidation mechanism (Equations 7.7-7.11) when it is irradiated by sunlight or UV-A light [146–151]. It is expected that, if iron supported alginate beads are used to entrap TiO_2 particles the photocatalytic pathway for the generation of oxidative species would be produced simultaneously to photo-Fenton reactions increasing the global effectiveness of the catalyst.

$$TiO_2 + h\nu \rightarrow e_{CB}^- + h_{VB}^+ \qquad\text{(Equation 7.7)}$$

$$h_{VB}^+ + H_2O \rightarrow HO\cdot + H^+ \qquad\text{(Equation 7.8)}$$

$$e_{CB}^- + O_2 \rightarrow O_2^-\cdot \qquad\text{(Equation 7.9)}$$

$$O_2^-\cdot + H^+ \rightarrow HO_2\cdot \qquad\text{(Equation 7.10)}$$

$$2\,HO_2\cdot \rightarrow H_2O_2 + O_2 \qquad\text{(Equation 7.11)}$$
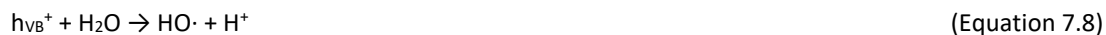
This chapter presents our research on the modifications of Fe/alginate catalyst to promote its stability and efficiency. A physical dehydration process was conducted and the contribution of homogeneous Fenton reaction was evaluated in the view of the main variables evolution as iron release, pH, SMX and TOC removal and H_2O_2 consumption. Furthermore, some modifications by embedding cerium in iron alginate gel beads and by entrapping zero valent iron (ZVI) and TiO_2 particles to this new dehydrated catalyst were

tested. The study was conducted in Milli-Q and naturally buffered waters (bottled drinking water and secondary effluent).

7.2. MATERIALS AND METHODS

7.2.1. Reactor set-up

In order to perform the experiments which results can be found in this chapter, a 4 L batch reactor with a similar configuration to the one used on previous chapters was used. The reactor was scaled-up to allow the incorporation of mechanical stirring, which was necessary to ensure the catalyst distribution over all reaction volume. The increase of density due to its dehydration made impossible to keep the catalyst suspended by only using magnetic stirring, as on previous experiments. A detailed description of the experimental device can be found in chapter 3, "Materials and Methods".

7.2.2. Samples preparation and characterization

4 L samples were prepared by spiking SMX into a distilled, bottled water or wastewater matrix to an initial concentration of 10 mg L^{-1}. Solutions were mixed overnight with a magnetic stirrer to ensure the total dissolution of the antibiotic.

Bottled drinking water and wastewater were selected as natural buffered water matrixes to perform the experiments. A detailed explanation about their collection and their characterization can be found in chapter 3, "Materials and Methods".

7.2.3. Catalysts' synthesis

A detailed explanation about the preparation procedure of all catalysts used in this chapter can be found in chapter 3, "Materials and Methods".

7.3. RESULTS AND DISCUSSION

7.3.1. Fe(III)/alginate dehydrated catalyst characterization

As it can be seen in Figure 7.1, after the dehydration process the catalyst size reduces considerably from an average of 1.9 mm to 0.72 mm, measured by using a caliper and through SEM respectively. A change of color can also be appreciated from an intense orange to a very dark brown-red.
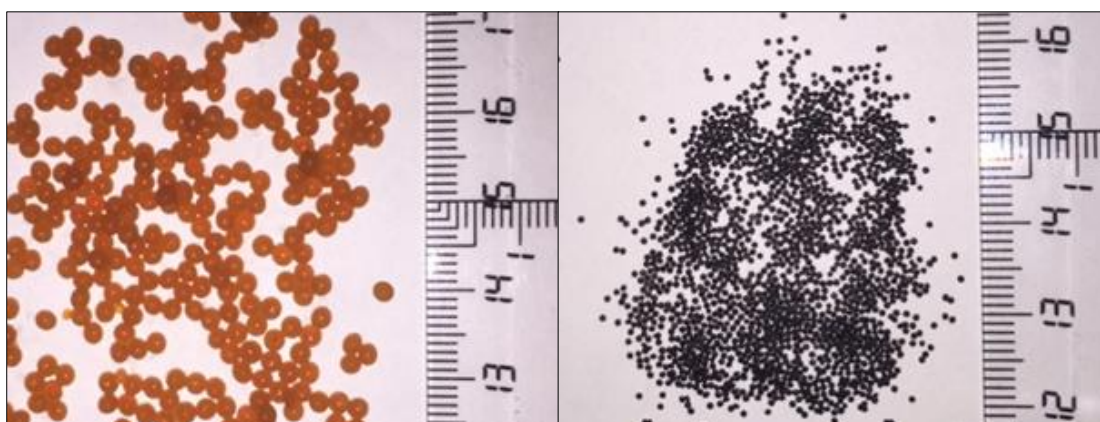
Figure 7.1. Images of the Fe(III)/alginate catalyst before (left) and after (right) the dehydration process (Scale shown is in cm).

In order to determine the total iron content of Fe(III)/alginate catalyst, 2 g of catalyst were weighted and digested in a HNO_3:$HClO_4$ solution. The digested solution Fe concentration was determined with ICP-OES. Results showed that average Fe mass percentage on both type of catalyst was 11.15 % with a determination error of 1.3 % (Table 7.1).

SEM images were taken to observe the surface morphology of the dry Fe(III)/alginate catalyst.

Figure 7.2.a shows the spherical shape of a single unit of dehydrated Fe/alginate catalyst. This sphere corresponds to a drop of sodium alginate that falls into the $FeCl_3$ hardening solution during the catalyst synthesis.
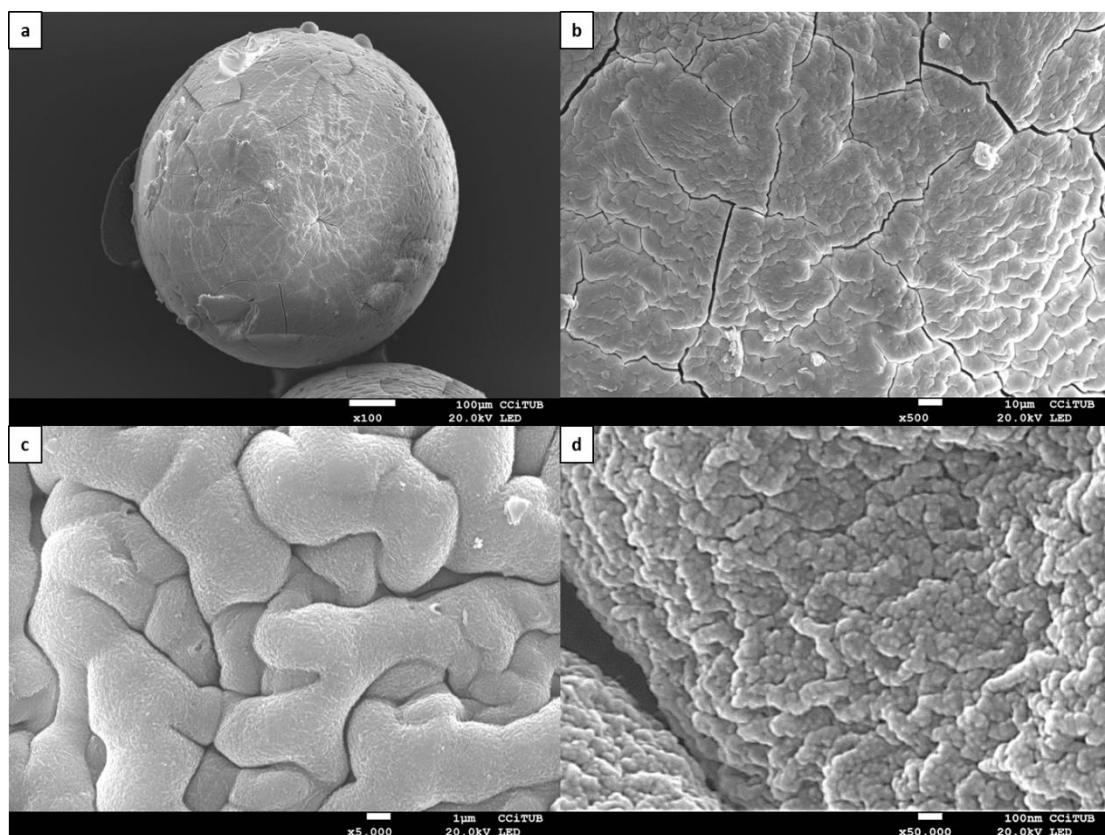
Figure 7.2. SEM images of the dehydrated Fe/alginate catalyst at different magnifications. a) x100 b) x500 c) x5,000 d) x50,000

In Figure 7.2.b it can be observed that the catalyst presents a wrinkled wavy surface. It also shows fractures along all catalyst surface. These fractures are attributed to the tensions generated on the solid structure surface during the dehydration process, which end collapsing.

In Figure 7.2.c and Figure 7.2.d it can be seen with more detail the wrinkled surface in which photo-Fenton reaction takes place. Despite this irregular morphology, the continuous homogeneity of the material composition along all the catalyst surface confirms that iron is included on alginate chains as a cross-linking agent at molecular level and that the excess of Fe that was not linked   to alginate was removed during the catalyst cleaning stage.

FTIR analysis was applied to the catalyst before and after the dehydration process in order to identify possible changes at molecular level during the drying process. Despite the presence of a high amount of water on the hydrated catalyst increased considerably the absorbance and also smothered the peaks, results didn't show significant variations between both forms of the catalyst (Figure 7.3).
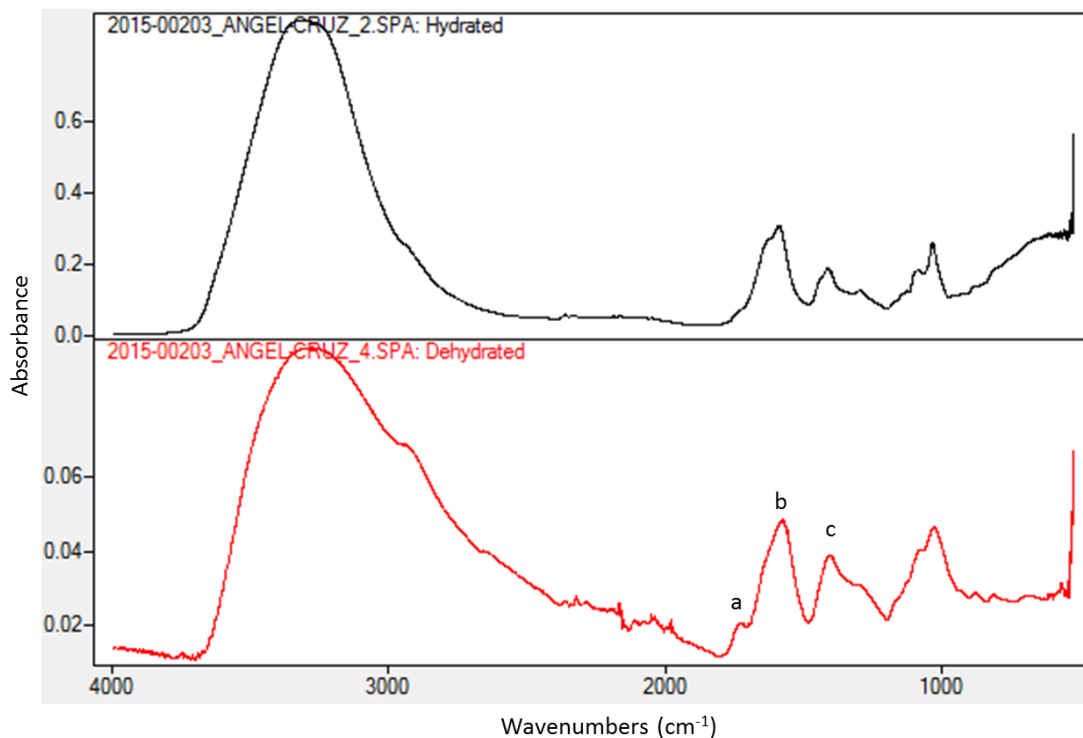
Figure 7.3. FTIR analysis results for Fe(III)/alginate catalyst before and after the dehydration process.

The IR diagrams show a wide vibration band from 3000 cm^{-1} to 3600 cm^{-1}, corresponding to the stretching frequency of hydroxyl groups [106]. Peak (a), centered at 1700 cm^{-1}, corresponds to the adsorption vibrations of the carboxyl group of alginate molecule [112]. Peaks (b) and (c) centered at 1573 cm^{-1} and 1401 cm^{-1} correspond to the asymmetric and symmetric stretching vibrations of the carboxyl groups of alginate molecule [152].

BET analysis performed on the catalyst determined a BET surface area of 1.2203 ± 0.0047 m^2 g^{-1}. Based on BJH analysis, the cumulative volume of pores between

1.5 nm and 300 nm width was 0.001617 cm^3 g^{-1} and the average pore width was 4.8897 nm. A mesoporous structure with pore size distribution in the range of 2-10 nm with a major abundance of pores centered in a pore size of about 3.5 nm was observed (Figure 7.4).
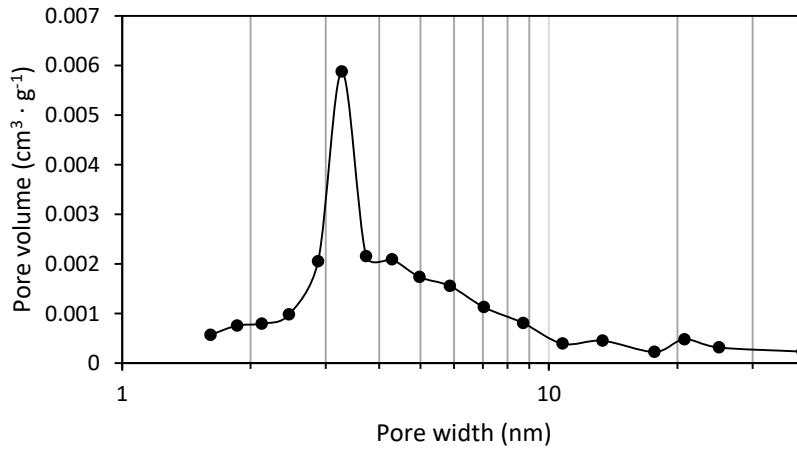
Figure 7.4. Pore width distribution for dehydrated Fe(III)/alginate catalyst.

The adsorption/desorption isotherms in Figure 7.5 show a hysteresis phenomenon that is associated to the capillary condensation on mesoporous structures that occurs at pressures lower than the saturation on narrow capillaries. The hysteresis observed shows that both isotherms are relatively asymptotic to the vertical p/p_0=1. According to IUPAC classification this hysteresis could be type H3, which is usually associated to rigid aggregates of plate shaped particles which form indented pores [153].
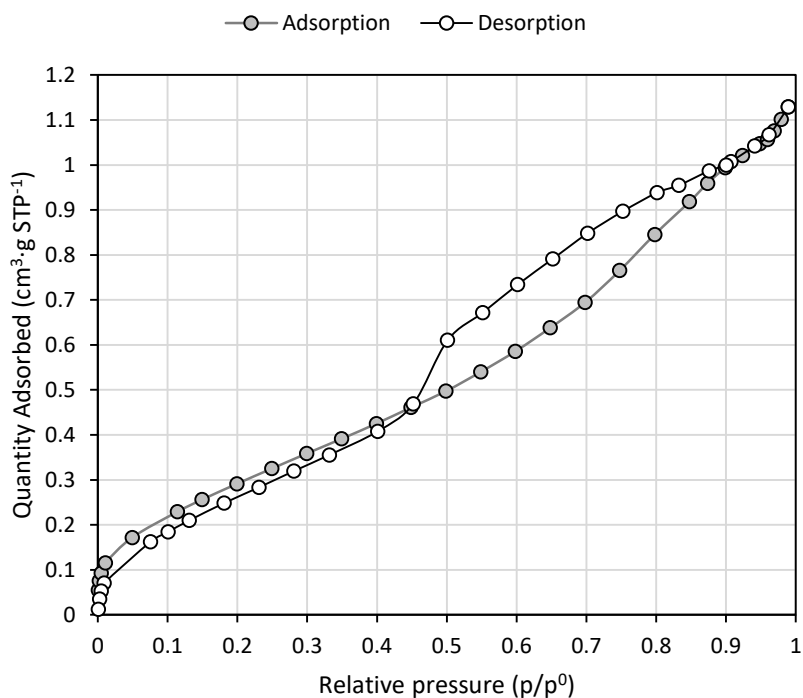
Figure 7.5. N$_2$ adsorption/desorption isotherms of Fe(III)/alginate dehydrated catalyst at 40°C on BET analysis.

7.3.2. Fe(III)/alginate dehydrated catalyst: photocatalytic activity and stability

<u>*Non-buffered water matrix experiments*</u>

First of all, the effectiveness of the dehydrated catalyst in comparison with the commonly used hydrated form was evaluated. Photo-Fenton experiments were performed in the same operational conditions to a SMX pure water solution. The amount of catalyst used was 0.5 g L^{-1} in dry basis for both catalysts. The samples were prepared by spiking sulfamethoxazole to a concentration of 10 mg L^{-1} on a MilliQ water matrix. 20 mg L^{-1} of H$_2$O$_2$ were added on both samples just before the experiment and then the reactor was irradiated for 120 min. Sulfamethoxazole removal, soluble iron concentration, H$_2$O$_2$ concentration, TOC and pH were monitored along the treatment.

Figure 7.6.a shows the performance of both catalysts on the degradation of sulfamethoxazole. The hydrated one presents a higher degradation on minute 30, but then

110

was unable to achieve the total removal of the target compound. On the other hand, the dehydrated Fe(III)/alginate catalyst reached the total pollutant removal within 60 minutes of reaction. This impossibility to achieve the total removal of SMX could be attributed to the increasing competition produced by the TOC released into the sample when working with the hydrated form of the catalyst, according to Figure 7.6.c.
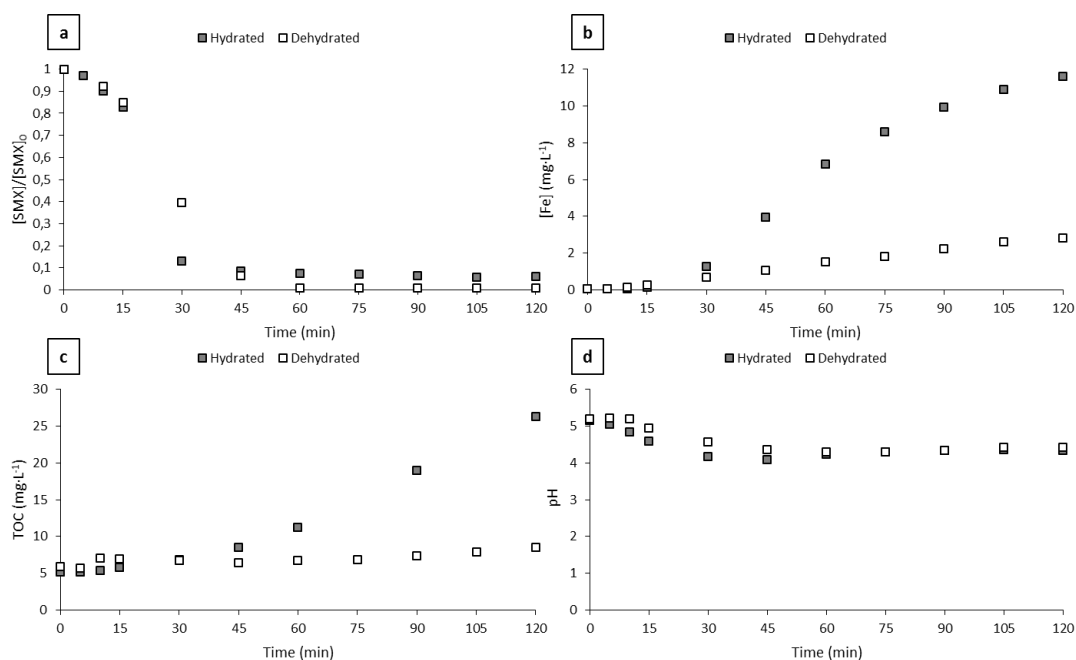
Figure 7.6. SMX degradation, soluble iron, TOC and pH comparison of experiments performed by using hydrated and dehydrated Fe(III)/alginate catalyst in a MilliQ water matrix. ([SMX]$_0$ = 10 mg L^{-1}, catalyst amount (dry basis) = 0.5 g L^{-1}, [H$_2$O$_2$]$_0$ = 20 mg L^{-1})

When looking at the iron release along reaction (Figure 7.6.b), it can be seen that the dehydrated form of the catalyst is far more stable at long times of reaction. The dehydrated form releases less than 3 mg L^{-1} of Fe after 120 min, unlike the hydrated one, which liberates about 11.5 mg L^{-1} on the same period of time. These amounts released supposed approximately 5.4 % and 20.0 % of the total iron content in catalyst, respectively. Similar phenomena can be observed on TOC measurements (Figure 7.6.c). Although in both cases

an increase of TOC can be observed, the use of the dehydrated form of the catalyst releases less than 2 mg L^{-1} after 120 min. On the contrary, the hydrated one produces an increase of more than 20 mg L^{-1} after the same time of reaction. This increase of TOC on both experiments comes from the catalyst itself, which is self-degraded by the HO· radicals formed on its surface during the photo-Fenton reaction and also from solubilization in the case of the hydrated form.

All these results can be explained according to the study of the contribution of homogeneous catalysis using alginate-based catalysts, which can be found in detail elsewhere [113]. It was found that alginate chains get protonated when the medium pH decays under its pK_a, which depending on some factors can be found from 3.4 to 5.0 [102–104]. At this point, the Fe cations, which bond alginate chains, are replaced by protons and released as a source of soluble iron, triggering the homogeneous photo-Fenton reaction.

These experiments were performed in MilliQ water, which means that the samples have no buffering capacity. As the photo-Fenton reaction is done in the presence of organic compounds, the sample pH starts reducing (Figure 7.6.d) due to the formation of small amounts of carboxylic acids [136,137]. By comparison of pH's profile with other parameters' profiles, the moment pH reach this pKa value is when Fe starts to increase in solution. Although at this pH the homogeneous photo-Fenton reaction does not show its best efficiency, it is enough to generate sufficient HO· radicals to attack the surface of the catalyst, solubilizing the alginate and releasing more iron into the sample, which exponentially increase the contribution of the homogeneous reaction.

As it can be seen in Figure 7.6, this effect is strongly minimized when using the dehydrated form of the catalyst, but not avoid.

Despite the amounts of iron released on both experiments are totally different at 120 minutes, the effects over SMX look to be very similar. If we focus on the effective time of removal for SMX when working with the hydrated catalyst, it can be seen that SMX is almost fully degraded before arriving to the alginate pK_a point, in which the major Fe release starts

112

(at minute 30 approximately). At this point, H_2O_2 concentration has been reduced by more than half (Figure 7.7), which palliates the visible effects over the SMX concentration profile. When working with the dehydrated catalyst, there is still a considerable amount of H_2O_2 and SMX at the pK_a point, but its higher stability holds the homogeneous reaction at bay. A major difference among SMX profiles would have been observed if the concentration of SMX had been still considerable at the pKa point. Even so, the difference of Fe release, even after the total consumption of H_2O_2, gives an idea of the improved stability of the hydrated catalyst.
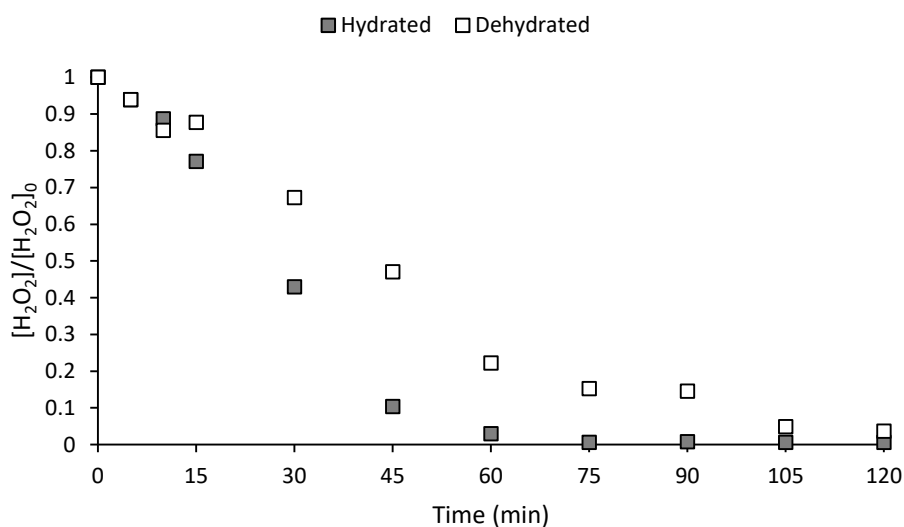
Figure 7.7. H_2O_2 consumption of experiments performed by using hydrated and dehydrated Fe(III)/alginate catalyst in a MilliQ water matrix. ([SMX]$_0$ = 10 mg L^{-1}, catalyst amount (dry basis) = 0.5 g L^{-1}, [H$_2$O$_2$]$_0$ = 20 mg L^{-1}).

Buffered water matrix experiments

The performance of the dehydrated Fe(III)/alginate catalyst in bottled drinking water and wastewater as sample matrixes was studied. The natural buffering compounds in drinking water and wastewater matrixes allowed keeping the pH of the samples above this limit value in which iron starts releasing due to protonation. Also, alkalinity in these real matrixes was proven as the best way to keep pH constant. Some tests performed with buffers

113

resulted in some Fe leaching due to the increase of monovalent cations coming from them, which partially replaced Fe in catalyst structure. After 2 hours of reaction pH remained over 7.0 for both water matrixes. Considering that at this neutral pH iron is not released due to the pH effect previously described, these experiments helped to study the dehydrated catalyst when only the heterogeneous photo-Fenton reaction was produced. For comparison purposes SMX initial concentration, H_2O_2 initial concentration and catalyst amount were kept the same as the ones used on MilliQ water matrix experiments ($[SMX]_0$ = 10 mg L^{-1}, catalyst amount (dry basis) = 0.5 mg L^{-1}, $[H_2O_2]_0$ = 20 mg L^{-1}).

Figure 7.8 presents the SMX degradation profiles by using the dehydrated Fe(III)/alginate catalyst in MilliQ water, drinking water and wastewater matrixes. It can be seen that the effectiveness of the catalysts on SMX removal becomes almost zero when using a sample matrix with buffering effect. After 120 minutes of reaction only 0.3 mg L^{-1} of Fe were detected when using bottled drinking water as sample matrix and 0.05 mg L^{-1} when using wastewater in comparison with the 2.8 mg L^{-1} measured at the same time of reaction when working with a MilliQ water matrix. It could be fair to think that previous results performed by using MilliQ water were only due to homogeneous reaction produced because of Fe release, since a deeper study on the other parameters involved in reaction suggests that there is also heterogeneous reaction.
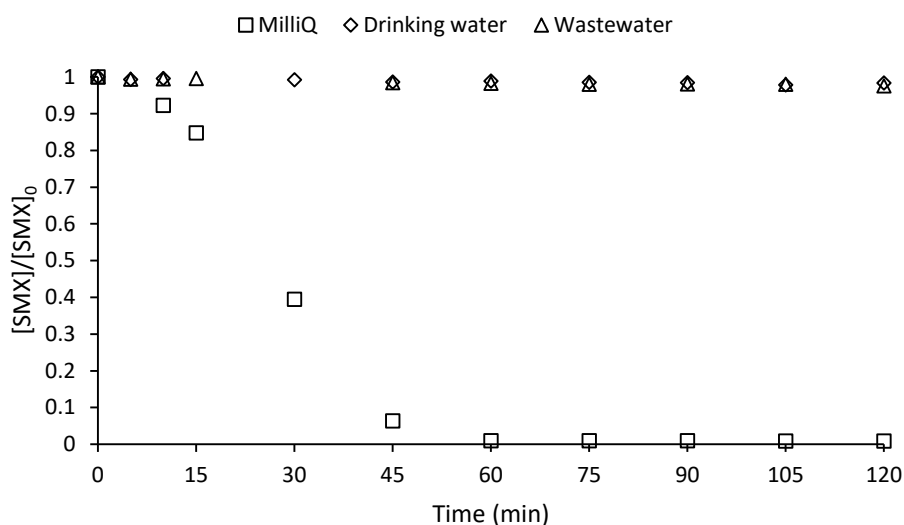
Figure 7.8. SMX degradation of experiments performed by using dehydrated Fe(III)/alginate catalyst in MilliQ water matrix, drinking water matrix and wastewater matrix at an initial pH of 7.5. ([SMX]$_0$ = 10 mg L^{-1}, catalyst amount = 0.5 g L^{-1}, [H$_2$O$_2$]$_0$ = 20 mg L^{-1})

Figure 7.9 shows the H$_2$O$_2$ consumption profiles of the experiments performed by using the three different water matrixes. It can be observed that when using a buffered matrix the concentration of H$_2$O$_2$ after 2 hours is about a 20% of the initial. In this conditions in which homogeneous reaction is avoided, this H$_2$O$_2$ reduction means that it is turned into HO· by means of the heterogeneous reaction produced on the catalyst surface. Although the reaction is produced, the low rate of H$_2$O$_2$ disappearance indicates a low efficiency in HO· production. As these radicals are formed on the surface of the catalyst and alginate organic chains mainly form this catalyst, these HO· are quenched by the organic alginate chains, turning the catalyst into a strong scavenger.
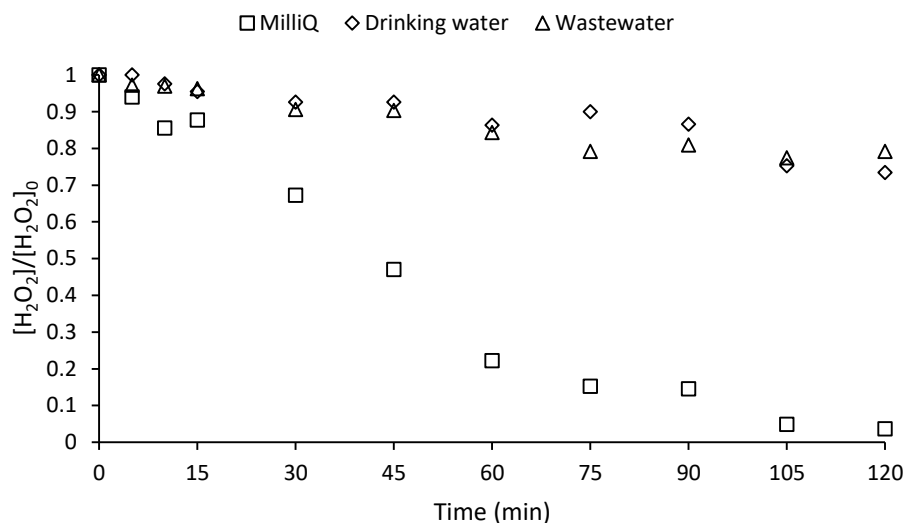
Figure 7.9. H$_2$O$_2$ consumption of experiments performed by using dehydrated Fe(III)/alginate catalyst in MilliQ water matrix, drinking water matrix and wastewater matrix at an initial pH of 7.5. ([SMX]$_0$ = 10 mg L^{-1}, catalyst amount (dry basis) = 0.5 g L^{-1}, [H$_2$O$_2$]$_0$ = 20 mg L^{-1})

Due to this, a partial oxidation of the catalyst is produced, which at long times of reaction could also solubilize alginate releasing a bit amount of TOC and soluble Fe. Despite this, at pHs near the neutrality, this low amount of soluble iron released makes that the contribution to homogeneous reaction can be considered negligible.

7.3.3. Fe(III)/alginate modified catalysts characterization

In order to evaluate the content of cerium, TiO$_2$ and ZVI in the modified catalysts, they were submitted to a digestion in different conditions according to each compound and lately analyzed by triplicates through ICP-OES. Results can be found in Table 7.1.

Results show that the amount of Fe linked to alginate chains remains almost the same despite the addition of another linking agent as Cerium. Even so, the different concentration of Fe and Ce despite the hardening concentration had a 1:1 molar ratio of both elements can be attributed to the different size of both cations. Fe, with an atomic number of 26 is significantly smaller than Ce, which core is formed of 58 protons. This difference in size can

make more difficult for Ce to diffuse through alginate structure during the hardening stage of the synthesis, even more as long as Fe forms bonds with alginate chains, reducing the intermolecular free space. This results in a lower diffusion rate of Ce and possibly a major distribution of this element on the outer layers of the catalyst.

Table 7.1. Fe, Ce, TiO$_2$ and ZVI content of the dehydrated Fe(III)/alginate catalyst and its three modifications.

Catalyst	Total Fe (Mass %)	Total Ce (Mass %)	TiO$_2$ (Mass %)
Fe(III)/alginate	11.15 ± 0.15	-	-
Fe(III)/Ce(III)/alginate	11.19 ± 0.23	1.12 ± 0.02	-
Fe(III)/TiO$_2$/alginate	11.28 ± 0.04	-	1.18 ± 0.01
Fe(III)/ZVI/alginate	11.58 ± 0.10	-	-

For TiO$_2$ and ZVI modifications, which introduce low size particles by encapsulating them inside the Fe(III)/alginate, the amount of Fe linked to alginate stays also unaltered. The mass of these particles detected on their respective catalyst modifications was a bit lower than the theoretical because during the synthesis process part of the particles were lost, attached to syringe walls.

The four catalysts' morphologies were observed and compared by using SEM images at different magnification levels (Figures 7.10-7.12).
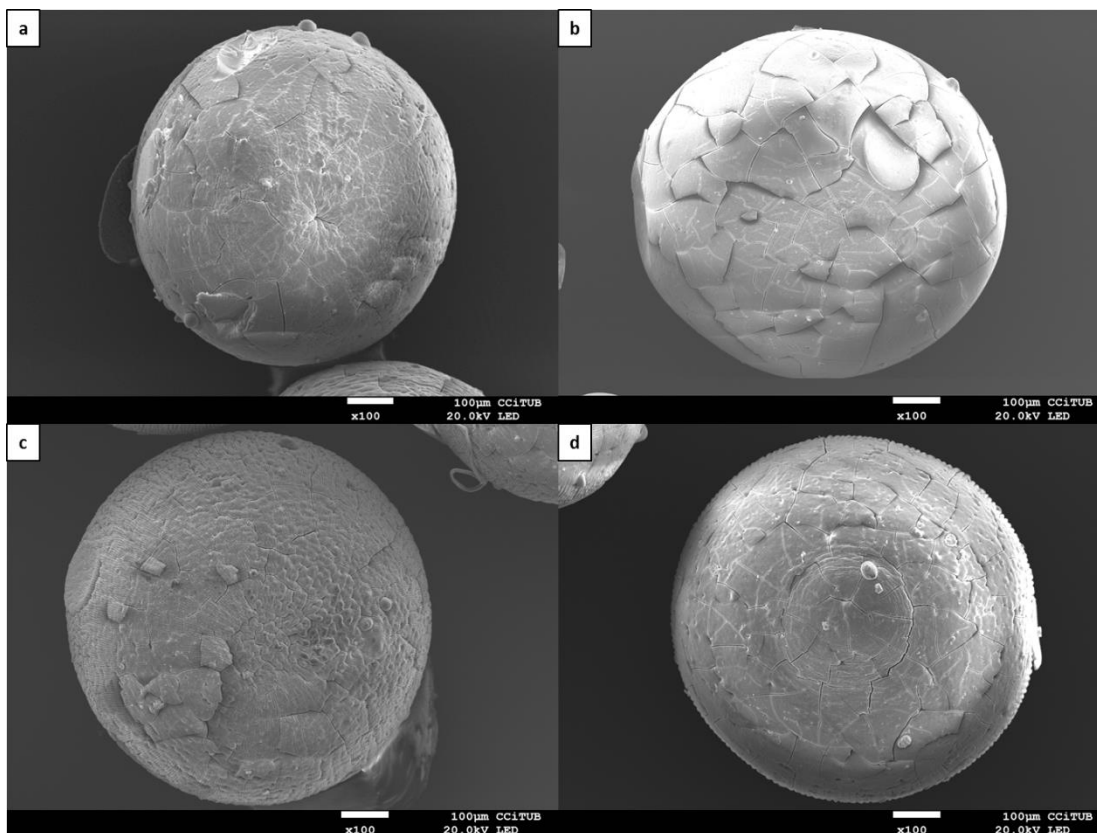
Figure 7.10. SEM images of (a) dehydrated Fe(III)/alginate catalyst, (b) Fe(III)/Ce(III)/alginate catalyst, (c) Fe(III)/TiO₂/alginate catalyst and (d) Fe(III)/ZVI/alginate catalyst at a magnification of x100.

Figure 7.10 shows a single catalyst unit of all four catalysts. It can be observed that the spherical shape and size is barely constant for all of them, but they present some variation on their surfaces.

In Figure 7.11, the surface of the four catalysts can be observed at a magnification of x500. Figure 7.11.b shows that the inclusion of Ce in the catalyst structure produces the same kind of major fractures observed previously on the dehydrated Fe(III)/alginate catalyst, but also an increase of smaller fractures along all the surface. This effect can be attributed to the variable tensions generated because of the presence of both, Fe(III) and Ce(III) cations, linking the alginate chains. At this magnification level it can be also observed that the surface is apparently less wavy than the non-modified catalyst. Figure 7.11.c and Figure 7.11.d show the morphology of the TiO_2 and ZVI modifications of the catalyst. At this

118

magnification, a more directional distribution of the surface waves than in the non-modified catalyst can be guessed, which will be confirmed in Figure 7.12, at a higher magnification level.
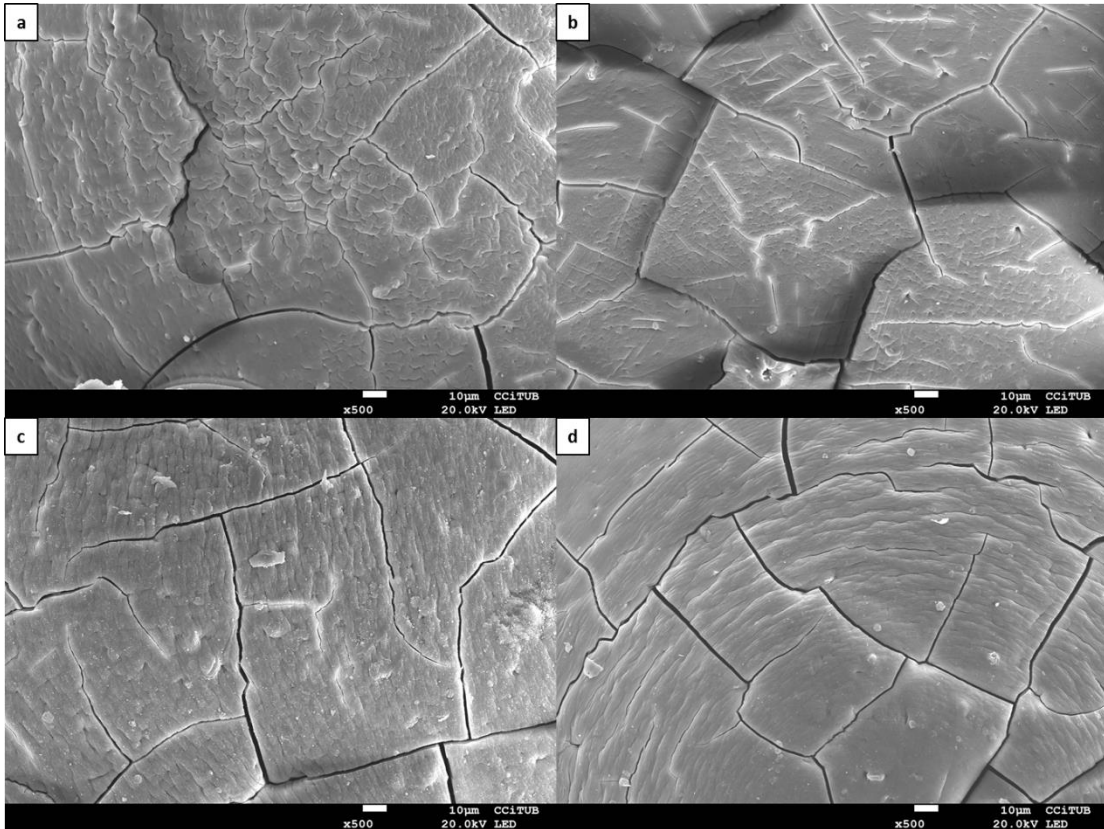
Figure 7.11. SEM images of (a) dehydrated Fe(III)/alginate catalyst, (b) Fe(III)/Ce(III)/alginate catalyst, (c) Fe(III)/TiO$_2$/alginate catalyst and (d) Fe(III)/ZVI/alginate catalyst at a magnification of x500.

In Figure 7.12, at a magnification level of x5,000, the differences between surface morphology of the four catalysts are more clear. Figure 13.a shows the wrinkled wavy surface of the Fe(III)/alginate catalyst previously observed. After modifying the catalyst by including Ce(III) in its structure (Figure 7.12.b) the minor linear fractures can be clearly seen. The presence of this secondary fractures also turn the catalyst surface into a less wrinkled one.
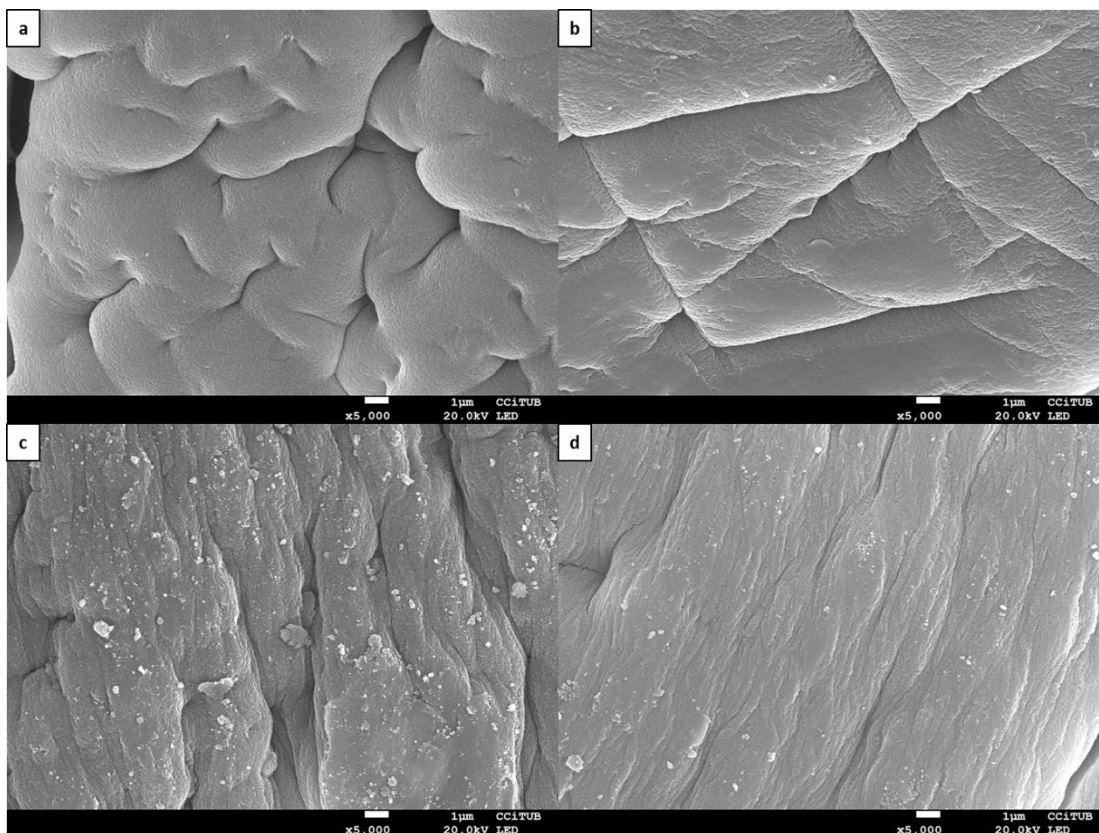
Figure 7.12. SEM images of (a) dehydrated Fe(III)/alginate catalyst, (b) Fe(III)/Ce(III)/alginate catalyst, (c) Fe(III)/TiO₂/alginate catalyst and (d) Fe(III)/ZVI/alginate catalyst at a magnification of x5,000.

Figure 7.12.c and Figure 7.12.d, as previously intuited, reveal a totally different morphology for TiO_2 and ZVI catalyst modifications. As this more directional surface morphology can be observed only on those catalysts prepared by the inclusion of solid particles on its volume, it is fair to think that the presence of solid microparticles inside the catalyst during the dehydration process is responsible for this change of morphology. The presence of these solid particles (TiO_2 and ZVI) can be also observed in Figure 7.12.c and Figure 7.12.d. These solid particles were suspended on alginate aqueous solution during the synthesis process and were supposed to be distributed along all catalyst volume. These images confirm that the particles that were fixed on the surface are still firmly attached after both catalysts synthesis processes and their storage and manipulation.

7.3.4.   Fe(III)/alginate modifications: photocatalytic activity and stability

Non-buffered water matrix experiments

In order to test the efficiency of the modified catalysts, a set of experiments were performed by using the same experimental conditions of previous experiments with the dehydrated catalyst ($[SMX]_0$ = 10 mg L^{-1}, $[H_2O_2]_0$ = 20 mg L^{-1}, catalyst amount = 0.5 g L^{-1}, MilliQ water matrix and pH0 = 5.5). Figure 7.13 shows these parameters profiles.

Figure 7.13. SMX degradation, soluble iron, H_2O_2 consumption and TOC comparison of experiments performed by using dehydrated Fe(III)/alginate catalyst and its three modifications with Ce, ZVI and TiO$_2$ in a MilliQ water matrix. ($[SMX]_0$ = 10 mg L^{-1}, $[H_2O_2]_0$ = 20 mg L^{-1}, pH$_0$ = 5.5, catalyst amount = 0.5 g L^{-1})

As it can be seen the SMX degradation profiles for the dehydrated Fe(III)/alginate catalyst and its three modifications. The one including TiO$_2$ has a SMX degradation rate on its linear stage of 0.42 mg L^{-1} min^{-1}, higher than the original Fe(III)/alginate catalyst (0.26 mg L^{-1}), achieving the total degradation more than 15 min before. This performance is consistent with the existence of a secondary pathway for the formation of oxidative species. TiO$_2$ particles on the surface of the catalyst absorb part of the incident UV-A light and generate

HO· radicals, among others. The higher degradation rate suggests that despite TiO_2 particles absorb UV-A light in competence with Fe(III)/alginate, the efficiency of TiO_2 compensates it achieving a higher global oxidation capacity.

When analyzing the performance of the cerium catalyst modification, a very similar performance to the non-modified catalyst is observed, with the exception of H_2O_2 consumption rate, which presents a little reduction.

By incorporating cerium into the catalyst structure, a small increase on the initial SMX consumption rate can be appreciated (0.35 mg L^{-1}), but no other significant variation can be appreciated in other parameters' profiles. This initial improvement of SMX degradation rate can be explained because cerium is initially included as Ce(III), which is its active specie for Fenton-like reactions.

The inclusion of ZVI particles in the Fe(III)/catalyst resulted in a lower Fe release, a lower H_2O_2 consumption and a lower SMX degradation, but avoiding TOC release. Iron linked to alginate in Fe(III)/alginate dehydrated catalyst was 11.15 % and the sum of iron linked to alginate and ZVI particles was 11.58 %, of which about 2% was ZVI. Considering that the same mass of catalyst was added in all experiments, the incorporation of ZVI particles to the catalyst replaced part of the iron linked to alginate. Considering that ZVI particles did not present significant activity on the tested conditions because there was not a strong acidic pH nor enough dissolved O_2 abundance, which according to its widely accepted mechanism are the main factors affecting the efficiency of ZVI particles [154–156], this general efficiency decay could be explained.

HO· scavenging experiments

Some experiments using Fe(III)/alginate dehydrated catalyst and its modifications were performed by using a MilliQ water matrix and adding tert-butyl alcohol (TBA) on a concentration of 500 mg L^{-1} as quenching probe. Other experimental conditions were kept as in previous experiments in order to compare ($[SMX]_0$ = 10 mg L^{-1}, $[H_2O_2]_0$ = 20 mg L^{-1}, catalyst amount = 0.5 g L^{-1}, pH_0 = 5.5). TBA is recognized as a powerful HO· scavenger due to

its fast reaction kinetics with this radical. By applying it on excess during this experiments it was ensured that the HO· produced during reaction were consumed by this compound, so if some degradation could be observed over SMX it should come from other oxidative species. Adsorption is not considered because previous experiments performed demonstrated that adsorption was negligible (results not shown).

Figure 7.14 shows the SMX degradation profiles by using the Fe(III)/alginate dehydrated catalyst and its three modifications. It can be observed the same performance for the basic catalyst, the one modified with ZVI and the one modified wit TiO_2, with a SMX degradation of about 15% after 120 min and the one modified with Ce, with a degradation of about 25%.
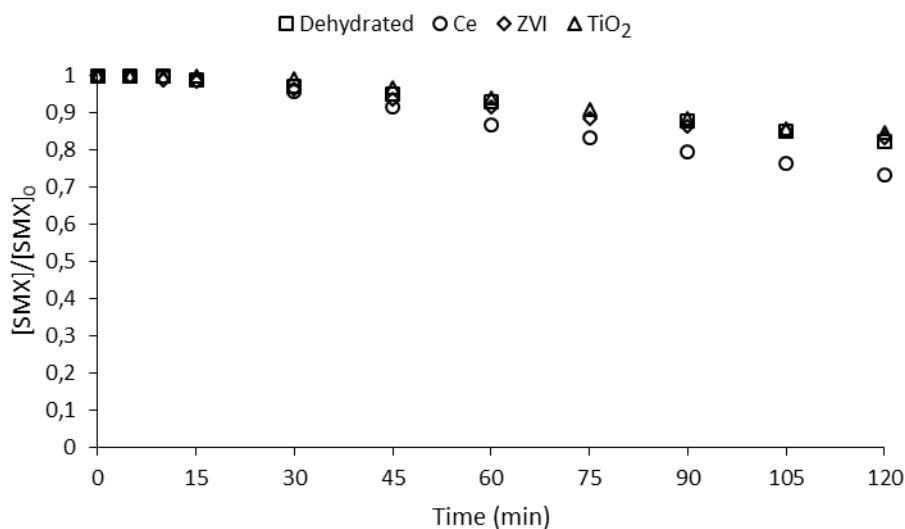
Figure 7.14. SMX degradation profiles of experiments performed by adding 500 mg L^{-1} of TBA into a MilliQ water matrix and by using dehydrated Fe(III)/alginate catalyst and its three modifications including cerium, ZVI and TiO_2. ([SMX]$_0$ = 10 mg L^{-1}, catalyst amount = 0.5 g L^{-1}, [H$_2$O$_2$]$_0$ = 20 mg L^{-1})

This results, compared to the previous performed without TBA, demonstrated that the main specie responsible for SMX oxidation was HO·. Despite this, it can be seen that some secondary oxidative species are generated and have a significant role during reaction. The similarity of all profiles suggest that this oxidative species are formed due to the reaction

with Fe(III)/alginate and not because of the modifications, except for the one modified by including Ce.

When the Fe/Ce/alginate catalyst is prepared, the concentration of Fe^{3+} in the hardening solution and the time of immersion of alginate drops in it are not designed to achieve a bonding saturation of alginate chains but to establish enough links Fe-alginate to ensure a stable solid sphere on a suitable time of preparation. As Ce^{3+} is added on hardening solution besides Fe^{3+}, the amount of links formed must be higher. Also, both species shouldn't be in competition for this linking spots, as it was proved on previous experiments that alginate could accept much more amount of Fe cations on its structure (results not shown). According to this, the generation of oxidative species that can be the result of the reactions involving Ce or Fe could explain this increase of efficiency.

Equation 5.1, proposed as part of the mechanism for Fe(III)/alginate, suggested the formation of the hydroperoxyl radical ($HO_2\cdot$) as an intermediate that supposed to react later on equation 5.3. Although the oxidative potential of this radical ($E°_{25°C}$ = 1.70 V) is not as high as the one of $HO\cdot$ ($E°_{25°C}$ = 2.80 V), it is a possible candidate responsible for this secondary oxidation.

As a result, the amount of $HO_2\cdot$ radicals produced by the Ce (Equation 7.1), as well as the SMX degradation observed, should be additive to the amount and degradation produced by Fe (Equation 5.1). Despite it is not possible to evaluate which radical comes from which element, it is sure that the sum is higher than just the ones produced by Fe, which is consistent with the results.

Buffered water matrix experiments

All the modified Fe(III)/alginate dehydrated catalysts were tested in bottled drinking water as self-buffered matrix to study their performance at neutral pH. The experimental conditions were kept the same as previous experiments ($[SMX]_0$ = 10 mg L^{-1}, $[H_2O_2]_0$ = 20 mg L^{-1}, catalyst amount = 0.5 g L^{-1}, pH_0 = 5.5).

In Figure 7.15 the main results obtained along the experiments with the Fe(III)/alginate catalyst and its three modifications can be seen.
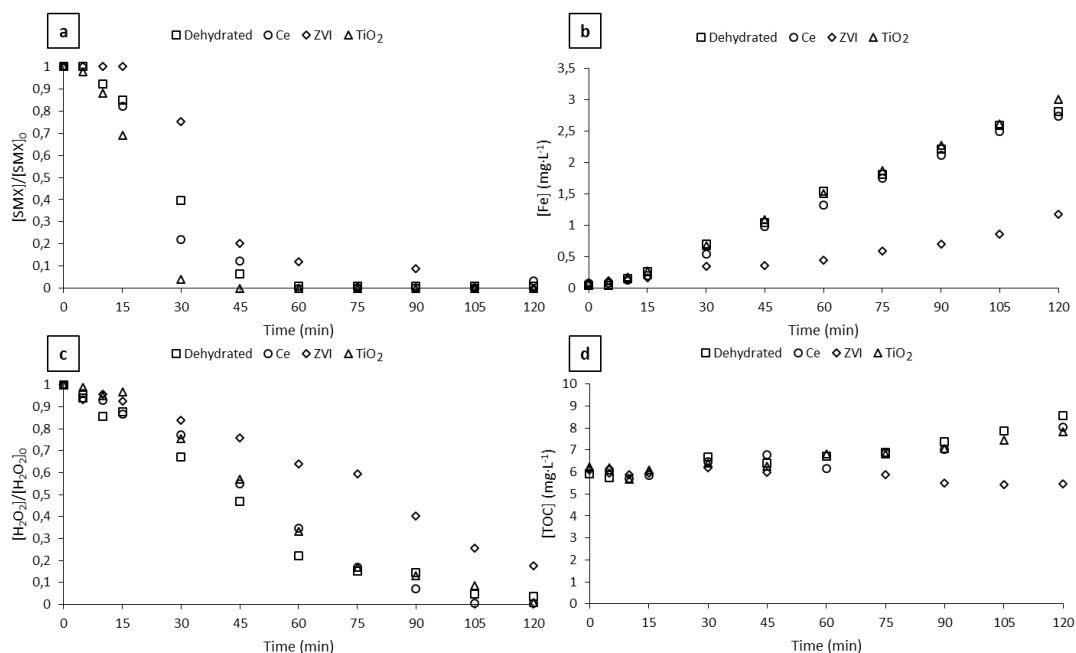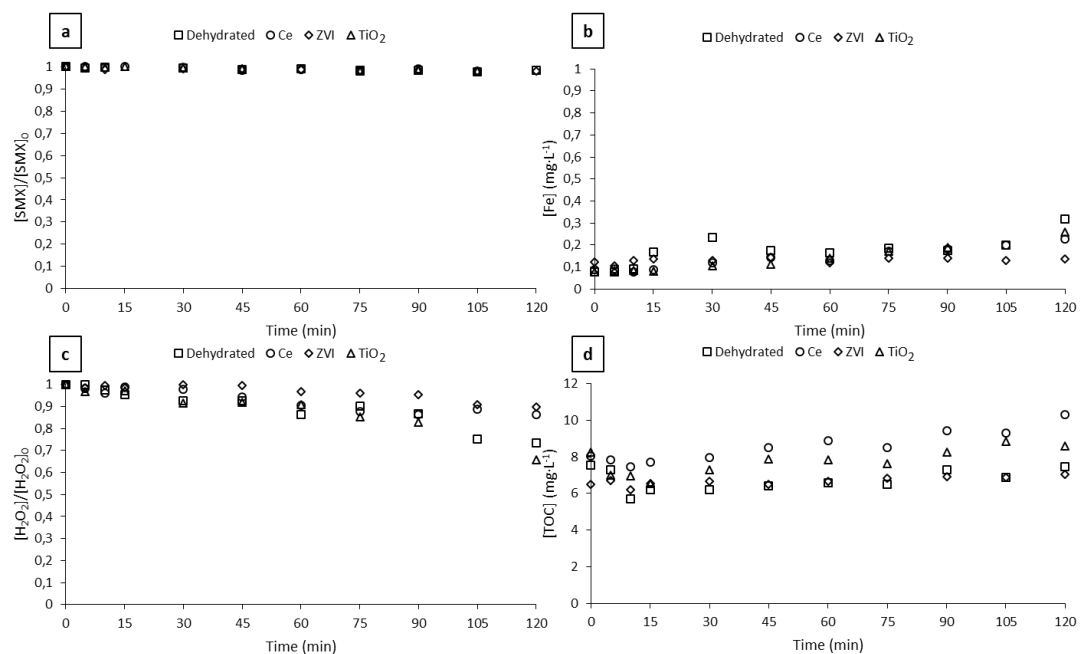

Figure 7.15. SMX degradation, soluble iron, H_2O_2 consumption and TOC comparison of experiments performed by using dehydrated Fe(III)/alginate catalyst and its three modifications with Ce, ZVI and TiO$_2$ in a drinking water matrix. ([SMX]$_0$ = 10 mg L^{-1}, [H$_2$O$_2$]$_0$ = 20 mg L^{-1}, pH$_0$ = 7.5, catalyst amount = 0.5 mg L^{-1})

Despite the improvements observed during its application on MilliQ water, SMX degradation rates still were null. There was also some H_2O_2 consumption indicating that the heterogeneous reaction was produced but its effects cannot be observed on SMX. The scavenging effect of alginate itself is too high to overcome only by the heterogeneous reaction produced on catalyst surface, even after being modified to increase its effectiveness for HO· production. This makes these catalysts not a good alternative to perform heterogeneous photo-Fenton reaction on buffered waters at circumneutral pH, in which the homogeneous pathway is totally avoided.

7.4. CONCLUSIONS

Fe/alginate based catalysts can be found in literature as heterogeneous catalysts for Fenton reactions. In previous chapters it was demonstrated that the homogeneous photo-Fenton reaction have a very significant role in the overall degradation mechanism due to Fe leakage when pH decreases below alginate's pK_a.

This chapter has proposed a more stable form of this catalyst by applying a thermal dehydration process. The dehydrated Fe(III)/alginate catalyst as much as efficient as the hydrated one when imitating photo-Fenton reaction at circumneutral pH, but with a scarce iron and TOC release.

Despite this, this work have shown that the use of this catalyst on buffered waters at neutral or slightly basic pH, when the homogeneous reaction is avoided, didn't have a visible oxidative effect over the reference compound studied (sulfamethoxazole).

In order to improve the effectiveness of the catalyst, some modifications by using cerium, zero valent iron and titanium dioxide have been tested. The combination of photo-Fenton reaction by iron coordinated with alginate together with the photocatalytic contribution of entrapped TiO_2 significantly improved the SMX removal rate. The use of cerium and zero valent iron proved useless to improve the effectiveness of dehydrated Fe(III)/alginate catalyst at circumneutral pH.

It can be concluded that, although some modifications can improve the efficiency, catalysts based on big organic chains act as powerful scavengers that consumes the HO· produced on its surface, turning its application meaningless if the homogeneous reaction is totally avoided.

8. Heterogeneous catalysts intended for Fenton and photo-Fenton at neutral pH

8.1. INTRODUCTION

Previous chapters of this doctoral thesis were focused on the synthesis, performance and improvement of alginate-based heterogeneous catalysts intended for photo-Fenton reaction, which are catalysts of organic nature. One of the main drawbacks observed during this investigation was the HO· scavenging effect produced by alginate due to its organic easy-degradable nature, which consumed the oxidant species produced and solubilized producing a TOC increase.

On this chapter, some heterogeneous catalysts of inorganic nature were studied when applied to Fenton reaction at acidic and cicumneutral pH conditions. Moreover, the same catalysts were used for photo-Fenton reaction at neutral pH in order to compare its performance with the already studied alginate-based catalysts. Part of the experiments found on this chapter were performed during a three months stay in the Group of Environment, Reaction, and Separation Engineering (GERSE) of the Chemical Engineering Department of the University of Coimbra (Portugal), which also provided the heterogeneous catalysts tested.

Considering iron as the most effective catalytic element for Fenton and photo-Fenton reactions, it was decided to evaluate the performance for Fenton and photo-Fenton of some heterogeneous catalysts containing this element.

Ce was considered a specie which presented Fenton-like activity and also it is considered to improve the global efficiency of the reaction due to its storage oxygen capacity that plays an important role in iron redox cycle [157]. Because of this, a Fe/Ce/O heterogeneous

catalyst was synthetized and tested. Also, an available Fe/Mn/O commercial catalyst (NORIT N-150) was tested.

Apart from these two synthetic catalysts, iron shavings, considered as a residue from metallurgic industry, and volcanic rocks from Azores islands were also tested as possible cheap heterogeneous catalysts for Fenton and photo-Fenton reactions.

8.2. MATERIALS AND METHODS

8.2.1. Reactors set-up

Dark Fenton experiments were performed at room temperature (25°C) and by using a 400 mL batch reactor. Reactors were magnetically stirred (Fe/Ce/O and volcanic rocks) or mechanically stirred (Fe/Mn/O and iron shavings) depending on the magnetic nature of the catalysts.

Photo-Fenton experiments were conducted by using a 2 L batch reactor including magnetic stirring and temperature control (25°C). Also, three 8 W UV-A lamps (λ_{max} = 365 nm) with a total emission of 4.74 x 10^{-6} Einstein s^{-1} were immersed inside the reaction volume.

A detailed description of the experimental devices can be found in chapter 3, "Materials and Methods".

8.2.2. Samples preparation

All samples were prepared by spiking SMX into distilled water to an initial concentration of 10 mg L^{-1}. Solutions were mixed overnight with a magnetic stirrer to ensure the total dissolution of the antibiotic.

8.2.3. Catalysts' synthesis and preparation

Fe/Ce/O catalyst was synthetized by means of a co-precipitation process, then crushed and sieved to obtain particles of a size lower than 250 µm. Commercially supplied Fe/Mn/O catalyst and volcanic rocks were crushed and sieved to obtain particles of a size lower than 250 µm. Due to the heterogeneity of size of iron shavings and its origin as residue, they were applied directly as obtained. Fe(III)/alginate dehydrated catalyst was prepared as described in chapter 3, "Materials and methods".

A detailed description of the Fe/Ce/O catalyst synthesis process and all inorganic base catalysts characterization can be found on chapter 3, "Materials and Methods". Fe(III)/alginate dehydrated catalyst detailed characterization can be found in chapter 7.

8.3. RESULTS AND DISCUSSION

8.3.1. Blank experiments

Before performing any Fenton experiment, a 10 mg L^{-1} SMX sample was spiked with H_2O_2 to a final concentration of 500 mg L^{-1}. HPLC analysis performed after 120 min revealed a SMX decay of less than 1 %, indicating that H_2O_2 direct oxidation over SMX was negligible.

Moreover, 1 g L^{-1} of each of the four catalysts was added into four 10 mg L^{-1} SMX samples to evaluate the possible effect of absorption. None of the catalysts presented a SMX concentration reduction higher than 1 % after 120 minutes of contact, what confirmed that absorption was also negligible.

UV-A irradiation blank experiments were already performed for the experimentation presented in chapter 5, which demonstrated that there was no photolysis effect over SMX at the experimental conditions applied.

8.3.2. Fenton experiments

The four heterogeneous catalysts selected were tested when applied to dark Fenton reaction by using 400 mL samples which were spiked with SMX to an initial concentration of 10 mg L^{-1}. Considering that dark Fenton reactions require a higher amount of H_2O_2 than photo-Fenton ones to achieve good results, an initial H_2O_2 concentration of 500 mg L^{-1} was selected for all experiments. To allow a direct comparison between experiments, a catalyst amount of 1 g L^{-1} was applied to all experiments except for the ones performed by using iron shavings. In this case, it was considered that due to its nature and its lower surface area per gram, a higher amount should be used, so 3 g L^{-1} were applied. All catalysts were tested for dark Fenton reaction at pH 3.0, as this reaction is conventionally conducted, and also at an initial pH of 7.0 to evaluate its efficiency when applied at circumneutral pH.

SMX, H_2O_2 and soluble iron concentrations were monitored along the experiments.

Acidic pH dark Fenton experiments

Figure 8.1 shows the SMX concentration profiles of the experiments performed by using the four catalysts at an initial pH of 3.0. No degradation was observed when applying Fe/Mn/O catalyst nor volcanic rocks as catalysts. A removal of about 20 % of the initial SMX was observed after 120 min when using Fe/Ce/O catalyst. This catalyst presented a constant SMX degradation rate of 0.002 mg L^{-1} min^{-1}. Also, by using iron shavings as catalyst no SMX was detected when the first sample was collected after 5 minutes of experiment.

Figure 8.1. SMX concentration along four dark Fenton experiments conducted by using four different catalysts at an initial pH of 3.0. $[SMX]_0$ = 10 mg L^{-1}, $[H_2O_2]_0$ = 500 mg L^{-1}, [Fe/Ce/O catalyst]$_0$ = 1.0 g L^{-1}, [Fe/Mn/O catalyst]$_0$ = 1.0 g L^{-1}, [Volcanic rocks]$_0$ = 1.0 g L^{-1}, [Iron shavings]$_0$ = 3.0 g L^{-1}.

Figure 8.2 shows the H_2O_2 consumption along the four experiments performed at acidic pH. A quick reduction of about 95 % of the initial H_2O_2 in less than 5 minutes was observed when applying Fe/Mn/O catalyst. The experiment performed by using iron shavings as catalyst also showed a quick H_2O_2 consumption profile, with a reduction of about 40 % of the initial in 5 minutes, when SMX concentration was already not detected. On the contrary, by using volcanic rocks as catalyst, no H_2O_2 consumption was detected in 120 minutes. By using Fe/Ce/O, an intermediate consumption profile was observed, achieving the total consumption of the initial 20 mg L^{-1} between 90 and 120 minutes of experiment.

The absence of H_2O_2 consumption nor SMX concentration reduction when applying volcanic rocks as catalyst suggested that Fenton reaction was not produced.

The experiments conducted by using Fe/Ce/O and iron shavings as catalysts presented both, SMX degradation and H_2O_2 consumption, which indicated the existence of Fenton reaction.

131

Figure 8.2. H$_2$O$_2$ concentration along four dark Fenton experiments conducted by using four different catalysts at an initial pH of 3.0. [SMX]$_0$ = 10 mg L^{-1}, [H$_2$O$_2$]$_0$ = 500 mg L^{-1}, [Fe/Ce/O catalyst]$_0$ = 1.0 g L^{-1}, [Fe/Mn/O catalyst]$_0$ = 1.0 g L^{-1}, [Volcanic rocks]$_0$ = 1.0 g L^{-1}, [Iron shavings]$_0$ = 3.0 g L^{-1}.

The high H$_2$O$_2$ consumption without observable effects over SMX concentration when using Fe/Mn/O catalyst suggested that no Fenton reaction was produced and H$_2$O$_2$ disappearance was due to a different reaction which did not produce oxidative species. Some tests performed with this catalyst at pH 7.0 allowed seeing the instantaneous formation of a gas when H$_2$O$_2$ was put in contact with the catalyst. A deeper review about this phenomena revealed that some manganese oxides are able to decompose H$_2$O$_2$ into oxygen and water [158], what discarded this Fe/Mn/O catalyst for further Fenton-related experiments and its application to any AOP which includes the use of H$_2$O$_2$.

Figure 8.3 shows the soluble iron profiles of the experiments conducted by using Fe/Ce/O and volcanic rocks as catalysts. It can be observed that the experiment conducted with Fe/Ce/O catalyst presented a gradual iron increase until reaching more than 1 mg L^{-1} after 90 minutes of reaction. Because of this leaching, and considering the global SMX removal obtained after 120 minutes of experiment ($\approx$ 20 %), it can be stated that there was a significant contribution of the homogeneous Fenton reaction into the overall SMX removal. On the contrary, the concentration of Fe when applying volcanic rocks as catalyst was

constant from the beginning and along all the reaction, so it did not present leaching. As the catalyst was sieved to be of a size less than 250 µm but no inferior size limit was established, the low amount of iron observed could be attributed to the smallest catalyst particles, with a size small enough to pass through the 0.45 µm pore size filter used to remove the catalyst from samples before soluble iron analysis. This iron content, less than 0.2 mg L^{-1}, did not produce any effect over SMX. Even so, volcanic rocks presented a brown-orange color which can be usually related to Fe(III) species. As in dark Fenton reaction mechanism there is no significant recovery from Fe(III) to Fe(II), which is the reactive specie generating HO·, a major or total presence of iron on its not active specie could be the reason of the absence of Fenton reaction and consequently the lack of SMX degradation.
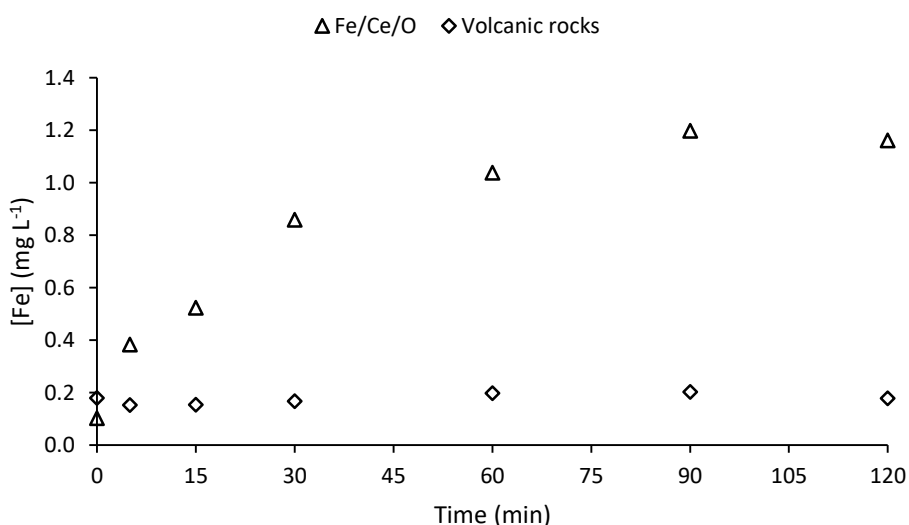
Figure 8.3. Iron concentration along two dark Fenton experiments conducted by using Fe/Ce/O and volcanic rocks as catalysts at an initial pH of 3.0. $[SMX]_0$ = 10 mg L^{-1}, $[H_2O_2]_0$ = 500 mg L^{-1}, [Fe/Ce/O catalyst]$_0$ = 1.0 g L^{-1}, [Volcanic rocks]$_0$ = 1.0 g L^{-1}.

In the experiment performed using iron shavings, due to the strongly acidic pH, large amounts of iron solubilized and also precipitated. Thus, the amount of iron leached from the catalyst was not possible to quantify. Because of this high amount of soluble iron, the quick SMX degradation rate observed can be attributed totally to the conventional homogeneous Fenton reactions.

Circumneutral pH dark Fenton experiments

Figure 8.4 shows the SMX concentration profiles of the experiments performed by using the three catalysts at an initial pH of 7.0. No SMX removal was observed when using volcanic rocks and the overall SMX removal by using Fe/Ce/O catalyst (7 %) and iron shavings (3 %) was very low.
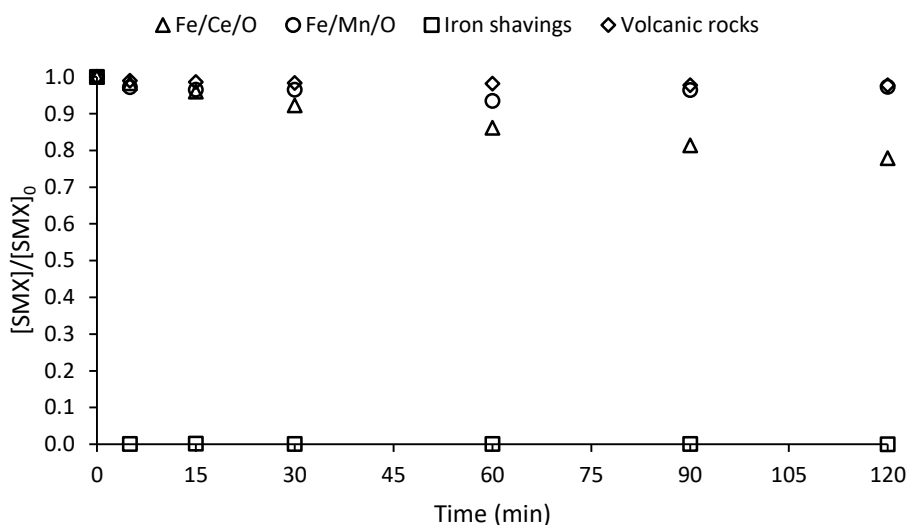

Figure 8.4. SMX concentration along three dark Fenton experiments conducted by using three different catalysts at an initial pH of 7.0. [SMX]$_0$ = 10 mg L^{-1}, [H$_2$O$_2$]$_0$ = 500 mg L^{-1}, [Fe/Ce/O catalyst]$_0$ = 1.0 g L^{-1}, [Volcanic rocks]$_0$ = 1.0 g L^{-1}, [Iron shavings]$_0$ = 3.0 g L^{-1}.

Regarding H$_2$O$_2$ (Figure 8.5), the experiments using iron shavings and volcanic rocks as catalyst had a very low consumption, which agrees to previous SMX profiles in which no degradation was observed. The lack of H$_2$O$_2$ reduction indicates that Fenton reaction is not being produced. Even so, when Fe/Ce/O catalyst was applied, H$_2$O$_2$ totally disappeared after 90 minutes of experiment. Considering Fenton reactions stoichiometry, the consumption of this amount of H$_2$O$_2$ should have produced enough HO· to observe a decrease of SMX concentration. These results suggest that, as it happened with Fe/Mn/O catalyst, part of the H$_2$O$_2$ could be directly decomposed without forming effective oxidative species but at a lower rate than when using Fe/Mn/O catalyst.
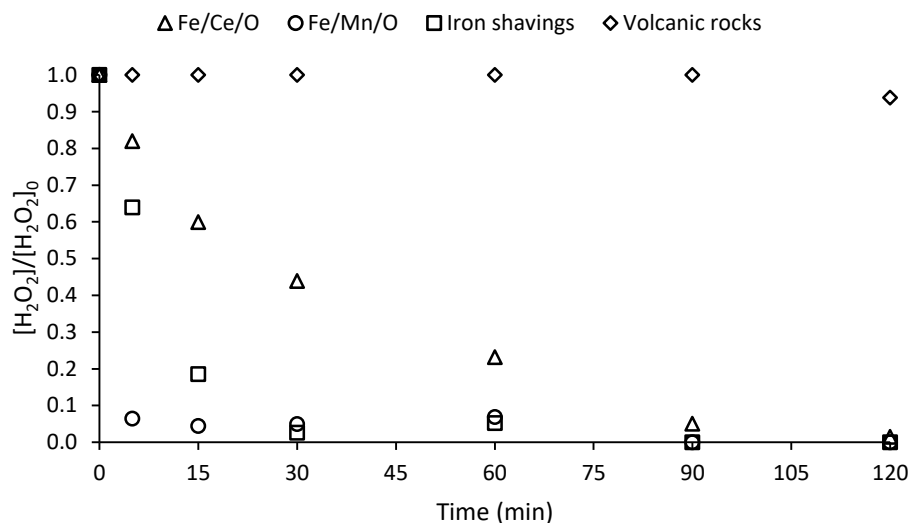
Figure 8.5. H_2O_2 concentration along three dark Fenton experiments conducted by using three different catalysts at an initial pH of 7.0. $[SMX]_0$ = 10 mg L^{-1}, $[H_2O_2]_0$ = 500 mg L^{-1}, [Fe/Ce/O catalyst]$_0$ = 1.0 g L^{-1}, [Volcanic rocks]$_0$ = 1.0 g L^{-1}, [Iron shavings]$_0$ = 3.0 g L^{-1}.

Figure 8.6 shows the soluble iron concentration of the three experiments performed at an initial pH of 7.0.

Volcanic rocks, as it happened when performing the experiment at acidic pH, do not present iron leaching nor SMX degradation, so not homogeneous nor heterogeneous Fenton catalytic activity was observed.

When applying iron shavings as catalyst at neutral pH, no iron was detected, but neither SMX degradation, which confirmed that the experiment performed at acidic pH was fully homogeneous Fenton. This catalyst mechanism was considered to work as zero valent iron, which is also metallic iron but changing mainly their particle size. ZVI nanoparticles mechanism at neutral pH need the presence of a high dissolved oxygen concentration to produce the catalyst surface oxidation and the consequently gradual dissolution of the iron, which acts as homogeneous catalyst but with a controlled release.

The use of Fe/Ce/O catalyst did not show significant iron leaching during reaction. Even so, as it happened with volcanic rocks, a low amount of iron was detected since the addition

135

of the catalyst. This confirmed that the strong acidic medium combined with the high H_2O_2 concentration were the responsible of the iron release observed at acidic pH and also reinforced the idea of a major contribution of the homogeneous Fenton reaction.
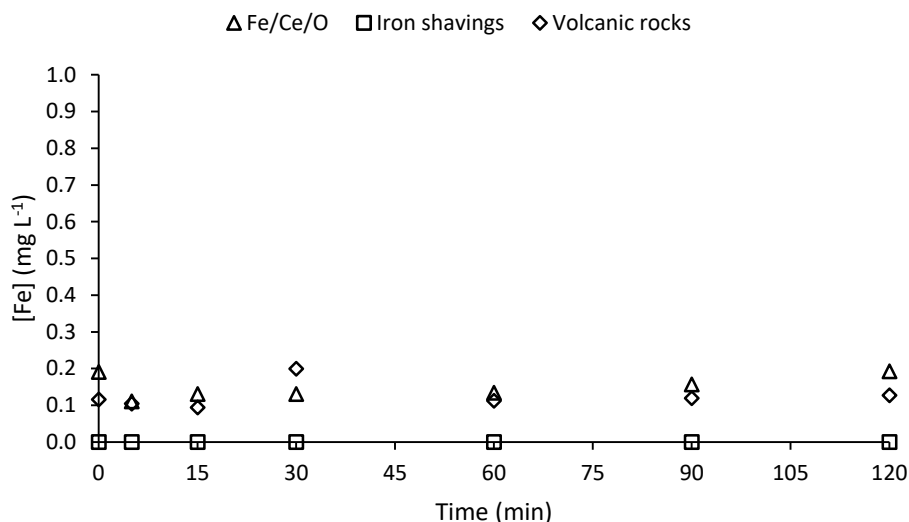
Figure 8.6. Iron concentration along three dark Fenton experiments conducted by using Fe/Ce/O, iron shavings and volcanic rocks as catalysts at an initial pH of 7.0. [SMX]$_0$ = 10 mg L^{-1}, [H$_2$O$_2$]$_0$ = 500 mg L^{-1}, [Fe/Ce/O catalyst]$_0$ = 1.0 g L^{-1}, [Volcanic rocks]$_0$ = 1.0 g L^{-1}.

8.3.3.   Photo-Fenton experiments

After the evaluation of the tested catalysts results by using dark Fenton reactions, it was considered that, among the selected catalysts, only Fe/Ce/O catalyst and volcanic rocks could produce an improvement by including UV-A light and consequently adding photo-Fenton reactions to the global mechanism. Thus, Fe(III) and Ce(IV) non-reactive species which did not produce any effects through dark Fenton reaction could possibly be turned into Fe(II) and Ce(III) active species by UV-A irradiation. Iron shavings were discarded due to their high iron release at acidic pH and its lack of activity at neutral pH Fenton experiments. For this reason, only Fe/Ce/O and volcanic rocks were tested as heterogeneous photo-Fenton catalyst at neutral pH.

136

Fe/Ce/O and volcanic rocks were applied as photo-Fenton heterogeneous catalysts to treat 4 L distilled water matrix samples spiked to an initial SMX concentration of 10 mg L^{-1}. The experimental conditions were kept the same as the ones applied when studying the performance of Fe(III)/alginate dehydrated catalyst in order to compare ($[H_2O_2]_0$ = 20 mg L^{-1}, catalyst amount = 0.5 g L^{-1}, pH_0 = 7.0). SMX degradation profiles can be found in Figure 8.7.
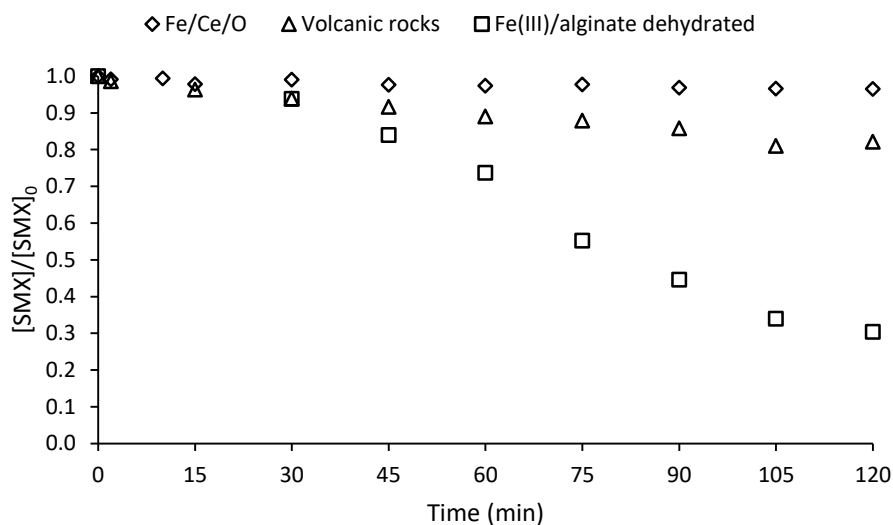
Figure 8.7. SMX degradation along three photo-Fenton experiments conducted by using three different catalysts at an initial pH of 7.0. $[SMX]_0$ = 10 mg L^{-1}, $[H_2O_2]_0$ = 20 mg L^{-1}, [Fe/Ce/O catalyst]$_0$ = 0.5 g L^{-1}, [Volcanic rocks]$_0$ = 0.5 g L^{-1}, [Fe(III)/alginate dehydrated catalyst]$_0$ = 0.5 g L^{-1}.

A very little SMX degradation (3 %) was observed after 120 minutes of treatment when using Fe/Ce/O catalyst. Moreover, when applying volcanic rocks as catalyst, a low SMX degradation rate of 0.018 mg L^{-1} min^{-1} was obtained, achieving a final degradation of about 20 % after 120 minutes. In comparison with Fe(III)/alginate dehydrated catalyst, which was able to remove about a 70 % of the initial SMX in the same time, both catalysts presented significantly lower efficiency.

Figure 8.8 shows the H_2O_2 consumption profiles of the experiments performed by using the three catalysts. The experiments performed by using volcanic rocks and the alginate-based catalyst show a similar initial H_2O_2 consumption, with a linear rate of about

0.17 mg L^{-1} min^{-1} during the first 60 minutes of reaction. They finally achieved a total consumption of 65 % and 75 %, respectively. On the contrary, the experiment performed by using Fe/Ce/O catalyst shows a very quick consumption rate which achieves the total H_2O_2 consumption before 30 minutes of treatment.
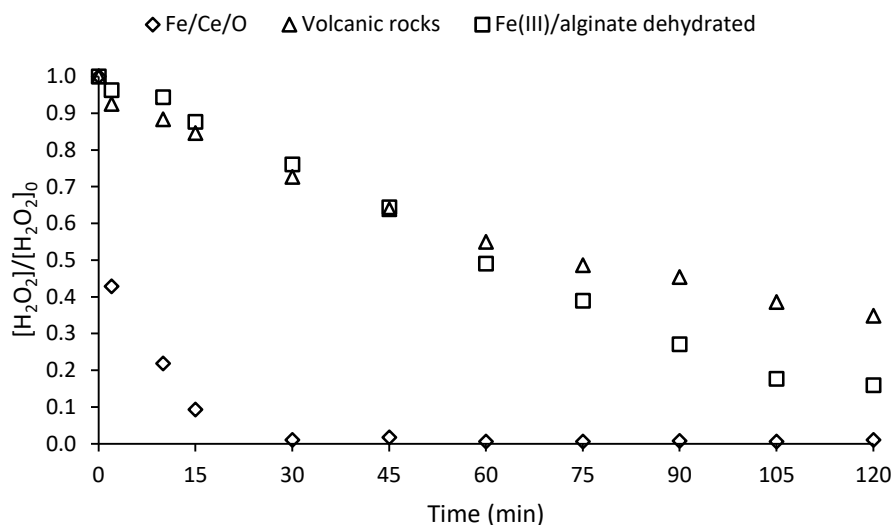
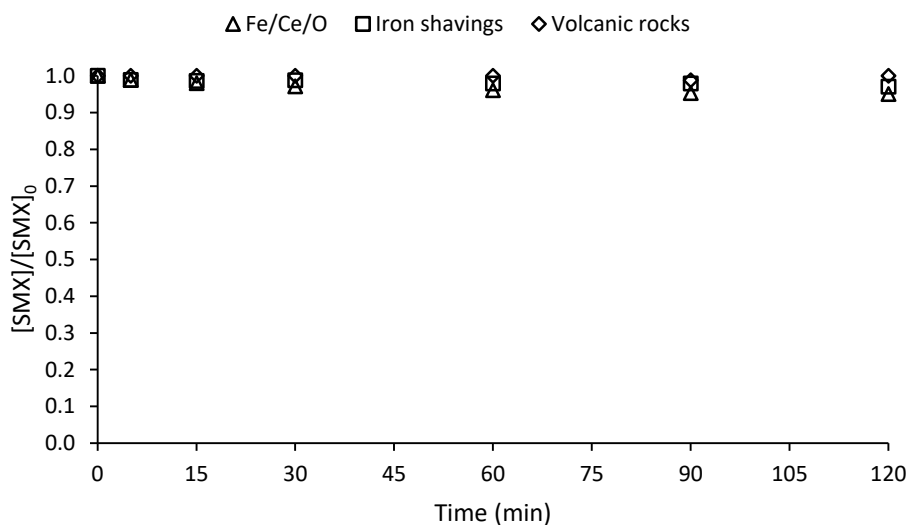**Figure 8.8. H_2O_2 concentration along three photo-Fenton experiments conducted by using three different catalysts at an initial pH of 7.0. [SMX]$_0$ = 10 mg L^{-1}, [H_2O_2]$_0$ = 20 mg L^{-1}, [Fe/Ce/O catalyst]$_0$ = 0.5 g L^{-1}, [Volcanic rocks]$_0$ = 0.5 g L^{-1}, [Fe(III)/alginate dehydrated catalyst]$_0$ = 0.5 g L^{-1}.**

Some conclusions can be drawn by comparing volcanic rocks and Fe(III)/alginate dehydrated catalysts results after the 120 minutes of treatment. Alginate-based catalyst consumed 2.5 mg L^{-1} of H_2O_2 per mg L^{-1} of SMX removed while volcanic rocks' ratio was only of 7.5 mg L^{-1} of H_2O_2 per mg L^{-1} of SMX depleted (Figure 8.9). This difference indicates that Fe(III)/alginate dehydrated catalyst photo-Fenton reaction was more efficient on the production of HO· per mg L^{-1} of H_2O_2 consumed.

The total H_2O_2 consumption of Fe/Ce/O catalyst with no significant SMX removal, which results in a ratio of 59.8 mg L^{-1} of H_2O_2 per mg L^{-1} of SMX depleted (Figure 8.9) confirmed the already mentioned H_2O_2 decomposition produced by this catalyst without the formation of

effective oxidative species. No references to this phenomenon were found in scientific literature but the results obtained pinpoint to this conclusion.
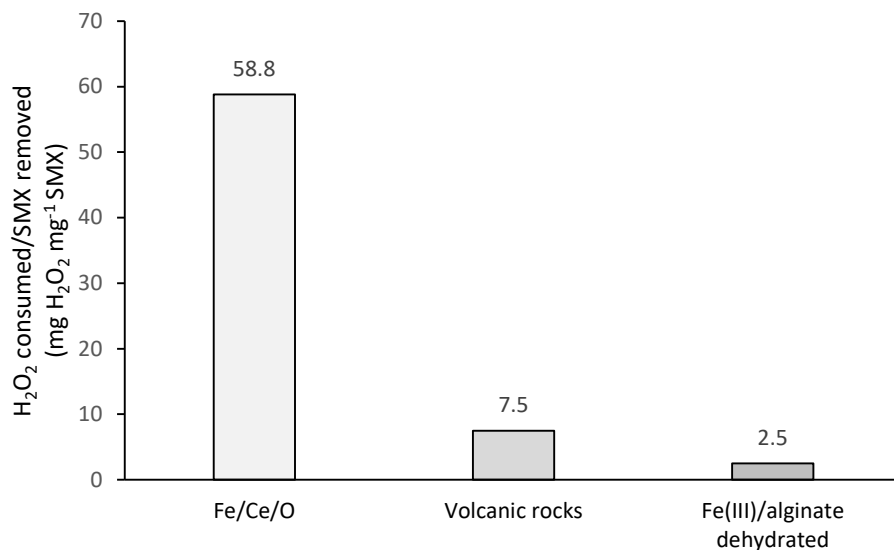
Figure 8.9. Ratio of H_2O_2 consumed per SMX removed after 120 minutes of treatment by using three different catalysts at an initial pH of 7.0. $[SMX]_0$ = 10 mg L^{-1}, $[H_2O_2]_0$ = 20 mg L^{-1}, [Fe/Ce/O catalyst]$_0$ = 0.5 g L^{-1}, [Volcanic rocks]$_0$ = 0.5 g L^{-1}, [Fe(III)/alginate dehydrated catalyst]$_0$ = 0.5 g L^{-1}.

Figure 8.10 shows the monitoring of soluble iron concentration during the experiments by using the three catalysts. As it happened on previous experiments, volcanic rocks and Fe/Ce/O catalyst presented an initial small amount of iron. When applying these catalysts to photo-Fenton reaction, no iron leaching was detected. The alginate-based catalyst, on the contrary, released iron as the reaction progressed, what was already explained on previous chapters.
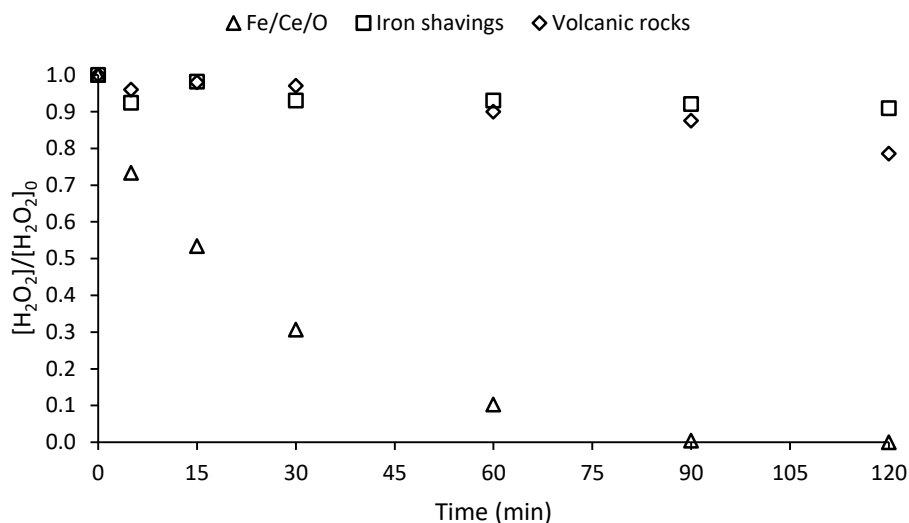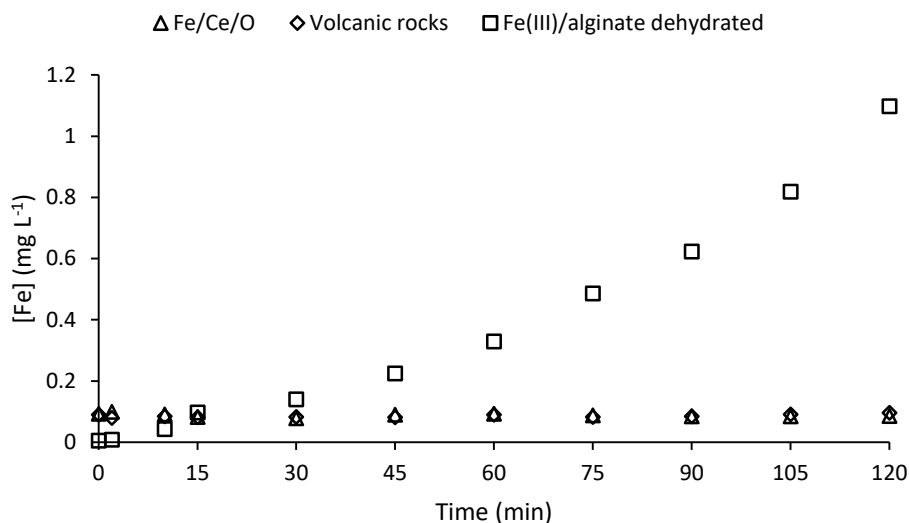
Figure 8.10. Dissolved iron concentration along three photo-Fenton experiments conducted by using three different catalysts at an initial pH of 7.0. $[SMX]_0$ = 10 mg L^{-1}, $[H_2O_2]_0$ = 20 mg L^{-1}, [Fe/Ce/O catalyst]$_0$ = 0.5 g L^{-1}, [Volcanic rocks]$_0$ = 0.5 g L^{-1}, [Fe(III)/alginate dehydrated catalyst]$_0$ = 0.5 g L^{-1}.

As the soluble iron concentration measured in experiments performed with volcanic rocks and Fe/Ce/O catalyst was almost the same (about 0.1 mg L^{-1}), the 3 % SMX degradation observed when applying the catalyst containing cerium could be attributed to homogeneous photo-Fenton reaction. Thus, the difference in SMX degradation observed between both catalysts could be considered as effective heterogeneous photo-Fenton reaction produced on volcanic rocks surface. Additionally, as no SMX degradation was observed when applying this catalyst to dark Fenton reaction, it could be considered that iron in volcanic rocks is mainly in the form of Fe(III) species, which are not active for Fenton reaction. Thus, the irradiation of the catalyst allowed transforming this Fe(III) species into Fe(II), which are able to catalyse H_2O_2 decomposition producing HO·.

Table 8.1 presents the main observations done during the evaluation of the experimental results in this chapter. It can be concluded that the only viable catalysts for its application on the removal of SMX through photo-Fenton at circumneutral pH are volcanic rocks and, with much higher effectiveness, Fe(III)/alginate dehydrated catalyst.

Table 8.1. Global resume of the main experimental observations done in this chapter.

Process	pH	Fe/Ce/O	Fe/Mn/O	Iron shavings	Volcanic rocks	Fe(III)/alginate
Fenton	Acidic pH (3.0)	H_2O_2 direct decomposition Homogeneous 22% SMX removal	H_2O_2 direct decomposition No SMX removal	Homogeneous Excessive Fe release	No SMX removal	Homogeneous Excessive Fe release
	Neutral pH (7.0)	H_2O_2 direct decomposition Homogeneous 7% SMX removal	H_2O_2 direct decomposition No SMX removal	No SMX removal	No SMX removal	No SMX removal
Photo-Fenton	Neutral pH (7.0)	H_2O_2 direct decomposition Homogeneous 3% SMX removal	H_2O_2 direct decomposition No SMX removal	No SMX removal	18 % SMX removal	70% SMX removal

8.4. CONCLUSIONS

Experimental results shown in this chapter presented the performance of some inorganic nature heterogeneous catalyst when applied to dark Fenton at acidic and neutral pH and photo-Fenton at neutral pH.

Fe/Mn/O catalyst was early discarded for Fenton-like reactions due to its ability to instantly decompose H_2O_2 into water and oxygen, making impossible to conduct this kind of reactions that use H_2O_2 as precursor for the formation of HO· as oxidative specie.

Also, the use of iron shavings as a possible low cost Fenton catalyst was discarded. Its application at acidic pH led to the release of enormous amounts of iron into samples, which was undesired. Furthermore, when applied at neutral pH, it was not able to catalyze the reaction.

The application of the synthetized Fe/Ce/O catalyst also presented H_2O_2 direct decomposition without the production of oxidative species, as it happened with Fe/Mn/O catalyst, but with a lower rate. Some degradation was observed when applied as dark Fenton catalyst at acidic pH, but the SMX degradation observed was attributed to the homogeneous contribution that was produced due to the iron leaching that happened at acidic pH in the presence of a high concentration of the oxidant H_2O_2.

Volcanic rocks catalytic activity was confirmed only when applied to photo-Fenton reaction. This catalyst was supposed to be formed mainly by Fe(III) non-catalytic species that required to be irradiated with UV-A light to be turned into Fe(II) active species. Even so, the efficiency obtained by this catalyst was low.

As a global conclusion, the use of catalysts of inorganic nature applied to Fenton and photo-Fenton reaction presented low or no catalytic activity in comparison to Fe(III)/alginate dehydrated catalyst, whose nature is organic. To be able to act as Fenton catalyst, iron in catalysts must be able to change from Fe(II) to Fe(III). Organic nature catalysts as Fe(III)/alginate looks to permit this change of valence easier, but in consequence, they are more prone to release this iron into water increasing the contribution of homogeneous reaction pathway.

9. Conclusions and recommendations

9.1. CONCLUSIONS

The main objective of this thesis was to evaluate the synthesis and the further application of alginate-based catalysts for heterogeneous Fenton-like and photo-Fenton like reactions for micropollutants removal and disinfection.

The conclusions to each interim goal proposed in chapter 2 have been provided at the end of chapters 4 to 8. A summary of all these conclusions obtained can be found below:

Chapter4: Fe(III)/alginate catalyst development

➢ Fe (III) resulted to be the more convenient oxidation state to use for the catalyst synthesis due to the better mechanical properties of the catalyst after preparation.

➢ Alginate solution concentration determined the amount of available spots for iron to act as cross-linking agent. The higher the concentration, the higher the amount of iron that alginate was able to absorb.

➢ Iron concentration in hardening solution determined the diffusion rate of iron cations through alginate during hardening stage. Thus, the higher the concentration, the higher the amount of iron that got bond with alginate or he same hardening time.

➢ Alginate solution temperature was found to be key (or determinant) factor in the production smaller spheres of catalyst. A slightly higher temperature varied significantly the solution viscosity allowing smaller drops of the alginate solution when added over hardening solution.

➢ An adequate cleaning stage was essential to remove the non-cross-linked iron from catalyst and consequently avoid the homogeneous reactions due to the residual iron from hardening solution.

➢ The use of a 2.5 % (w/w) alginate solution, a $FeCl_3$ 0.05 M hardening solution and 6 hours of hardening time resulted to be the optimal conditions for the preparation of the Fe/alginate catalyst for its application to photo-Fenton process.

Chapter 5: Fe(III)/alginate catalyst mechanism and stability

➢ pH plays a very important role on alginate-based catalysts stability. It's been demonstrated that iron release as soluble iron is linked with solutions pH when below alginate carboxylic groups' pK_a, increasing the contribution of the homogenous photo-Fenton reaction mechanism.

➢ When Fe(III)/alginate catalyst is applied in non-buffered samples, the acidification tendency of Fenton reactions triggers the release of soluble iron and turns the initially fully heterogeneous reaction into simultaneous homogeneous and heterogeneous reactions. The more iron is released, the higher is the contributions of the homogeneous one until heterogeneous reaction can be considered negligible.

➢ Alginate itself, due to its organic, easy-to-degrade nature, acts as a competitor for the oxidative species formed during reaction, which turns itself into a strong HO· radicals scavenger and reduces significantly the overall removal efficiency. Consequently, a release of iron and TOC is produced.

➤ Fe(III)/alginate catalyst activity as heterogeneous catalyst for photo-Fenton reaction at circumneutral pH have been proved to exist but its observable efficiency when applied to SMX depletion was very low because of the alginate scavenging effect.

➤ The sequential reutilization of Fe(III)/alginate catalyst obtained lower efficiencies after each use due to the catalyst self-degradation, that reduced gradually the catalyst size and consequently the surface area in which the heterogeneous reaction was produced.

Chapter 6: Fe(III)/alginate catalyst applied for disinfection

➤ Fe(III)/alginate catalyst was able to achieve total inactivation of Escherichia Coli when applied as photo-Fenton heterogeneous catalyst in distilled water, with minimal contribution of homogeneous photo-Fenton reaction.

➤ Fe(III)/alginate catalyst applied as photo-Fenton heterogeneous catalyst in bottled drinking water inactivated more than 99 % of the initial 1.14×10^4 CFU mL^{-1} of Escherichia Coli but 14 CFU mL^{-1} were still detected after 60 minutes. The lower contribution of homogeneous reaction due to the naturally buffered medium produced a reduction of the overall disinfection rate and did not allow the total inactivation.

➤ Compared to other disinfection technologies, the non-harmful nature of alginate catalysts suppose an advantage when applied to waters intended for human consumption. Thus, it could be a suitable candidate for disinfection of effluents with low organic loads in compliance with the soluble iron limits in current water legislation (0.2 mg L^{-1}). Even so, the reaction conditions must be adjusted to

minimize iron release and according to the microbiological population to ensure total disinfection.

➢ Fe(III)/alginate catalyst was applied to the inactivation of M4 bacteriophage virus, which is a specially resistant to AOPs microorganism, achieved a removal of 98.5% of the initial virus spiked in samples, which indicates that it is not totally efficient to inactivate resistant microorganisms on the applied conditions.

Chapter 7: Fe(III)/alginate catalyst modifications

➢ The application of a controlled dehydration process to Fe(III)/alginate catalyst allow to synthetize the dehydrated Fe(III)/alginate catalyst, which proved to be as much as efficient as the hydrated one when imitating photo-Fenton reaction at circumneutral pH, but with a scarce iron and TOC release.

➢ The use of dehydrated Fe(III)/alginate catalyst on naturally buffered water at neutral or slightly basic pH, when the homogeneous reaction is avoided, didn't have a visible oxidative effect over the reference compound studied (sulfamethoxazole).

➢ The combination of photo-Fenton reaction by iron coordinated with alginate together with the photocatalytic contribution of entrapped TiO_2 significantly improved the SMX removal rate.

➢ The inclusion of cerium and zero valent iron into the catalyst proved useless to improve the effectiveness of dehydrated Fe(III)/alginate catalyst at circumneutral pH.

Chapter 8: Heterogeneous catalysts intended for Fenton and photo-Fenton at neutral pH

➢ Fe/Mn/O catalyst was discarded for Fenton-like reactions due to manganese oxides' ability to instantly decompose H_2O_2 into water and oxygen, making impossible to conduct reactions that use H_2O_2 as precursor for the formation of HO· as oxidative specie.

➢ Irons shavings from metallurgic industry were discarded as possible low cost Fenton catalyst due to the lack of reaction observed at neutral pH and the enormous amount of iron released when conducting the reaction on acidic conditions.

➢ Fe/Ce/O catalyst proved to produce H_2O_2 direct decomposition without the production of oxidative species, as it happened with Fe/Mn/O catalyst, but with a lower rate.

➢ Fenton experiments performed with Fe/Ce/O catalyst presented some SMX degradation at acidic pH. Global results suggested that the strong acidic pH and the high concentration of H_2O_2 produced the partial solubilization of Fe from the catalyst. Thus, the observed SMX depletion could be attributed to homogeneous Fenton reaction.

➢ Volcanic rocks catalytic activity was confirmed only when applied to photo-Fenton reaction. This catalyst was supposed to be formed mainly by Fe(III) non-catalytic species that required to be irradiated with UV-A light to be turned into Fe(II) active species. Even so, the efficiency obtained by this catalyst was low.

➢ Fe(III)/alginate dehydrated catalyst proved to be more efficient on the degradation of sulfamethoxazole through photo-Fenton reaction at circumneutral pH than all other heterogeneous catalysts tested.

147

As a global conclusion, the use of alginate-based catalysts intended for photo-Fenton reaction presents three main drawbacks: the iron release produced at pHs below its pK_a, the HO· radicals scavenging effect produced by the catalyst itself due to its organic nature and the consequent release of soluble iron and TOC.

Even so, when the photo-Fenton reaction conditions were carefully controlled, Fe(III)/alginate catalyst proved to be able to remove SMX and also able to be used for disinfection with a minimal iron and TOC release.

Also, the inclusion of TiO_2 in Fe(III)/alginate catalyst can be a suitable way of increasing the overall removal efficiency by adding a second radical production pathway into the process.

9.2. RECOMMENDATIONS

Regarding the results in chapter 6 and considering the improvement achieved by the dehydrated catalyst that have been observed in chapter 7, it would be interesting to test this modified catalyst applied for disinfection.

Also, its application for disinfection could be studied deeply by using different kind of low organic load matrixes and different microorganisms' concentrations to optimize the process and know the optimal conditions to achieve total disinfection depending on the effluent.

Moreover, considering that the modification of this catalyst by entrapping TiO_2 particles resulted in an increase of its efficiency, it could be of interest the optimization of this catalyst by varying the amount of TiO_2 added during its preparation. Also, regarding this TiO_2 modified catalyst, it could be necessary to evaluate possible discharge of TiO_2 into the effluent during the treatment.

To conclude, once the operational conditions of these processes were optimized, it would be necessary to perform an economical study by comparing the use of this technology with

some other ones which serve to the same purpose, as the disinfection with UV-C lamps or the addition of chlorine.

10. Other works

During the execution of this PhD thesis, some other promising works were performed.

10.1. DISINFECTION THROUGH AOPS FOR THE DESALINATION OF SEAWATER BY REVERSE OSMOSIS

This work was performed on the first year of this PhD thesis was fund and conducted in collaboration with the R+D+i department of ACCIONA AGUA in El Prat de Llobregat (SPAIN). It was englobed inside the project SISIFO (IDI-20101742) and had the aim of studying the application of a disinfection process through AOPs prior to the desalination of seawater by using reverse osmosis membranes. This was proposed as a possible way of reducing the formation of biofouling and consequently the membranes lifetime [159].

This project focused on the application of ozonation and UV-C/H_2O_2 processes for disinfection of seawater. Also, UV-C alone was tested.

Fresh samples were regularly collected from sea at the beach of Gavà (SPAIN) and then submitted to these processes in 2 L batch reactors in experiments from 1 to 15 minutes. A concentration of 5 mg L^{-1} of H_2O_2 and three 8 W low pressure mercury UV-C lamps were used for UV-C/H_2O_2 process and the same lamps but without H_2O_2 for direct disinfection by UV-C light. Ozone was generated in-situ and applied by using a bubbles diffusor. The transferred dose of ozone was of 0.131 mg L^{-1} min^{-1}.

Disinfection was evaluated by two different processes. The first one was the use of specific culture mediums to count bacteria populations along the experiments. The target microorganisms were selected by ACCIONA according to their previous experience. These microorganisms were *Escherichia Coli*, coliform bacteria, *Vibrio algynoliticus* and *Vibrio parahaemolyticus*. Also total bacteria population was evaluated by using marine agar as a general culture media. The second way of evaluating disinfection was through the quantification of Adenosin Tri-Phosphate (ATP). This compound is a molecule responsible

for most energy transactions inside cells. Cellular ATP and free ATP were measured during the processes. The reduction of cellular ATP indicated the destruction of the cell membranes from bacteria, what consequently caused their death.

Total disinfection was achieved in 15 minutes, 10 minutes and 5 minutes by using UV, UV-C/H_2O_2 and ozonation, respectively.

After the disinfection, samples were submitted to a regrowth process in dark for 10 days to evaluate the possible reappearance of bacteria that survived the process, as it would happen in reverse osmosis membranes.

50 %, 7 % and 17 % of the initial amount of cellular ATP measured before the treatments was observed after the regrowth process by using UV-C, UV-C/H_2O_2 and ozonation, respectively. This indicated that UV-C/H_2O_2 was the best solution as disinfection pre-treatment for reverse osmosis.

Also, some pieces of reverse osmosis membranes provided by ACCIONA were directly submitted to these treatments and lately analyzed by them to evaluate possible negative effects of the treatments over the membranes.

10.2.   NEW DISINFECTION INDICATORS FOR AOP PROCESSES

This work was conducted for 18 months simultaneously to part of the work presented previously in this thesis. It was done in collaboration with the *Microbiology of water related to the health* group (*MARS*) from the Microbiology Department of the University of Barcelona. The project consisted on the evaluation of different microorganisms proposed by the *MARS* group that were considered more resistant to disinfection than the current indicator in legislation, which is *Escherichia Coli*. Thus, the inactivation of this microorganisms could ensure the total disinfection of most other harmful microorganisms that still can be present in water after *Escherichia Coli* have been totally inactivated by a disinfection process.

For this purpose, bacteria *Escherichia Coli*, the somatic coliphages PDR1 (*Tectiviridae*) and φX174 (*Microviridae*) as well as the F-specific RNA bacteriophage MS2 (*Leviviridae*) and the M4 bacteriophage virus were tested by using diverse AOPs as disinfection processes.

The AOP's applied were UV-C/H_2O_2 in a batch reactor, UV-C/H_2O_2 in a recirculating tubular reactor, heterogeneous photo-Fenton at neutral pH in a batch rector by using Fe(III)/alginate hydrated catalyst and homogeneous photo-Fenton at neutral pH by using a solar simulator Solar-BOX.

After evaluating the performance of all microorganisms submitted to these processes, UV-C/H_2O_2 in a batch reactor was discarded because the irradiation of the available lamps were too powerful and achieved total disinfection in less than 1 minute for all microorganisms. The solar simulator was also discarded because the temperature inside the reactor was too high and interfered significantly with the disinfection process.

Finally, experiments by using UV-C/H_2O_2 in a tubular recirculated reactor and through heterogeneous photo-Fenton with alginate beads were selected for the experimentation.

A publication including all these experiments is being written with the aim of being submitted soon.

10.3.   STUDY OF THE FORMATION OF FOULING IN UV-C LOW PRESSURE MERCURY LAMPS' SLEEVES

This work was performed during a 5 moth stay in the Research Center for Eco-Environmental Science (RCEES) of the Chinese Academy of Sciences in Beijing (CHINA).

The aim of this project was to evaluate the formation of inorganic fouling in UV-C low pressure mercury lamps' sleeves, study its composition and measure the mitigation effects produced over UV-C lamps emission.

For this purpose it was necessary to design a reactor that operates in the adequate conditions to promote the formation of this fouling in a short time. According to EPA, the main fouling agents in UV lamp sleeves are calcium, alkalinity, hardness, iron and manganese [37]. Literature mainly indicated that the deposition of this compounds was favored by high temperature and slow flowrates [160,161].

Three reactors of 5 L, each one coupled with a recirculation tank of 50L were used. The reactors included a Hg low pressure UV lamp of 15 W, two micro fluorescent silica detector (MFSD) for UV fluency measurement and a thermostatic bath for inlet water temperature control (25°C). Reactors operated during 21 days with three different Beijing tap water matrix feed waters spiked with different amounts of Fe(III), which was considered the main compound affecting UV mitigation due to its high absorbance (Reactor A: No addition, Reactor B: 0.3 mg L^{-1} of Fe(III) addition, Reactor B: 0.5 mg L^{-1} of Fe(III) addition). Its flow rate was set to 60 L h^{-1} in order to promote fouling formation in a short time. After this time, inorganic fouling from sleeves was recovered by using an acidic solution and main metallic compounds (Fe, Ca, Mg, K, Na) were analyzed by means of inductively coupled plasma atomic emission spectroscopy (ICP-AES). Results can be observed at Figure 10.1.
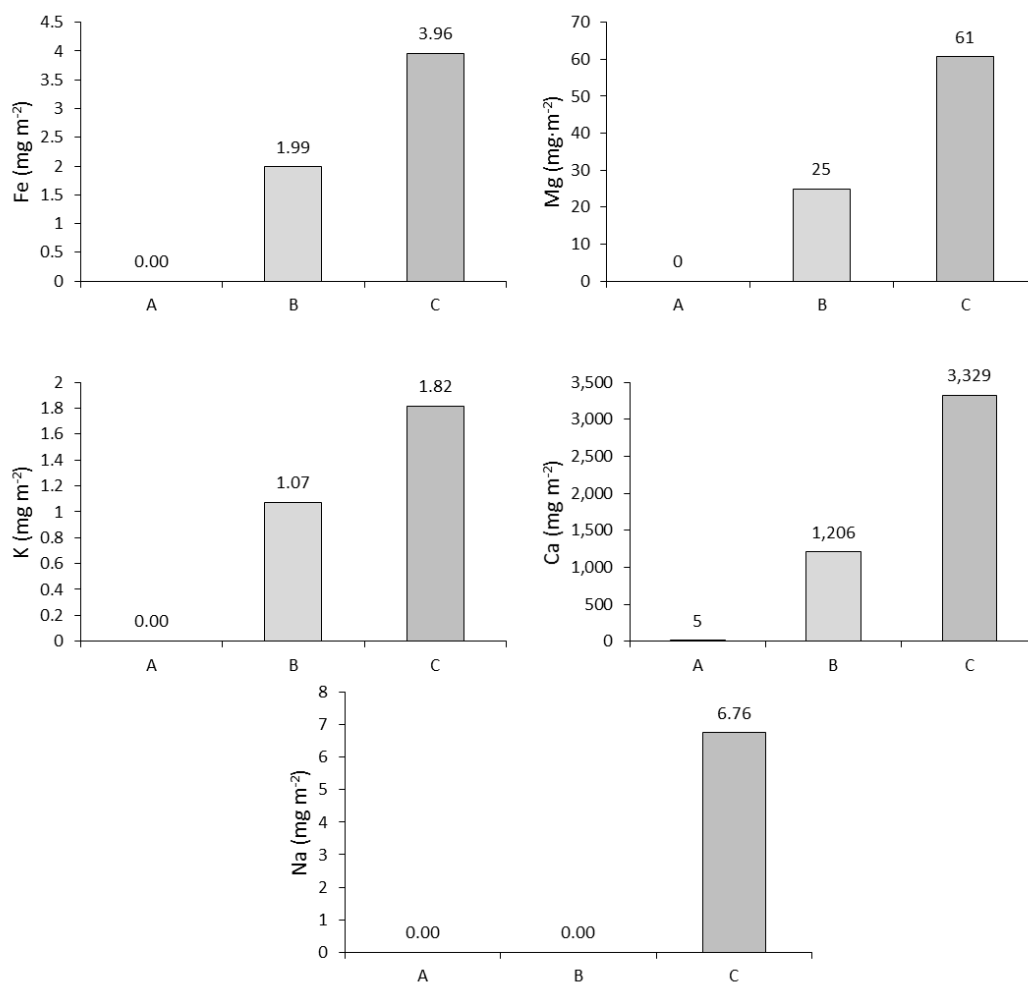
Figure 10.1. Fe, Mg, K, Ca and Na amount measured through ICP-AES of the reactors A, B and C lamps' sleeves after 21 days of operation.

Also, Figure 10.2 shows the visual aspect of lamps's sleeves after these 21 days of operation.
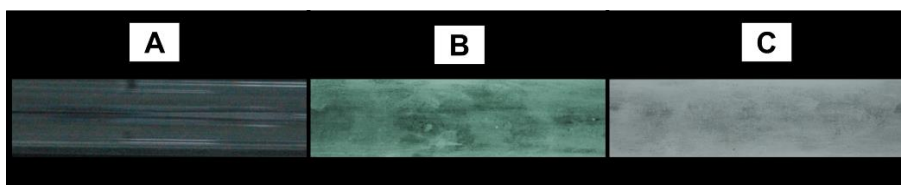
Figure 10.2.Visual aspect of lamps' sleeves of reactors by using A) Beijing tap water, B) Beijing tap water + 0.3 mg L^{-1} of Fe(III) and C) Beijing tap water + 0.5 mg L^{-1} of Fe(III) after 21 days of operation.

155

Despite these promising initial results, due to logistical problems the reactors were not ready until the last month of stay so only the preliminary experimentation was performed and no further data was obtained.

11. References

[1]   H.H.. Savenije, Water scarcity indicators; the deception of the numbers, Phys. Chem. Earth, Part B Hydrol. Ocean. Atmos. 25 (2000) 199–204. doi:10.1016/S1464-1909(00)00004-6.

[2]   U. Nations, D. Programme, Human Development Report 2006, 2006.

[3]   M. Falkenmark, C. Widstrand, Population and water resources: a delicate balance., Popul. Bull. 47 (1992) 1–36.

[4]   United Nations, International Decade for Action "Water for Life" 2005-2015. Focus Areas: Water scarcity, (n.d.). http://www.un.org/waterforlifedecade/scarcity.shtml (accessed March 27, 2017).

[5]   FAO Corporate Document Repository, Wastewater treatment, (n.d.). http://www.fao.org/docrep/t0551e/t0551e05.htm (accessed March 27, 2017).

[6]   J. Melgarejo, D. Prats, A. Molina, A. Trapote, A case study of urban wastewater reclamation in Spain: comparison of water quality produced by using alternative processes and related costs, J. Water Reuse Desalin. (2015) jwrd2015147. doi:10.2166/wrd.2015.147.

[7]   A. Jelic, M. Gros, A. Ginebreda, R. Cespedes-Sánchez, F. Ventura, M. Petrovic, D. Barcelo, Occurrence, partition and removal of pharmaceuticals in sewage water and sludge during wastewater treatment, Water Res. 45 (2011) 1165–1176. doi:10.1016/j.watres.2010.11.010.

[8]   M. Clara, B. Strenn, O. Gans, E. Martinez, N. Kreuzinger, H. Kroiss, Removal of selected pharmaceuticals, fragrances and endocrine disrupting compounds in a membrane bioreactor and conventional wastewater treatment plants, Water Res. 39 (2005) 4797–4807. doi:10.1016/j.watres.2005.09.015.

[9]   S. Glassmeyer, E.T. Furlong, D.W. Kolpin, J.D. Cahill, S.D. Zaugg, S.L. Werner, M.T. Meyer, D.D. Kryak, Transport of chemical and microbial contaminants from known wastewater discharges: potential for use as indicators of human fecal contamination, Environ. Sci. Technol. 39 (2005) 5157–5169.

[10]   European Comission, Introduction to the new EU Water Framework Directive - Environment - European Commission, (n.d.). http://ec.europa.eu/environment/water/water-framework/info/intro_en.htm (accessed March 27, 2017).

[11]   European Comission, Priority Substances and Certain Other Pollutants according to Annex II of Directive 2008/105/EC - Environment - European Commission, (n.d.). http://ec.europa.eu/environment/water/water-framework/priority_substances.htm (accessed March 28, 2017).

[12]   M. Petrović, S. Gonzalez, D. Barceló, Analysis and removal of emerging contaminants in wastewater and drinking water, TrAC Trends Anal. Chem. 22 (2003) 685–696. doi:10.1016/S0165-9936(03)01105-1.

[13]   M. la Farré, S. Pérez, L. Kantiani, Fate and toxicity of emerging pollutants, their metabolites and transformation products in the aquatic environment, TrAC Trends Anal. Chem. 27 (2008) 991–1007. doi:10.1016/j.trac.2008.09.010.

[14]   S.D. Richardson, M.J. Plewa, E.D. Wagner, R. Schoeny, D.M. DeMarini, Occurrence, genotoxicity, and carcinogenicity of regulated and emerging disinfection by-products in drinking water: A review and roadmap for research, Mutat. Res. Mutat. Res. 636 (2007) 178–242. doi:10.1016/j.mrrev.2007.09.001.

[15]   Y. Luo, W. Guo, H.H. Ngo, L.D. Nghiem, F.I. Hai, J. Zhang, S. Liang, X.C. Wang, A review on the occurrence of micropollutants in the aquatic environment and their fate and removal during wastewater treatment, Sci. Total Environ. 473 (2014) 619–641. doi:10.1016/j.scitotenv.2013.12.065.

[16]   A. Ginebreda, I. Muñoz, M.L. de Alda, R. Brix, J. López-Doval, D. Barceló, Environmental risk assessment of pharmaceuticals in rivers: Relationships between hazard indexes and aquatic macroinvertebrate diversity indexes in the Llobregat River (NE Spain), Environ. Int. 36 (2010) 153–162. doi:10.1016/j.envint.2009.10.003.

[17]   G. Teijon, L. Candela, K. Tamoh, A. Molina-Díaz, A.R. Fernández-Alba, Occurrence of emerging contaminants, priority substances (2008/105/CE) and heavy metals in treated wastewater and groundwater at Depurbaix facility (Barcelona, Spain), Sci. Total Environ. 408 (2010) 3584–3595. doi:10.1016/j.scitotenv.2010.04.041.

[18]   D.W. Kolpin, M.T. Meyer, Pharmaceuticals , Hormones , and Other Organic Wastewater Contaminants in U . S . Streams , 1999 - 2000 : A National Reconnaissance, Environ. Sci. Technol. 36 (2002) 1202–1211. doi:10.1021/es011055j.

[19]   P.J. Phillips, S.G. Smith, D.W. Kolpin, S.D. Zaugg, H.T. Buxton, E.T. Furlong, K. Esposito, B. Stinson, Pharmaceutical formulation facilities as sources of opioids and other pharmaceuticals to wastewater treatment plant effluents, Environ. Sci. Technol. 44 (2010) 4910–4916. doi:10.1021/es100356f.

[20]   C.G. Daughton, T.A. Ternes, Pharmaceuticals and personal care products in the environment: agents of subtle change, Environ. Health Perspect. (1999) 907–38. http://www.ncbi.nlm.nih.gov/pubmed/10592150 (accessed March 28, 2017).

[21]   I. Muñoz, M.J. Gómez-Ramos, A. Agüera, A.R. Fernández-Alba, J.F. García-Reyes, A. Molina-Díaz, Chemical evaluation of contaminants in wastewater effluents and the environmental risk of reusing effluents in agriculture, TrAC Trends Anal. Chem. 28 (2009) 676–694. doi:10.1016/j.trac.2009.03.007.

[22]   H.Y. Kim, T.-H. Kim, S.M. Cha, S. Yu, Degradation of sulfamethoxazole by ionizing radiation: Identification and characterization of radiolytic products, Chem. Eng. J. 313 (2017) 556–566. doi:10.1016/j.cej.2016.12.080.

[23]   D.C.G. Bedor, T.M. Gonçalves, M.L.L. Ferreira, C.E.M. de Sousa, A.L. Menezes, E.J.

Oliveira, D.P. de Santana, Simultaneous determination of sulfamethoxazole and trimethoprim in biological fluids for high-throughput analysis: Comparison of HPLC with ultraviolet and tandem mass spectrometric detection, J. Chromatogr. B Anal. Technol. Biomed. Life Sci. 863 (2008) 46–54. doi:10.1016/j.jchromb.2007.12.027.

[24]   J.C. Underwood, R.W. Harvey, D.W. Metge, D.A. Repert, L.K. Baumgartner, R.L. Smith, T.M. Roane, L.B. Barber, Effects of the antimicrobial sulfamethoxazole on groundwater bacterial enrichment, Environ. Sci. Technol. 45 (2011) 3096–3101. doi:10.1021/es103605e.

[25]   M. Touraki, I. Niopas, C. Kastritsis, Bioaccumulation of trimethoprim, sulfamethoxazole and N-acetyl-sulfamethoxazole in Artemia nauplii and residual kinetics in seabass larvae after repeated oral dosing of medicated nauplii, Aquaculture. 175 (1999) 15–30. doi:10.1016/S0044-8486(99)00036-8.

[26]   M. Chair, H.J. Nelis, P. Leger, P. Sorgeloos, A.P. de Leenheer, Accumulation of trimethoprim, sulfamethoxazole, and N-acetylsulfamethoxazole in fish and shrimp fed medicated Artemia franciscana., Antimicrob. Agents Chemother. 40 (1996) 1649–52. http://www.ncbi.nlm.nih.gov/pubmed/8807056 (accessed March 28, 2017).

[27]   K.B. Barnes, J. Steward, J.E. Thwaite, M.S. Lever, C.H. Davies, S.J. Armstrong, T.R. Laws, N. Roughley, S. V. Harding, T.P. Atkins, A.J.H. Simpson, H.S. Atkins, Trimethoprim/sulfamethoxazole (co-trimoxazole) prophylaxis is effective against acute murine inhalational melioidosis and glanders, Int. J. Antimicrob. Agents. 41 (2013) 552–557. doi:10.1016/j.ijantimicag.2013.02.007.

[28]   J. Lienert, K. Güdel, B.I. Escher, Screening method for ecotoxicological hazard assessment of 42 pharmaceuticals considering human metabolism and excretory routes, Environ. Sci. Technol. 41 (2007) 4471–4478. doi:10.1021/es0627693.

[29]   T. Ternes, A. Joss, Human pharmaceuticals, hormones and fragrances : the challenge of micropollutants in urban water management, IWA Publishing, 2007.

[30]   R. Andreozzi, V. Caprio, A. Insola, R. Marotta, Advanced oxidation processes (AOP) for water purification and recovery, Catal. Today. 53 (1999) 51–59. doi:10.1016/S0920-5861(99)00102-9.

[31]   M. Klavarioti, D. Mantzavinos, D. Kassinos, Removal of residual pharmaceuticals from aqueous systems by advanced oxidation processes, Environ. Int. 35 (2009) 402–417. doi:10.1016/j.envint.2008.07.009.

[32]   P.R. Gogate, A.B. Pandit, A review of imperative technologies for wastewater treatment I: oxidation technologies at ambient conditions, Adv. Environ. Res. 8 (2004) 501–551. doi:10.1016/S1093-0191(03)00032-7.

[33]   M. Agulló-Barceló, M.I. Polo-López, F. Lucena, J. Jofre, P. Fernández-Ibáñez, Solar Advanced Oxidation Processes as disinfection tertiary treatments for real wastewater: Implications for water reclamation, Appl. Catal. B Environ. 136–137 (2013) 341–350. doi:10.1016/j.apcatb.2013.01.069.

[34]   M.I. Polo-López, I. Oller, P. Fernández-Ibáñez, Benefits of photo-Fenton at low concentrations for solar disinfection of distilled water. A case study: Phytophthora capsici, Catal. Today. 209 (2013) 181–187. doi:10.1016/j.cattod.2012.10.006.

[35]   Y. Penru, A.R. Guastalli, S. Esplugas, S. Baig, Application of UV and UV/H_2O_2 to seawater: Disinfection and natural organic matter removal, J. Photochem. Photobiol. A Chem. 233 (2012) 40–45. doi:10.1016/j.jphotochem.2012.02.017.

[36]   A.C. Miranda, M. Lepretti, L. Rizzo, I. Caputo, V. Vaiano, O. Sacco, W.S. Lopes, D. Sannino, Surface water disinfection by chlorination and advanced oxidation processes: Inactivation of an antibiotic resistant E. coli strain and cytotoxicity evaluation, Sci. Total Environ. 554 (2016) 1–6. doi:10.1016/j.scitotenv.2016.02.189.

[37]   M. Pirnie, K.G. Linden, J.P.J. Malley, Ultraviolet disinfection guidance manual for the final long term 2 enhanced surface water treatment rule, Environ. Prot. 2 (2006) 1–436.

[38]   D. Gerrity, S. Gamage, J.C. Holady, D.B. Mawhinney, O. Quiñones, R.A. Trenholm, S.A. Snyder, Pilot-scale evaluation of ozone and biological activated carbon for trace organic contaminant mitigation and disinfection, Water Res. 45 (2011) 2155–2165. doi:10.1016/j.watres.2010.12.031.

[39]   S. Parsons, Advanced oxidation processes for water and wastewater treatment, IWA Publishing, n.d. https://books.google.es/books/about/Advanced_Oxidation_Processes_for_Water_a. html?id=7NeNgJWaavgC&source=kp_cover&redir_esc=y (accessed March 31, 2017).

[40]   G. V. Buxton, C.L. Greenstock, W.P. Helman, A.B. Ross, Critical Review of rate constants for reactions of hydrated electrons, hydrogen atoms and hydroxyl radicals ($\cdot$OH/$\cdot$O $^-$ in Aqueous Solution, J. Phys. Chem. Ref. Data. 17 (1988) 513–886. doi:10.1063/1.555805.

[41]   Y. Lee, U. von Gunten, Oxidative transformation of micropollutants during municipal wastewater treatment: Comparison of kinetic aspects of selective (chlorine, chlorine dioxide, ferrateVI, and ozone) and non-selective oxidants (hydroxyl radical), Water Res. 44 (2010) 555–566. doi:10.1016/j.watres.2009.11.045.

[42]   I. Gültekin, N.H. Ince, Synthetic endocrine disruptors in the environment and water remediation by advanced oxidation processes, J. Environ. Manage. 85 (2007) 816–832. doi:10.1016/j.jenvman.2007.07.020.

[43]   C. Comninellis, A. Kapalka, S. Malato, S.A. Parsons, I. Poulios, D. Mantzavinos, Advanced oxidation processes for water treatment: advances and trends for R&D, J. Chem. Technol. Biotechnol. 83 (2008) 769–776. doi:10.1002/jctb.1873.

[44]   S. Malato, J. Blanco, A. Vidal, C. Richter, Photocatalysis with solar energy at a pilot-plant scale: an overview, Appl. Catal. B Environ. 37 (2002) 1–15. doi:10.1016/S0926-3373(01)00315-0.

[45]   M. Petrovic, J. Radjenovic, D. Barcelo, ADVANCED OXIDATION PROCESSES (AOPs)

162

APPLIED FOR WASTEWATER AND DRINKING WATER TREATMENT. ELIMINATION OF PHARMACEUTICALS, Holist. Approach to Environ. 1 (2011) 63–74. http://hrcak.srce.hr/index.php?show=clanak&id_clanak_jezik=103247&lang=en (accessed March 31, 2017).

[46]   F. Morel, J.G. Hering, F. Morel, Principles and applications of aquatic chemistry, Wiley, 1993.

[47]   J. Hoigné, Chemistry of Aqueous Ozone and Transformation of Pollutants by Ozonation and Advanced Oxidation Processes, in: Springer Berlin Heidelberg, 1998: pp. 83–141. doi:10.1007/978-3-540-68089-5_5.

[48]   F. Millero, F.J. Millero, K. Matsunaga, F.M.M. Morel, N. Hakem, T. Prussin, C.P. Moore, Speciation of metals in natural waters, Geochim. Cosmochim. Acta. 63 (2001) 3487. doi:B104809K.

[49]   P.L. Huston, J.J. Pignatello, Degradation of selected pesticide active ingredients and commercial formulations in water by the photo-assisted Fenton reaction, Water Res. 33 (1999) 1238–1246. doi:10.1016/S0043-1354(98)00330-3.

[50]   M. Pérez, F. Torrades, X. Domènech, J. Peral, Fenton and photo-Fenton oxidation of textile effluents, Water Res. 36 (2002) 2703–2710. doi:10.1016/S0043-1354(01)00506-1.

[51]   T. Rigg, W. Taylor, J. Weiss, The Rate Constant of the Reaction between Hydrogen Peroxide and Ferrous Ions, J. Chem. Phys. 22 (1954) 575–577. doi:10.1063/1.1740127.

[52]   C. Walling, A. Goosen, Mechanism of the ferric ion catalyzed decomposition of hydrogen peroxide. Effect of organic substrates, J. Am. Chem. Soc. 95 (1973) 2987–2991. doi:10.1021/ja00790a042.

[53]   B.H.J. Bielski, D.E. Cabelli, R.L. Arudi, A.B. Ross, Reactivity of HO_2 /O_2^- Radicals in

Aqueous Solution, J. Phys. Chem. Ref. Data. 14 (1985) 1041–1100. doi:10.1063/1.555739.

[54] J.J. Pignatello, E. Oliveros, A. MacKay, Advanced Oxidation Processes for Organic Contaminant Destruction Based on the Fenton Reaction and Related Chemistry, Crit. Rev. Environ. Sci. Technol. 36 (2006) 1–84. doi:10.1080/10643380500326564.

[55] S.M. Arnold, W.J. Hickey, R.F. Harris, Degradation of Atrazine by Fenton's Reagent: Condition Optimization and Product Quantification, Environ. Sci. Technol. 29 (1995) 2083–2089. doi:10.1021/es00008a030.

[56] O. Rozas, D. Contreras, M.A. Mondaca, M. Pérez-Moya, H.D. Mansilla, Experimental design of Fenton and photo-Fenton reactions for the treatment of ampicillin solutions, J. Hazard. Mater. 177 (2010) 1025–1030. doi:10.1016/j.jhazmat.2010.01.023.

[57] C.C.A. Loures, M.A.K. Alcântara, H.J. Izário Filho, A.C.S. TEIXEIRA, F.T. Silva, T.C.B. Paiva, G.R.L. Samanamud, Advanced oxidative degradation processes: fundamentals and applications, Int Rev Chem Eng. 5 (2013) 102–120.

[58] J.M. Monteagudo, A. Durán, R. Culebradas, I. San Martín, A. Carnicer, Optimization of pharmaceutical wastewater treatment by solar/ferrioxalate photo-catalysis, J. Environ. Manage. 128 (2013) 210–219. doi:10.1016/j.jenvman.2013.05.013.

[59] E.S. Elmolla, M. Chaudhuri, Degradation of the antibiotics amoxicillin, ampicillin and cloxacillin in aqueous solution by the photo-Fenton process, J. Hazard. Mater. 172 (2009) 1476–1481. doi:10.1016/j.jhazmat.2009.08.015.

[60] E.S. Elmolla, M. Chaudhuri, Combined photo-Fenton–SBR process for antibiotic wastewater treatment, J. Hazard. Mater. 192 (2011) 1418–1426. doi:10.1016/j.jhazmat.2011.06.057.

[61] I.R. Bautitz, R.F.P. Nogueira, Photodegradation of lincomycin and diazepam in

sewage treatment plant effluent by photo-Fenton process, Catal. Today. 151 (2010) 94–99. doi:10.1016/j.cattod.2010.02.018.

[62]   A.G. Trovó, R.F. Pupo Nogueira, A. Agüera, A.R. Fernandez-Alba, S. Malato, Degradation of the antibiotic amoxicillin by photo-Fenton process – Chemical and toxicological assessment, Water Res. 45 (2011) 1394–1402. doi:10.1016/j.watres.2010.10.029.

[63]   C. Sirtori, A. Zapata, W. Gernjak, S. Malato, A. Lopez, A. Agüera, Solar photo-Fenton degradation of nalidixic acid in waters and wastewaters of different composition. Analytical assessment by LC–TOF-MS, Water Res. 45 (2011) 1736–1744. doi:10.1016/j.watres.2010.11.023.

[64]   P. Miró, A. Arques, A.M. Amat, M.L. Marin, M.A. Miranda, A mechanistic study on the oxidative photodegradation of 2,6-dichlorodiphenylamine-derived drugs: Photo-Fenton versus photocatalysis with a triphenylpyrylium salt, Appl. Catal. B Environ. 140 (2013) 412–418. doi:10.1016/j.apcatb.2013.04.042.

[65]   O. González, C. Sans, S. Esplugas, Sulfamethoxazole abatement by photo-Fenton toxicity, inhibition and biodegradability assessment of intermediates., J. Hazard. Mater. 146 (2007) 459–64. doi:10.1016/j.jhazmat.2007.04.055.

[66]   L.S.-J. Jordá, M.M.B. Martín, E.O. Gómez, A.C. Reina, I.M.R. Sánchez, J.L.C. López, J.A.S. Pérez, Economic evaluation of the photo-Fenton process. Mineralization level and reaction time: The keys for increasing plant efficiency, J. Hazard. Mater. 186 (2011) 1924–1929. doi:10.1016/j.jhazmat.2010.12.100.

[67]   A.P.S. Batista, R.F.P. Nogueira, Parameters affecting sulfonamide photo-Fenton degradation – Iron complexation and substituent group, J. Photochem. Photobiol. A Chem. 232 (2012) 8–13. doi:10.1016/j.jphotochem.2012.01.016.

[68]   R.P. Cavalcante, L. da Rocha Sandim, D. Bogo, A.M.J. Barbosa, M.E. Osugi, M. Blanco, S.C. de Oliveira, M. de Fatima Cepa Matos, A. Machulek, V.S. Ferreira, Application of

Fenton, photo-Fenton, solar photo-Fenton, and UV/H_2O_2 to degradation of the antineoplastic agent mitoxantrone and toxicological evaluation, Environ. Sci. Pollut. Res. 20 (2013) 2352–2361. doi:10.1007/s11356-012-1110-y.

[69] Y. Zhang, K. Pagilla, Treatment of malathion pesticide wastewater with nanofiltration and photo-Fenton oxidation, Desalination. 263 (2010) 36–44. doi:10.1016/j.desal.2010.06.031.

[70] M.J. Farré, X. Doménech, J. Peral, Assessment of photo-Fenton and biological treatment coupling for Diuron and Linuron removal from water, Water Res. 40 (2006) 2533–2540. doi:10.1016/j.watres.2006.04.034.

[71] I. Nitoi, T. Oncescu, P. Oancea, Mechanism and kinetic study for the degradation of lindane by photo-Fenton process, J. Ind. Eng. Chem. 19 (2013) 305–309. doi:10.1016/j.jiec.2012.08.016.

[72] M.M. Ballesteros Martín, J.A. Sánchez Pérez, J.L. Casas López, I. Oller, S. Malato Rodríguez, Degradation of a four-pesticide mixture by combined photo-Fenton and biological oxidation, Water Res. 43 (2009) 653–660. doi:10.1016/j.watres.2008.11.020.

[73] J.M. Monteagudo, A. Durán, M. Aguirre, I. San Martín, Optimization of the mineralization of a mixture of phenolic pollutants under a ferrioxalate-induced solar photo-Fenton process, J. Hazard. Mater. 185 (2011) 131–139. doi:10.1016/j.jhazmat.2010.09.007.

[74] M. Tamimi, S. Qourzal, N. Barka, A. Assabbane, Y. Ait-Ichou, Methomyl degradation in aqueous solutions by Fenton's reagent and the photo-Fenton system, Sep. Purif. Technol. 61 (2008) 103–108. doi:10.1016/j.seppur.2007.09.017.

[75] H. Katsumata, S. Kaneco, T. Suzuki, K. Ohta, Y. Yobiko, Degradation of linuron in aqueous solution by the photo-Fenton reaction, Chem. Eng. J. 108 (2005) 269–276. doi:10.1016/j.cej.2005.02.029.

[76]   T.A. de F. Matos, A.L.N. Dias, A.D.P. Reis, M.R.A. da Silva, M.M. Kondo, Degradation of Abamectin Using the Photo-Fenton Process, Int. J. Chem. Eng. 2012 (2012). doi:10.1155/2012/915724.

[77]   A.M.T. Silva, N.R. Zilhão, R.A. Segundo, M. Azenha, F. Fidalgo, A.F. Silva, J.L. Faria, J. Teixeira, Photo-Fenton plus Solanum nigrum L. weed plants integrated process for the abatement of highly concentrated metalaxyl on waste waters, Chem. Eng. J. 184 (2012) 213–220. doi:10.1016/j.cej.2012.01.038.

[78]   M. Simunovic, H. Kusic, N. Koprivanac, A.L. Bozic, Treatment of simulated industrial wastewater by photo-Fenton process: Part II. The development of mechanistic model, Chem. Eng. J. 173 (2011) 280–289. doi:10.1016/j.cej.2010.09.030.

[79]   A. Coelho, A. V. Castro, M. Dezotti, G.L. Sant'Anna, Treatment of petroleum refinery sourwater by advanced oxidation processes, J. Hazard. Mater. 137 (2006) 178–184. doi:10.1016/j.jhazmat.2006.01.051.

[80]   S.A.O. Galvão, A.L.N. Mota, D.N. Silva, J.E.F. Moraes, C.A.O. Nascimento, O. Chiavone-Filho, Application of the photo-Fenton process to the treatment of wastewaters contaminated with diesel, Sci. Total Environ. 367 (2006) 42–49. doi:10.1016/j.scitotenv.2006.01.014.

[81]   O.R.S. da Rocha, R.F. Dantas, M.M.M. Bezerra Duarte, M.M. Lima Duarte, V.L. da Silva, Solar photo-Fenton treatment of petroleum extraction wastewater, Desalin. Water Treat. 51 (2013) 5785–5791. doi:10.1080/19443994.2013.792136.

[82]   Y.-H. Huang, Y.-J. Huang, H.-C. Tsai, H.-T. Chen, Degradation of phenol using low concentration of ferric ions by the photo-Fenton process, J. Taiwan Inst. Chem. Eng. 41 (2010) 699–704. doi:10.1016/j.jtice.2010.01.012.

[83]   O.B. Ayodele, J.K. Lim, B.H. Hameed, Degradation of phenol in photo-Fenton process by phosphoric acid modified kaolin supported ferric-oxalate catalyst: Optimization and kinetic modeling, Chem. Eng. J. 197 (2012) 181–192.

doi:10.1016/j.cej.2012.04.053.

[84]   S.S. da Silva, O. Chiavone-Filho, E.L. de Barros Neto, C.A.O. Nascimento, Integration of processes induced air flotation and photo-Fenton for treatment of residual waters contaminated with xylene, J. Hazard. Mater. 199 (2012) 151–157. doi:10.1016/j.jhazmat.2011.10.070.

[85]   K.R.B. Nogueira, A.C.S.C. Teixeira, C.A.O. Nascimento, R. Guardani, Use of solar energy in the treatment of water contaminated with phenol by photochemical processes, Brazilian J. Chem. Eng. 25 (2008) 671–682. doi:10.1590/S0104-66322008000400005.

[86]   J.-H. Sun, S.-P. Sun, M.-H. Fan, H.-Q. Guo, Y.-F. Lee, R.-X. Sun, Oxidative decomposition of p-nitroaniline in water by solar photo-Fenton advanced oxidation process, J. Hazard. Mater. 153 (2008) 187–193. doi:10.1016/j.jhazmat.2007.08.037.

[87]   X. Xue, K. Hanna, C. Despas, F. Wu, N. Deng, Effect of chelating agent on the oxidation rate of PCP in the magnetite/H_2O_2 system at neutral pH, J. Mol. Catal. A Chem. 311 (2009) 29–35. doi:10.1016/j.molcata.2009.06.016.

[88]   Y. Sun, J.J. Pignatello, Photochemical reactions involved in the total mineralization of 2,4-D by iron(3+)/hydrogen peroxide/UV, Environ. Sci. Technol. 27 (1993) 304–310. doi:10.1021/es00039a010.

[89]   L.F. González-Bahamón, F. Mazille, L.N. Benítez, C. Pulgarín, Photo-Fenton degradation of resorcinol mediated by catalysts based on iron species supported on polymers, J. Photochem. Photobiol. A Chem. 217 (2011) 201–206. doi:10.1016/j.jphotochem.2010.10.009.

[90]   M. Pariente, F. Martínez, J. Melero, J. Botas, T. Velegraki, N. Xekoukoulotakis, D. Mantzavinos, Heterogeneous photo-Fenton oxidation of benzoic acid in water: Effect of operating conditions, reaction by-products and coupling with biological treatment, Appl. Catal. B Environ. 85 (2008) 24–32. doi:10.1016/j.apcatb.2008.06.019.

[91]   R. Gonzalez-Olmos, M.J. Martin, A. Georgi, F.-D. Kopinke, I. Oller, S. Malato, Fe-zeolites as heterogeneous catalysts in solar Fenton-like reactions at neutral pH, Appl. Catal. B Environ. 125 (2012) 51–58. doi:10.1016/j.apcatb.2012.05.022.

[92]   A.F. Rossi, N. Amaral-Silva, R.C. Martins, R.M. Quinta-Ferreira, Heterogeneous Fenton using ceria based catalysts: Effects of the calcination temperature in the process efficiency, Appl. Catal. B Environ. 111–112 (2012) 254–263. doi:10.1016/j.apcatb.2011.10.006.

[93]   R.C. Martins, L.R. Henriques, R.M. Quinta-Ferreira, Catalytic activity of low cost materials for pollutants abatement by Fenton's process, Chem. Eng. Sci. 100 (2013) 225–233. doi:10.1016/j.ces.2013.03.024.

[94]   J. Herney-Ramirez, M.A. Vicente, L.M. Madeira, Heterogeneous photo-Fenton oxidation with pillared clay-based catalysts for wastewater treatment: A review, Appl. Catal. B Environ. 98 (2010) 10–26. doi:10.1016/j.apcatb.2010.05.004.

[95]   W. Schmid, K.M. Picker-Freyer, Tableting and tablet properties of alginates: characterisation and potential for Soft Tableting., Eur. J. Pharm. Biopharm. 72 (2009) 165–72. doi:10.1016/j.ejpb.2008.10.006.

[96]   M.J.M. Villena, F. Lara-Villoslada, M.A.R. Martínez, M.E.M. Hernández, Development of gastro-resistant tablets for the protection and intestinal delivery of Lactobacillus fermentum CECT 5716., Int. J. Pharm. 487 (2015) 314–9. doi:10.1016/j.ijpharm.2015.03.078.

[97]   P. Lee, M.A. Rogers, Effect of calcium source and exposure-time on basic caviar spherification using sodium alginate, Int. J. Gastron. Food Sci. 1 (2012) 96–100. doi:10.1016/j.ijgfs.2013.06.003.

[98]   V.A. Solah, D.A. Kerr, C.D. Adikara, X. Meng, C.W. Binns, K. Zhu, A. Devine, R.L. Prince, Differences in satiety effects of alginate- and whey protein-based foods., Appetite. 54 (2010) 485–91. doi:10.1016/j.appet.2010.01.019.

[99]   B. Lupo, A. Maestro, M. Porras, J.M. Gutiérrez, C. González, Preparation of alginate microspheres by emulsification/internal gelation to encapsulate cocoa polyphenols, Food Hydrocoll. 38 (2014) 56–65. doi:10.1016/j.foodhyd.2013.11.003.

[100]   A. Haug, B. Larsen, O. Smidsrod, A study of the constitution of alginic acid by partial acid hydrolysis, Acta Chem Scand. (1966). http://actachemscand.org/pdf/acta_vol_20_p0183-0190.pdf (accessed April 4, 2017).

[101]   B.H. a Rehm, Alginates: Biology and Applications, Springer Berlin Heidelberg, Berlin, Heidelberg, 2009. doi:10.1007/978-3-540-92679-5.

[102]   K.J. Sreeram, H. Yamini Shrivastava, B.U. Nair, Studies on the nature of interaction of iron(III) with alginates, Biochim. Biophys. Acta - Gen. Subj. 1670 (2004) 121–125. doi:10.1016/j.bbagen.2003.11.001.

[103]   T. Coradin, J. Livage, Synthesis and Characterization of Alginate/Silica Biocomposites, J. Sol-Gel Sci. Technol. 26 (2003) 1165–1168. doi:10.1023/A:1020787514512.

[104]   A. Maureira, B.L. Rivas, Metal ions recovery with alginic acid coupled to ultrafiltration membrane, Eur. Polym. J. 45 (2009) 573–581. doi:10.1016/j.eurpolymj.2008.11.021.

[105]   H. Titouhi, J.-E. Belgaied, Removal of ofloxacin antibiotic using heterogeneous Fenton process over modified alginate beads, J. Environ. Sci. 45 (2016) 84–93. doi:10.1016/j.jes.2015.12.017.

[106]   S. Ben Hammouda, N.N. Adhoum, L. Monser, Chemical oxidation of a malodorous compound, indole, using iron entrapped in calcium alginate beads, J. Hazard. Mater. 301 (2016) 350–361. doi:10.1016/j.jhazmat.2015.09.012.

[107]   S. Ben Hammouda, N. Adhoum, L. Monser, Synthesis of magnetic alginate beads based on Fe_3O_4 nanoparticles for the removal of 3-methylindole from aqueous solution using Fenton process, J. Hazard. Mater. 294 (2015) 128–136.

doi:10.1016/j.jhazmat.2015.03.068.

[108] H. Niu, Dizhang, Z. Meng, Y. Cai, Fast defluorination and removal of norfloxacin by alginate/Fe@Fe$_3$O$_4$ core/shell structured nanoparticles, J. Hazard. Mater. 227 (2012) 195–203. doi:10.1016/j.jhazmat.2012.05.036.

[109] K.V. de Souza, P. Peralta-Zamora, S.F. Zawadzki, Imobilização de ferro (II) em matriz de alginato e sua utilização na degradação de corantes têxteis por processos Fenton, Quim. Nova. 31 (2008) 1145–1149. doi:10.1590/S0100-40422008000500041.

[110] J. Fernandez, M.R. Dhananjeyan, J. Kiwi, Y. Senuma, J. Hilborn, Evidence for Fenton Photoassisted Processes Mediated by Encapsulated Fe ions at Biocompatible pH Values, J. Phys. Chem. B. 104 (2000) 5298–5301. doi:10.1021/jp9943777.

[111] S. Barreca, J.J. Velez Colmenares, A. Pace, S. Orecchio, C. Pulgarin, Escherichia coli inactivation by neutral solar heterogeneous photo-Fenton (HPF) over hybrid iron/montmorillonite/alginate beads, J. Environ. Chem. Eng. 3 (2015) 317–324. doi:10.1016/j.jece.2014.10.018.

[112] Y. Dong, W. Dong, Y. Cao, Z. Han, Z. Ding, Preparation and catalytic activity of Fe alginate gel beads for oxidative degradation of azo dyes under visible light irradiation, Catal. Today. 175 (2011) 346–355. doi:10.1016/j.cattod.2011.03.035.

[113] A. Cruz, L. Couto, S. Esplugas, C. Sans, Study of the contribution of homogeneous catalysis on heterogeneous Fe(III)/alginate mediated photo-Fenton process, Chem. Eng. J. 318 (2016) 272–280. doi:10.1016/j.cej.2016.09.014.

[114] Y. Dong, W. Dong, Y. Cao, C. Liu, Degradation of azo dye in water through a heterogeneous Fenton process catalyzed by Fe alginate gel beads, 2009 Int. Conf. Energy Environ. Technol. ICEET 2009. 2 (2009) 492–495. doi:10.1109/ICEET.2009.357.

[115] S. Barreca, J.J.V. Colmenares, A. Pace, S. Orecchio, C. Pulgarin, Neutral solar photo-Fenton degradation of 4-nitrophenol on iron-enriched hybrid montmorillonite-

alginate beads (Fe-MABs), J. Photochem. Photobiol. A Chem. 282 (2014) 33–40. doi:10.1016/j.jphotochem.2014.02.008.

[116] S. Ben Hammouda, F. Fourcade, A. Assadi, I. Soutrel, N. adhoum, A. Amrane, L. Monser, Effective heterogeneous electro-Fenton process for the degradation of a malodorous compound, indole, using iron loaded alginate beads as a reusable catalyst, Appl. Catal. B Environ. 182 (2016) 47–58. doi:10.1016/j.apcatb.2015.09.007.

[117] O. Iglesias, J. Gómez, M. Pazos, M.Á. Sanromán, Electro-Fenton oxidation of imidacloprid by Fe alginate gel beads, Appl. Catal. B Environ. 144 (2014) 416–424. doi:10.1016/j.apcatb.2013.07.046.

[118] E. Rosales, O. Iglesias, M. Pazos, M.A.A. Sanromán, Decolourisation of dyes under electro-Fenton process using Fe alginate gel beads., J. Hazard. Mater. 213–214 (2012) 369–77. doi:10.1016/j.jhazmat.2012.02.005.

[119] M.Á. Fernández de Dios, E. Rosales, M. Fernández-Fernández, M. Pazos, M.Á. Sanromán, Degradation of organic pollutants by heterogeneous electro-Fenton process using Mn-alginate composite, J. Chem. Technol. Biotechnol. 90 (2015) 1439–1447. doi:10.1002/jctb.4446.

[120] R.C. Martins, N. Amaral-Silva, R.M. Quinta-Ferreira, Ceria based solid catalysts for Fenton's depuration of phenolic wastewaters, biodegradability enhancement and toxicity removal, Appl. Catal. B Environ. 99 (2010) 135–144. doi:10.1016/j.apcatb.2010.06.010.

[121] R.C. Martins, R.M. Quinta-Ferreira, Phenolic wastewaters depuration and biodegradability enhancement by ozone over active catalysts, Desalination. 270 (2011) 90–97. doi:10.1016/j.desal.2010.11.026.

[122] Standard Methods for the Examination of Water and Wastewater, 21st ed., American Public Health Association/American Water Works Association/Water Pollution Control Federation, Washington, DC, USA, 2005.

[123] R.F.P. Nogueira, M.C. Oliveira, W.C. Paterlini, Simple and fast spectrophotometric determination of H_2O_2 in photo-Fenton reactions using metavanadate., Talanta. 66 (2005) 86–91. doi:10.1016/j.talanta.2004.10.001.

[124] H.J. Kuhn, S.E. Braslavsky, R. Schmidt, Chemical actinometry (IUPAC Technical Report), Pure Appl. Chem. 76 (2004) 2105–2146. doi:10.1351/pac200476122105.

[125] N. De la Cruz, V. Romero, R.F. Dantas, P. Marco, B. Bayarri, J. Giménez, S. Esplugas, o-Nitrobenzaldehyde actinometry in the presence of suspended TiO2 for photocatalytic reactors, Catal. Today. 209 (2013) 209–214. doi:10.1016/j.cattod.2012.08.035.

[126] K.L. Willett, R.A. Hites, Chemical Actinometry: Using o-Nitrobenzaldehyde to Measure Lamp Intensity in Photochemical Experiments, J. Chem. Educ. 77 (2000) 900. doi:10.1021/ed077p900.

[127] O. Levenspiel, Flujo de fluidos e intercambio de calor, Reverté, 1993.

[128] N. Perez-Moral, M.C. Gonzalez, R. Parker, Preparation of iron-loaded alginate gel beads and their release characteristics under simulated gastrointestinal conditions, Food Hydrocoll. 31 (2013) 114–120. doi:10.1016/j.foodhyd.2012.09.015.

[129] A. Banerjee, D. Nayak, S. Lahiri, A new method of synthesis of iron doped calcium alginate beads and determination of iron content by radiometric method, Biochem. Eng. J. 33 (2007) 260–262. doi:10.1016/j.bej.2006.11.005.

[130] P.V. Finotelli, M.A. Morales, M.H. Rocha-Leão, E.M. Baggio-Saitovitch, A.M. Rossi, Magnetic studies of iron(III) nanoparticles in alginate polymer for drug delivery applications, Mater. Sci. Eng. C. 24 (2004) 625–629. doi:10.1016/j.msec.2004.08.005.

[131] O. Iglesias, M.A.F. de Dios, T. Tavares, M.A. Sanromán, M. Pazos, Heterogeneous electro-Fenton treatment: preparation, characterization and performance in groundwater pesticide removal, J. Ind. Eng. Chem. 27 (2015) 276–282.

doi:10.1016/j.jiec.2014.12.044.

[132] O. Iglesias, J. Meijide, E. Bocos, M.Á. Sanromán, M. Pazos, New approaches on heterogeneous electro-Fenton treatment of winery wastewater, Electrochim. Acta. 169 (2015) 134–141. doi:10.1016/j.electacta.2015.04.062.

[133] A. Banerjee, D. Nayak, S. Lahiri, Speciation-dependent studies on removal of arsenic by iron-doped calcium alginate beads., Appl. Radiat. Isot. 65 (2007) 769–75. doi:10.1016/j.apradiso.2007.02.007.

[134] L.K. Jang, D. Nguyen, G.G. Geese, Effect of pH on the absorption of Cu(II) by alginate gel, Water Res. 29 (1995) 315–321. doi:10.1016/0043-1354(94)E0091-J.

[135] W.H. Glaze, J.-W. Kang, D.H. Chapin, The Chemistry of Water Treatment Processes Involving Ozone, Hydrogen Peroxide and Ultraviolet Radiation, Ozone Sci. Eng. 9 (1987) 335–352. doi:10.1080/01919518708552148.

[136] A.G. Trovó, R.F.P. Nogueira, A. Agüera, A.R. Fernandez-Alba, C. Sirtori, S. Malato, Degradation of sulfamethoxazole in water by solar photo-Fenton. Chemical and toxicological evaluation., Water Res. 43 (2009) 3922–31. doi:10.1016/j.watres.2009.04.006.

[137] A. Wang, Y.-Y. Li, A.L. Estrada, Mineralization of antibiotic sulfamethoxazole by photoelectro-Fenton treatment using activated carbon fiber cathode and under UVA irradiation, Appl. Catal. B Environ. 102 (2011) 378–386. doi:10.1016/j.apcatb.2010.12.007.

[138] J.F. Barona, D.F. Morales, L.F. González-Bahamón, C. Pulgarín, L.N. Benítez, Shift from heterogeneous to homogeneous catalysis during resorcinol degradation using the solar photo-Fenton process initiated at circumneutral pH, Appl. Catal. B Environ. 165 (2015) 620–627. doi:10.1016/j.apcatb.2014.10.053.

[139] D. Vione, S. Khanra, S.C. Man, P.R. Maddigapu, R. Das, C. Arsene, R.-I. Olariu, V.

174

Maurino, C. Minero, Inhibition vs. enhancement of the nitrate-induced phototransformation of organic substrates by the •OH scavengers bicarbonate and carbonate, Water Res. 43 (2009) 4718–4728. doi:10.1016/j.watres.2009.07.032.

[140]   R. Hofmann, R.C. Andrews, Impact of H2O2 and (bi)carbonate alkalinity on ammonia's inhibition of bromate formation, Water Res. 40 (2006) 3343–3348. doi:10.1016/j.watres.2006.07.032.

[141]   S. Giannakis, M.I.P. López, D. Spuhler, J.A.S. Pérez, P.F. Ibáñez, C. Pulgarin, Solar disinfection is an augmentable, in situ-generated photo-Fenton reaction-Part 2: A review of the applications for drinking water and wastewater disinfection, Appl. Catal. B Environ. 198 (2016) 431–446. doi:10.1016/j.apcatb.2016.06.007.

[142]   S. Silva Martínez, J. Vergara Sánchez, J.R. Moreno Estrada, R. Flores Velásquez, FeIII supported on ceria as effective catalyst for the heterogeneous photo-oxidation of basic orange 2 in aqueous solution with sunlight, Sol. Energy Mater. Sol. Cells. 95 (2011) 2010–2017. doi:10.1016/j.solmat.2010.06.038.

[143]   A.D. Bokare, W. Choi, Review of iron-free Fenton-like systems for activating H_2O_2 in advanced oxidation processes, J. Hazard. Mater. 275 (2014) 121–135. doi:10.1016/j.jhazmat.2014.04.054.

[144]   L. Santos-Juanes, F.S. García Einschlag, A.M. Amat, A. Arques, Combining ZVI reduction with photo-Fenton process for the removal of persistent pollutants, Chem. Eng. J. 310 (2017) 484–490. doi:10.1016/j.cej.2016.04.114.

[145]   Y. Pan, M. Zhou, X. Li, L. Xu, Z. Tang, M. Liu, Novel Fenton-like process (pre-magnetized Fe^0/H_2O_2) for efficient degradation of organic pollutants, Sep. Purif. Technol. 169 (2016) 83–92. doi:10.1016/j.seppur.2016.06.011.

[146]   S. Garcia-Segura, E. Brillas, Applied photoelectrocatalysis on the degradation of organic pollutants in wastewaters, J. Photochem. Photobiol. C Photochem. Rev. 31 (2017) 1–35. doi:10.1016/j.jphotochemrev.2017.01.005.

[147] N. De La Cruz, V. Romero, R.F. Dantas, P. Marco, B. Bayarri, J. Giménez, S. Esplugas, O-Nitrobenzaldehyde actinometry in the presence of suspended TiO_2 for photocatalytic reactors, Catal. Today. 209 (2013) 209–214. doi:10.1016/j.cattod.2012.08.035.

[148] R.P. Cavalcante, R.F. Dantas, B. Bayarri, O. González, J. Giménez, S. Esplugas, A. Machulek, Photocatalytic mechanism of metoprolol oxidation by photocatalysts TiO_2 and TiO_2 doped with 5% B: Primary active species and intermediates, Appl. Catal. B Environ. 194 (2016) 111–122. doi:10.1016/j.apcatb.2016.04.054.

[149] S. Rtimi, S. Giannakis, M. Bensimon, C. Pulgarin, R. Sanjines, J. Kiwi, Supported TiO_2 films deposited at different energies: Implications of the surface compactness on the catalytic kinetics, Appl. Catal. B Environ. 191 (2016) 42–52. doi:10.1016/j.apcatb.2016.03.019.

[150] N. Miranda-García, S. Suárez, B. Sánchez, J.M. Coronado, S. Malato, M.I. Maldonado, Photocatalytic degradation of emerging contaminants in municipal wastewater treatment plant effluents using immobilized TiO2 in a solar pilot plant, Appl. Catal. B Environ. 103 (2011) 294–301. doi:10.1016/j.apcatb.2011.01.030.

[151] L. Andronic, L. Isac, S. Miralles-Cuevas, M. Visa, I. Oller, A. Duta, S. Malato, Pilot-plant evaluation of TiO2 and TiO2-based hybrid photocatalysts for solar treatment of polluted water, J. Hazard. Mater. 320 (2016) 469–478. doi:10.1016/j.jhazmat.2016.08.013.

[152] S.K. Papageorgiou, E.P. Kouvelos, E.P. Favvas, A.A. Sapalidis, G.E. Romanos, F.K. Katsaros, Metal-carboxylate interactions in metal-alginate complexes studied with FTIR spectroscopy, Carbohydr. Res. 345 (2010) 469–473. doi:10.1016/j.carres.2009.12.010.

[153] J.L. Figueiredo, J.L. Figueiredo, Catálise heterogénea, Fund. C. Gulbenkian, 1989.

[154] M. Tomizawa, S. Kurosu, M. Kobayashi, Y. Kawase, Zero-valent iron treatment of dark

brown colored coffee effluent: Contributions of a core-shell structure to pollutant removals, J. Environ. Manage. 183 (2016) 478–487. doi:10.1016/j.jenvman.2016.08.081.

[155] W. Zhang, H. Gao, J. He, P. Yang, D. Wang, T. Ma, H. Xia, X. Xu, Removal of norfloxacin using coupled synthesized nanoscale zero-valent iron (nZVI) with H_2O_2 system: Optimization of operating conditions and degradation pathway, Sep. Purif. Technol. 172 (2017) 158–167. doi:10.1016/j.seppur.2016.08.008.

[156] A. Khan, S.M. Prabhu, J. Park, W. Lee, C.-M. Chon, J.S. Ahn, G. Lee, Azo dye decolorization by ZVI under circum-neutral pH conditions and the characterization of ZVI corrosion products, J. Ind. Eng. Chem. 47 (2017) 86–93. doi:10.1016/j.jiec.2016.11.017.

[157] A. Trovarelli, P. Fornasiero, World Scientific (Firm), Catalysis by ceria and related materials, Imperial College Press, 2013.

[158] S.-H. Do, B. Batchelor, H.-K. Lee, S.-H. Kong, Hydrogen peroxide decomposition on manganese oxide (pyrolusite): Kinetics, intermediates, and mechanism, Chemosphere. 75 (2009) 8–12. doi:10.1016/j.chemosphere.2008.11.075.

[159] G. Petrucci, M. Rosellini, Chlorine dioxide in seawater for fouling control and post-disinfection in potable waterworks, Desalination. 182 (2005) 283–291. doi:10.1016/j.desal.2005.02.029.

[160] I.W. Wait, C.T. Johnston, E.R. Blatchley, The influence of oxidation reduction potential and water treatment processes on quartz lamp sleeve fouling in ultraviolet disinfection reactors., Water Res. 41 (2007) 2427–36. doi:10.1016/j.watres.2007.02.057.

[161] I.W. Wait, Multiple-Barrier Disinfection by Chlorination and UV Irradiation for Desalinated Drinking Waters: Chlorine Photolysis and Accelerated Lamp-Sleeve Fouling Effects, Water Environ. Res. 80 (2008) 2183–2188.

doi:10.2175/106143008X304668.

[162] A. De Luca, R.F. Dantas, S. Esplugas, Assessment of iron chelates efficiency for photo-Fenton at neutral pH., Water Res. 61 (2014) 232–42. doi:10.1016/j.watres.2014.05.033.

12. Resumen en castellano

12.1. INTRODUCCIÓN

Desde la antigüedad el agua ha sido un bien preciado entorno al cual han prosperado las civilizaciones. A medida que la tecnología evolucionó, el hombre ha sido capaz de no solo establecer sus pueblos y ciudades próximos a este recurso sino de canalizarlo y hacerlo disponible para su uso en casi cualquier ubicación del territorio. Hoy en día, con una población mundial de casi 7.5 millones de habitantes, la ciencia se plantea nuevos retos para satisfacer esta demanda de agua.
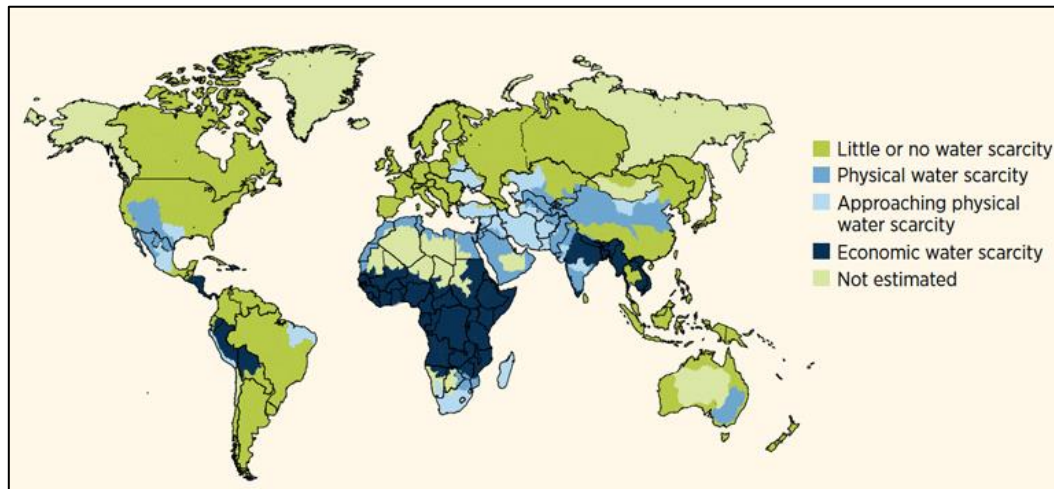
Figura 12.1. Escasez de agua económica y física en el mundo. Fuente: World water development report 4. World Water Assessment Program (WWAP), marzo de 2012.

Pese a que existe una cantidad de agua suficiente para sustentar la población en cuanto a necesidades básicas (bebida, cocina, higiene personal…), este preciado recurso también es necesario para otras actividades imprescindibles como la agricultura y la industria, que son las que actualmente efectúan mayores consumos [1]. El hecho de que este recurso no esté distribuido de forma uniforme en el territorio hace que existan zonas en las que se considera que existe escasez de agua, ya sea por motivos físicos (ausencia de recursos

hídricos próximos) o económicos (falta de suficientes fondos para hacer llegar este recurso a la población) (Figura 12.1).

Las Naciones Unidas estimaron en su *Human Development Report* (2006) que en el año 2025 más de 3 billones de personas podrían estar viviendo en países en situación de escasez de agua [2].

Considerando estos hechos y previsiones, la gestión y conservación de los recursos hídricos existentes se considera actualmente un asunto crítico para la sociedad.

Toda actividad humana en que se hace uso del agua, deja además una huella en forma de contaminación que empeora la calidad del agua adicionando materia orgánica y compuestos químicos que de no ser tratados acaban descargándose en el medio ambiente e incrementando gradualmente la calidad de los recursos existentes.

La ingeniería ambiental se ha encargado de preservar el medio ambiente de estas fuentes de contaminación antropogénica mediante la implementación de plantas depuradoras de agua residual previas a su descarga al medio, ya sean ríos, lagos o el mar. Aun así, últimamente se ha visto que estas plantas, que eliminan principalmente sólidos (tratamiento primario) y materia orgánica (tratamiento terciario), no son suficientes para devolver el agua al medio en las condiciones suficientes para no producir efectos negativos sobre él. Numerosos estudios han detectado que existen ciertos compuestos, de carácter recalcitrante, que no son capaces de eliminar de la forma tradicional y acaban en el efluente de descarga y por consiguiente siendo vertidos [3-5]. Debido a esto, hoy en día se empiezan a aplicar tratamientos adicionales que permitan eliminar estos compuestos.

Entre los más preocupantes, se encuentran los conocidos como contaminantes emergentes (CE). De acuerdo a Farré et al. [6], estos contaminantes se definen como compuestos actualmente no considerados en la legislación vigente en materia de agua, los cuales no se han estudiado previamente y que son considerados como potenciales riesgos para el medio ambiente y la salud humana. Dentro de esta definición se encuentran la mayoría de productos farmacéuticos, drogas de abuso, productos de higiene y cuidado

180

personal, esteroides, hormonas, surfactantes, compuestos perfluorinados, retardantes de llama, aditivos industriales, y muchos otros que por su carácter novedoso y su uso habitual suponen una preocupación.

Una de las tecnologías desarrolladas para evitar la acumulación de todos estos productos en el medio son los Procesos de Oxidación Avanzada (POA). Estos son procesos basados en reacciones químicas que generan especies altamente oxidantes, normalmente el radical hidroxilo (HO·), las cuales son capaces de oxidar la mayoría de compuestos recalcitrantes, tóxicos y no biodegradables a subproductos o productos que no lo son, e incluso son capaces de alcanzar la mineralización total [7,8]. Además, estos procesos también son capaces de desinfectar, pues la oxidación de la membrana celular de bacterias y otros microorganismos evita la proliferación de estas.

Entre estos procesos de oxidación avanzada se encuentran los procesos Fenton y foto-Fenton. El primero se basa en la generación de radicales hidroxilo mediante la descomposición catalítica del peróxido de hidrógeno (H_2O_2) en presencia de sales de Fe(II). Durante la cadena de complejas reacciones simultáneas, el Fe (II) se convierte en Fe (III), por lo que el rendimiento de la reacción baja de forma considerable una vez todo el Fe(II) disponible se ha consumido, convirtiéndose en la especie limitante [9]. Para mejorar este proceso, se descubrió que la irradiación con luz ultravioleta UV-A permitía al Fe(III) que ya no era activo volver a su valencia Fe(II) de una forma rápida, por lo que el rendimiento de la reacción mejoraba de forma significativa y no era necesaria la adición de grandes cantidades de sales de hierro al inicio de la reacción.

Pese a todo, la poca solubilidad de las especies de hierro a pH neutro, así como la poca actividad que presentaban a pH neutro llevó a aplicar el proceso a su pH óptimo, que se encuentra por debajo de 3.0 [10-11]. Consecuentemente, antes de verter los efluentes tratados por este proceso se requiere un proceso de neutralización en el que se generan grandes cantidades de fangos de hierro por precipitación de hidróxidos de hierro.

Para evitar estos inconvenientes, actualmente se investigan diversas formas de llevar a cabo este proceso a un pH neutro o cercano a la neutralidad. Entre ellas, las más aceptadas son el uso de agentes quelantes [12], que complejan el hierro y lo mantienen en solución, y la utilización de catalizadores heterogéneos de hierro [13-16], que también permiten realizar la reacción a pH neutro y además son sencillos de separar mediante un proceso de separación física.

Dentro de las diversas categorías de catalizadores heterogéneos que se están investigando en la actualidad, existen los catalizadores en base alginato. Este compuesto es un polisacárido natural extraído de las algas marrones el cual tiene la propiedad de formar geles en presencia de cationes divalentes y trivalentes. Estos cationes actúan de enlace entre cadenas de alginato formando estas estructuras sólidas. Además, debido a sus propiedades (no tóxico y comestible) se ha considerado como un buen candidato para ejercer de soporte para el hierro y formar así catalizadores heterogéneos para las reacciones de tipo Fenton y foto-Fenton que puedan ser aplicados a aguas cuyo destino es el consumo humano [17-21].

12.2. OBJETIVOS

El objetivo principal de esta tesis es explorar la utilización de catalizadores heterogéneos de hierro para llevar a cabo reacciones de tipo Fenton y foto-Fenton a pH neutro o cercano a la neutralidad, con especial atención a los catalizadores en base alginato.

Para alcanzar este objetivo se han propuesto los siguientes objetivos intermedios:

- Optimizar el proceso de síntesis de catalizadores en base alginato para su aplicación a reacciones de tipo foto-Fenton heterogéneas.
- Estudiar el comportamiento de estos catalizadores cuando son aplicados en reacciones de tipo Fenton o foto-Fenton heterogéneas para la eliminación del antibiótico sulfametoxazol (SMX) como compuesto de referencia. Se hará

especial hincapié en la contribución de la reacción homogénea al rendimiento global, así como a la estabilidad del catalizador.
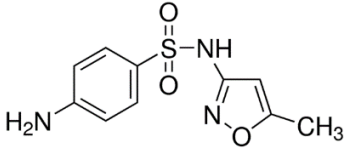
- Estudiar la posible aplicación de este catalizador de Fe/alginato en procesos de desinfección.

- Mejorar la eficiencia y estabilidad de este catalizador para obtener mejores rendimientos y menor lixiviación de hierro.

- Estudiar el comportamiento de estos catalizadores mejorados frente a otros catalizadores heterogéneos actualmente en estudio para su aplicación a reacciones de tipo Fenton y foto-Fenton.

12.3. MATERIALES Y MÉTODOS

12.3.1. Compuestos de referencia

Se utilizó el antibiótico sulfametoxazol (SMX, Sigma-Aldrich) (Tabla 12.1) como contaminante modelo en los experimentos para la eliminación de microcontaminantes y cultivos de bacteria *Escherichia Coli* para los estudios de desinfección.

Tabla 12.1. Principal información del antibiótico sulfametoxazol (SMX).

Fórmula química	$C_{10}H_{11}N_3O_3S$
Nombre químico	4-Amino-N-(5-metil-3-isoxazolil) benzenosulfonamida, N^1-(5-Metilisoxazol-3-iyl) sulfanilamida
Estructura química	
Masa molar	253.28 g mol^{-1}
Número CAS	723-46-6

183

12.3.2. Síntesis y preparación de catalizadores

Catalizador de Fe(III)/alginato hidratado

Se preparó de acuerdo al método desarrollado durante este trabajo. Para ello, una solución 2,5% en alginato de sodio a 40 °C se vertió gota a gota sobre una solución de cloruro de hierro (FeCl$_3$) 0,05 M. Posteriormente se mantuvo en agitación durante 6 horas hasta obtener esferas de catalizador de Fe(III)/alginato hidratadas. Posteriormente el exceso de solución endurecedora de cloruro de hierro se eliminó mediante un proceso de lavado.

Catalizador de Fe(/alginato deshidratado

Se preparó mediante el proceso de preparación del catalizador de Fe(III)/alginato hidratado y posteriormente se sometió a un proceso de deshidratación controlada a 40 °C durante 24h.

Catalizador de Fe(III)/Ce/alginato

Se preparó de la misma manera que el catalizador de Fe(III)/alginato deshidratado pero se añadieron 0,05 M de cloruro de cerio (CeCl$_3$) en la solución endurecedora.

Catalizador de Fe(III)/TiO$_2$/alginato

Se preparó de forma homóloga al catalizador de Fe(III)/alginato deshidratado pero se adicionaron partículas de TiO$_2$ en suspensión a la solución de alginato de sodio previamente a su adición sobre la solución endurecedora. De esta manera el TiO$_2$ quedó atrapado en la estructura del catalizador.

Catalizador de Fe(III)/ZVI/alginato

Se preparó siguiendo el mismo proceso que el catalizador de Fe(III)/alginato deshidratado pero se añadieron partículas de hierro monovalente (ZVI) en suspensión dentro de la solución de alginato de sodio antes de ser añadido sobre la solución de cloruro de hierro, quedando así distribuidas en el catalizador.

Catalizador de Fe/Ce/O

Se preparó mediante un proceso de co-precipitación en medio básico. Una solución de Fe/Ce con un ratio molar 70:30 se adicionó gota a gota sobre una solución de hidróxido de sodio 3 M. El precipitado formado se lavó con agua y secó a 105 °C durante 12 h. Posteriormente se calcinó a 300 °C por 3 h y se molió y tamizó para obtener tamaños de partícula inferiores a 250 µm.

Otros catalizadores

También se utilizó el catalizador de Fe/Mn/O comercial NORIT N-150, rocas volcánicas recogidas en las islas Azores y limaduras de hierro consideradas residuo de la industria metalúrgica.

12.3.3. Principales técnicas analíticas

Las principales técnicas analíticas utilizadas fueron:

- Cromatografía Líquida de Alta Precisión (HPLC) para la determinación del contenido de sulfametoxazol.
- Medida de hierro disuelto mediante colorimetría basado en su reacción fon 1,10-fenantrolina.
- Medida de peróxido de hidrógeno mediante colorimetría basado en su reacción con metavanadato de amonio.
- Determinación de carbono orgánico total (COT)
- Viscosimetría
- Recuento bacteriano de Escherichia Coli en medio selectivo Chromocult® TBX Agar.
- Medidas actinométricas para la determinación de los flujos fotónicos característicos de cada reactor.
- Microscopía electrónica de barrido (SEM) para la observación de los catalizadores
- Análisis BET y porosimetría

185

- Análisis de metales mediante ICP-OES

- Análisis FTIR

12.3.4. Dispositivos experimentales

Se utilizaron reactores encamisados por cargas de 2L y 4L dependiendo de los experimentos a realizar. Todos los reactores estaban refrigerados a 25 °C y disponían de agitación magnética en el caso de los reactores de 2 L y mecánica en el caso del reactor de 4 L. El reactor de 2 L utilizado para la eliminación de SMX utilizando el catalizador de Fe(III)/alginato hidratado constaba de tres lámparas UV-A de luz negra Philips TL 8W FAM con una emisión en el rango de 350-400 nm de 4,74 x 10^{-6} Einstein s^{-1}. El reactor de 2 L utilizado para desinfección constaba de una sola lámpara de la misma clase con una emisión de 1,58 x 10^{-6} Einstein s^{-1}. El reactor de 4 L constaba de tres lámparas de igual modelo y una emisión de 5,13 x 10^{-6} Einstein s^{-1}. El esquema del reactor de 4 L, muy similar al de los otros dos, puede observarse en la Figura 12.2.
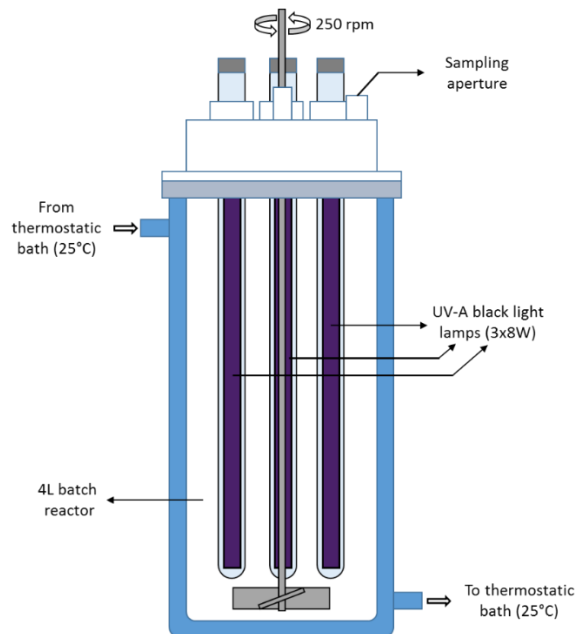

Figura 12.2. Esquema del reactor de 4 L utilizado para los experimentos de eliminación de SMX con catalizador de Fe(III)/alginato deshidratado y sus modificaciones.

12.4.   RESULTADOS Y DISCUSIÓN

12.4.1. Capítulo 4: Desarrollo del catalizador de Fe(III)/alginato

El estudio realizado en este capítulo busca evaluar el efecto que tienen los diferentes parámetros implicados en la síntesis de los catalizadores de Fe/alginato sobre sus propiedades, así como sentar las bases para la optimización de un proceso de preparación estandarizado para todo el trabajo.

Para ello se estudiaron el efecto de la concentración de alginato en la solución de alginato de sodio y su viscosidad, la concentración y especie de hierro en la solución endurecedora, el tiempo de endurecimiento y el tamaño de catalizador.

Se observó que la utilización de sales de Fe(III) producía catalizadores con mejores propiedades mecánicas que los sintetizados con Fe(II), pues establecían un mayor número de enlaces entre cadenas poliméricas.

También se comprobó que una mayor concentración de alginato de sodio en la solución inicial permitía la aceptación de mayor cantidad de hierro en la estructura del catalizador final (Figura 12.3). Aun así, una concentración superior a 2,5 % resultó difícil de preparar, por lo que se consideró que 2,5 % era la concentración adecuada a utilizar. Además, se observó que la viscosidad de esta solución influía de forma directa en el tamaño de las gotas a adicionar sobre la solución endurecedora, por lo que determinaba directamente el tamaño final del catalizador. Así, se vio que incrementando la temperatura de la solución a 40 °C suponía una mejora substancial en este parámetro permitiendo así obtener esferas de catalizador de tamaño inferior.

Figura 12.3. Contenido en hierro de catalizadores de Fe/alginato preparados utilizando soluciones de alginato de sodio de concentraciones 1%, 2%, 2,5% y 3%, una solución endurecedora 0,05M en FeCl$_3$ y 6 horas de endurecimiento.

También se observó que la variación de la concentración de hierro en la solución endurecedora repercutía linealmente en la cantidad de hierro en el catalizador preparado (Figura 12.4).

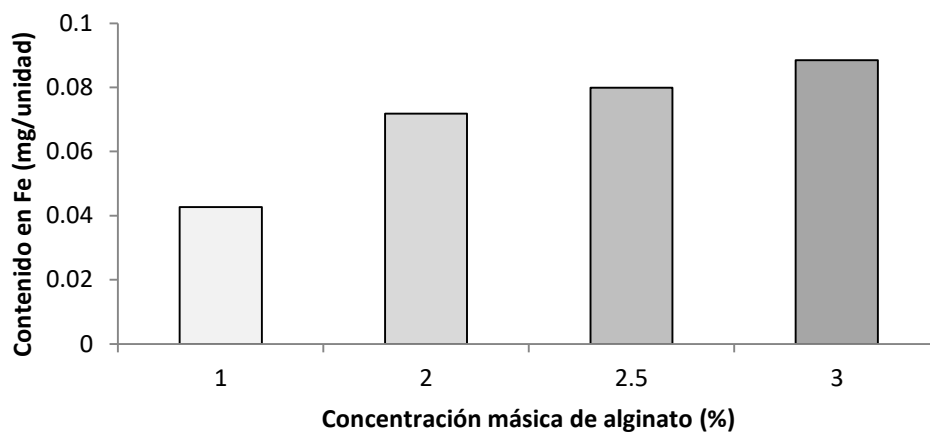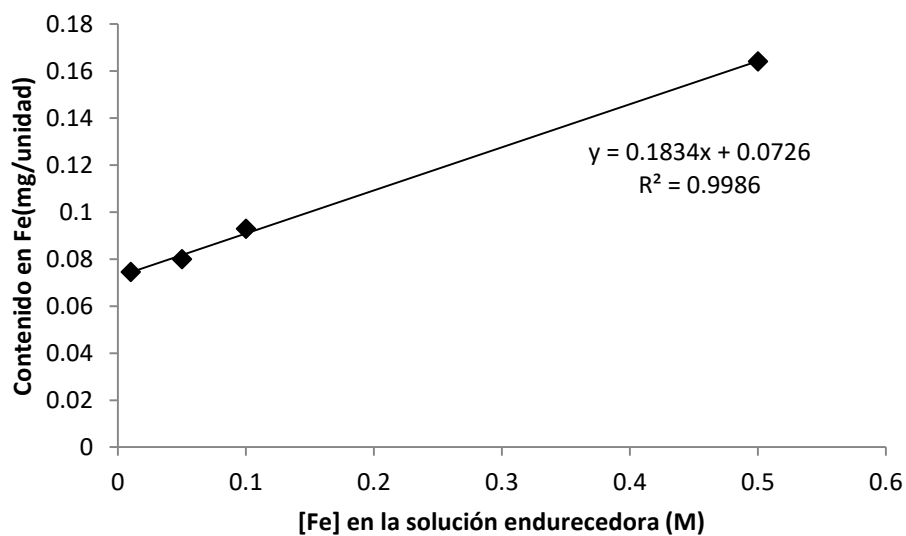**Figura 12.4. Contenido en hierro de catalizadores de Fe/alginato preparados utilizando una solución de alginato de sodio 2,5% (m/m), 6 horas de endurecimiento y concentraciones de solución endurecedora de 0,01M, 0,05M, 0,1M y 0,5M en FeCl$_3$.**

Por último, se comprobó que el método de adición más adecuado para la síntesis del catalizador era la utilización de una cámara de vacío conectada a diversas jeringuillas, pues permitía la producción de grandes cantidades de catalizador de forma homogénea y en poco tiempo.

12.4.2. Capítulo 5: Mecanismo y estabilidad del catalizador de Fe(III)/alginato

En este capítulo se vio que el comportamiento del catalizador de Fe(III)/alginato cuando se aplicaba a la eliminación de SMX mediante la reacción de tipo foto-Fenton en agua destilada dependía de forma significativa del pH inicial al que se encontraba la solución tratada (Figura 12.5). Se pudo observar también una tendencia en todos los experimentos a estabilizarse en un pH final de 4,2 excepto aquellos que empezaron a un pH ya inferior. Además, se observó que cuando alcanzaban este pH se iniciaba la liberación del hierro ligado en el catalizador, así como el incremento de COT medido en la muestra. En cambio, cuando se llevaron a cabo los experimentos de forma homóloga pero utilizando agua de botella como matriz de agua naturalmente tamponada se observó que no se producía eliminación de SMX, pero tampoco una significativa liberación de hierro ni de COT.
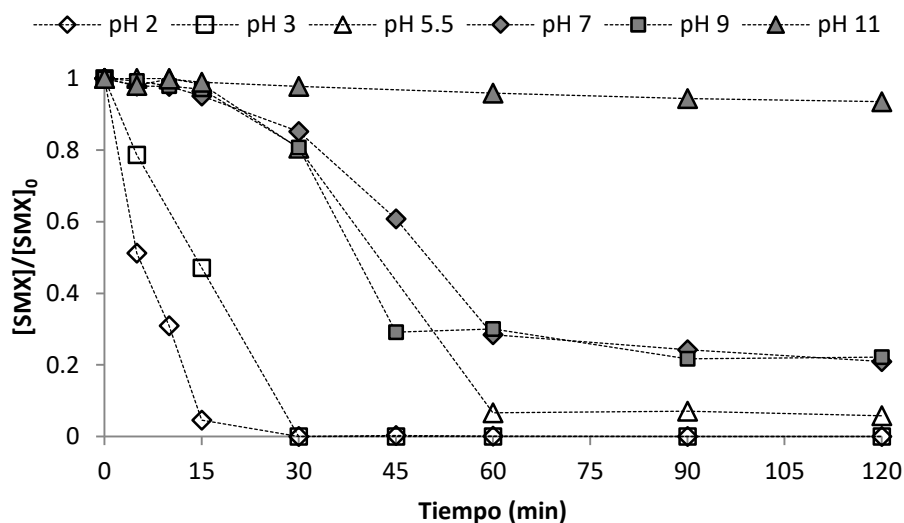
Figura 12.5. Eliminación de SMX mediante foto-Fenton heterogéneo a diferentes pH inicial utilizando 0,5 g L^{-1} (base seca) de catalizador, [H$_2$O$_2$]$_0$ = 20 mg L^{-1}, [SMX]$_0$ = 10 mg L^{-1} y agua destilada como matriz.

Estos datos llevaron a formular un mecanismo en el que se tenía en cuenta el pH como parámetro principal en la estabilidad del catalizador. Cuando el pH alcanzaba el pK$_a$ del alginato, que es de 4,2 [22-24], las cadenas de alginato se protonaban perdiendo así el hierro sus enlaces con el alginato, lo que desencadenaba su liberación gradual y el incremento de la contribución de la reacción foto-Fenton homogénea.

A su vez, las cadenas de alginato quedaban libres y acababan solubilizándose, lo que producía el incremento de COT, que actuaba en competición directa con el SMX por los radicales hidroxilos generados.

12.4.3. Capítulo 6: Catalizador de Fe(III)/alginato aplicado a desinfección

Después de observar la gran liberación de hierro producida por la reducción de pH, se decidió estudiar la aplicación de este catalizador en condiciones más suaves, intentando alargar la etapa inicial en que el pH de la solución se encontraba por encima del pKa del alginato, minimizando de esta manera la contribución de la vía homogénea de la reacción

foto-Fenton. Para ello se decidió que su aplicación a desinfección podía ser eficiente, pues es conocido que se requieren bajas dosis de oxidante para conseguirlo.

Se vio que tanto en matrices de agua destilada como en matrices de agua de botella se conseguía el efecto deseado sobre la inactivación de bacterias *Escherichia Coli*, aunque en el agua ligeramente tamponada la velocidad de inactivación se vio reducida e incluso no llegó a alcanzar la desinfección total después de 60 minutos de tratamiento (Figura 12.6). Esta mejora se atribuyó a una pequeña contribución de la vía homogénea en la matriz no tamponada, aunque la concentración de hierro se mantuvo por debajo de los límites legales para uso humano establecidos por la Directiva del Consejo 98/83/EC (0.2 mg L^{-1}).
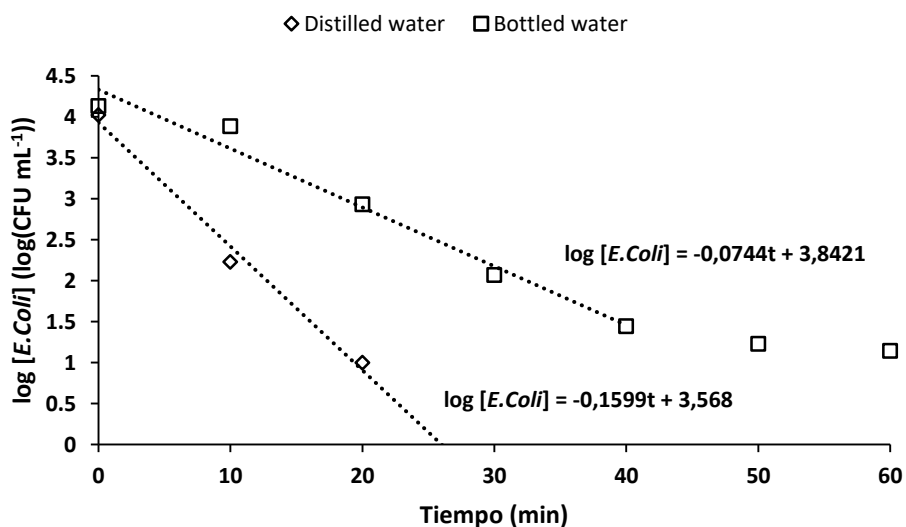
Figura 12.6. Inactivación de *Escherichia Coli* mediante foto-Fenton heterogéneo en matrices de agua destilada y agua de botella. Condiciones experimentales: 0,5 g L^{-1} de catalizador de Fe(III)/alginato (base seca) y 20 mg L^{-1} de H_2O_2.

Además, se aplicó el mismo tratamiento en una matriz de agua de botella sobre el virus bacteriófago M4, aislado en trabajos previos por el grupo MARS del Departamento de Microbiología de la Universidad de Barcelona. Este virus se aisló de los supervivientes de un tratamiento foto-Fenton solar, por lo que se considera un indicador adecuado para la comparación de la efectividad de procesos de oxidación avanzada aplicados a desinfección.

Se obtuvo un 98,5% de eliminación, pero no se consiguió alcanzar la desinfección total después de 40 minutos de tratamiento (Figura 12.7).

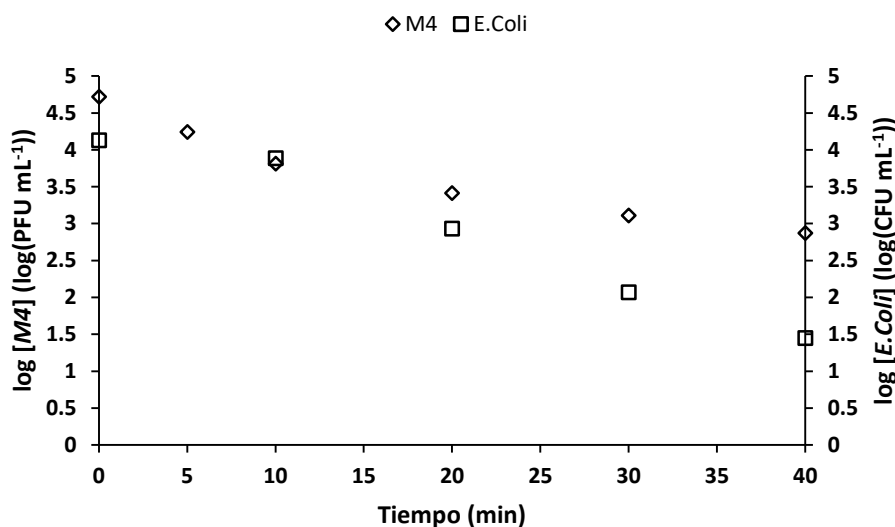**Figura 12.7. Inactivación del virus bacteriófago M4 y de Escherichia Coli mediante foto-Fenton heterogéneo en una matriz de agua embotellada. Condiciones experimentales: $[M4]_0$ = 5,3 x 10^4 PFU mL^{-1}, $[E.Coli]_0$ = 1,4 x 10^4 CFU mL^{-1}, 0.5 g L^{-1} de catalizador de Fe(III)/alginato y 20 mg L^{-1} de H_2O_2.**

12.4.4. Capítulo 7: Modificaciones del catalizador de Fe(III)/alginato

Con la intención de mejorar la estabilidad y eficiencia del catalizador básico de Fe(III)/alginato, algunas modificaciones fueron realizadas.

Primero se añadió una fase de deshidratación controlada a tras el proceso estándar de síntesis del catalizador. Los resultados de los experimentos realizados en las mismas condiciones para los catalizadores de Fe(III)/alginato hidratado y deshidratado pueden verse en la Figura 12.8. Se observa que las eliminaciones de SMX tienen un perfil muy similar. Aun así, el catalizador hidratado presenta un ligero aumento respecto al deshidratado en la velocidad inicial de eliminación de SMX, pero no es capaz de eliminar completamente el antibiótico después de 2 horas de tratamiento. Esto es debido al COT liberado, como se aprecia en la misma figura. Si nos centramos en el gráfico que muestra la liberación de hierro, se puede observar que, pese a que el catalizador deshidratado libera

aproximadamente 3 mg L^{-1} de hierro tras 2 horas de tratamiento, esta cantidad es considerablemente inferior a los 11 mg L^{-1} que libera el catalizador hidratado, por lo que claramente el proceso de deshidratación confiere una mayor estabilidad al catalizador de Fe(III) alginato.

Figura 12.8. Comparación de la degradación de SMX, hierro soluble, COT y pH de experimentos llevados a cabo utilizando los catalizadores de Fe(III)/alginato hidratados y deshidratados. ([SMX]$_0$ = 10 mg L^{-1}, cantidad de catalizador (base seca) = 0,5 g L^{-1}, [H$_2$O$_2$]$_0$ = 20 mg L^{-1})

Además, como ya se ha comentado previamente, el COT liberado también es significativamente inferior, por lo que el efecto de competencia con el compuesto de referencia por los radicales hidroxilos también será menor. En cuanto al pH, se ve que ambos siguen la misma tendencia a bajar hasta estabilizarse cuando el pH es igual al pK$_a$ del alginato (pK$_a$=4,2).

Pese a que claramente mejora la estabilidad y reduce la contribución de la vía homogénea de la reacción foto-Fenton, la eficiencia del proceso no mejora con el proceso de deshidratación. Por ello, otras modificaciones se aplicaron sobre este catalizador más

estable. Con este fin, se decidió incluir cerio en la estructura del catalizador, aprovechando que el Ce(III) puede incorporarse en el catalizador de la misma manera que el hierro. También se decidió probar la inclusión de partículas de hierro monovalente (ZVI) y partículas de TiO_2 utilizando el catalizador como agente aglomerante. La Figura 12.9 muestra los resultados los experimentos realizados utilizando estos tres catalizadores modificados en comparación con el catalizador de F(III)/alginato deshidratado.
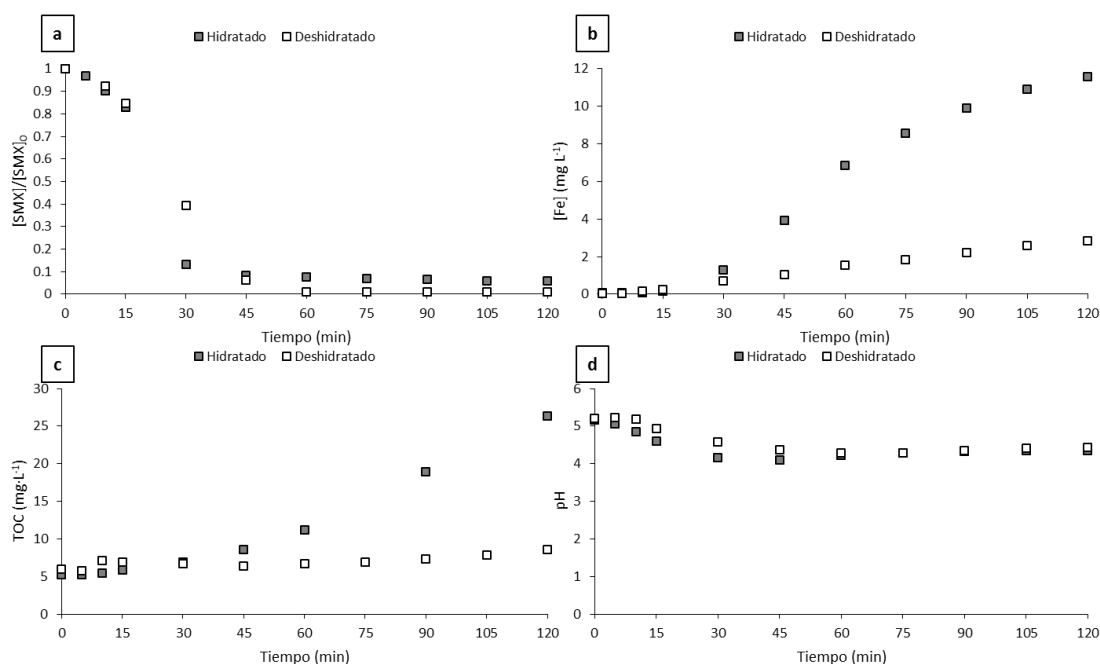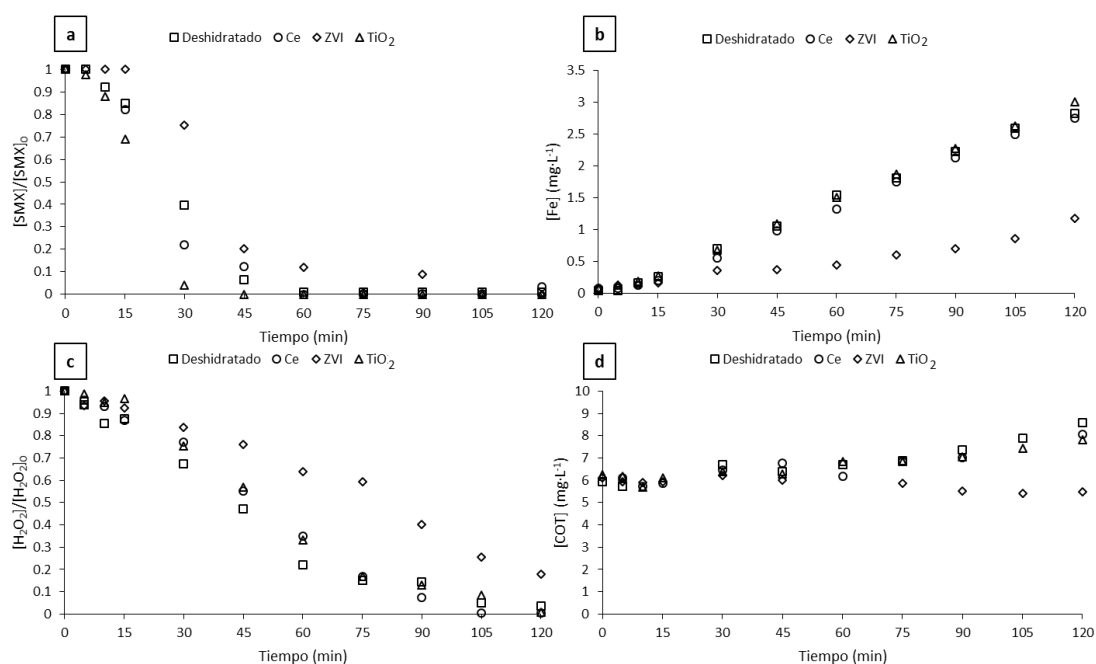

Figura 12.9. Comparación de la degradación de SMX, hierro soluble, H_2O_2 y pH de experimentos llevados a cabo utilizando los catalizadores de Fe(III)/alginato hidratado y sus tres modificaciones con Ce, ZVI y TiO_2. ([SMX]$_0$ = 10 mg L^{-1}, cantidad de catalizador (base seca) = 0,5 g L^{-1}, [H$_2$O$_2$]$_0$ = 20 mg L^{-1})

El catalizador modificado con TiO_2 incrementó considerablemente su eficiencia respecto al catalizador de Fe(III)/alginato básico, consiguiendo la eliminación total del compuesto aproximadamente 30 minutos antes. Esto fue debido a la vía fotocatalítica de generación de especies oxidantes que aporta el TiO_2, la cual es simultánea y aditiva a la ya existente. En cuanto a los demás parámetros, solo se detectaron variaciones despreciables respecto al catalizador sin modificar.

194

El catalizador que incorpora ZVI empeoró de forma considerable en cuanto a degradación de SMX y no consiguió alcanzar la eliminación total después de 120 minutos de tratamiento. Se piensa que las partículas de ZVI no aportaron actividad catalítica al catalizador y dada su densidad, substituyeron a parte de la masa de catalizador que sí que proporcionaba actividad. Esto concuerda con la menor liberación de hierro y el menor consumo de H_2O_2 que también se pueden observar.

El catalizador que incorpora cerio en su estructura, a diferencia de los otros dos, no mostró variaciones significativas respecto de ningún parámetro excepto en la velocidad inicial de eliminación de SMX. Al incluir el cerio en su forma activa (Ce(III)) este aportó un extra de velocidad inicial respecto al catalizador básico, pero parece que tras 30 minutos de tratamiento perdió eficacia respecto al catalizador sin modificar, por lo que es posible que la eficiencia en la recuperación de Ce(IV) a Ce(III) mediante la luz UV-A sea baja.

Globalmente, se observó que la única modificación que realmente aportó una mejora significativa fue la incorporación de TiO_2, abriendo así una segunda vía de producción de especies oxidantes.

12.4.5. Capítulo 8: Catalizadores heterogéneos aplicados a reacciones de tipo Fenton y foto-Fenton a pH neutro.

Algunos catalizadores heterogéneos para las reacciones tipo Fenton y foto-Fenton que actualmente están en estudio se seleccionaron con el fin de comparar la efectividad del catalizador de Fe(III)/alginato deshidratado. Los catalizadores seleccionados fueron un catalizador comercial de Fe/Mn/O y un catalizador sintetizado de Fe/Ce/O, así como piedras volcánicas y limaduras de hierro como catalizadores de bajo coste.

La Figura 12.10 muestra los resultados de la eliminación de SMX para los cuatro catalizadores aplicándolos a la reacción Fenton a pH ácido (3,0). Se puede observar que las limaduras de hierro presentaron una degradación extremadamente rápida, eliminando completamente el compuesto de referencia antes de 5 minutos. Esto fue debido a la

disolución de grandes cantidades de hierro debido al pH ácido, lo que produjo una intensa actividad de la reacción Fenton homogénea. El catalizador de Fe/Ce/O presentó cierta degradación, consiguiendo aproximadamente un 20% de eliminación en 120 minutos de tratamiento. Posteriormente se observó que debido al medio fuertemente ácido y a la elevada concentración de oxidante (500 mg L^{-1}) se produjo la lixiviación de hierro procedente del catalizador, por lo que los resultados de eliminación de SMX utilizando este catalizador tenían una parte de contribución de la reacción de Fenton homogénea. El resto de catalizadores no consiguieron reducir la concentración inicial del antibiótico. Cabe destacar que el catalizador de Fe/Mn/O fe descartado debido a que descompuso de forma instantánea el H$_2$O$_2$ en oxígeno y agua, cosa que pudo comprobarse posteriormente en la literatura científica [25].

Figura 12.10. Degradación de SMX durante cuatro experimentos Fenton llevados a cabo utilizando cuatro diferentes catalizadores heterogéneos a un pH inicial de 3,0. [SMX]$_0$ = 10 mg L^{-1}, [H$_2$O$_2$]$_0$ = 500 mg L^{-1}, [Fe/Ce/O]$_0$ = 1,0 g L^{-1}, [Fe/Mn/O]$_0$ = 1,0 g L^{-1}, [Piedras volcánicas]$_0$ = 1.0 g L^{-1}, [Limaduras de hierro]$_0$ = 3,0 g L^{-1}.

Tras repetir los experimentos Fenton en ausencia de luz a un pH inicial de 7,0, ninguno de los catalizadores mostró actividad alguna, por lo que no se obtuvo degradación del SMX. Después de este experimento se descartaron las limaduras de hierro como posible catalizador, pues se consideró que su comportamiento era homólogo al de las partículas de

hierro monovalente, pues su composición era la misma y diferían principalmente en el tamaño de partícula.

Por último, se realizaron experimentos foto-Fenton a pH neutro (7,0) para utilizando los catalizadores de Fe/Ce/O y piedras volcánicas. Los resultados de la eliminación de SMX, comparados con los obtenidos utilizando el catalizador de Fe(III)/alginato deshidratado pueden verse en la Figura 12.11. Se puede observar que el catalizador de Fe/Ce/O no consiguió producir ninguna eliminación de SMX, por lo que se confirmó que carecía de actividad catalítica para la reacción foto-Fenton y que la eliminación previamente obtenida en el experimento Fenton a pH ácido era en su totalidad debida a la vía homogénea, puesto que en este caso no hubo lixiviación de hierro. Además, este catalizador presentó un consumo de H_2O_2 del 100%, por lo que se consideró que tenía un comportamiento similar al catalizador de Fe/Mn/O pero con una velocidad de descomposición del H_2O_2 inferior.
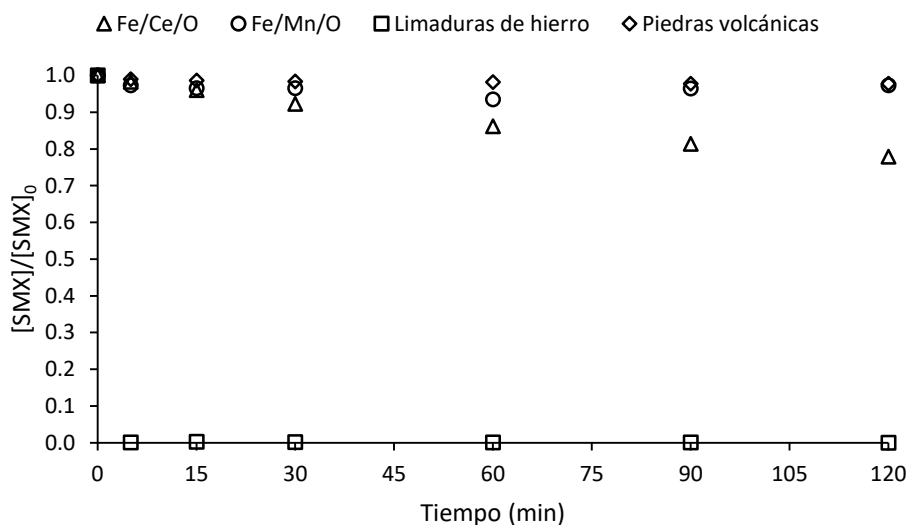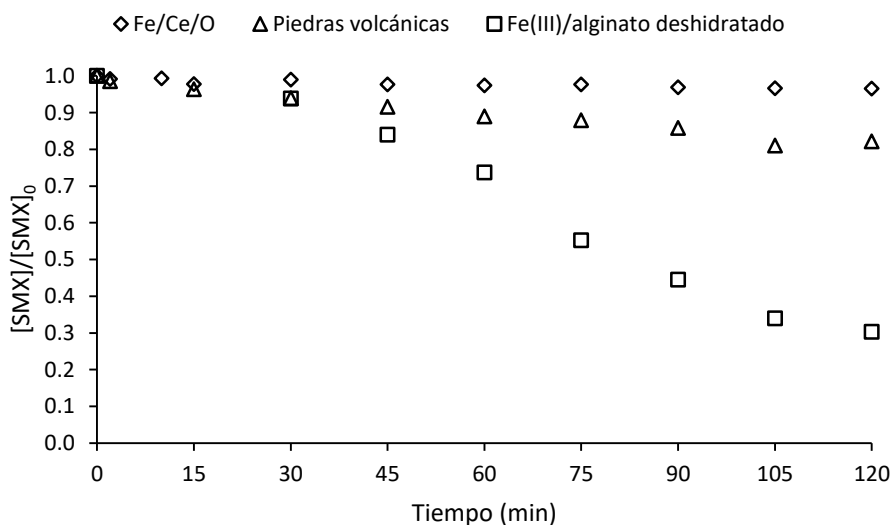

Figura 12.11. Degradación de SMX a lo largo de tres experimentos foto-Fenton llevados a cabo utilizando tres diferentes catalizadores heterogéneos a un pH inicial de 7,0. $[SMX]_0$ = 10 mg L^{-1}, $[H_2O_2]_0$ = 20 mg L^{-1}, $[Fe/Ce/O]_0$ = 0,5 g L^{-1}, $[Piedras volcánicas]_0$ = 0,5 g L^{-1}, $[Fe(III)/alginato deshidratado]_0$ = 0,5 g L^{-1}.

En cuanto a las piedras volcánicas, mostraron una ligera degradación de aproximadamente un 20 % del SMX inicial. Esta mejora respecto a los experimentos

197

anteriores se justificó debido a que el contenido de hierro en este catalizador se encontraba principalmente en forma de especies de Fe(III), las cuales no son activas para la reacción Fenton y requerían de la irradiación con luz UV-A para transformarse en especies de Fe(II) que sí que lo eran.

Comparando estos resultados con los del catalizador de Fe(III)/alginato, se puede observar que pese a los problemas de competencia que puede generar este catalizador debido a su naturaleza orgánica, su eficiencia en la eliminación de SMX mediante la reacción de tipo foto-Fenton es muy superior a la de los catalizadores probados.

12.5. CONCLUSIONES

El principal objetivo de esta tesis era evaluar la síntesis de catalizadores heterogéneos basados en alginato y su posterior aplicación a las reacciones tipo Fenton y foto-Fenton para la eliminación de microcontaminantes y para desinfección. Las conclusiones obtenidas en cada uno de los capítulos puedes verse a continuación:

Capítulo 4: Desarrollo del catalizador de Fe(III)/alginato

- El Fe(III) resultó ser más adecuado en la síntesis del catalizador de Fe/alginato debido a las mejores propiedades mecánicas del catalizador tras su preparación.
- La concentración de la solución de alginato determinó la cantidad de hierro que puede ligarse con las cadenas de alginato.
- La concentración de la solución endurecedora determinó la velocidad de difusión del hierro a través del alginato durante la fase de endurecimiento, por lo que mayores concentraciones consiguieron ligar más cantidad de hierro y más rápido.
- La temperatura de la solución de alginato resultó fundamental a la hora de determinar el tamaño del catalizador debido a su influencia sobre la viscosidad y consecuentemente sobre el tamaño de las gotas que se convierten en catalizador tras ponerse en contacto con la solución endurecedora.

- La limpieza del catalizador para la eliminación de la solución endurecedora tras el proceso de síntesis fue esencial para evitar la reacción homogénea debido a restos de esta solución.

- El uso de una solución de alginato 2,5% (m/m), una solución endurecedora de $FeCl_3$ 0,05M y 6 horas de endurecimiento fueron las condiciones óptimas de preparación del catalizador de Fe/alginato para su aplicación al proceso foto-Fenton a pH cercano a la neutralidad.

Capítulo 5: Mecanismo y estabilidad del catalizador de Fe(III)/alginato

- El pH juega un papel importante en la estabilidad de los catalizadores en base alginato. Se ha demostrado que la liberación del hierro ligado se produce cuando el pH desciende por debajo del pK_a de los grupos carboxilo del alginato, incrementando la contribución de la reacción foto-Fenton homogénea.

- Cuando el catalizador de Fe(III)/alginato se aplica a aguas no tamponadas, la tendencia a la acidificación de las reacciones Fenton activan la liberación de hierro soluble y convierten la reacción inicialmente heterogénea en un proceso simultáneo de las reacciones homogénea y heterogénea.

- El alginato, debido a su naturaleza orgánica, actúa como agente secuestrante de las especies oxidantes reduciendo significativamente la eficiencia de la reacción.

- Se ha comprobado la existencia de actividad heterogénea del catalizador de Fe(III)/alginato aplicado a la reacción foto-Fenton a pH cercano a la neutralidad para la eliminación de SMX, pero la eficiencia es baja debido al efecto secuestrante del propio alginato.

Capítulo 6: Catalizador de Fe(III)/alginato aplicado a desinfección

- El catalizador de Fe(III)/alginato es capaz de producir la inactivación de la bacteria Escherichia Coli cuando se aplica como catalizador heterogéneo de la reacción foto-Fenton en agua destilada, con una contribución mínima de la vía homogénea.

- El catalizador de Fe(III)/alginato aplicado como catalizador heterogéneo de la reacción foto-Fenton en agua potable embotellada inactivó más de 99% de los $1,14 \times 10^4$ CFU mL^{-1} iniciales de Escherichia Coli pero 14 CFU mL^{-1} aún se detectaron después de 60 minutos. La menor contribución de la reacción homogénea debido al medio natural tamponado produjo una reducción de la tasa de desinfección total y no permitió la inactivación total.

- En comparación con otras tecnologías de desinfección, la naturaleza no dañina de los catalizadores de alginato supone una ventaja cuando se aplica a aguas destinadas al consumo humano. Por lo tanto, podría ser un candidato adecuado para la desinfección de efluentes con bajas cargas orgánicas en cumplimiento con los límites de hierro soluble en la legislación actual sobre el agua (0,2 mg L^{-1}). Aun así, las condiciones de reacción deben ser ajustadas para minimizar la liberación de hierro y de acuerdo con la población microbiológica para asegurar la desinfección total.

- Se aplicó el catalizador de Fe (III) / alginato a la inactivación del virus del bacteriófago M4, que es especialmente resistente a los procesos de oxidación avanzada, y consiguió una eliminación del 98,5% del virus inicial, lo que indica que no es totalmente eficiente para inactivar microorganismos resistentes en las condiciones aplicadas.

Capítulo 7: Modificaciones del catalizador de Fe(III)/alginato

- La aplicación de un proceso de deshidratación controlada al catalizador de Fe (III)/alginato permite sintetizar el catalizador de Fe (III)/alginato deshidratado, que demostró ser tan eficiente como el hidratado aplicado a la reacción foto-Fenton a pH próximo a la neutralidad, pero con una escasa liberación de hierro y COT.

- El uso de catalizador de Fe(III)/alginato deshidratado en agua natural tamponada a pH neutro o ligeramente básico, cuando se evita la reacción homogénea, no

tuvo un efecto oxidativo visible sobre el compuesto de referencia estudiado (sulfametoxazol).

- La combinación de la reacción foto-Fenton con hierro coordinado con alginato junto con la contribución fotocatalítica de las partículas de TiO_2 atrapadas mejoró significativamente la tasa de eliminación de SMX.

- La inclusión de cerio y partículas de hierro de d valencia cero en el catalizador resultó inútil para mejorar la eficacia del catalizador de Fe(III)/alginato deshidratado a pH próximo a la neutralidad.

Capítulo 8: Catalizadores heterogéneos aplicados a reacciones de tipo Fenton y foto-Fenton a pH neutro

- Se desechó el catalizador de Fe/Mn/O para reacciones de tipo Fenton debido a la capacidad de los óxidos de manganeso para descomponer instantáneamente el H_2O_2 en agua y oxígeno, haciendo imposible realizar reacciones que utilicen H_2O_2 como precursor para la formación de HO· como especie oxidativa.

- Las limaduras de hierro de la industria metalúrgica fueron descartadas como posible catalizador de Fenton de bajo costo debido a la falta de reacción observada a pH neutro y a la enorme cantidad de hierro liberado cuando se llevaba a cabo la reacción en condiciones ácidas.

- El catalizador de Fe/Ce/O demostró producir la descomposición directa del H_2O_2 sin la producción de especies oxidativas, como ocurrió con el catalizador Fe/Mn/O, pero a una menor velocidad.

- Los experimentos de Fenton realizados con el catalizador de Fe/Ce/O presentaron alguna degradación de SMX a pH ácido. Los resultados globales sugirieron que el pH ácido fuerte y la alta concentración de H_2O_2 produjeron la solubilización parcial de Fe procedente del catalizador. Por lo tanto, la disminución de SMX observada podría atribuirse a la reacción homogénea de Fenton.

- La actividad catalítica de las rocas volcánicas se confirmó sólo cuando se aplicó a la reacción foto-Fenton. Se supuso que este catalizador estaba formado principalmente por especies no catalíticas de Fe(III) que necesitaban irradiarse con luz UV-A para convertirse en especies activas de Fe(II). Aun así, la eficiencia obtenida por este catalizador fue baja.

- El catalizador deshidratado de Fe(III)/alginato demostró ser más eficiente en la degradación del sulfametoxazol a través de la reacción foto-Fenton a pH cercano a la neutralidad que todos los demás catalizadores heterogéneos probados.

12.6.   REFERENCIAS

[1]   H.H.. Savenije, Water scarcity indicators; the deception of the numbers, Phys. Chem. Earth, Part B Hydrol. Ocean. Atmos. 25 (2000) 199–204. doi:10.1016/S1464-1909(00)00004-6.

[2]   U. Nations, D. Programme, Human Development Report 2006, 2006.

[3]   A. Jelic, M. Gros, A. Ginebreda, R. Cespedes-Sánchez, F. Ventura, M. Petrovic, D. Barcelo, Occurrence, partition and removal of pharmaceuticals in sewage water and sludge during wastewater treatment, Water Res. 45 (2011) 1165–1176. doi:10.1016/j.watres.2010.11.010.

[4]   M. Clara, B. Strenn, O. Gans, E. Martinez, N. Kreuzinger, H. Kroiss, Removal of selected pharmaceuticals, fragrances and endocrine disrupting compounds in a membrane bioreactor and conventional wastewater treatment plants, Water Res. 39 (2005) 4797–4807. doi:10.1016/j.watres.2005.09.015.

[5]   S. Glassmeyer, E.T. Furlong, D.W. Kolpin, J.D. Cahill, S.D. Zaugg, S.L. Werner, M.T. Meyer, D.D. Kryak, Transport of chemical and microbial contaminants from known wastewater discharges: potential for use as indicators of human fecal contamination, Environ. Sci. Technol. 39 (2005) 5157–5169.

[6]   M. la Farré, S. Pérez, L. Kantiani, Fate and toxicity of emerging pollutants, their metabolites and transformation products in the aquatic environment, TrAC Trends Anal. Chem. 27 (2008) 991–1007. doi:10.1016/j.trac.2008.09.010.

[7]   M. Klavarioti, D. Mantzavinos, D. Kassinos, Removal of residual pharmaceuticals from aqueous systems by advanced oxidation processes, Environ. Int. 35 (2009) 402–417. doi:10.1016/j.envint.2008.07.009.

[8]   P.R. Gogate, A.B. Pandit, A review of imperative technologies for wastewater treatment I: oxidation technologies at ambient conditions, Adv. Environ. Res. 8 (2004) 501–551. doi:10.1016/S1093-0191(03)00032-7.

[9]   J.J. Pignatello, E. Oliveros, A. MacKay, Advanced Oxidation Processes for Organic Contaminant Destruction Based on the Fenton Reaction and Related Chemistry, Crit. Rev. Environ. Sci. Technol. 36 (2006) 1–84. doi:10.1080/10643380500326564.

[10] M. Pérez, F. Torrades, X. Domènech, J. Peral, Fenton and photo-Fenton oxidation of textile effluents, Water Res. 36 (2002) 2703–2710. doi:10.1016/S0043-1354(01)00506-1.

[11] S.M. Arnold, W.J. Hickey, R.F. Harris, Degradation of Atrazine by Fenton's Reagent: Condition Optimization and Product Quantification, Environ. Sci. Technol. 29 (1995) 2083–2089. doi:10.1021/es00008a030.

[12] A. De Luca, R.F. Dantas, S. Esplugas, Assessment of iron chelates efficiency for photo-Fenton at neutral pH., Water Res. 61 (2014) 232–42. doi:10.1016/j.watres.2014.05.033.

[13] L.F. González-Bahamón, F. Mazille, L.N. Benítez, C. Pulgarín, Photo-Fenton degradation of resorcinol mediated by catalysts based on iron species supported on polymers, J. Photochem. Photobiol. A Chem. 217 (2011) 201–206. doi:10.1016/j.jphotochem.2010.10.009.

[14] M. Pariente, F. Martínez, J. Melero, J. Botas, T. Velegraki, N. Xekoukoulotakis, D. Mantzavinos, Heterogeneous photo-Fenton oxidation of benzoic acid in water: Effect of operating conditions, reaction by-products and coupling with biological treatment, Appl. Catal. B Environ. 85 (2008) 24–32. doi:10.1016/j.apcatb.2008.06.019.

[15] R. Gonzalez-Olmos, M.J. Martin, A. Georgi, F.-D. Kopinke, I. Oller, S. Malato, Fe-zeolites as heterogeneous catalysts in solar Fenton-like reactions at neutral pH, Appl. Catal. B Environ. 125 (2012) 51–58. doi:10.1016/j.apcatb.2012.05.022.

[16] A.F. Rossi, N. Amaral-Silva, R.C. Martins, R.M. Quinta-Ferreira, Heterogeneous Fenton using ceria based catalysts: Effects of the calcination temperature in the process efficiency, Appl. Catal. B Environ. 111–112 (2012) 254–263. doi:10.1016/j.apcatb.2011.10.006.

[17] S. Ben Hammouda, N.N. Adhoum, L. Monser, Chemical oxidation of a malodorous compound, indole, using iron entrapped in calcium alginate beads, J. Hazard. Mater. 301 (2016) 350–361. doi:10.1016/j.jhazmat.2015.09.012.

[18] H. Niu, Dizhang, Z. Meng, Y. Cai, Fast defluorination and removal of norfloxacin by alginate/Fe@Fe3O4 core/shell structured nanoparticles, J. Hazard. Mater. 227 (2012) 195–203. doi:10.1016/j.jhazmat.2012.05.036.

[19] J. Fernandez, M.R. Dhananjeyan, J. Kiwi, Y. Senuma, J. Hilborn, Evidence for Fenton Photoassisted Processes Mediated by Encapsulated Fe ions at Biocompatible pH Values, J. Phys. Chem. B. 104 (2000) 5298–5301. doi:10.1021/jp9943777.

[20] Y. Dong, W. Dong, Y. Cao, Z. Han, Z. Ding, Preparation and catalytic activity of Fe alginate gel beads for oxidative degradation of azo dyes under visible light irradiation, Catal. Today. 175 (2011) 346–355. doi:10.1016/j.cattod.2011.03.035.

[21] E. Rosales, O. Iglesias, M. Pazos, M.A.A. Sanromán, Decolourisation of dyes under electro-Fenton process using Fe alginate gel beads., J. Hazard. Mater. 213–214 (2012) 369–77. doi:10.1016/j.jhazmat.2012.02.005.

204

[22] K.J. Sreeram, H. Yamini Shrivastava, B.U. Nair, Studies on the nature of interaction of iron(III) with alginates, Biochim. Biophys. Acta - Gen. Subj. 1670 (2004) 121–125. doi:10.1016/j.bbagen.2003.11.001.

[23] T. Coradin, J. Livage, Synthesis and Characterization of Alginate/Silica Biocomposites, J. Sol-Gel Sci. Technol. 26 (2003) 1165–1168. doi:10.1023/A:1020787514512.

[24] A. Maureira, B.L. Rivas, Metal ions recovery with alginic acid coupled to ultrafiltration membrane, Eur. Polym. J. 45 (2009) 573–581. doi:10.1016/j.eurpolymj.2008.11.021.

[25] S.-H. Do, B. Batchelor, H.-K. Lee, S.-H. Kong, Hydrogen peroxide decomposition on manganese oxide (pyrolusite): Kinetics, intermediates, and mechanism, Chemosphere. 75 (2009) 8–12. doi:10.1016/j.chemosphere.2008.11.075.